

**STUDIES ON SOLUTE BINDING PROTEINS FROM  
CANDIDATUS LIBERIBACTER ASIATICUS**

**Ph.D THESIS**

*by*

**GUNJAN SAINI**



**DEPARTMENT OF BIOTECHNOLOGY  
INDIAN INSTITUTE OF TECHNOLOGY ROORKEE  
ROORKEE-247667(INDIA)  
JULY, 2018**



**STUDIES ON SOLUTE BINDING PROTEINS FROM  
CANDIDATUS LIBERIBACTER ASIATICUS**

**A THESIS**

*Submitted in partial fulfilment of the  
requirements for the award of the degree*

*of*

**DOCTOR OF PHILOSOPHY**

*in*

**BIOTECHNOLOGY**

*by*

**GUNJAN SAINI**

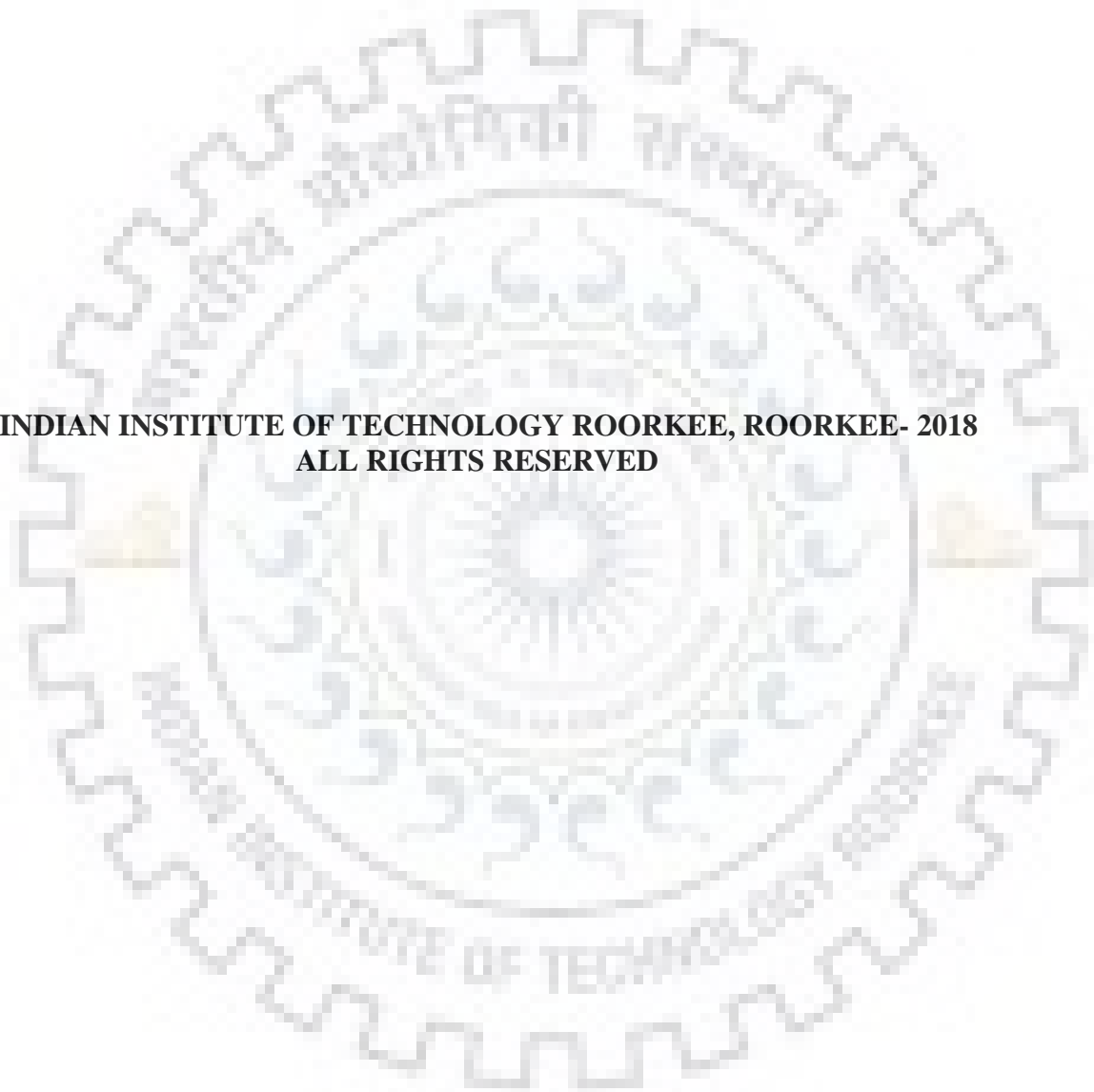


**DEPARTMENT OF BIOTECHNOLOGY  
INDIAN INSTITUTE OF TECHNOLOGY ROORKEE  
ROORKEE-247667(INDIA)  
JULY, 2018**





**©INDIAN INSTITUTE OF TECHNOLOGY ROORKEE, ROORKEE- 2018  
ALL RIGHTS RESERVED**





# INDIAN INSTITUTE OF TECHNOLOGY ROORKEE ROORKEE

## CANDIDATE'S DECLARATION

I hereby certify that the work which is being presented in the thesis entitled "**STUDIES ON SOLUTE BINDING PROTEINS FROM *CANDIDATUS LIBERIBACTER ASIATICUS***" in partial fulfilment of the requirements for the award of the degree of Doctor of Philosophy and submitted in the Department of Biotechnology of the Indian Institute of Technology Roorkee, Roorkee is an authentic record of my own work carried out during a period from January, 2013 to July, 2018 under the supervision of Dr. Ashwani Kumar Sharma, Professor, Department of Biotechnology, Indian Institute of Technology Roorkee, Roorkee.

The matter presented in the thesis has not been submitted by me for the award of any other degree of this or any other institution.

(GUNJAN SAINI)

This is to certify that the above statement made by the candidate is correct to the best of my knowledge.

(Ashwani Kumar Sharma)  
Supervisor

The Ph.D. Viva-Voce Examination of **Gunjan Saini**, Research Scholar, has been held on .....

Chairman, SRC

Signature of External Examiner

This is to certify that the student has made all the corrections in the thesis.

Signature of Supervisor (s)  
Dated:

Head of Department

## ABSTRACT

---

Huanglongbing or citrus greening is the most destructive disease of citrus orchards all over the world. This disease causes the substantial losses in citrus production. HLB is caused by three species of phloem-limited, unculturable, Gram-negative fastidious  $\alpha$ -proteobacteria; *Candidatus Liberibacter asiaticus* (Las), *Candidatus Liberibacter africanus* (Laf) and *Candidatus Liberibacter americanus*. Of the three species, *Candidatus Liberibacter asiaticus* is widely distributed and most virulent strain. It is transmitted by Asian citrus psyllid (*Diaphorina citri* Kuwayama). HLB was mainly identified by blotchy chlorosis /mottling of leaves, yellow shoot, stunted growth, vein corking. HLB affected fruits are small in size, of lower quality, often lopsided and contain aborted seeds. HLB disease is seriously affecting the citrus world by decreasing the lifespan of the citrus trees and lowering the yield as well as the quality of fruits. Currently, no strategies have been developed to manage the HLB disease and to stop the spreading of this disease to new citrus areas. The recommended control strategy is to chemically control the psyllids and removal of the infected trees.

Transition metals such as manganese, zinc and iron sequestration or uptake are essential for bacterial survival and proliferation in the environment as well as within host. They are essential for the activity of a wide range of enzymes, involved in DNA replication, protein synthesis, cell wall synthesis, and oxidative stress management. Metal deficiency greatly inhibits the growth of the bacteria. Therefore, inhibition of the uptake of metal can be a possible strategy for the development of antibacterial agents against the pathogenic bacteria. ATP binding cassette (ABC) family is one of largest family, found in all kingdoms of life. These proteins transport a large range of substrates such as metals, sugars, amino acids, cholesterol, phospholipids, peptides, proteins, polysaccharides and other metabolites. Metal ions such as  $Zn^{2+}$ ,  $Mn^{2+}$  and  $Fe^{2+}$  uptake across the membrane is facilitated by the ATP- binding cassette (ABC-type) transport system. This system works by using the solute binding protein (SBPs) present in periplasm in Gram-negative bacteria and linked to the cytoplasmic membrane in Gram-positive bacteria, to capture the molecule and deliver the substrate for translocation by trans membrane domain of ABC transporter powered by the hydrolysis of ATP by nucleotide binding domain of the membrane. The SBPs involved in the



capture of divalent metal ions like  $Zn^{2+}$ ,  $Mn^{2+}$ , and  $Fe^{2+}$  belongs to Cluster A-1 family of substrate binding proteins.

The Znu system, a member of ABC transporter family, is critical for survival and pathogenesis of *Candidatus Liberibacter asiaticus* (CLA). The two gene clusters have been identified as homologues of the *znuABC* transporter in CLA. The studies demonstrated that only genes from one of the two *znuABC* clusters were able to functionally complement the system in these  $\Delta znuABC$  *E. coli* and  $\Delta znuABC$  *S. meliloti*. The ZnuA gene from the *znuABC* cluster, which is unable to complement  $\Delta znuABC$  *E. coli* and *S. meliloti*, encodes for a periplasmic solute-binding protein (CLas-ZnuA2), which show homology to Mn/Fe-specific rather than Zn-specific proteins in Cluster A-I SBPs. Previously, in our lab, crystal structure analysis of CLas-ZnuA2, a periplasmic solute binding protein from second of the two gene clusters of Znu system in CLA in metal-free state, intermediate state of metal binding,  $Mn^{2+}$ -bound state and  $Zn^{2+}$ -bound state revealed that the mechanistic resemblance of CLas-ZnuA2 seems to be closer to the Zn-specific rather than Mn-specific SBPs of cluster A-I family. Biophysical characterization of CLas-ZnuA2 suggested that it is a low metal binding affinity protein. The subtle communications within and between domains from crystal structure analysis revealed that protein seems to prefer a metal-free state. The unique features of CLas-ZnuA2 included a highly restrained loop L3 and presence of a proline in linker helix. In the present work, we further extended our work by mutation studies, particularly in L3 and linker helix, to understand the nature of interactions and their overall effect. Also, *in-silico* studies on CLas-ZnuA1, a  $Zn^{2+}$  solute binding protein from first of the two gene clusters of Znu system and Esbp, an extracellular solute binding proteins involved in uptake of iron, in CLA were carried out. The 3-dimensional structures were predicted through homology modeling and further virtual screening with molecular docking was used to identify the small molecule inhibitor(s) against these proteins. The thesis has been divided into four chapters.

**CHAPTER 1** reviews the literature describing the bacterial ABC transporter system and their mechanism to transport the substrate across the membrane, importance of metal in biological processes and mechanism of metal binding and release of Cluster A-I proteins and their role in virulence of pathogenic bacteria. The chapter also describes the history of HLB disease, causal Organism, identification, diagnosis, vector and also detection and genome analysis of CLas and it's virulence mechanism and strategies to manage the disease.

**CHAPTER 2** deals with the mutational studies of CLas-ZnuA2 and their characterization using X-ray crystallography, surface plasmon resonance (SPR) and circular dichroism (CD). The ZnuA gene from second of the two gene clusters encodes for a periplasmic solute binding protein (CLas-ZnuA2) which shows homology to Mn/Fe-specific rather than Zn-specific cluster A-I SBPs. The subtle internal communications through an intricate network of interactions play a key role in metal-binding and release and maintaining structural integrity in periplasmic metal uptake proteins. Six mutations Ser38Ala; Tyr68Phe; Pro153Ala; Glu159Ala; Asn193Ala and Pro153Ala/Glu159Ala has been created in CLas-ZnuA2 using site-directed mutagenesis and expressed in *E. coli* BL21-DE3 host cell and purified by Ni-NTA chromatography. All mutations except for S38A and Y68F resulted in destabilization/degradation of the protein. The bioinformatics analysis revealed the creation of hot spot due to P153A mutation in linker helix making CLas-ZnuA2 susceptible to destabilization and degradation. The crystal structure analysis of S38A and Y68F mutants in metal-free and metal-bound forms showed variations in interactions, an increase in the number of alternate conformations and distortions in secondary structure elements. The S38A mutation in CLas-ZnuA2 showed major changes in structure and interactions at the domain interface in loop L3 at the opening of the metal-binding cleft. The metal-free state of S38A CLas-ZnuA2 showed the major sideward shift of part of L3 as compared to metal-free wild-type CLas-ZnuA2 where L3 is displaced away from metal-binding cleft exhibiting an open conformation. Due to mutation of Ser38 to Ala, the particular hydrogen bond between the side-chains of Ser38 and Tyr68 ceases to exist and now the Tyr68 forms hydrogen bond with the main-chain oxygen of Ala38. This conformation is partly similar to the one which occurs on metal-binding in wild-type structure where a larger inward shift of part of the L3 loop (residues 38-40) is observed. The mutation of S38A demonstrated that the sliding of Ser38 present on restrained L3 during metal-binding is part of the metal-binding mechanism for this low metal-binding affinity protein. The mutation to Ala leads to disruption of that mechanism along with disruption of the intricate network of interactions affecting the overall fine-tuned structure. While no sideward shift of L3 was observed in Y68F mutations. The Y68F mutation completely abolished any interaction between mutated Phe68 and Ser38. In the metal-bound form of Y68F CLas-ZnuA2, the inward shift of L3 is not complete to bring His39 within coordinating distance with metal. There were notable changes in interactions of metal coordinating residues with second shell residues in both mutant structures as compared to wild-type metal-free and metal-bound structures of CLas-ZnuA2 were observed. The results suggested that any change in critical residues could alter the subtle

internal communications and result in disturbing the fine-tuned structure required for optimal functioning. Both S38A and Y68F mutations in CLas-ZnuA2 resulted in the notable alterations in the network of interactions which might affect the mechanism of action of the protein. Although the thermal and binding affinity studies did not show significant change as compared to wild-type CLas-ZnuA2 may be due to very low metal-binding affinities can be explained by the mutational study in PsaA (Mn-binding protein from *Streptococcus pneumoniae*), where, two engineered disulphide bond at the C-terminal helix restricts the flexibility through cross-linking and resulted in the significant decrease in the binding capacity of the mutant PsaA for  $Mn^{2+}$  and  $Zn^{2+}$ .

**CHAPTER 3** deals with the computational approach to identify the small molecule inhibitor(s) against CLas-ZnuA1, which can block the binding of Zn and might be able to inhibit the CLA growth. ZnuA1 is the periplasmic component of ZnuABC transporter system, involved in uptake of Zn metal ion in CLA. Thus, inhibiting this process may be a promising approach to design a drug against CLA. CLas-ZnuA1 has been cloned in the pET-28c expression vector. In order to select the novel lead molecules, the model of CLas-ZnuA1 was used for virtual screening of drug-like molecules from the ZINC database by utilizing virtual screening tool PyRx 0.8. 50 drug-like molecules were identified having higher binding energy as the comparison to the binding energy of reference molecule RDS51 (PDB ID: 4BBP) which showed concomitantly binding with Zn (II) and inhibit the growth of *Salmonella enterica*. Five molecules were selected for further analysis on the basis of comparison of the binding affinity energy of the AutoDock Tools and AutoDock Vina. Molecular dynamics were performed for determined the dynamics and stability of CLas-ZnuA1-RDS51 and CLas-ZnuA1-inhibitor(s) complexes. MMPBSA method has been employed for binding free energy calculations. The results reveal that ZINC15670529, ZINC92774705, ZINC06510089, ZINC79841324, and ZINC69594834 were found to bind at the active site of CLas-ZnuA1 and inhibit its binding to Zn metal ion.

**CHAPTER 4** deals with the computational approach to identify the small molecule against Esbp, which can block the binding of Fe and might be able to inhibit the CLA growth. Gram-negative pathogenic microorganisms have developed a range of various high-affinity iron uptake systems for survival like small iron chelators “siderophores”. Another uptake system is also used, which is directly involved in the acquisition of iron from transferrin and/or lactoferrin. Further transport across the membrane is facilitated by the ATP- binding cassette (ABC-type) transport system.

Therefore, affecting the binding process of iron by identifying the small molecule inhibitor at the metal binding site will interrupt the function of CLas-Esbp and thus inhibit the iron uptake process, and this strategy could be used in the discovery of antimicrobial agent against the pathogenic microorganism. CLas-Esbp has been cloned in pET-28c expression vector. The 3-dimensional structure of CLas-Esbp was predicted by homology modeling. The Drug like molecules was retrieved from ZINC database and used for virtual screening. 50 molecules were identified on the basis of binding affinity, fulfilling the range of Lipinski rule of five. Three molecules were selected for further analysis based on the comparison of binding affinity from AutoDock Tools and AutoDock Vina. Furthermore, the protein-ligand complexes were subjected to molecular dynamics simulation to understand the dynamics and stability of the complex(s). Molecular Mechanic/Poisson-Boltzmann Surface Area (MMPBSA) was employed for binding free energy calculation. The results revealed that ZINC03143779, ZINC05491830, and ZINC19210425 were found to be bind at the binding site of CLas-Esbp protein. This computational approach provides an idea in the further development of inhibitor designing against essential proteins of pathogenic microorganisms.

## LIST OF PUBLICATIONS

- 1.) **Gunjan Saini**, Nidhi Sharma, Vikram Dalal, Ashish Warghane, Dilip Kumar Ghosh, Pravindra Kumar<sup>1</sup> and Ashwani Kumar Sharma. The analysis of subtle internal communications through mutation studies in periplasmic metal uptake protein CLas-ZnuA2 (2018) Journal of Structural Biology 204 : 228-239
- 2.) Nidhi Sharma, Purushotham Selvakumar, **Gunjan Saini**, Ashish Warghane, Dilip Kumar Ghosh and Ashwani Kumar Sharma. Crystal structure analysis in Zn<sup>2+</sup> -bound state and biophysical characterization of CLas-ZnuA2 (2016). Biochimica et Biophysica Acta 1864: 1649-1657
- 3.) **Gunjan Saini**, Vikram Dalal, D.N. Gupta, Ashwani Kumar Sharma. Identification of small molecule inhibitors against ZnuA1 of *Candidatus Liberibacter asiaticus* by structure-based design (under review)
- 4.) **Gunjan Saini**, Vikram Dalal, Brajesh Kumar Savita, Ashwani Kumar Sharma. Structure based virtual screening of the novel inhibitors and docking analysis for Esbp from *Candidatus Liberibacter asiaticus* (Manuscript under preparation)

## WORKSHOPS/CONFERENCE ATTENDED

- 1.) Attended **Indo-US conference on “Recent advances in Structural Biology and Drug Discovery”** held in Department of Biotechnology, IIT Roorkee, India from October 9-11, **2014**.
- 2.) Attended **“42nd National Seminar on Crystallography”** held in Jawaharlal Nehru University, New Delhi, India from November 21-23, 2013.



## ACKNOWLEDGEMENT

---

*Before writing my final acknowledgement I would like to share my thoughts. After finishing my thesis writing I was about to write my feelings, memories which I have shared here and outside this environment. Because I know, no one is going to read your “whole” thesis besides your mentor, examiner and of course yourself. Your dear ones always look forward to see your acknowledgement and look for their names only. So I thought I should mention each and every person who played a very important role in my life not only professionally but more importantly emotionally. Because these are your emotions which always make you do something extraordinary not for yourself but for them who believe in you more than yourself. Before acknowledging anyone in this thesis, I dedicate it to my “Papa” & “Mummy” for their endless love, support and encouragement. My papa always dreamed to see me to get a degree from IIT Roorkee, more precisely from Biotechnology Department. And my mummy dreamed to see the Dr.” Prefix before my name. Now, this is the time when their dreams really coming true. A special thanks to my bhai Bhanu, who always motivate and support me. I would not have finished this work without his support and encouragement. Words are not enough to express how grateful I am to my sister Rachna di and Lalit jiju, for their encouragement, moral support, personal attention and care. I express my love to my sweet nephew Parikshit whose innocence refreshed me during my difficult times.*

*At this moment of accomplishment, first of all I am indebted to express my heartfelt thanks to my venerable supervisor Dr. Ashwani Kumar Sharma for his expert guidance, outstanding advice, encouraging attitude and critical comments that made difficult task simple. His encouragement, supervision and support from the preliminary to the concluding level enabled me to develop and understand the subject. This work would not have been possible without his constant guidance and rock solid support at every step from almost past five and half years. He is a mentor who not only supported academically but also emotionally through the rough road to finish this thesis and gave me moral support that I needed during the difficult time. I have learnt a lot from his wisdom and experience, both professionally and personally. I thank him for his patience, kind nature, for many fruitful discussions and also for rectifying my mistakes.*

*I would like to express my sincere thanks towards Dr. Pravindra Kumar for providing Macromolecular Crystallographic Unit facilities. I am courteous to him for his unwavering help and support during structure solution. I am indebted to him for his valuable advice, constant encouragement and precious time without which this work was a very difficult task.*

*I feel overwhelmed in thanking to Prof. R. Prasad and Prof. Partha Roy (former) Head, Department of Biotechnology for providing necessary facilities, support and cooperation in the Department. I would also like to express my sincere thanks to the members of my research committee Prof. R.P. Singh (SRC chairman) Department of Biotechnology, Prof. Partha Roy (internal expert) Department of Biotechnology and Dr. Ramesh Chandra (external expert) Institute Instrumentation Center for their intellectual suggestions, prudent admonitions and immense concern throughout my research period. I am courteous to Prof. R. Prasad, Chairman DRC, Department of Biotechnology for his support and encouragement.*

*I would also like to express my gratitude towards Dr. Shailly Tomar for her precious suggestions especially for SPR experiments. I feel really blessed to have an opportunity to learn from her. My thanks are due to Akshay Pareek and Neetu Singh for their valuable suggestions and untried help during SPR experiment. I am much indebted to both of them for their valuable advice and precious times to analyse my SPR results. I would like to extend my sincere gratitude and special thanks to Dr. Dilip Ghosh for kind help towards my research work by proving genomic DNA, without which this work would not have been possible.*

*Here I take this opportunity to convey my sincere regards, gratitude and special thanks to all faculty members of Department of Biotechnology, IIT Roorkee, for their constant encouragement and support during my research work. I am so indebted to them for providing me necessary help time to time in the form of valuable advice or assistance in handling the instruments.*

*I am obliged to my labmates Dr. Selva kumar, Dr. Prabhat Tomar, Dr. Bibekananda kar, Dr. Anamika Singh, Dr. Preeti Verma, Mr. Pranav Kumar, Mr. Brajesh Kumar Savita, Mr. Deena Nath Gupta, Ms. Sweta, Ms. Sapna, Ms. Harry, Mr. Yogesh kumar and Mr. Gaurav for their honest efforts, friendly attitude and assistance while working in lab. Very special thanks are due to my labmates as well as my friends Dr. Prabhat Tomar, Dr. Bibekananda kar, Dr. Nidhi Sharma, Dr. Anamika Singh, Dr. Preeti Verma, Mr. Brajesh Kumar Savita and Mr. Deena Nath Gupta, for wonderful assistance, motivation and support whenever and wherever required and for providing*

*pleasurable laboratory atmosphere and nice time during this research work. I would like to acknowledge my sincere thanks to Dr. Nidhi Sharma for her wise input at each step of this work. I thank him for raising critical questions and lending me a receptive ear. I am forever grateful for his unwavering support and belief in my abilities. I am very much indebted to my juniors for providing a stimulating and fun-filled environment especially Brajesh, Deena, Vedita, Benazir, Akshay and Swasti. A special thanks to Vikram, for giving his time from tight schedule and all his efforts in completing my thesis work and respect to all of them for their, encouragement, support, and understanding. I would like to thanks Mr. Rajat for his immense support and encouragement. Through all my good and bad times during my thesis, he was with me all the time and helped me in every way.*

*Friends are always most valuable asset anyone can treasure and this list is incomplete without acknowledging. I would like to thank my loving friends, Dr. Richa Katiyar, Ms. Ritu Varshney, Ms. Rukmini Roy, Ms. Neha Singh, Ms. Archana Mishra, Ms. Noopur Singh Parmar who have always been there for me and without whom I could not imagine surviving this journey. Richa Katiyar always pushes me to do things on time. I want to give my love to my sweetest junior Vedita who became very late precisely in my last phase of Ph.D. but she turns out be my lovable friend. She always motivates and pushes me to forward during my journey of work.*

*Outside this campus there are lot people who do so much for me in every aspect say research and no research. My friends who always made me realise that I am doing great, thanks to you all Kiran, Pooja, Tripti and Poonam.*

*Also to be acknowledged with love and appreciation in the memorable concern, affection and care from my senior, batchmates and juniors Dr. Sonali, Dr. RajBala, Dr. Aarti, Dr. Manju Narwal, Dr. Megha, Dr. Mansi, Dr. Meenu, Dr. Rekha, Dr. Ravi, Ms. Swati Mr. Madhu, Mr. Rajesh, Mr. Shailendra Singh Khichi, Mr. Harvijay, Mr. Vijay, Ms. Anchal, Ms. Raman, Ms. Pooja, Ms. Anjali, Ms. Neetu, Ms. Poonam, Mr. Jai, Ms. Monica, Ms. Supreeti and many others.*

*I am also grateful to the Institute Sports Club as well as the Institute Hospital. Both helped me in maintaining physical fitness so that I could accomplish my studies contained in this thesis. I also appreciate the help from the institute Library. It provides a wonderful academic atmosphere during my thesis writing. I would like to express my gratitude toward Mr. Sudheshwar Ram, Institute Library for his time to time help for my thesis. In recognition of all the help and support, I*



would like to mention all the office staff of the Biotechnology Department in particular Mr. Subhash Jain, Mr. Yogeendra Walthare, Mr. Shashi Pal chauhan, Mr. Lokesh, Mrs. Surita, Mr. Y.P.Singh, Mr. Rajesh, Mr. Anil, Mr. Padam, Mr. Pradeep, Ms. Naziya and Mr. Rohit. I would like to thanks to all the cleaning and gardener staff of the Biotechnology Department in particular Sharvan, Anil, Padam and Vijendra for maintaining the healthy and beautiful environment in the department.

Lastly, I will be delighted to say a big thanks to my parents, for giving birth to me at the first place. I pleased to thank my brother for his never ending encouragement throughout my PhD tenure and lifting up my spirits whenever I felt low. I take this opportunity to sincerely acknowledge the Ministry of Human Resource Development (MHRD), New Delhi, for providing financial assistance in the form of Senior Research Fellowship making me to work calmly.

Finally, I thank almighty God for blessing me and keeping me strong and calm during all good and hard times throughout my life.



# CONTENTS

---

## CANDIDATE'S DECLARATION

<b>ABSTRACT.....</b>	<b>i-v</b>
<b>LIST OF PUBLICATIONS.....</b>	<b>vi</b>
<b>ACKNOWLEDGEMENT.....</b>	<b>vii-x</b>
<b>CONTENTS.....</b>	<b>xi-xv</b>
<b>LIST OF FIGURES.....</b>	<b>xvi-xix</b>
<b>LIST OF TABLES.....</b>	<b>xx-xxi</b>
<b>ABBREVIATIONS.....</b>	<b>xxii-xxiv</b>
<b>INTRODUCTION.....</b>	<b>1-3</b>

## **Chapter -1 REVIEW OF LITERATURE**

1.1	ABC transporter	4
	1.1.1. Introduction	4
	1.1.2. Mechanism of ABC transporter proteins	5
	1.1.3. Crystal structures of ABC transporter	6
	1.1.4. Role in virulence	7
	1.1.5. Periplasmic Solute binding proteins	9
	1.1.5.1. Classification of Substrate binding proteins	11
	1.1.5.2. Cluster A-1SBPs	12
	1.1.5.3. Metal transporter	14
	1.1.5.4. Structures of Cluster A-1 SBPs	15
	1.1.5.5. Mechanism of metal binding and release	18
	1.1.5.6. Role of Cluster A -1 in virulence	18
1.2.	Citrus Huanglongbing	19
	1.2.1. Introduction	19
	1.2.2. Historical overview	20
	1.2.3. Causal Organism, identification, diagnosis	21
	1.2.4. Symptoms	22

1.2.4.1. Foliage symptoms	22
1.2.4.2. Fruit symptoms	23
1.2.4.3. Internal changes	23
1.2.5. Disease vector and population dynamics	25
1.2.5.1. Transmission of pathogen	25
1.2.5.2. Pathogen detection system	26
1.2.6. Genome analysis of CLas	27
1.2.6.1. Metabolic pathway	27
1.2.6.2. Transport proteins and types of secretion systems	28
1.2.6.3. Secretion systems	28
1.2.6.4. Proteome and transcriptome analysis of citrus plants and CLas infection	29
1.2.7. Virulence mechanism	29
1.2.7.1. Phloem blockage and aberrations	30
1.2.7.2. Metabolic imbalances by nutrient depletion	30
1.2.7.3. Hormone	31
1.2.7.4. Suppression or avoidance of plant defense	31
1.2.7.5. Prophages SC1 and SC2	32
1.2.7.6. Serralysin and hemolysin	32
1.2.8. Metabolite signature of CLas infection	33
1.2.9. Management practices to control the pathogen	34
1.2.9.1. Cultural Practices	34
1.2.9.2. Biological control of the vector population	34
1.2.9.3. Chemotherapy	35
1.2.10. ABC transporters in CLas	35

**Chapter -2 MUTATION STUDIES IN PERIPLASMIC METAL UPTAKE  
PROTEIN CLas-ZnuA2 FROM *CANDIDATUS LIBERIBACTER  
ASIATICUS***

2.1. Introduction	37
2.2. Materials & Methods	38
2.2.1. Site-directed mutagenesis, expression and, purification of mutant	38

CLas-ZnuA2	
2.2.2. Crystallization and data collection	39
2.2.3. Structure solution and refinement	40
2.2.4. Accession number	40
2.2.5. CD spectroscopy	40
2.2.6. Surface plasmon resonance	40
2.2.7. Determination of kinetics and affinities	41
2.2.8. Prediction of Aggregation effect of mutation	42
2.3. Results	42
2.3.1. Crystal structures of CLas-ZnuA2 mutants	42
2.3.1.1. Crystal Structure of S38ACLas-ZnuA2	42
2.3.1.1.1. Quality of the model	42
2.3.1.1.2. Overall structure and its comparison with wild-type CLas-ZnuA2	44
2.3.1.2. Crystal structure of Y68F CLas-ZnuA2	56
2.3.1.2.1. Quality of the model	56
2.3.1.2.2. Overall structure and its comparison with wild-type CLas-ZnuA2	57
2.3.2. Circular dichroism	66
2.3.3. Surface plasmon resonance	73
2.3.4. Aggregation effect of mutation	75
2.4. Discussion	78
2.5. Conclusion	83
<b>Chapter-3</b>	<b>CLONING AND STRUCTURE BASED IDENTIFICATION OF INHIBITORS AGAINST ZnuA1 FROM CANDIDATUS LIBERIBACTER ASIATICUS</b>
3.1. Introduction	85
3.2. Material & Method	87
3.2.1. Cloning and expression of CLas-ZnuA1	87

3.2.2. Sequence analysis	87
3.2.3. Homology modelling and Structure validation	88
3.2.4. Virtual screening	88
3.2.5. Molecular docking	88
3.2.6. Molecular dynamic simulation	92
3.2.7 MMPBSA binding free energy calculation	93
3.3. Results	93
3.3.1. Cloning and expression of CLas-ZnuA1	93
3.3.2. Bioinformatics analysis of CLas-ZnuA1	94
3.3.2.1. Prediction of signal peptide	94
3.3.2.2. Physico-chemical parameters	94
3.3.2.3. Model building and structure validation	95
3.3.2.4. Amino acid sequence similarity search by NCBI-BLAST	96
3.3.3. Virtual screening	100
3.3.4. Molecular docking	102
3.3.5. Molecular dynamics simulation	108
3.3.5.1. Root mean square deviation (RMSD)	108
3.3.5.2. Root mean square fluctuation (RMSF)	111
3.3.5.3. Radius of gyration (Rg)	112
3.3.5.4. Solvent accessible surface area (SASA)	113
3.3.5.5. Hydrogen bond analysis	114
3.3.5.6. MMPBSA binding free energy calculation	116
3.4. Discussion	118
3.5. Conclusion	121

**Chapter- 4 CLONING AND STRUCTURE BASED IDENTIFICATION OF INHIBITORS AGAINST Esbp FROM CANDIDATUS LIBERIBACTER ASIATICUS**

4.1. Introduction	123
4.2. Material & Method	125
4.2.1. Cloning and expression of CLas-Esbp	125
4.2.2. Sequence analysis	125

4.2.3. Homology modeling and Structure validation	126
4.2.4. Virtual screening	126
4.2.5. Molecular docking	126
4.2.6. Molecular dynamics simulation	129
4.2.7. MMPBSA binding free energy calculation	130
4.3. Results	130
4.3.1. Cloning and expression of CLas-Esbp	130
4.3.2. Bioinformatics analysis	131
4.3.2.1. Prediction of the signal peptide	131
4.3.2.2. Amino acid sequence similarity search by NCBI-BLAST	132
4.3.2.3. Physico-chemical parameters	133
4.3.2.4. Model building and structure validation	133
4.3.3. Virtual screening	135
4.3.4. Molecular docking	137
4.3.5. Molecular dynamics simulation	139
4.3.5.1. Root mean square deviation (RMSD)	140
4.3.5.2. Root mean square fluctuation (RMSF)	142
4.3.5.3. Radius of gyration (Rg)	143
4.3.5.4. Solvent accessible surface area (SASA)	144
4.3.5.5. Hydrogen bond analysis	145
4.3.6. MMPBSA binding free energy calculation	147
4.4. Discussion	149
4.5. Conclusion	152
<b>REFERENCES</b>	<b>153</b>

## LIST OF FIGURES

Fig. 1.1: Schematic of the mechanism of substrate transport by SBP-dependent ATP-binding cassette transporter across the membrane of Gram-negative bacteria.....	6
Fig. 1.2: Ribbon representation of the four crystal structures of full ABC transporters.....	7
Fig. 1.3: Ribbon representation of the zinc-specific cluster A-I solute-binding protein ZnuA from <i>Escherichia coli</i> bound to zinc.....	13
Fig. 1.4: Current global distribution of HLB disease.....	22
Fig. 1.5: Symptoms of HLB in infected citrus plants.....	24
Fig. 1.6: HLB-associated vector Asian citrus psyllid and bacteria <i>Candidatus Liberibacter asiaticus</i> (CLas).....	25
Fig. 2.1: Superposition of S38A CLas-ZnuA2 with wild-type CLas-ZnuA2.....	45
Fig. 2.2: The shift observed in L3 in CLas-ZnuA2 mutants.....	47
Fig. 2.3: The comparison of interactions of residues Ser/Ala38 and Asp247 between wild-type and S38A CLas-ZnuA2.....	48
Fig. 2.4: The comparison of interactions involving metal coordinating residues in S38A CLas-ZnuA2 and wild-type CLas-ZnuA2.....	50
Fig. 2.5: The comparison of the interaction involving residues Asn193, Glu172, and Arg198 of S38A CLas-ZnuA2 and wild-type CLas-ZnuA2.....	53
Fig. 2.6: Superposition of Y68F CLas-ZnuA2 with wild-type CLas-ZnuA2.....	58

Fig. 2.7: The comparison of the interaction of residues Tyr/Phe68 and Asp247 between wild-type and Y68F CLas-ZnuA2.....	59
Fig. 2.8: The electron density map A) The electron density is shown around residues in L3 in the metal-bound state of Y68F CLas-ZnuA2.....	60
Fig. 2.9: The comparison of interaction of metal coordinating residues of Y68F CLas-ZnuA2 with wild-type CLas-ZnuA2.....	61
Fig. 2.10: The comparison of CD spectra of A) metal-free S38A CLas-ZnuA2, Mn <sup>2+</sup> -bound, Zn <sup>2+</sup> -bound CLas-ZnuA2, .....	67
Fig. 2.11: CD spectra showing differences in temperature of the unfolding of Apo S38A CLas-ZnuA2 and after adding MnCl <sub>2</sub> in different concentrations.....	68
Fig. 2.12: CD spectra showing differences in temperature of the unfolding of Apo S38A CLas-ZnuA2 and after adding ZnCl <sub>2</sub> in different concentrations.....	69
Fig. 2.13: CD spectra showing differences in temperature of the unfolding of Apo Y68F CLas-ZnuA2 and after adding MnCl <sub>2</sub> in different concentrations.....	70
Fig. 2.14: CD spectra showing differences in temperature of the unfolding of Apo Y68F CLas-ZnuA2 and after adding ZnCl <sub>2</sub> in different concentrations.....	71
Fig. 2.15: SPR sensograms showing S38A Clas-ZnuA2 and Y68F Clas-ZnuA2 interaction with Mn <sup>2+</sup> and Zn <sup>2+</sup> .....	75
Fig. 2.16: Hot spot area graphics. Hot spot area plot for A) Wild CLas-ZnuA2 protein .....	77
Fig. 2.17: The comparison of interactions between L3, L5, L7 and helix e are shown in the metal-free state of A) wild-type CLas-ZnuA2.....	82



Fig. 3.1: Agarose gel electrophoresis confirming the positive clones.....	94
Fig. 3.2: Prediction of the signal sequence in CLas-ZnuA1.....	95
Fig. 3.3: Cartoon representation of the predicted model of CLas-ZnuA1.....	96
Fig. 3.4: Sequence similarity search of CLas-ZnuA1 using NCBI BLAST search tool.....	97
Fig. 3.5: Multiple sequence alignment of CLas-ZnuA1 with other related.....	98
Fig. 3.6: Phylogenetic tree of CLas-ZnuA1 and related proteins present in.....	99
Fig. 3.7: Ramachandran plot of CLas-ZnuA1 model, showing distribution.....	100
Fig. 3.8: Electrostatic potential surface view of CLas-ZnuA1 protein.....	103
Fig. 3.9: Docking interaction analysis of .....	107
Fig. 3.10: Root mean square deviation of protein.....	109
Fig. 3.11: Root mean square fluctuation profiles of .....	111
Fig. 3.12: Radius of gyration of CLas-ZnuA1.....	112
Fig. 3.13: Solvent accessible surface area profiles of CLas-ZnuA1.....	113
Fig. 3.14: Hydrogen bond analysis of CLas-ZnuA1.....	115
Fig. 3.15: Pictographic representation of interaction involved in .....	120
Fig. 4.1: Agarose gel electrophoresis confirming the positive clones.....	131

Fig. 4.2: Prediction of the signal sequence in CLas-Esbp.....	132
Fig. 4.3: Sequence similarity search of CLas-Esbp using NCBI BLAST search tool.....	133
Fig. 4.4: Cartoon representation of the 3-dimensional model of the CLas- Esbp protein.....	134
Fig.4.5: Ramachandran plot of CLas- Esbp model.....	135
Fig.4.6: Docking interaction analysis of CLas-Esbp.....	139
Fig. 4.7: Root mean square deviation of protein-inhibitor(s) .....	141
Fig. 4.8: Root mean square fluctuation profiles of CLas-Esbp.....	142
Fig. 4.9: Radius of gyration of CLas-Esbp.....	143
Fig. 4.10: Solvent accessible surface area profiles of of CLas-Esbp.....	144
Fig. 4.11: Hydrogen bond analysis of CLas-Esbp.....	146
Fig. 4.12: Pictographic representation of interaction involved in binding of inhibitor(s) to CLas-Esbp using Maestro 11.2.....	151

## LIST OF TABLES

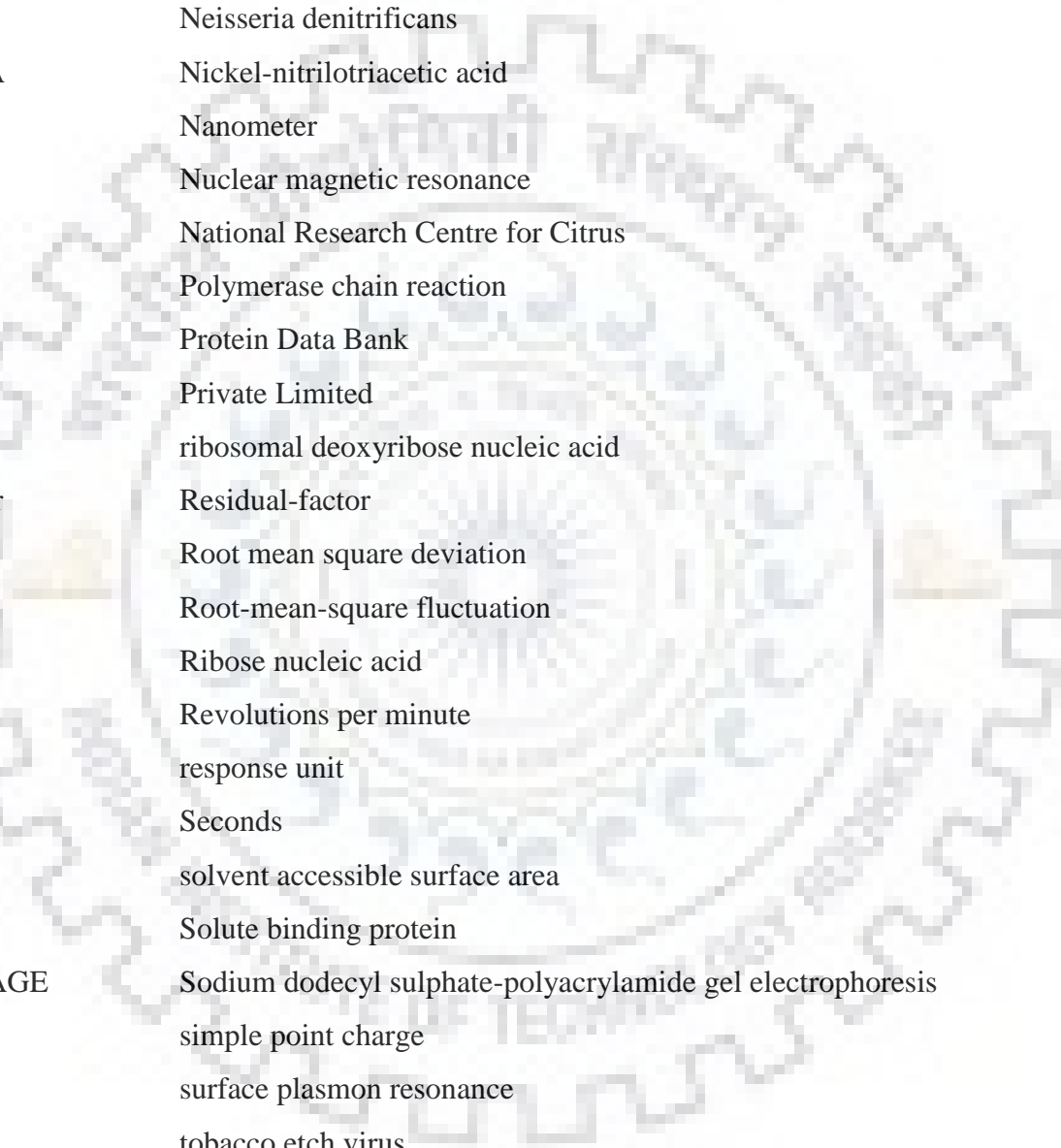
Table 1.1: Selected ABC transporters that play a role in full virulence.....	8
Table 1.2 Classification of substrate binding proteins.....	12
Table 1.3: Structurally characterized cluster A-I SBPs.....	15
Table.2.1:Primers used for site-directed mutagenesis.....	39
Table 2.2: Crystal parameters, data collection and structure refinement.....	43
Table 2.3: Comparison of Exclusive interactions of Metal-free S38A CLas-ZnuA2 and wild-type CLasZnuA2.....	54
Table 2.4: Comparison of interactions of Mn-bound S38A CLas-ZnuA2 and wild -type CLas-ZnuA2.....	55
Table 2.5: Comparison of interactions of Metal-free Y68F CLas-ZnuA2 and wild-type CLas-ZnuA2.....	64
Table 2.6: Comparison of interactions of Metal-bound Y68F CLas-ZnuA2 and wild-type CLas-ZnuA2.....	65
Table 2.7: Effect of Metal ions concentration on Temperature of the unfolding of Mutants CLas-ZnuA2 Protein.....	72
Table 2.8: Comparison of different AGGRESCAN parameters for CLas-ZnuA2.....	76
Table 3.1: Chemical name and structure of selected compounds from the ZINC database.....	89

Table 3.2: Chemical formulae of selected compounds from the ZINC database.....	91
Table 3.3: Physico-chemical properties.....	101
Table 3.4: A detailed summary of the docking binding affinities.....	104
Table 3.5: Average values of RMSD, RMSF, radius of gyration, SASA and intra-H bond of CLas-ZnuA1-RDS51 complex and CLas-ZnuA1- inhibitor(s) complexes.....	110
Table 3.6: Binding free energies calculation of CLas-ZnuA1-RDS51 complex and CLas-ZnuA1- inhibitor(s) complexes by MMPBSA.....	117
Table 4.1: Chemical name and structure of selected compounds from the ZINC database.....	127
Table 4.2: Physico-chemical properties (molecular weight, LogP, H-bond donor, H-bond acceptor) of all selected ZINC IDs fulfilling the Lipinski rule of five.....	136
Table 4.3: A detailed summary of the docking binding affinities .....	137
Table 4.4: Average values of RMSD, RMSF, Radius of gyration, SASA and intra-H bond of CLasEsbp- inhibitor(s) complexes.....	140
Table 4.5: Binding free energies calculation of CLas-Esbp-inhibitor(s).....	148

## LIST OF ABBREVIATIONS USED

---

C	Degree Centigrade
Å	Angstrom
ABC	ATP-binding cassette
B-factor	Debye-Waller factor/Temperature factor
Bp	Base pair
CD	Circular dichroism
CLas	<i>Candidatus Liberibacter asiaticus</i>
Da	Daltons
DNA	Deoxyribose nucleic acid
dNTPs	Deoxy nucleotide triphosphates
E. coli	Escherichia coli
EDTA	Ethylene diamine tetracetic acid
e.g.	For example
<i>et al.</i>	et alia
Fe	iron
gm	Gram
h	Hours
H-bond	Hydrogen bond
HLB	Huanglongbing
IITR	Indian Institute of Technology Roorkee
IPTG	Isopropyl $\beta$ -D-thiogalactoside
K	Kelvin
kDa	Kilo Daltons
LB	Luria Bertani
M	Molar
Mg	milligram
min	Minute
ml	millilitre



MMPBSA	Molecular Mechanic/Poisson-Boltzmann Surface Area
Mn	Manganese
MnCl <sub>2</sub>	manganese chloride
NaCl	Sodium Chloride
NCBI	National Centre for Biotechnology Information
Nde	Neisseria denitrificans
Ni-NTA	Nickel-nitrilotriacetic acid
nm	Nanometer
NMR	Nuclear magnetic resonance
NRCC	National Research Centre for Citrus
PCR	Polymerase chain reaction
PDB	Protein Data Bank
Pvt Ltd	Private Limited
rDNA	ribosomal deoxyribose nucleic acid
R-factor	Residual-factor
RMSD	Root mean square deviation
RMSF	Root-mean-square fluctuation
RNA	Ribose nucleic acid
rpm	Revolutions per minute
RU	response unit
s	Seconds
SASA	solvent accessible surface area
SBP	Solute binding protein
SDS-PAGE	Sodium dodecyl sulphate-polyacrylamide gel electrophoresis
SPC	simple point charge
SPR	surface plasmon resonance
TEV	tobacco etch virus
USA	United States of America
UV	ultra-violet
Xho	Xanthomonas holcicola
Zn	Zinc
ZnCl <sub>2</sub>	zinc chloride

A	Alpha
B	Beta
$\gamma$	Gamma
$\mu\text{g}$	Microgram
$\mu\text{l}$	Microlitre



### Introduction

Proteins are the basic biological macromolecule of all living system. Proteins are constructed by 20 different amino acids. They play an important functional and structural role in all living organism. They are unique for underpinning every reaction of the biological system. The functional versatility of proteins is due to their structural diversity. They may be existing in the single unit or in the combination of several units to perform different functions. Protein interaction with other biomolecules depends upon the three-dimensional structure of the protein and its nature of amino acid side chains. They are linked covalently or non-covalently to the biomolecule such as lipids, carbohydrates, nucleic acids, phosphate groups and metal ions. Protein function is linked to the protein flexibility. The interaction with other molecule causes the conformation changes in the protein which may be very small like the rearrangement of side chains of few amino acids or it may be large, like folding of the entire protein. Different inter and intramolecular bond like hydrogen, electrostatic, van der Waals forces and hydrophobic interaction are formed by the proteins. These interactions are necessary for the structure and activity of the proteins. A Component like heme or metal ions called as the prosthetic group. Complex with lipids is called as lipoproteins, those with carbohydrates known as glycoproteins and with metal ions forms metalloproteins [1, 2]. Physiological conditions like temperature, pH and salt concentration also affect the structure and function of the proteins. Proteins play important role in several biological processes like defense (e.g. antibodies), transport of other molecules (e.g. hemoglobin), reaction catalysis (enzymes), regulatory role (hormones), structural role (e.g. collagen and elastin) and gene regulation by maintaining chromosome structure. Apart from proteins, there are also other factors which contribute to innate host defenses such as reactive nitrogen species [3]. In microorganisms, various proteins are involved in adaption to changes in environments by signal transduction [4, 5]. Over a long period of time, proteins evolve in terms of the sequence through mutation and selection and therefore in structure to perform different biological functions [5, 6].

Metal uptake or sequestration is critical for survival and proliferation of bacteria in the atmosphere and as well as in the host. Transition metals such as manganese, zinc, and iron are crucial for various biological processes since it is used as cofactors for a very wide number of enzymes and



proteins. Manganese acts as the metal cofactor for the range of enzymatic processes including phosphorylation, hydrolysis, carbon metabolism, decarboxylation and oxidative stress response. Zinc is essential for many structural and catalytic activities of all major classes of enzymes and also involved in DNA replication, transcription and cell wall synthesis. Iron is required for the proliferation of bacteria because it is major components of the large range of enzyme including ribonucleotide reductase and cytochromes. It is found in many proteins that are involved in metabolic processes from dioxygen transport and energy transducing pathways to hydrogen and nitrogen fixation. Therefore, these metal ions are important determinants for survival and virulence of microorganism. Metal ion uptake across the membrane is facilitated by ATP- binding cassette type (ABC-type) transport system. This system uses substrate binding protein (SBPs) to capture the molecule and deliver the substrate for translocation by transmembrane domain of ABC transporter powered by the hydrolysis of ATP by nucleotide binding domain of the membrane. SBPs are periplasmic proteins and extracellular lipoproteins in gram negative and gram positive bacteria respectively. The SBPs which transport divalent metal ions belong to the Cluster A-I family which includes zinc, manganese and iron transporters.

Citrus Greening (huanglongbing) is a widespread, extremely destructive citrus plant disease. It causes extensive economic losses by reducing the lifespan of infected trees. HLB is related with three species of phloem-limited, gram-negative fastidious  $\alpha$ - proteobacteria: ‘*Candidatus Liberibacter asiaticus*’ (Las), ‘*Ca. L. africanus*’ (Laf) and ‘*Ca. L. americanus*’. Of the three species, *Ca. L. asiaticus* is widely distributed and most virulent strain. It is transmitted by Asian citrus psyllid (*Diaphorina citri* Kuwayama). Symptoms include blotchy chlorosis and /or mottling of leaves: stunted growth; malformed fruits and finally death. Vahling –Armstrong et al. demonstrated that CLA encodes two ZnuABC homologous systems. To understand the role of these protein homologs, a complementation assay was devised to check their ability to reinstate a partially- inactivated Znu system in *Escherichia coli* and *Sinorhizobium meliloti*. The Result from assay proposed that only genes from one of the two ZnuABC clusters were able to functionally complement the system in these  $\Delta znuABC$  *E. coli* and  $\Delta znuABC$  *S. meliloti*. The ZnuA gene from Znu ABC cluster, which is unable to complement  $\Delta znuABC$  *E. coli* and *S. meliloti* encodes periplasmic solute binding protein (CLas- ZnuA2) which show high homology to Mn/Fe- specific rather than Zn- specific protein in Cluster A-1 SBPs. Earlier in our lab, crystal structure analysis of CLas-ZnuA2, a periplasmic solute binding protein from second of the two gene clusters of Znu

system in CLA in metal-free state, intermediate state of metal binding,  $Mn^{2+}$ -bound state and  $Zn^{2+}$ -bound state revealed that the mechanistic resemblance of CLAs-ZnuA2 seems to be closer to the Zn-specific rather than Mn-specific SBPs of cluster A-I family and it preferred square pyramidal geometry for both  $Mn^{2+}$  and  $Zn^{2+}$ . Biophysical characterization of CLAs-ZnuA2 suggested that it is a low metal binding affinity protein. The unique features of CLAs-ZnuA2 included a highly restrained loop L3 and presence of a proline in linker helix.

In the present work, we further extended this work through mutational study particularly in residues critical for structure and function of L3 loop and linker helix and further analyze the overall effect on the structure of fine-tuned structure of the CLAs-ZnuA2 protein. We have done site-directed mutagenesis in CLAs-ZnuA2, expression, purification of mutant proteins. The biochemical and biophysical characterization of mutant proteins have been performed by using circular dichroism and surface plasmon resonance in order to explore the thermal stability and binding affinity of metal ions towards mutant proteins. We have also determined the high-resolution crystal structures of two mutant S38A and Y68F CLAs-ZnuA2 proteins in metal free and metal bound states. The comparison of mutant CLAs-ZnuA2 proteins to the wild CLAs-ZnuA2 suggest that any change in critical residues could alter the subtle internal communications and result in disturbing the fine-tuned structure required for optimal functioning. Also, *in-silico* studies on CLAs-ZnuA1, a  $Zn^{2+}$  solute binding protein from first of the two gene clusters of Znu system and Esbp, an extracellular solute binding proteins involved in uptake of iron, in CLA were carried out. Homology modeling was used to predict the 3-dimensional structures of CLAs-ZnuA1 and CLAs-Esbp proteins. Virtual screening was used to identify the novel potent molecule against both proteins. Molecular docking program was used for interaction analysis of small molecule with the CLAs-ZnuA1 and CLAs-Esbp proteins. Furthermore, molecular dynamics were performed to understand the stable behaviour of the CLAs-ZnuA1-inhibitor(s) complexes. Molecular Mechanic/Poisson-Boltzmann Surface Area (MMPBSA) assay was used to calculate the binding free energy of the complexes. We successfully identified the small molecules which might be suggested as novel potent compounds to inhibit the binding of Zn and Fe metals to the CLAs-ZnuA1 and CLAs-Esbp proteins, respectively.

# CHAPTER – 1

## REVIEW OF LITERATURE

---

### 1.1. ABC transporter

#### 1.1.1. Introduction

ATP-binding cassette (ABC) transporters are well-known among living organisms from prokaryotes to human representing one of the largest protein families [7, 8]. These transporters are observed in all species and are related evolutionarily. Nevertheless, they are functionally different performing roles in a variety of important cellular functions including translocation of various substrates across membranes such as metabolic products, lipids and sterols, and drugs [9, 10].

ABC transporters may function as an exporter (as in all the kingdoms) or as an importer (exclusively in bacteria and kingdom Plantae). This group of transport protein maintains a balance of transport system across the cellular membranes and are responsible for vital activities in living organisms [11, 12]. Transportation activity of ABC Transporters is regulated precisely so that balance in the transport system is maintained, which is important whether for the fulfilment of nutrient requirements or removal of toxic effects of the substrates. ABC exporters transport various substrates eg. Proteins, Antibiotics, and lipids etc. Whereas, ABC importers transport specific substrate across the membrane of archaea and bacteria, into their cytoplasm [13].

ABC importers transport a large range of substrates such as metals, sugars, amino acids, peptides, and other metabolites [14]. The mechanism of binding and transportation of substrate across the membrane is the same for both importers and exporters [15]. The generic structural conformation of ABC transporters consists of two transmembrane domains (TMDs) and two cytoplasmic nucleotide-binding domains (NBDs). TMDs provide a route for the substrate being transported and NBDs bind and hydrolyze the ATP. The TMDs and NBDs are separate polypeptide chains in ABC importers while in bacterial exporters; both TMDs and NBDs are fused, generating a ‘half transporter’ that forms a homodimer or heterodimer to form the functional unit. In eukaryotes, most of the ABC exporters expressed as a single polypeptide chain consist of all four domains. The majority of bacterial ABC transporters that import the cargo into the cell needs an extracellular SBP [16]. In case of gram-negative bacteria, the SBP inhabits the periplasm.

While gram-positive bacteria use lipoprotein SBPs tethered to the surface of the cell or fused to the membrane permease. This ABC-SBP complex binds to the cargo with high affinity and with precise specification and delivered to the membrane permease for transportation into the cytoplasm.

### **1.1.2. Mechanism of ABC transporter proteins**

Several models on the mechanism of ABC Transporter Proteins have been proposed based on their architectural and biochemical data. The most notable mechanism models of ABC Transporter are “alternating site” [17], “switch” [15] and “constant contact” [18, 19]. All of these models have common elementary steps, like ATP-dependent dimerization of NBD and switching of the TMD between inward- and outward-facing conformations, the variation is in few details of the mechanism. An important bullet which needs to be mentioned is that there is very little evidence that proved all ABC transporters function by the very same mechanism. For instance, the best-structurally and mechanistically characterized importers are the *E. coli* maltose [20, 21] (a type I) and vitamin B12 [22-24] (a type II) uptake systems.

A series of steps involved in the catalytic cycle of ABC transporter from the ground state or “apo” state. In resting state, the substrate-binding site of permease is found in an inward-facing orientation and the cytosolic NBDs are apart from each other. When a loaded SBP become associated with the inward facing permease, both NBDs are brought together. The binding of ATP to the NBDs initiate a series of conformational changes in all components of the translocation machinery. The conformational changes in the ATP- bound NBDs reconstitute a productive catalytic site for ATP hydrolysis and trigger the permease to adopt an outward-facing conformation. This reorientation of the TMDs is linked to the opening of the SBP, which delivers the cargo to the permease. Following ATP hydrolysis, the permease returns to its inward-facing conformation and the substrate is free to diffuse to the cytoplasm and transporter is at the ground state for the next cycle (Fig.1.1).

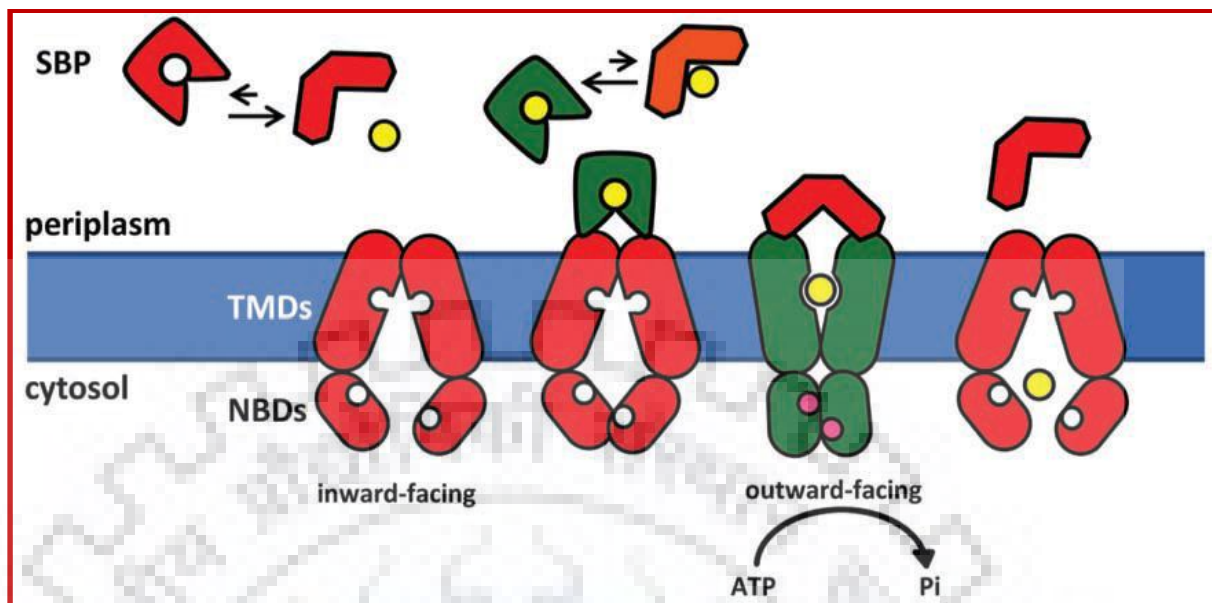


**Fig. 1.1:** Schematic representation of the mechanism of substrate transport by SBP-dependent ATP-binding cassette transporter across the membrane of Gram-negative bacteria [25].

Recently, a direct visualization of the mechanism of conformational changes in the transition of ABC associated SBDs was made using single-molecule FRET which permits a kinetics and structural information of SBDs [26].

### 1.1.3. Crystal structures of ABC transporter

There are numbers of crystal structure of ABC importers and exporters are solved. The vitamin B<sub>12</sub> transporter BtuCD from *E. coli*, the molybdate/tungstate transporter ModBC from *A. fulgidus* [27] reported in complex with ModA protein and the another one is the metal-chelate-type transporter HI1470/1 from *H. influenzae* [28], the multidrug transporter Sav1866 from *S. aureus* [29, 30] (Fig. 1.2), a high affinity methionine uptake transporter MetNI from *E. coli* [31], a homologous of multidrug transporter, TmrAB from *Thermus thermophilus*[32], the nucleotide-free and Glutathione-bound Mitochondrial ABC Transporter Atm1 [33], the intact folate ECF transporter from *Lactobacillus brevis* [34]



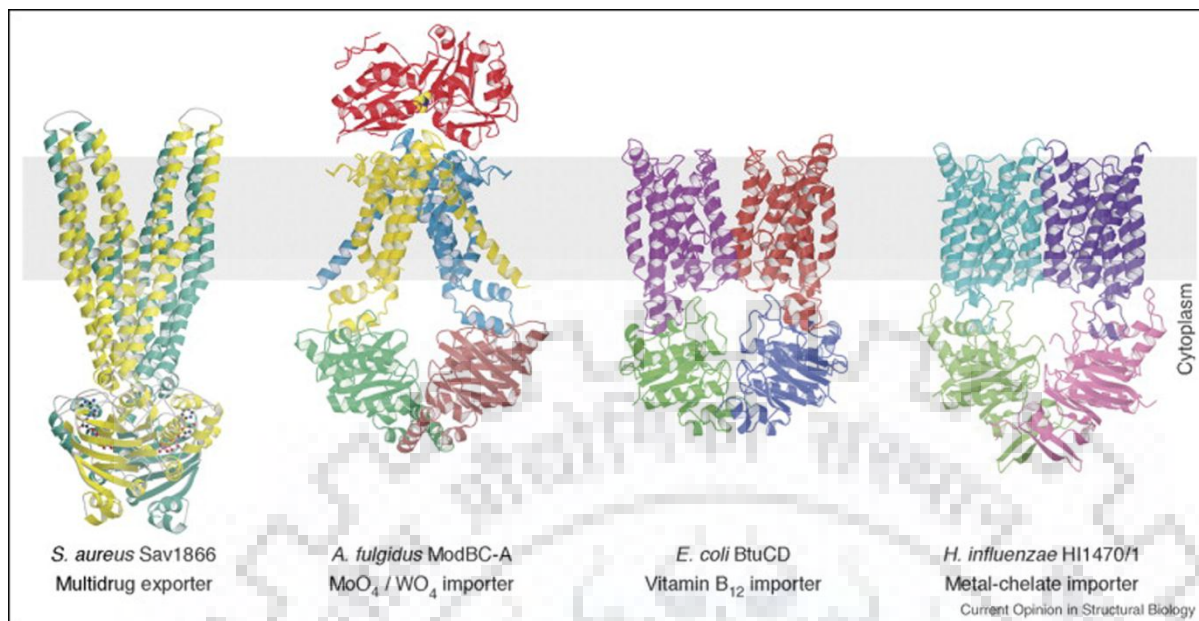


**Fig. 1.2:** Cartoon representation of the crystal structures of full ABC transporters, with the source organism, transporter name, and putative function. PDB ID: 2HYD 2HYD and 2ONJ for Sav1866, 2ONK for ModB2C2A, 1L7V for BtuCD, and 2NQ2 for HI1470/71. Grey box indicate the position of membrane. TMDs of exporters, like Sav1866 are fused to the NBDs, whereas TMDs and NBDs are separate subunits in the importers ModBC, BtuCD, and HI1470/71. ModA is the cognate molybdate/tungstate binding protein of ModBC. The stoichiometries of the assembled transporters/complexes are (Sav1866)<sub>2</sub>, ModB<sub>2</sub>C<sub>2</sub>A, BtuC<sub>2</sub>D<sub>2</sub>, (HI1470)<sub>2</sub>(HI1471)<sub>2</sub>[35].

#### 1.1.4. Role in virulence

The colonization of bacteria is dependent on their ability to get the nutrients from the surrounding environment. Bacteria have evolved in the variety of genus & species depending upon their ability to utilize available nutrients to maintain homeostasis and pathogenesis. To restrict the growth of bacteria, the host may attack the site of infection with anti-bacterial mechanisms or limit the nutrients available to the pathogen to prevent further colonization [36]. Many of the importers play the vital role in the delivery of nutrients such as, ECF transporters for delivery of riboflavin are found in the *Listeria monocytogenes*, *Clostridium difficile* and *Bacillus subtilis* whereas, Type I importer of zinc, ZnuABC is found in *Yersinia pestis*, *Brucella abortus* and *Proteus mirabilis* [37, 38].

Pathogenic micro-organism quickly adapts to dynamic host microenvironment, through uptake of nutrient by choosing ABC transporters. The nutrient uptake mechanisms are the main

virulence determinants employed by the causal organism to mediate the disease. There are several important nutrients that micro-organism required for survival, however in several cases; there remains an absence of knowledge linking these systems to infective agent virulence, initially tested by transporter mutants in the animal model of diseases. Whereas, several key transports stay to be known, selected ABC importers are shown to be crucial for virulence of the micro-organism, illustrating these proteins as the factor of virulence in Table 1.1. The virulence factor transports a long list of a substrate including transition metals, amino acid, and peptides.

**Table 1.1: Selected ABC transporters that play a role in full virulence [39].**

Substrate	Name	Organism
Metal transporters Zinc	ZnuABC	<i>B. abortus</i> , <i>S. Typhimurium</i> , <i>C. jejuni</i> , <i>M. catarrhalis</i> , uropathogenic <i>E. coli</i> , <i>A. baumannii</i> , <i>Y. pestis</i> , <i>P. mirabilis</i>
Manganese and iron	SitABCD	Avian pathogenic <i>E. coli</i> , APEC O78 strain X7122, <i>B. henselae</i>
Manganese and zinc	MntABC	<i>S. Typhimurium</i> , <i>N. gonorrhoea</i>
Manganese and zinc	PsaABC	<i>S. pneumoniae</i>
Nickel and cobalt	CntABCDF	<i>S. aureus</i>
Amino acid transporter Glutamate	Glt <sup>TM</sup> , SBP (NMB1964)	<i>N. meningitides</i>
Glutamine	GlnHPQ	<i>S. Typhimurium</i> , <i>N. gonorrhoeae</i> , Group B Streptococci, <i>S. pneumoniae</i> (spd1098-1099, spd0411-0412)
Alanine	DalS, SBP of putative Dalaninetransporter	<i>S. Typhimurium</i>
Cysteine	CtaP, SBP of putative oligopeptide transporter	<i>L. monocytogenes</i>

Lysine, Ornithine	SBP1, SBP3, SBPs putative amino acid transporter	<i>M. catarrhalis</i>
Methionine	MetNIQ	<i>M. catarrhalis</i>
Methionine	MetQNP	<i>S. pneumoniae</i>
Peptide transporter Peptides	OppABCDF	<i>M. catarrhalis</i> and <i>B. thuringiensis</i>
AMPs	SapABCDF	Nontypable <i>H. influenzae</i> and <i>H. ducreyi</i>
AMPs	YejABEF	<i>B. melitensis</i> (BMNI_I0006-BMNI_I00010) and <i>S. Typhimurium</i>

### 1.1.5. Periplasmic Solute binding proteins

Periplasm acts as a “nutrient bank” to the cytoplasm by both supplying nutrients and depletion of the same. Thus, periplasm plays a crucial role in the homeostasis of essential transition metals [40]. A wide variety of proteins with their various specific functions are present in the periplasmic space of Gram-negative bacteria which are responsible for nutrient metabolism, chemotaxis, antibiotic resistance, transport, and energy utilization [41]. There are “about a dozen” such periplasmic proteins that are responsible for transportation of small polar substrates itself across the inner membrane of the bacteria. The actual working of the protein is that it acts as a mediator by binding with the solute in the periplasm and transfers the solute across the inner membrane of the bacteria. Further, binding of the periplasmic protein of Gram-negative bacteria with the solute changes their own molecular rearrangement, this leads to facilitation of transmembrane chemoreceptors interaction [42]. Transmembrane chemoreceptors are also known as transport proteins.

The periplasmic binding proteins (also referred as PBPs or PSBPs in further text) actually represent a widely distributed protein superfamily [41, 43]. The size of PSBPs may vary from 25–70 kDa, in spite of the varieties of the proteins their overall structural organization is highly conserved. An exclusive characteristic of the PSBPs is having two large domain connected



via flexible tethers in its structure; thus binding of ligand induces a crucial conformational change in a manner that two domain fold simultaneously or say trapping takes place between the two lobes. Thus the term Venus flytrap has been given to this double-lobed simultaneously folding formed structure. PSBPs are supposed to function through a mechanism named “Venus-flytrap” which has an open, solvent-accessible ligand-free state and a closed bound state that exist in kinetic equilibrium. When the ligand binds with the PSBPs, it shifts the equilibrium towards the state of closed conformation [44]. Comprehensive list of PSBPs is easily accessible over the internet in the Entrez program at <http://www.ncbi.nlm.nih.gov/Entrez/>, enter "periplasmic binding proteins") [45]. The PSBPs after binding with the substrate form a complex with membrane-bound transporters or chemotaxis receptors (CR). This transport complex generally comprises of two integral membrane proteins and two ATPases subunit attached on the surface of the cytoplasm [13]. The PSBP-Substrate-CR structure resembles multiple drug-resistant structure that secretes substrate from the cells but in contrast, this complex commonly transports substrates into the cells.

The substrate-binding domains (SBDs) and Substrate-binding proteins (SBPs) form a class of proteins that are related to membrane protein complexes employed for transport or signal transduction [46]. Also, the review of the literature on PSBPs or SBPs says that originally these proteins were found in prokaryotic ABC-transporters, as well as also the part of other membrane protein complexes too. The table below is showing such examples with references. Such as:

PSBPs Complexes explored by researchers	Research Reference
prokaryotic tripartite ATP-independent periplasmic (TRAP)-transporters	[47-49]
prokaryotic two-component regulatory systems	[50]
eukaryotic guanylate cyclase-atrial natriuretic peptide receptors	[43, 51]
G-protein coupled receptors (GPCRs) and ligand-gated ion channels	[52]
prokaryotic DNA-binding proteins play role in gene regulation	[53-55]

### 1.1.5.1. Classification of Substrate binding proteins

The SBPs are classified into various clusters on the basis of overall structural organization of the proteins [56]. Transporter Classification Database which is available on the web at <http://www.tcdb.org/> divides the ABC superfamily into three different families (ABC1–3) based on the homology of membrane proteins [57-60]. To correlate the cargo specificity and function, the further divided into multiple sub-families on the basis of phylogeny [61, 62].

Traditionally, the ABC superfamily was illustrated by homology among the components of ATPase.

Sequence resemblance was used to group SBPs into 8 classifications [41], and later nine classifications [63, 64] and topology of secondary structure classified them into 3 broad classes [65, 66]. A structural classification, classified SBPs in six groups (A-F), on the basis of their conserved scaffold [46] (Table 1.2).

- A-I subcluster involved in binding to zinc, iron, manganese ions,

- A-II involved in binding to chelated metal forms like iron-siderophores and vitamin B12. These are found to be of particular interest because numbers of studies suggest that they are main virulence factors for a various number of human disease-causing organisms [67].

**Table 1.2: Classification of substrate binding proteins given by Ronnie P.A. Berntsson *et al.***

Clusters		Types of substrates
A	I	Divalent metal ions
	II	Siderophores
B		Carbohydrates, Leu, Ile, Val, Autoinducer-2, Natriuretic peptide
C		Di- and oligopeptides, Arg, cellobiose, nickel
D	I	Carbohydrates
	II	Putrescine, thiamine
	III	Tetrahedral oxyanions
	IV	Iron ions
E		Sialic acid, 2-keto acids, ectoine, pyroglutamic acid
F	I	Trigonal planar anions
	II	Methionine
	III	Compatible solutes
	IV	Amino acids

### 1.1.5.2. Cluster A-1SBPs

The Cluster A-1 SBPs are needed for transportation of essential transition metals such as  $Mn^{2+}$ ,  $Zn^{2+}$ , or  $Fe^{2+}$  by using ABC transporter systems in the microorganism. An exclusive

characteristic of Cluster A is a long  $\alpha$ -helix connecting two domains. The helix maintains the rigidity of the structure; only allow a tiny movement of each domain upon cargo binding (Fig. 1.3). In many cases, one or number of transport systems may be existing for each element in a particular bacterium. A knockout study of specific SBP, lead to initiate growth defects in media restricted within the particular of interest. For instance, disruption of *Zinc uptake A (znuA)* SBP, specifically involved in binding to Zn, in *Escherichia coli* inhibits its growth in Zn-restricted media [68]. For pathogenic microorganism, this interprets to attenuated virulence in animal models, suggesting bacterial metal ABC transporter system as a potential target for designing of novel antibiotics [67, 69]. Initially, Cluster A-1 SBPs were detected in *Streptococcus* species as cell surface adhesions [70-72]. These genes were found at adjacent to those of ABC transporters and evidence from experiment linking this type of system with the transport of manganese [64, 73] whereas, a physiological role in uptake of metal for streptococcal cluster A-I SBPs, is dynamically established and uncertainty in their function of cell adhesion [74-77]. It has been prompted that they may act for both, through zinc mediation, an interaction forms between SBP and extracellular protein like laminin [78, 79].

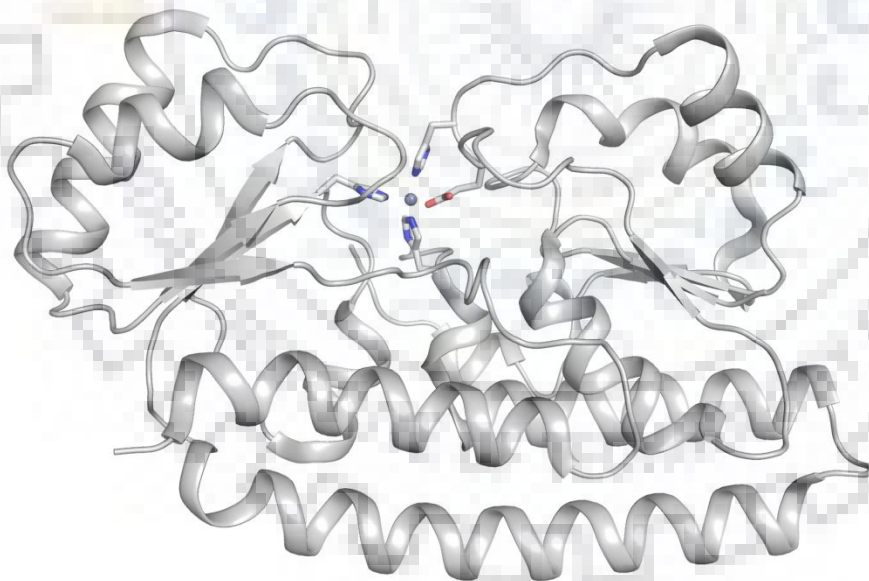


**Fig. 1.3:** Cartoon representation of the Zn-specific cluster A-I solute-binding protein ZnuA from *Escherichia coli* bound to Zn (PDB code: 2OSV).

### 1.1.5.3. Metal transporter

Essential metals are required by all bacteria to perform various metabolic processes. All the trace elements like Iron (Fe), Cobalt (Co), Nickel (Ni), Copper (Cu), Zinc (Zn), and Manganese (Mn) as important in various metabolic activities where they act as precursor (enzyme cofactor), catalysts in biochemical reactions or structural component of protein [80, 81]. To fulfill the requirement of trace elements, bacteria employ the various metal transport system for regulation of the uptake of metal ions, removal of an excess metal ion to avoid toxicity and control homeostasis. Mammals possess advanced ways to limit the presence of the essential trace element in the host environment to prevent the invasion of bacteria, this process known as nutritional immunity [82].

Among transition metals, Zinc is needed for stability and proper folding of proteins in a cell and also acts as a catalyst for several enzymes. Despite the fact, that Zinc is a vital nutrient, It conjointly plays a role within the host to defend the bacterial invasion, an increased level of zinc is often toxic to bacteria [83]. In addition to alternative transport proteins, ZnuABC, provide assistance to the survival of pathogen within the infected host.

Taking another example of Manganese, manganese is required for free radical detoxification and to protect the cell against oxidative damage prompted by peroxide. MntABC, PsaABC, YfeABCD, SitABCD have all been involved in transportation of manganese [84, 85]. These importers are associated with virulence of many bacteria likewise; in *S. Typhimurium* and *Neisseria gonorrhoea* [86].

In case of iron, several forms of iron are needed for the important functions in bacteria, like iron deficiency affect the nucleotide synthesis, production of ATP and also affect the activity of various important enzymes [80, 87]. Gram-negative pathogenic microorganisms have developed a range of various high-affinity iron uptake systems for survival like iron chelator “siderophores”. An alternate iron uptake system, also used by Gram-negative bacteria has been found in many human and veterinary diseases causing microorganism. These bacteria consist of an outer membrane receptor which directly involved in the acquisition of iron from transferrin and/or lactoferrin [88-91].

#### 1.1.5.4. Structures of Cluster A-1 SBPs

Most of the Cluster A-I proteins involved in binding to specific divalent metal ions with high affinities, but some Cluster A-I proteins bind to more than one metal with similar affinities [66, 92]. The first crystal structure of Cluster A-I SBP member was determined for PsaA from *Streptococcus pneumonia* [93] in Zn(II) bound form although physiologically this protein binds to Mn(II). Hitherto, Cluster A-I protein structures are available for receptors involved in the transport of transition metals Zn(II), Mn(II), and Fe(II) (Table 1.3). The differences in their 3d-orbital occupancies of these transition metals make them act rather differently from each other. Mn(II) and Fe(II) have partially filled 3d-orbital and prefer “hard” ligands, like oxygen atoms present in carboxylate groups in side chains of aspartate and glutamate. These metals prefer ligand coordination number of 6 with octahedral coordination geometry. In contrast, Zn(II) has complete 3d orbital and favors “soft” ligands such as the amide group of histidine residues. The preferred coordination number of Zn(II) for ligands is 4 with a tetrahedral coordination geometry [94, 95]. The specificity of the metal ion in Cluster A-I proteins is considered to be a result of the particular coordination chemistry preferred by individual metal-binding sites. However, most Cluster A-I proteins bind to multiple divalent metal ions *in vitro*.

**Table 1.3: Structurally characterized cluster A-I SBPs. ‘Ligand’ refers to the metal bound in the structures indicated by PDB code [96].**

Protein	Organism	Ligand	PDB codes	Kd	References
ZnuA	<i>Salmonella enterica</i>	Zn Apo (mut) Zn/PHa	2XQV, 2XY4 2XH8, 4BBP	<20 nM, $\mu$ M range Zn <sup>40</sup>	[97, 98]
ZnuA	<i>E. coli</i>	Zn  Co Apo	2OSV, 2OGW, 2PS0, 2PRS 2PS9	<20nM Zn <sup>42</sup>	[99-101]

			2PS3		
ZnuA	<i>Synechocystis</i> 6803	Zn Apo	1PQ4, 2OV3 2OV1	7 nM, 9 $\mu$ M Zn <sup>45</sup>	[102, 103]
TroA	<i>Streptococcus</i> <i>suis</i>	Zn	3MFQ	434nM Zn 254nM Mn <sup>46</sup>	[104]
TroA	<i>Treponema</i> <i>pallidum</i>	Zn Apo	1TOA 1K0F	23 nM Zn 7.1 nM Mn <sup>49,50</sup>	[66, 105]
Lbp	<i>Streptococcus</i> <i>pyogenes</i>	Zn	3GI1	nd	[78]
MntA	<i>Listeria</i> <i>monocytogenes</i>	Apo	5HX7	nd	Unpublished
Lmb	<i>Streptococcus</i> <i>agalactiae</i>	Zn	3HJT, 4H0F	nd	[79, 106]
MntC	<i>Synechocystis</i> 6803	Mn Zn/Mn	1XVL 3UJP	nd	[107, 108]
MntC	<i>Staphylococcus</i> <i>aureus</i>	Mn Zn Apo/Abb	4K3V 4NNO 4NNP	4 nM Mn <sup>54</sup>	
PsaA	<i>Streptococcus</i> <i>pneumoniae</i>	Zn Mn Apo Cd	1PSZ 3ZTT, 3ZKA 3ZK7, 3ZK8, 3ZK9 4UTP, 4UTO	231nM Zn 3.3 nM Mn <sup>60</sup>	[93, 109-111]



SitA	<i>Staphylococcus pseudintermedius</i>	Mn Zn/Apo	4OXR 4OXQ	Low nM Zn and Mn <sup>61</sup>	[111]
ZnuA	<i>Bacillus subtilis</i>	Mn	2O1E	nd	Unpublished
AdcAII	<i>Streptococcus pneumoniae</i>	Zn	3CX3	nd	[112]
ZnuA2	<i>Candidatus liberibacter</i>	Mn Apo Zinc	4UDO, 4CL2 4UDN 5AFS	430 μM Zn, 370 μM Mn <sup>65</sup>	[113]
MtsA	<i>Streptococcus pyogenes</i>	Iron	3HH8	4.3 μM Fe(II) 50 μMMn	[114]
AztC	<i>Paracoccus denitrificans</i>	Zinc	4XRV	0.3 nM Zn 52nM Mn	[115]

In cluster A-1 proteins, four positions are involved for binding to the metal ion. Generally, the same types of the ligand are found to be present in three of these positions; two Nε2 atoms from conserved histidine residues and a carboxylate group from a glutamate or an aspartate residue. The fourth position is observed to be important in receptor-metal ion specificity. For Zn specific SBPs, this position is occupied by the by the “soft” Nε2 atom of histidine residue whereas, in case of Mn and Fe SBPs, this is occupied by a carboxylate group of a glutamate residue.

However, a discrepancy to this metal binding mode has been observed in ZnuA structure from *Salmonella enterica*. In the Zn-bound structure of *Salmonella enterica* ZnuA, one of the metal ligands is contributed by the Nε2 atom of histidine residue present in the histidine-rich loop which is unique to ZnuA homologs [98]. Additionally, ZnuA of *E.coli* has a second Zn atom bound to a histidine residue near to the histidine-rich loop, but absent in the primary metal-binding



site [101]. These structures suggest the presence of low affinity, the secondary metal binding site in ZnuA, which might play a role in the translocation of Zn in and out of the high-affinity primary metal binding site [101, 102]. Although the physiological role of the histidine-rich loop in ZnuA-like SBPs is not yet clear, it has also been suggested to play a regulatory role in ZnuA-like proteins, functioning as a sensor for high Zn(II) concentrations [98].

#### **1.1.5.5. Mechanism of metal binding and release**

The reported crystal structures of cluster A-I SBPs, both in apo and bound states, have disclosed the differences in the mechanism of metal binding and release. In Zn(II) binding SBPs, metal binding and release are mainly through local conformational changes without the involvement of any significant change in domain movements and linker helix. In the case of *Trepanoma pallidum* TroA and *Synechocystis* ZnuA SBPs metal binding site remains identical in apo and bound state with the only minor flipping of side chains was observed while in ZnuA of *E. coli*, the loop displacement was also observed. However, in Mn(II) binding SBPs *Staphylococcus aureus* Mntc and PsaA flipping of metal binding residues along with a movement of C-domain and partial unfolding of linker helix at C-terminal was observed. In ZnuA2 of *Candidatus Liberibacter asiaticus*, inward flipping of the side chain of one of the metal coordinating residue has been observed in the metal bound state [101, 104, 111, 113, 116]. Several techniques have been utilized to examine the stoichiometry, metal binding affinity and specificity including isothermal titration calorimetry (ITC), equilibrium dialysis and binding assay with fluorescent chelators or absorbent. These analyses suggest that Cluster A-1 SBPs have the capability to bind various transition metals. Specificity explained from the higher affinity for a specific metal within the range from subnanomolar to low micromolar of dissociation constants (Kd) (Table 1.3).

#### **1.1.5.6. Role of Cluster A -1 in virulence**

Pathogenic bacteria secrete many virulence factors including proteins to invade the host immune system contributing in the pathogenicity and also some toxins for disease development [117-126]. The transition metal ions requirement is crucial for colonization and virulence of bacteria and cluster A-I SBPs have an essential role in this process [69, 81, 127]. Mn(II) is a metal cofactor playing role in a broad range of enzymatic processes such as phosphorylation, hydrolysis, carbon metabolism, decarboxylation and oxidative stress response [128]. ABC permeases which

transport Mn(II) have been identified in almost all disease-causing bacteria. The Mn(II)-ABC permease of *S. pneumoniae*, consists of the Cluster A-I SBP PsaA and the ABC transporter PsaBC, is required for virulence, although not necessary for growth [111, 129]. The requirement of Mn(II) for proliferation and virulence has also been reported in other pathogenic bacteria such as *S. pyogenes*, *S. mutans*, *S. suis*, *Neisseria gonorrhoeae*, and *S. aureus* [130-134]. Iron has the key role in a wide range of process including respiration, photosynthesis and nitrogen fixation. MtsABC has been shown to be important for manganese and iron transport, oxidative stress resistance and virulence of *S. pyogenes* [131]. Zn(II) play significant structural and/or catalytic roles in different classes of enzymes and has the function in transcription and replication factors [135, 136]. Consequently, acquisition of Zn *in vivo* is important for determining virulence in numerous pathogenic bacteria. The Zn(II)-ABC permease of *S. pneumoniae* is vital for colonization of the host environment [63, 137]. ABC permease ZnuABC mediated Zn(II) acquisition is also involved in the virulence of *E. coli* O157:H7 [138], *E. coli* CFT073 [139, 140], *Listeria monocytogenes*, and *Salmonella enterica* [141, 142].

PsaA has been proposed to be a candidate protein target for antimicrobial development. Recently, novel pneumococcal PsaA inhibitors have been identified using fragment-based drug design approaches [143]. PsaA binds to Mn<sup>2+</sup> reversibly and Zn<sup>2+</sup> irreversibly, therefore extracellular Zn<sup>2+</sup> inhibits the acquisition of the essential metal Mn<sup>2+</sup> by competing for binding to PsaA irreversibly and exploited by the host defense mechanism to inhibit the bacterial growth [109, 111]. Recently, structure-based functional studies identified an antibody fragment.

FabC1 caused the sterical blockage of the structurally conserved surface of *Staphylococcus aureus* MntC. This blockage prevents interaction of MntC with the MntB membrane importer thereby increasing *S. aureus* sensitivity to oxidative stress forming the basis for ABC importer inhibition by an engineered antibody fragment [144].

## **1.2. Citrus Huanglongbing**

### **1.2.1. Introduction**

India occupies the sixth rank in the production of citrus fruit in the world whereas citrus industry is the third largest fruit industry in India after mango and banana. So citrus occupies an important place in the horticultural wealth and economy of India. Other countries which are major

producers of citrus fruit include Spain, USA, Israel, Morocco, South Africa, Japan, Brazil, Turkey and, Cuba. Citrus fruits originated in the tropical and subtropical regions of South East Asia, particularly India and China. The native place of many citrus species is North East India. Citrus fruits are of particular interest because of its refreshing juice and high content of vitamin C. Of the various types of citrus fruits grown in India, orange (santra or mandarin), sweet orange (mosambi, malta or satgudi) and lime/lemon are of commercial importance. In India, citrus fruits are mainly produced in Maharashtra, Andhra Pradesh, Punjab, Karnataka, Uttaranchal, Bihar, Orissa, Assam, and Gujarat.

Huanglongbing or citrus greening is the most destructive disease of citrus orchards all over the world. Though there are many diseases which infect citrus plants caused by the number of pathogens like fungi, prokaryotes, nematodes, viroids, viruses and probable viruses, citrus huanglongbing has proved to be very devastating and has been reviewed extensively by various researchers [145-147]. The studies showed that the HLB pathogen co evolves as insect endosymbiont and later moves into the plant [148]. Initially, HLB-like symptoms were observed in central India in the 1700s and called to as dieback [149]. Research suggests that the vector can transmit this disease to a very long distance. On an average basis, this disease can cause the loss in yield up to 30 -100%, depends on the severity of HLB. After the first appearance of symptoms, it takes around 2-5 year to become completely unproductive, and the life of the tree is reduced by 7-10 years.

### **1.2.2. Historical overview**

Citrus fruits were first grown in China 4000 years ago and then India came second in citriculture [150]. The question first arises of where the disease HLB came from? As there was no record of any disease resemble this disease until 260 years ago. Maybe pathogens were absent in these two countries and were introduced in recent times through exotic species or wild rutaceous species and expansion of the disease took place after commercialization of citriculture. Garden citricultures were flourished in India for centuries, but the modern commercial industry was introduced during the last century. In South Africa, the citrus plant was first introduced in Western Cape during 17 century, [150], however, this disease was not noticed after expansion of citriculture in the northern part of the country [151]. In Asia, African pathogen was found to establish in the citrus orchard, transmitted by the insect vector. The first symptom of this disease was “dieback”

recorded in central part of India in the 18<sup>th</sup> century [149]. It was suggested that the Citrus tristeza virus was the main cause of this disease, Raychaudhuri et al, in 1969 explained that dieback was similar to greening [151]. In Southern China, this disease was first observed in Guangdong Province during the late 19<sup>th</sup> century [152], transmitted to the other parts and become a major problem of citrus orchids [153]. Research showed that the disease was transferred to China from India through trades of sea passage [154]. Gradually, HLB covers the citrus orchids of many countries of Asia, like Philippines [155] Taiwan [156], and Indonesia [157]. It was suggested that common ancestors of causal organism and vector were co-founded in Gondwana, later evolve in Asian and African species of both. Later suggested that, the disease was original, originated from Africa, and brought to India from Portuguese, [158], further this hypothesis was rejected and explained that three species of the pathogen have evolved many years ago [159].

### 1.2.3. Causal Organism, identification, diagnosis

Transmission of HLB through grafting and insect conclude that it was caused by the virus. whereas, Electron microscopy (EM) studies of infected plant suggest that mycoplasma-like organisms (MLOs) were found in phloem element, which was related to “yellows” diseases [160]. But on deeper study, it was found that the microorganism has thicker covering as compared to MLOs, showed that they were real bacteria [161]. Isolation of pure culture of this bacterium was remained unsuccessful, however, the combined study of EM along with enzymes treatments explained that this bacterium possesses a cell wall similar to Gram-negative bacteria [162]. 16S ribosomal DNA of two strains of these bacteria was amplified using universal primers and compared with GeneBank sequence and showed that these bacteria belonged to  $\alpha$ - proteobacteria. The Asian bacteria has been called *Candidatus Liberibacter asiaticus* and African bacteria named *Candidatus Liberibacter africanus* [163]. And the Brazilian species were named *Candidatus Liberibacter americanus* [164]. Distribution Map of HLB disease is shown in Fig. 1.4.

Current evidence showed that HLB was caused by three species of unculturable bacteria belongs to  $\alpha$ -Proteobacteria. These are limited to phloem, made up of a very thin cell wall, so can easily cross the sieve pores. *Candidatus Liberibacter asiaticus* is a heat tolerant species, can easily survive above 30<sup>0</sup>C. However, *Candidatus Liberibacter africanus* is suppressed by the increase in

temperature. The Brazilian species, *Candidatus Liberibacter americanus* have the resemblance to the temperature sensitivity of *Candidatus Liberibacter africanus* and latest report suggests that evidence of Asian form is gradually increasing [165].

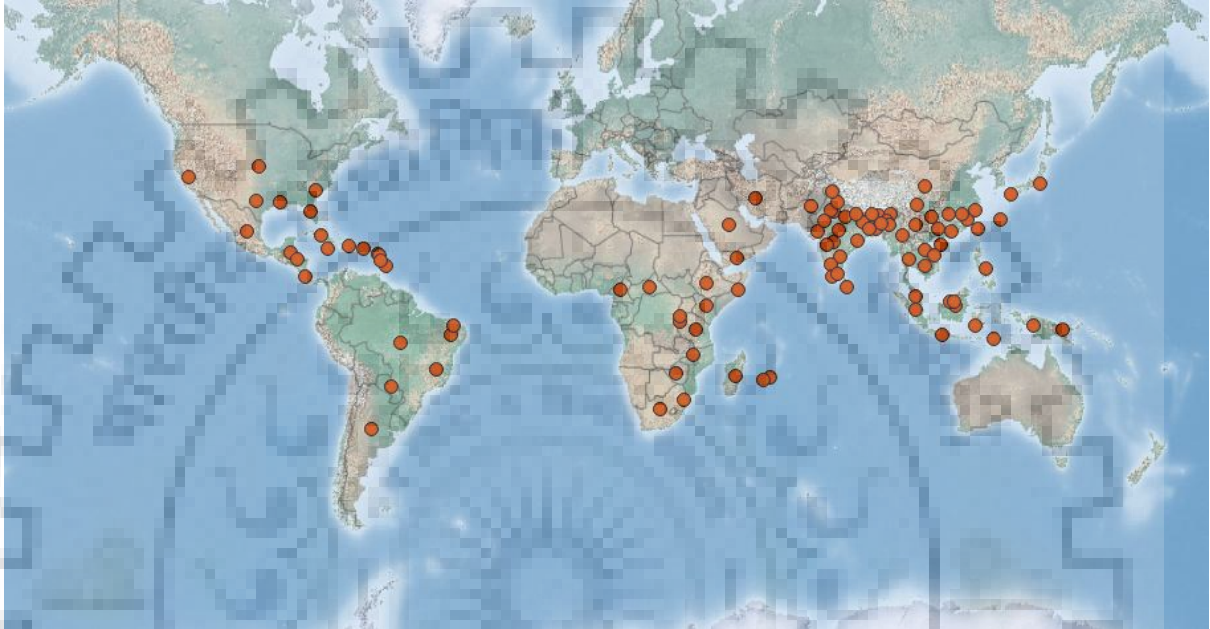


**Fig. 1.4:** Current global distribution of HLB disease as per CABI, current year. Invasive Species Compendium. Wallingford, UK: CAB International. [www.cabi.org/isc](http://www.cabi.org/isc).

#### 1.2.4. Symptoms

HLB symptoms are varied and share many common symptoms with other diseases as well. Some specific characteristics of HLB are that the trees infected with HLB will usually develop one or more yellow shoots thus the name “Yellow Shoot” disease. If the rest of the tree is seems healthy or without any visible symptom, the disease will take a sectoral appearance.

##### 1.2.4.1. Foliage symptoms:

Leaves usually on the lower part of the branches i.e. older ones turn yellow along their primary and secondary veins. The “yellow-vein” appearance later changes to a blotchy-mottle as the discoloration spreads towards the periphery of the leaves. Also leaves on short branches back



in the tree, and those on the more vigorous shoots that develop during the late summer flush develop these symptoms. The yellow discoloration usually develops post maturation of the leaves (Fig. 1.5A). Another symptom is that leaves of weak terminal twigs become small, show chlorosis, suggesting the iron and zinc deficiencies. Initially, small leaves become pale and later on, shows chlorosis on maturity. Sometimes, green blotches and green spots were also developed. The intensity of the symptoms of this disease varies a lot. It may be slight or well defined like small leaves at terminal mostly green and few of them showing chlorosis [43, 166] (Fig. 1.5B). Primary and secondary symptoms were distinguished based on the time of appearance. The primary symptoms become visible on leaves after normal maturation, while secondary symptoms developed on leafy shoots, grows from branches already having primary symptoms [167].

#### **1.2.4.2. Fruit symptoms:**

Citrus greening affected fruits are small in size, of lower quality, often lopsided. In the earlier season, they possess bitter and salty taste. Some fruits remain very small and start falling prematurely while those that enlarge which remain on the tree but the colour of the fruit never reach to colour of normal fruits. Very less sized fruits have no seed or possess abortive seed. More number of seeds may be observed in larger fruits, out of them mostly sterile (Fig. 1.5C).

#### **1.2.4.3. Internal changes:**

The HLB symptom shows resemblance to the symptoms caused by minerals deficiencies and initiate starvation caused by dislocation of food in the tree [167], and observed that local sieve tube damage in leaves, suggests blockage of translocation which causes the starch accumulation and faulty multiplication of cambial cells. The midribs of infected leaves have four fold more phloem with most of the sieve element faces necrosis. Thus, veins of infected leaves become swollen.

The phloem necrosis affects the normal development of fruits due to saccharide deficiency, and starch becomes failed to move out of the leaves. It commonly occurs in yellow leaves and typically within the vascular tube of undeveloped fruits [146, 166].

The symptoms of both Asian and African species are typically the same but Asian species affect the citrus more extensively and lead to the death of the tree.



**Fig. 1.5:** Symptoms of HLB in infected citrus plants. A) Yellowing of citrus tree B) chlorosis of citrus leaves C) HLB-affected sweet orange (adapted from the book entitled “Asian Citrus Psyllids”).

### 1.2.5. Disease vector and population dynamics

Transmission of citrus greening takes place through various means such as insect vector, diseased branched and cuscuta. The identified most potent vector of this disease is citrus psylla (Fig. 1.6). *Diaphorina citri* and *Trioza erytreae* are referred to vectors of Asiaticus, Americanus and Africanus species [168, 169]. The heat tolerance and sensitivity of these vector species similar to HLB type, *Diaphorina citri* is temperature tolerant whereas, *Triozaerytreae* is sensitive to increase in temperatures.



**Fig. 1.6:** HLB-associated vector Asian citrus psyllid and bacteria *Candidatus Liberibacter asiaticus* (CLas). A) and B) Asian citrus psyllid (*Diaphorina citri*) feeding on citrus plants [148].

#### 1.2.5.1. Transmission of pathogen

Research has been found that adults, as well as nymphs, can transmit the causal organism of HLB disease [170]. It was observed that nymphs are comparatively more efficient in transmitting and establishing the CLas pathogen [171]. Electron microscopy study shows the presence of bacteria similar to those found in citrus greening affected citrus [172]. HLB causing organism release a volatile chemical in host tree, which attracts the insect vector to feed on the host tree and pathogen also become injected in the insect vector [173]. The vector can have the



pathogen up to twelve weeks [174]. Multiplication of CLas pathogen in the haemolymph of *D.citri* suggests that it has all essential nutrient for CLas [168, 175, 176] .

The population of the vector was also affected by variation in temperature and humidity. The growth of African psyllid is negatively associated with the increase in temperature and saturation [177]. There is also great variation in times for acquisition and transmission of both species. Once the pathogen is established, the vector will retain and transmit the pathogen throughout its life.

#### **1.2.5.2. Pathogen detection system**

Scoring of HLB was done on the basis of different symptoms of the disease. While, HLB is a fastidious micro-organism which can survive within the host tissue for several years, beneath covert conditions. Thus, the presence of subtle technology that enables the fast detection of the causal organism is pre-requisite. A PCR-based detection system can be used for detection of the pathogen. It is cheaper to apply to different traditional technologies. In 2004, Das compared this method to the conventional method of HLB indexing. This PCR- based technique showed many advantages like rapid detection, need less time for completing the procedure and not affected by the uneven distribution of the pathogen in the host. Two type of PCR protocol was employed i.e. long and standard suggested that long protocol was more accurate and reliable as compared to standard. The long protocol has another set of DNA polymerase enzyme for proofreading. Studies suggest that long protocol PCR is more reliable in detecting the HLB in the host [178]. Loop-mediated isothermal amplification (LAMP) was also utilized for detection of the pathogen in the host [179]. Real-time PCR was also found to be highly sensitive in detection of HLB. It can recognize and quantify the HLB concentration in the host tissue. Real-time PCR is most effective in comparison to other PCR method for calculating the pathogen concentration in the host tissue, and it can also detect the pathogenicity at early stages. The pathogen detection system can increase the capability of the disease control system for the production of HLB free citrus trees. The digoxigenin labeled probe was proposed for *Candidatus Liberibacter asiaticus* for fast, simple and non-radioactive detection of the causal organism [180] Imaging techniques were also used for detection of HLB [181]. This technique measures the reflectance of infected and healthy leaves and observed a significant variation in values at 560 nm and 710 nm. In the same manner, Pourreza et al. (2013) measures reflectance at 591 nm and observed infected foliage with 100% accuracy

[182]. Extended spectral angle mapping (ESAM) was also proposed for detection and translocation of HLB disease.

### **1.2.6. Genome analysis of CLAs**

In spite of the limitation of culturing CLAs, therefore, it's difficult to obtain genomic DNA in pure form; it's been sequenced successfully and provides an idea for the evolution of metabolic and functional processes of the infectious agent [183, 184].

Genomic analysis of CLAs provided helpful insight in the study of biology and pathogenicity of the HLB. The identification of essential gene allows us to understand the requirement of nutrition for growth as well as give an idea of the potential target for the development of the antibacterial drug [185].

CLAs contains genetic features characteristics to obligate intracellular bacteria [186]. A complete circular genome of CLAs has been retrieved through metagenomics, by using the extraction of DNA from one CLAs-infected psyllid. The size of the genome is 1.23-Mb and it contains 36.5 % of GC content. Annotation discloses that a high percentage of genes concerned with cell motility (4.5%) and active transportation (8.0%), which can be responsible for its virulence. CLAs seems to possess a restricted capability for aerobic respiration and is probably auxotrophic for a minimum of 5 amino acids. Multiprotein phyletic analysis showed that CLAs is an extremely divergent member of the Rhizobiaceae family.

#### **1.2.6.1. Metabolic pathway**

CLAs have all fourteen genes that encode NADH dehydrogenase subunits [A-N] which is a significant component of the electron transport chain of respiration. While there is no homolog of the terminal stage of oxidative phosphorylation were found. Similarly, No, homologs of cytochrome bc1 complex ,cytochrome c oxidase, the cbb3-type, or the cytochrome bd complex were found in genome of CLAs while, all four cytochrome O ubiquinol oxidase subunits [I to IV] were observed, and the CLAs respiratory complex show resemblance with the citrus infectious agent *X. fastidiosa* [187], that has 1 terminal oxidase encoded for by the cyo-operon, and active solely beneath high oxygen condition [188, 189]. Thus, due to an absence of important enzymes

concerned with the oxidative phosphorylation as well as lack of various terminal oxidases, it can be suggested that CLas has restricted capability for aerobic respiration. CLas encodes an ATP/ADP translocase additionally to its ATP synthase, which permits it to synthesize ATP and direct uptake of energy from its environment. Moreover, the genes which are important for TCA (tricarboxylic acid ) cycle like, gene for citrate synthase (gltA), the main port of acetyl CoA entry in the TCA cycle that is typically associated with functional TCA cycle, were found in CLas which can make it use long range of amino acid for source of energy.

#### **1.2.6.2. Transport proteins and types of secretion systems**

Total 137 transport protein were identified in 'Ca. L. asiaticus', out of the nine protein refer to the channels/pores category of transporter, twenty-four proteins refer to electrochemical potential-driven transporters, ninety-two proteins come under the primary active transporter, 1 refer to the class of translocators and remaining eleven proteins can be put under incompletely characterized transport system of the transporter class. Out of the ninety-two primary active transporters, forty belongs to ABC transporter, that is of  $\alpha$ -Proteobacteria which have wide host range but in contrast to the similar sized intracellular bacterium, in which 15 ABC transporter is present [190]. It's quite possible that a number of these transporters have an effect on virulence, the range of host or symptoms stimulation, alone or conjointly. For instance, znuABC (zinc transport system) are needed for virulence in various organisms [191]. The znuABC genes in CLas involved in uptake of zinc from phloem, which result in localized zinc deficiency, therefore, mimicry of symptoms between the zinc deficient and HLB affected the plant.

#### **1.2.6.3. Secretion systems**

According to the intracellular life pattern of the disease causal organism whose passage of infection involves direct injection by psyllid into the host tissue, there is no type III or IV secretion systems including avirulence genes were identified. Also, cell wall degradation enzymes like cellulases, xylanases, pectinases, or endoglucanases which need type II secretion were not identified. While, all proteins needed for the general secretory pathway, the first step of the type II secretion system, that is responsible for the export of proteins to periplasm [192], were identified in CLas from Psy62. Additionally, ten putative proteins needed for pilin secretion and assembly as a

part of MTB (main terminal branch) were identified, which indicated its potential for type IV pilus secretion and assembly.

Various complete secretion systems of type I were found. Two main functions of the type I secretion system are elucidated. The primary one is defensive which involves the efflux of multidrug, protection of bacteria against harmful surrounding chemicals, antibiotics formed by another bacterium and phytoalexins released by hosts. Multidrug effluence has been reported as an important mechanism for microorganism survival in different genera like *Erwinia*, *Rhizobium*, *Agrobacterium*, *Bradyrhizobium*, and *Xanthomonas* [193]. Another function is offensive, which involves the secretion of a range of degradative enzymes and offensive effectors, some of them are antibiotics and others responsible for pathogenicity in plants and animals. Type I system involved n secretion of offensive enzymes and effectors includes a limited range of hydrolases such as (proteases, phosphatases, esterases, nucleases, and glucanases and a large number of toxins of proteins like RTX hemolysins and bacteriocins [194, 195].

#### **1.2.6.4. Proteome and transcriptome analysis of citrus plants and CLas infection**

Fan et al., uses the relative and absolute quantification (iTRAQ) technique, and found that important upregulation of protein related with defense/stress response, likewise four miraculin-like proteins, Cu/Zn superoxide dismutase, chitinase, and lipoxygenase sweet orange plants (*Citrus sinensis*). Also, Microarray technique suggests that stress associated genes were considerably upregulated during transcription in Cu/Zn superoxide dismutase and miraculin-like proteins. Moreover, the transcription patterns of both Cu/Zn superoxide dismutase and miraculin-like proteins were checked at different stages of disease development. In the combination of the transcriptomic study, the proteomic study may provide a better understanding of citrus stress/defense responses to HLB [196]. Similar results have been observed for grapefruit plants (*Citrus paradise*) on the basis of protein profiling by 2DE and mass-spectrometry [197].

#### **1.2.7. Virulence mechanism**

In order to design management strategies against CLas and controlling HLB, it is critical to understand the interaction between citrus and CLas and the virulence mechanism employed by CLas. However, due to the complexity in obtaining CLas in culture, limited information is available regarding the understanding of virulence mechanism with some promising improvement.

### **1.2.7.1. Phloem blockage and aberrations**

The main cause of development of citrus greening disease symptoms is might be suggested from blockage of phloem results from sieve pores plugging not from the aggregation of HLB bacteria [167, 198]. The blockage of phloem is due to a large amount of deposition of phloem protein and callose. The deposition of callose is confirmed by aniline blue staining whereas, phloem protein may be involved because PP2 gene was induced in diseased citrus [198]. PP2 gene has been suggested to involve in host defence response to limit the spreading of the pathogen in the sieve tubes. The callose deposition was also observed in sieve plates and around plasmodesmata units (PPUs) connecting companion cells and sieve tubes (Koh et al). The deposition of callose around PPUs was observed to be followed by deposition of starch in the chloroplast. The decrease in phloem loading efficiency was also observed due to blockage of the symplastic flow of solute from companion cell into sieve tubes caused by deposition of callose around PPUs in diseased leaves. This type of blockage is harmful to both plants as well as CLAs. CLAs might not be capable to survive in blocked sieve elements[198].

The accumulation of sucrose in diseased leaves, that the major photoassimilate of phloem, transported from mature leaves to sink organs, showed that photoassimilate translocation becomes disrupted by infection of CLAs, might be due to phloem blockage [198-201].

This decreased photoassimilate transportation might be responsible for the tiny, distorted, and inadequately colored fruit having undeveloped or partially developed seed. Deficiency of sucrose has been linked with seized fruit growth [202]. However, it's been noticed that many of the genes associated with the photosynthesis are repressed presumably due to higher levels of sucrose/glucose [198, 199, 203]. The establishment of HLB symptoms was correlated with microscopic aberrations increment including phloem necrosis, enormous deposition of starch in the plastids, abnormal cambial activity and excessive development and collapse of phloem [167, 198]. As a result, these changes are accountable for the mottling, leatheriness, yellowing, and vein clearing in diseased leaves[167].

### **1.2.7.2. Metabolic imbalances by nutrient depletion**

CLAs causes the imbalances of metabolism in the host by nutrient exhaustion or disturbed transportation resulting in symptoms of HLB [183]. The disruption in host cellular metabolic



functions might be due to the import of host-cell metabolites for growth and development eventually leading to the appearance of the disease. It was suggested that CLAs make use of fructose preferentially causing fructose reduction and the glucose accumulation in the infected host tissues [199]. The accumulation of glucose consequently leads to the suppression of enzymes responsible for photosynthesis causing the development of HLB symptom. CLAs encode comparatively less number of genes implicated in the biosynthesis of compounds, which are used from the host without much difficulty. Recently, Li et al. [204] found fourteen ABC transporter systems and seven non-transporting ABC proteins which could be used by the bacterium for importing metabolites and enzyme cofactors to resist organic solvent, lipid-like drugs, and heavy metal maintaining the composition of the outer membrane and secreting virulence factors. These numerous transporter proteins play a crucial role to provide necessary nutrients to CLAs resulting in a metabolic imbalance in citrus.

#### **1.2.7.3. Hormone**

Phytohormones play an important role in determining the set of citrus fruit, productivity, and plant response to infectious agent [205]. On the basis of comparison between symptomatic and asymptomatic fruits from infected and healthy sweet orange trees, Rosales and Burns found that ethylene production was reduced in infected plants whereas content of indole-3-acetic acid (IAA) and abscisic acid (ABA) in the stylar end, middle section, or stem end of fruit were more in symptomatic plants [205]. The lower content of IAA in symptomatic stem end suggested acceleration in abscission, while ethylene production in whole fruit is lower contrasting its role in abscission promotion. The content of IAA was higher in the deformed area in comparison to the normal-growing regions of symptomatic plants. The size of the hypodermal cell was also enlarged in the analogous regions. Thus, IAA has been found to play an important role in the development of distorted fruits [205].

#### **1.2.7.4. Suppression or avoidance of plant defense**

CLAs elicit a delayed defense response in plants [198] and this manipulation of defense response is crucial for its survival in the plant. The reduced genome of CLAs and psyllids mediated transmission might facilitate it to avoid pathogen-associated molecular pattern (PAMP)-triggered immunity. Peptidoglycan recognition proteins (PGRPs) are involved in the recognition of PAMP

[206]. Additionally, an absence of type II plant cell-wall degrading enzymes helps it in inhibition of defense responses on the basis of autodegradation products of the plant cell wall [207]. However, CLas has 57 genes for biogenesis of cell envelope [183] which might function as PAMPs. It has been revealed that a functional *flagene* is present in CLas which encodes flagellin and hook-associated protein of 452 amino acids that have the conserved flg22 [208]. Studies suggested that CLas flagellin may act as a PAMP and elicit host plant resistance to the bacteria [208]. Microarray analysis suggested that the CLas infection in citrus does not produce a noteworthy induction of defense-associated genes in the earlier stages [198, 203]. Besides, CLas could further inhibit the host defense. CLas contain a gene encoding a salicylate hydroxylase which is causing the conversion of salicylic acid (SA) into catechol for resistance suppression [209]. This gene is highly induced in planta in comparison to psyllid. SA has the role in plant defenses against pathogens for basal defense, the hypersensitive response and systemic acquired resistance [210]. Salicylate hydroxylase expression in plants demolishes plant defenses by degrading SA [211] which could be one of the mechanisms utilized by CLas to avoid responses of plant defense [212, 213] in accordance with the down-regulation of defense-related genes in CLas-infected citrus [92, 203].

#### **1.2.7.5. Prophages SC1 and SC2**

CLas contains an excision plasmid prophage, SC2 and a chromosomally integrated prophage, SC1 that gets lytic in citrus [214] and might impart in the pathogenicity of CLas. A lytic burst of CLas within phloem cell, mediated through SC1 genes, might elicit an apoptosis cascade, leading to death [198, 215]. SC1 and SC2 also contain many genes for virulence that might be the reason for the pathogenicity of CLas, for example, i) two peroxidases that might protect CLas against reactive oxygen species ii) two adhesins, which might be helpful in transmission by psyllids [214]. However, SC1 and SC2 involvement in the pathogenicity of CLas need to be further investigated.

#### **1.2.7.6. Serralysin and hemolysin**

The antimicrobial peptides and proteins production is one of the important defense strategies used by the plant in response to infection by disease-causing organisms. CLas encodes a putative type I secretion system (T1SS), serralysin, and its expression was observed to be up-



regulated in planta in comparison to psyllid [216]. Serralysin is a metalloprotease secreted by various microorganisms which inactivate antimicrobial proteins and peptides [217]. The upregulation of the serralysin biosynthesis gene in planta suggests that CLAs may exploit serralysin to alter the plant defenses, probably by degradation of plant antimicrobial peptides. It also helps in the acquirement of carbon and nitrogen by the proteolysis of host proteins and uptake of nutrient [218, 219], further aiding to bacterial survival in hosts. Due to possible challenge in selecting effective antimicrobial peptides against CLAs, the serralysin of CLAs could be suggested as a potential target in the screening of antimicrobial compounds for controlling HLB disease. Hemolysin is secreted by animal and insect pathogens which helps in survival of bacteria in plants by the various mechanism like cell lysis, necrosis, and apoptosis stimulation [220], availing the iron for pathogen [221], and induction ions, water, and small molecules leakage across plant cell [222]. Hemolysin is believed to play a significant role in proteins degradation produced responsibly for the defense reaction or uptake of crucial nutrients [223]. Therefore hemolysin production by CLAs might also play a significant role in the survival of CLAs by contributing to the acquisition of nutrient, ion transfer, and phloem necrosis.

#### **1.2.8. Metabolite signature of CLAs infection**

Symptoms of HLB include starch accumulation in the leaves and phloem impairment. Studies have reported that the concentration of sugars including fructose, glucose, sucrose, and proline decreases during CLAs infection reflecting altered carbohydrate transport. However phenylalanine, histidine, asparagine and limonin concentration is increased during CLAs infection in Valencia or Hamlin fruit [224]. In *Citrus sinensis* Valencia fruits, the concentration of sucrose is found to be reduced upon CLAs infection. Additionally, in infected fruits, many of the amino acids concentration like alanine, arginine, isoleucine, leucine, proline, threonine, and valine is reduced except the increased concentration of phenylalanine, asparagine, and histidine. Ascorbate, citrate, limonin and limonin glucoside concentrations were observed higher in infected fruits [225]. Micro X-ray fluorescence investigation discloses that Zin concentration in the phloem of healthy leaves of grapefruit was more than ten times higher than that in the HLB-affected leaves [226].

### **1.2.9. Management practices to control the pathogen**

Currently, no strategies have been developed to manage the HLB disease and to stop the spreading of this disease to new citrus areas. The only control strategy is to prevent trees from infection by removing the infected tree and minimizing the psyllid population. Recently, the combination of antibiotics was found to be effective in elimination or suppression of the CLas bacteria and providing a therapeutically, effective level to control the HLB disease, However more evaluation is needed [227].

#### **1.2.9.1. Cultural Practices**

Agronomical and horticulture practices have additionally been shown to manage the intensity of disease symptoms. Hand selective pruning in summer reduce the disease and observed a positive impact on citrus yield and fruit size [228]. Grafting in conjunction with pre-heat treatment additionally reduced the HLB disease with good efficiency [229]. “Intensive farming” was introduced, which has insect protection, pruning, and application of fertilizer to enhance the growth and production in diseased plants[230]. The continual foliar application of micronutrient like (ZnSO<sub>4</sub> + MnSO<sub>4</sub>) for seven weeks was found to be effective in enhancing the growth and production in diseased plants [231]. Recently, a new method, trap cropping was suggested to control the spreading of HLB disease in which an alternative insect host plants were grown to get away the insect from harvested agriculture. However, this method has not yet applied in citrus production [232].

#### **1.2.9.2. Biological control of the vector population**

The insect vector population was also regulated by natural occurring enemies like the wasp and fungal mycelia [233]. In France, the populations of the vector were regulated by the discharge of parasites on the island. In Indonesia, fungal mycelia were also used to control the HLB disease[234]. Recently, a toxicity test was performed on a strain *Serratia marcescens* KH-001 which is isolated from diseased *D. citri* nymph and analyses its effect on microbe’s community in *D. citri* by utilizing high-throughput sequencing. Results suggested that *Serratia marcescens* KH-001 kills 83%of *D. citri* nymph, [235] however, more work has to be done before applying this method.

### 1.2.9.3. Chemotherapy

Several types of antibiotics have recommended for disease management even, chemotherapy is not new. Various antibiotics suppress the symptoms of the disease in the infected plant [236]. Antibiotics such as achromycin and ledermycin effectively reduce the symptoms of the disease [237]. Combined dose of antibiotic and fertilizer was most effective in enhancing the quality and fruit yield [238]. An integrated approach of micropropagation and antibiotics was also helpful in reducing the disease symptoms. Two chemical agents, 2,2-dibromo-3-nitrilopropionamide (DBNPA) and penicillin G sodium were identified to eliminate and suppress the '*Ca. L. asiaticus*' bacterium [239]. A combination of penicillin and streptomycin was also found to effectively reduced or eliminate the '*Ca. L. asiaticus*' [240, 241]. A cryopreservation method has been employ for complete removal of pathogens which suppress the virus, bacteria, and phytoplasmas.

Other approaches for controlling HLB might involve targeting essential proteins for survival and developing inhibitor molecules against them to impair the protein function. Essential proteins of many pathogenic bacteria are potential targets for developing anti-bacterial drugs [242-251].

### 1.2.10. ABC transporters in CLAs

ABC transporters of CLAs may be involved in host metabolic imbalances in infected plants and development of HLB [183]. Wenlin Li et al have identified 14 ABC transporter systems and seven non-transporting ABC systems in CLAs. In the CLAs proteome, out of 14 ABC systems, 8 are responsible for uptake of essential nutrient from its environment. The substrate includes the amino acids, B family vitamins, ions and lipids [204]. Because it is advised that CLAs might exhaust the host's nutrient supply, which ultimately results in disease symptoms, these ABC systems might contribute to the death of the tree. The other 6 ABC systems have a wider range for substrates. These are associated with the biogenesis of the outer membrane, multiple drug resistance, and secretion of toxin proteins. These are predicted to function as the L-amino acid transporter, phosphate transporter, thiamine transporter, choline transporter, zinc transporter, and manganese and iron transporter. Vahling-Armstrong et al. demonstrated that the zinc transport ABC system (*znuABC* gene cluster #1) of CLAs is involved in high-affinity zinc uptake [252].

Their studies showed that both ZnuB and ZnuC genes from CLas were able to complement respectively  $\Delta$ ZnuB and  $\Delta$ ZnuC *Escherichia coli* and *Sinorhizobium meliloti* strains, however, CLas-ZnuA gene was not able to functionally complement  $\Delta$ ZnuA *E. coli* strain and only partially complement the  $\Delta$ znuA *S. meliloti* strain. Therefore, this system might contribute to the zinc deficiency associated with HLB-affected trees. Their studies have also shown that the gene cluster of Mn and Fe ABC transport system (*znuABC* gene cluster #2) was not able to functionally complement  $\Delta$ znuABC *E. coli* and *S. meliloti* strain.



**CHAPTER 2**

**MUTATION STUDIES IN PERIPLASMIC METAL UPTAKE PROTEIN**

**CLas-ZnuA2 FROM *CANDIDATUS LIBERIBACTER ASIATICUS***

---

---

### **2.1. Introduction**

The ATP-binding cassette-type (ABC-type) transport systems comprises of three components: a solute-binding protein (SBP), which is either found in the periplasm (Gram-negative bacteria) or linked to the cytoplasmic membrane (Gram-positive bacteria), a trans-membrane permease, and a nucleotide-binding protein (ATPase) [253]. The SBPs involved in the transport of metal ions across the membrane belong to cluster A-I family which include manganese, zinc and iron transporters. The crystal structures reported for zinc, manganese and iron transporting SBPs of the cluster A-I family [66, 93, 99, 101, 107, 113, 114] in metal-free and metal-bound states suggest that overall structure comprises a pair of N- and C-terminal ( $\alpha/\beta$ )<sub>4</sub> sandwich domains linked through a long backbone  $\alpha$ -helix running across the two domains. The N- and C-terminal domain interface constitutes the metal binding site. The crystal structures in metal-free and metal-bound states, despite having similar overall fold, have revealed differences in the mechanism of metal binding and release for different metal ions. In Zn-specific SBPs, metal binding and release occurs without any significant change in the relative domain position and the linker helix [99, 103, 105]. In contrast, Mn/Fe-transporting SBPs accomplish metal-binding and release through a rigid body movement of C-domain and unfolding and refolding of the C-terminal end of the linker helix [109]. Also, the changes in interaction among different secondary structural elements contribute towards the metal binding and release. The differences in their mechanisms could be to cater to subtle differences in their specificities in a particular system.

One of the clusters A-I family proteins characterized from *Candidatus Liberibacter asiaticus* (CLA) showed low metal-binding affinity [254]. The CLA, a phloem-limited, unculturable, Gram-negative bacterium causes Huanglongbing (HLB) or citrus greening, an extremely destructive, fast-spreading disease of citrus which causes severe economic losses worldwide [255]. The ZnuA gene from second of the two gene clusters encodes for a periplasmic solute binding protein (CLas-ZnuA2) which shows high homology to Mn-specific rather than Zn-specific cluster A-I SBPs. However, the crystal structure analysis in metal-free, intermediate and

metal-bound states revealed that the mechanistic resemblance of CLas-ZnuA2 seems to be closer to the Zn-specific rather than Mn-specific SBPs of cluster A-I family [113]. This seems to be the case of evolution of typical Mn-specific protein to a low affinity metal-binding protein to cater to specific needs. A detailed comparative analysis of interactions in all three states indicated towards a relative tendency of CLas-ZnuA2 structure to attain metal-free state. The key features, quite different from typical Mn-specific SBPs, included a highly restrained loop L3 and presence of proline in linker helix. The movement of L3 loop and flipping of His residue towards metal-binding site in metal-bound forms of CLas-ZnuA2 were achieved only at a very high concentration of metal in crystallization condition indicating a role of restrained loop in low metal affinity of the protein. Also, square pyramidal geometry and pentavalent coordination different from preferred octahedral and tetrahedral geometry for  $Mn^{2+}$  and  $Zn^{2+}$  respectively allows reversible binding for both metals. The presence of proline in linker helix results in disruption and bending of linker helix, with higher angle as compared to other Mn-specific SBPs, resulting in almost fixing and positioning of C-domain similar to metal-bound state of SBPs. The fixed domain positioning due to a curved rigid linker helix and the coordination geometry seems to be responsible for low metal-binding affinity of CLas-ZnuA2. This evolutionary change in Mn-specific SBPs, particularly in plant pathogens, could be attributed to avoid Zn-toxicity.

In the present work, we have carried out the crystal structure analysis, both in metal-free and metal-bound states, of CLas-ZnuA2 mutants to unravel the subtle changes in internal communications. All mutations, except for in L3 (Ser38Ala) and helix c (Tyr68Phe), resulted in destabilization or degradation of the protein. The crystal structures of S38A CLas-ZnuA2 and Y68F CLas-ZnuA2, in both metal-free and metal-bound states, revealed significant differences in interactions as compared to wild-type protein. We have also characterized the binding affinities and thermal stability of these mutants using surface plasmon resonance and circular dichroism and compared with the wild-type CLas-ZnuA2.

## **2.2. Materials & Methods**

### **2.2.1. Site directed mutagenesis, expression and purification of mutant CLas-ZnuA2**

Six mutations Ser38Ala; Tyr68Phe; Pro153Ala; Glu159Ala; Asn193Ala and Pro153Ala/Glu159Ala have been created in CLas-ZnuA2 using site directed mutagenesis. The



primers used for mutagenesis are shown in Table 2.1. The resulted plasmids were confirmed by DNA sequencing. All recombinant mutated CLas-ZnuA2 were expressed in *E.coli* BL21-DE3 host cell by induction with 0.4mM IPTG at 25 °C and purified by Ni-NTA chromatography similar to wild-type CLas-ZnuA2 purification [113].

**Table. 2.1: Primers used for site directed mutagenesis.**

S.N O.	Mutation	Forward primers and reverse primers
1.	Ser38Ala	(5'-GGGCAATGATGCTCATAGTTATC-3'), (5'-GCTTCTACTAAAGTGGTTAC-3')
2.	Tyr68Phe	(5'TGAAGAACTTTTATGAAGTATTTCACTAATTTAAAAAAG-3'), (5'-AGATGCAAGCCATTGCATAG-3')
3.	Pro153Ala;	(5' CAACAGCATTCTGGCGCTGAAAACCCG-3'), (5' CGGGTTTTCAGCGCCAGAATGCTGTTG-3')
4.	Glu159Ala	5'- TTAAAAACTAGAATTGCAAAAAGTGGACCCTG-3'), 5'- CAG GGT CCA CTT TTG CAA TTC TAG TTT TTA A -3')
5.	Asn193Ala	(5'-CTGGCCAATTGCTTCCGATTCTGAAAG-3'), (5'-AGATATAGTGATTTGAAACCAAATC-3')
6.	Pro153Ala/Glu159Ala	(5'- TTAAAAACTAGAATTGCAAAAAGTGGACCCTG -3'), 5'- CAG GGTCCACTTTTGCAATTCTAGTTTTTAA -3')

### 2.2.2. Crystallization and data collection

Two mutants (Ser38Ala and Tyr68Phe) of CLas-ZnuA2 were concentrated up to 7-10mg/ml. The crystallization experiments were undertaken as described for wild type CLas-ZnuA2 [113] using sitting drop vapour diffusion method in 96-well plates at 4 °C in 0.1 M sodium acetate trihydrate buffer, pH 4.6 containing 2.0 M ammonium sulphate. The drops contained 1µl of protein solution and 1µl of reservoir solution and equilibrated against 50µl reservoir solution. Metal-free and metal-bound states of mutant protein were prepared in similar manner as for wild-type CLas-ZnuA2 [113]. However, as no electron density was observed for metal, therefore both mutants (Ser38Ala; Tyr68Phe) were obtained in metal-bound state by soaking the crystals in precipitant solution containing 50mM MnCl<sub>2</sub> for 5 min. For cryo-protection, crystals of both the mutants

were exposed to well solution containing 20% glycerol, mounted in cryo-loop prior to collection of X-ray diffraction data. The data of metal-free and metal-bound states were collected on MAR 345 image plate detectors mounted on Rigaku Micromax 007HF rotating anode generator. The crystals and data collection parameters are given in Table 2.2. The diffraction data were processed and scaled with iMOSFLM and SCALA program in CCP4i suite.

### **2.2.3. Structure solution and refinement**

The structure were solved by molecular replacement method using Molrep [256], with the structure of metal-free and metal-bound state of wild-type CLas-ZnuA2 (PDBID: 4UDN and 4UDO) as search model. The initial models were subsequently rebuilt manually using COOT [257, 258] and refined using REFMAC 5.7 [259, 260] and PDB\_REDO web server ([http://xtal.nki.nl/PDB\\_REDO/](http://xtal.nki.nl/PDB_REDO/)). The quality of final models were validated by PROCHECK [261] and MOLPROBITY [262]. Structure alignments were done using superpose [263]. Structure figures were prepared using PyMOL [264] and Chimera [265].

### **2.2.4. Accession number**

The coordinates have been deposited in Protein Data Bank with accession code 5Z2J (S38A metal-free state), 5Z2K (S38A metal-bound state), 5Z35 (Y68F metal-free state) and 5ZHA (Y68F metal-bound state).

### **2.2.5. CD spectroscopy**

The CD studies were performed using JASCO-1500 CD spectrophotometer equipped with peltier thermostat in sodium cacodylate buffer pH 7.0. Far UV-CD spectra (190-260) were recorded using 0.2mg/ml of mutant CLas-ZnuA2 in 1mm quartz cell. The spectra were recorded at different temperature (20°C-90°C) to examine the thermal stability of CLas-ZnuA2 mutant forms. The intensities of CD spectra were expressed as mean residue ellipticity (MRE) in deg. cm<sup>2</sup> dmol<sup>-1</sup>.

### **2.2.6. Surface plasmon resonance**

All the SPR experiment were performed on BIAcore T200 (GE, Healthcare, USA) instrument with research grade CM5 sensor chips (BIAcore AB, Uppsala, Sweden). The

instrument operated with BIAcore T200 control software version 2.0. The analysis and sample preparation compartment temperature was set at 25 °C for all binding and kinetic experiment.

The amine coupling kit was purchased from (GE health care, BR-1000-50). The dextran surface of CM5 (carboxy methylated ) sensor chip was first activated by solution containing 0.05M N-hydroxy-succinimide (NHS) and 0.2M 1-ethyl-3-(3-dimethyl amino propyl carbodiimide (EDC) with flow rate of injection of solution of 10  $\mu$ l/min. For immobilization of ligand on sensor chip surface, final concentration of 100 $\mu$ g/ml was achieved by dissolving the 20 $\mu$ l of 1 mg/ml mutant CLas-ZnuA2 in 180 $\mu$ l immobilization buffer (100mM sodium acetate pH 4.5). The mutant CLas-ZnuA2 protein was injected and passed through the activated sensor surface at the flow rate of 10 $\mu$ l/min. After successful immobilization of ligand on sensor surface, 50mM NaOH was injected to remove any remaining ligand molecule. The effectiveness of protein coupling was monitored according to sensogram obtained after mutant CLas-ZnuA2 injection. The difference in response unit (RU) at the beginning and at the end of coupling reaction represents the quantity of mutant CLas-ZnuA2 bound on the chip.

### **2.2.7. Determination of kinetics and affinities**

After immobilization of CLas-ZnuA2 mutant, sodium cacodylate buffer, pH 7.0 was passed continuously until steady state was reached. For all SPR measurement, two flow cells monitored the responses for buffer flowing through two sensor chips that were coated with and without mutant CLas-ZnuA2 simultaneously and difference in RU value detected from two cells were referred as baseline value. Dilutions of different concentration of metal ions ranging from 0.0125mM to 1.6mM were prepared from 10mM stock solution of MnCl<sub>2</sub> and ZnCl<sub>2</sub> in 10mM sodium cacodylate buffer, pH 7.0. The metal solution was injected over the immobilised mutant protein at flow rate of 30  $\mu$ l/min with contact time 180s and dissociation time of 600s. The difference in response detected between two flow cells was subtracted from baseline value stating the bound quantity of metal ions over the sensor chips. For monitoring the dissociation, sodium cacodylate buffer was flown continuously over the sensor surface. After returning to stable baseline, the sample can be injected again. After each injection, sensor chip was regenerated by injecting 200mM EDTA. All the buffers used in this study were filtered using 0.22  $\mu$ m Millipore filters and degassed using Millipore degassing unit to avoid the formation of micro-bubbles. The

sensor chip could be stored in tube and stored dry at 4 °C for >5 months.  $K_D$  value was determined by using BIAcore T200 evaluation software version 2.0 as described earlier [254].

### **2.2.8. Prediction of Aggregation effect of mutation**

AGGRESCAN programme was used to study the Aggregation effect of mutation; Pro153Ala, Glu159Ala, Asn193Ala and Pro153Ala/Glu159Ala on CLas-ZnuA2 protein. AGGRESCAN is based on an aggregation propensity scale of natural amino acid. It predicts the aggregation “hot spot” and variation in aggregation propensity induced by the mutation in protein sequence [266].

## **2.3. Results**

### **2.3.1. Crystal structures of CLas-ZnuA2 mutants**

#### **2.3.1.1. Crystal Structure of S38ACLas-ZnuA2**

##### **2.3.1.1.1. Quality of the model**

The crystal structure of S38A CLas-ZnuA2 has been determined in metal-free and metal-bound states to 1.8 Å resolutions. The refinement data statistics in Table 2.2 show that both models are well refined with excellent stereochemistry and crystallographic R-factor values. The overall electron density in both states is well defined except for the three N-terminal residues and two loop regions. Residues 96-100 had weak electron density and 196-197 had no density in metal-free state; residues 98-99 had no density and 194-197 had weak electron density in metal bound state. The three N-terminal residues and some residues in loops (196-197 in metal-free state and 98-99 in metal bound state) were not included in the models.

The final model of metal-free state consists of 270 amino acid residues, 324 waters, 7 glycerol molecules, 8 acetate ions and 3 sulphate ions. Of the 270 residues, 14 residues (Ser9, Ser45, Thr73, Ile147, Arg148, Arg157, Ile158, Glu180, Ser186, Ile192, Ser212, Arg198, Leu260 and Val271) have been refined with alternate conformations. The final model of metal-bound state consist of 270 amino acid residues, one metal ion, 376 waters, 7 glycerol molecules, 6 acetate ions

and 1 sulphates ion. Of the 270 residues, 20 residues (Ser9, Ile13, Ser45, Met69, Thr73, Asp86, Ser94, Ile147, Arg148, Ser150, Arg157, Ile158, Glu180, Asp181, Ser186, Ser212, Asp253, Leu260, Val271 and Thr273) have been refined with alternate conformations. The metal ion was modelled as Mn(II).

**Table 2.2: Crystal parameters, data collection and structure refinement.**

	<b>Metal free - S38A CLas- ZnuA2</b>	<b>Mn-bound S38A CLas- ZnuA2</b>	<b>Metal free - Y68F CLas- ZnuA2</b>	<b>Mn bound Y68F CLas- ZnuA2</b>
Wavelength (Å)	1.5418	1.5418	1.5418	1.5418
Resolution range (Å)	42.12-1.87 (1.96-1.87)	42.14-1.80 (1.89-1.8)	40.8-1.79 (1.89-1.79)	40.8-1.84 (1.87-1.84)
Space group	<i>P</i> 3 <sub>2</sub> 21	<i>P</i> 3 <sub>2</sub> 21	<i>P</i> 3 <sub>2</sub> 21	<i>P</i> 3 <sub>2</sub> 21
Cell dimensions				
<i>a</i> ,	94.1	94.2	94.2	93.9
<i>b</i> ,	94.1	94.2	94.2	93.9
<i>c</i> (Å),	94.7	94.3	94.3	94.6
$\alpha, \beta, \gamma$ (°)	90, 90, 120	90, 90, 120	90, 90, 120	90, 90, 120
Total no of Reflections	232160	254539	260695	1086897
Unique reflections	40167	44692	44757	45940
Multiplicity	5.8 (5.3)	5.7(5.1)	5.8 (5.4)	6.4 (6.1)
Completeness (%)	97.9 (85.6)	97.9(85.8)	97.6 (84)	99.9 (100)
Mean I/sigma(I)	10.2 (2.3)	20.6(5.1)	10.1 (2.4)	23.5 (2.1)
Reflections used in refinement	38248	42404	42469	40046
Reflections used for R-free	1885	2254	2256	2040
R <sub>work</sub> (%)	15.8	14.6	17.0	14.0
R <sub>free</sub> (%)	19.1	16.4	19.7	18.9
RMSD (bonds)	0.019	0.014	0.015	0.018

RMSD (angles)	1.9	1.57	1.65	1.85
Number of non-hydrogen atoms	2640	2714	2590	2636
Macromolecules	2227	2266	2202	2155
Number of protein residues	270	270	268	263
Ramachandran favored (%)	96.3	96.4	95.8	97.9
Ramachandran Allowed (%)	3.7	3.6	4.2	2.1
Ramachandran outliers (%)	0	0	0	0
Clash Score	6.0	4.0	5.0	7.0
Side chain outliers (%)	2.5	1.7	1.7	1.3
Wilson B factor	19.7	18.3	20.4	25.3
Average B-factor (Å <sup>2</sup> ) Protein	28.4	24.6	28.3	28.5
Water atoms	37.0	37.3	38.7	39.7
All atoms	29.0	26.4	29.0	34.0

Values in parentheses are for the outermost shell.

<sup>a</sup>  $R_{merge} = \frac{\sum hkl \sum i |I_i(hkl) - \langle I(hkl) \rangle|}{\sum hkl \sum i I_i(hkl)}$ , where  $I_i(hkl)$  is the intensity of an observation and  $\langle I(hkl) \rangle$  is the mean value for its unique reflection; summations are over all reflections.

### 2.3.1.1.2. Overall structure and its comparison with wild-type CLas-ZnuA2

The overall structural organisation of S38A CLas-ZnuA2 is similar to previously reported CLas-ZnuA2 [113] consisting of a pair of N and C-terminal domains linked through a long rigid linker helix with the interface of two domains constituting the metal-binding cleft. The superposition of metal-free and metal-bound states of S38A CLas-ZnuA2 gave r.m.s.d values of 0.36 Å and 0.23 Å with metal-free and metal-bound states of wild-type CLas-ZnuA2 respectively.

However, there are notable differences in length of  $\beta$ -strands in C-domain of metal-free state of S38A CLas-ZnuA2 as compared to previously reported wild-type metal-free CLas-ZnuA2 structure (Fig. 2.1). The C-domain is made up of shortened parallel  $\beta$ -sheets (residues 167-169, 185-187, 217-221 and 239-244 forms strands E-H) in metal-free state of S38A CLas-ZnuA2, while no differences was observed in metal-bound S38A CLas-ZnuA2. The N-terminal domain is made



of four parallel  $\beta$ -sheets (residues 6-11, 27-32, 56-59 and 80-83 forms strands A-D) of similar length in both states of metal-free and metal-bound of S38A CLas-ZnuA2 as compared to both states of wild-type CLas-ZnuA2. There are no significant difference in number and length of helices in each domain of S38A CLas-ZnuA2. Each domain is made up of four helices (residues 12-23, 44-54, 69-72 and 110-129 forms helices a-d in N-domain and residues 175-183, 199-213, 226-237, 258-275 forms helices e-h in C-domain) in both metal-free and metal-bound state of S38A CLas-ZnuA2. The strands and helices are linked through loop (L1-L7 in -N and L10-L16 in C-domain) in similar manner as in wild-type CLas-ZnuA2. A long backbone  $\alpha$ -helix d' (residues 132-159) links N- and C-terminal domains in S38A CLas-ZnuA2 as in wild-type structure.

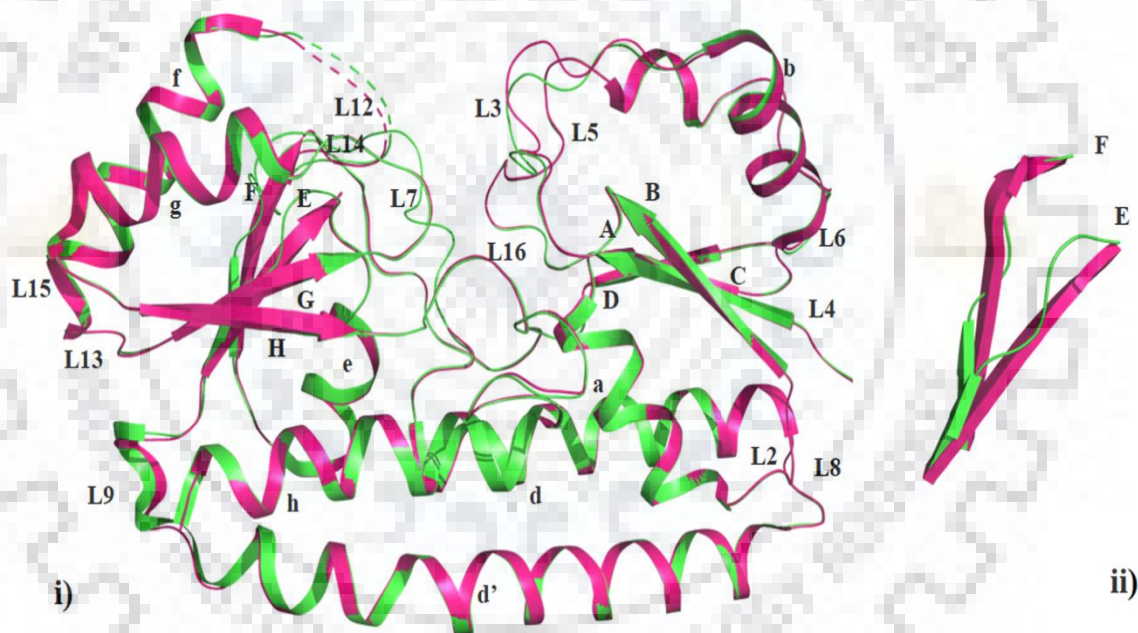


**Fig. 2.1 Superposition of S38A CLas-ZnuA2 with wild type CLas-ZnuA2** i) The superposition involving metal-free states of S38A CLas-ZnuA2 (green) and wild-type CLas-ZnuA2 (pink) (PDBID: 4UDN). ii) The variation in secondary structure elements in C- domain is shown.

The S38A mutation in CLas-ZnuA2 showed major changes in structure and interactions at domain interface in loop L3 at the opening of metal-binding cleft. The positions of metal and metal-coordinating residues His106 and Glu172 are almost same as in wild-type structure. The minor differences in orientation of Asp247 in S38A CLas-ZnuA2 as compared to wild-type CLas-ZnuA2 were observed. Also, changes in interactions of second shell residues were observed. The metal-free state of S38A CLas-ZnuA2 showed major sideward shift of part of L3 including residue 36-43 (~0.4Å, ~0.7Å, ~1.9Å, ~2.5Å, ~2.5Å, ~0.8Å, ~0.8Å, ~0.3Å C $\alpha$  displacement of Asn36, Asp37, Ser38, His39, Ser40, Tyr41, Gln42 and Val43 respectively) as compared to metal-free wild-type CLas-ZnuA2 (Fig. 2.2A and B) where L3 is displaced away from metal-binding cleft exhibiting an open conformation. The inward shift (~2.5Å C $\alpha$  displacement of His39) was observed in wild-type CLas-ZnuA2 on metal binding only. This shift seems to be due to change in the interaction between Ser38 and Tyr68.

In wild-type CLas-ZnuA2 structure, the side-chains of Ser38 and Tyr68 forms hydrogen bond. However, due to mutation of Ser38 to Ala, the particular hydrogen bond ceases to exist and now the Tyr68 forms hydrogen bond with main-chain oxygen of Ala38. This conformation is partly similar to the one which occurs on metal-binding in wild-type structure (Fig. 2A and C) where a larger inward shift of part of the L3 loop (residues 38-40) is observed. Due to this inward-shift in metal-free state of S38A CLas-ZnuA2, there is only minor C $\alpha$  displacement of His 39 with flipping of side-chain towards metal-binding site on metal-binding as compared to wild-type protein where a substantial movement of part of L3 was observed on metal-binding. This inward-shift of L3 in metal-free state of S38A CLas-ZnuA2 leads to the alterations of many interactions as compared to wild-type structure.

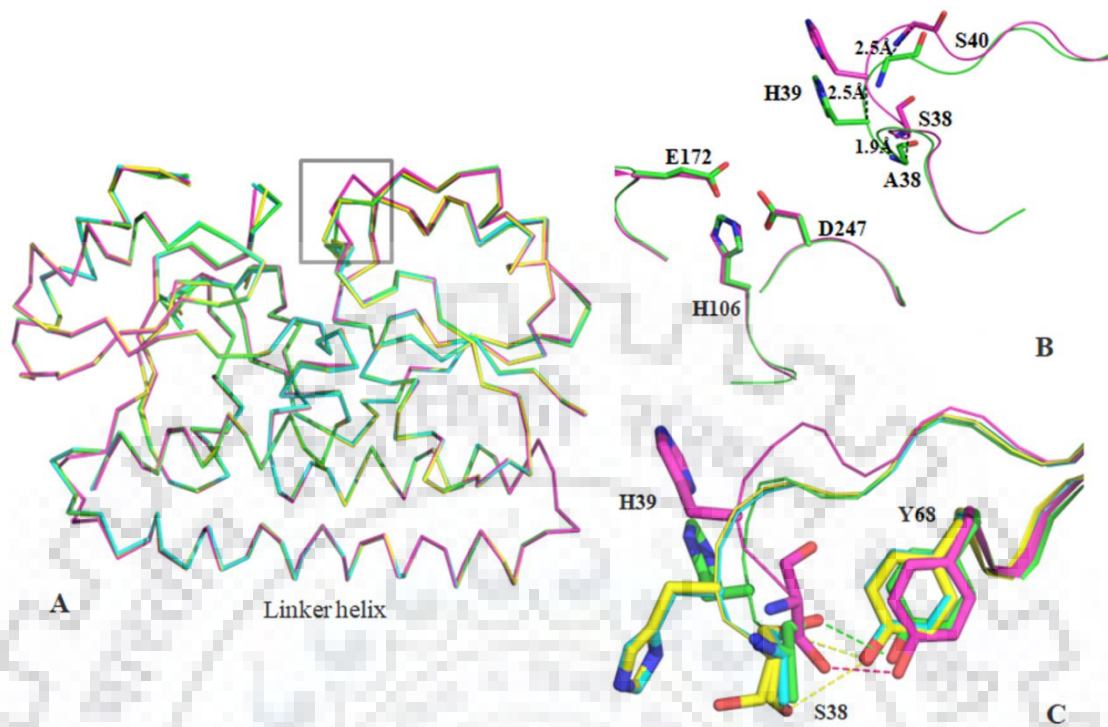


**Fig. 2.2: The shift observed in L3 in CLas-ZnuA2 mutants.** **A)** The superposition of metal-free (green) and metal-bound (cyan) states of S38A CLas-ZnuA2 with metal-free (pink) and metal-bound states of wild-type CLas-ZnuA2 (yellow) revealing inward shift of the L3 loop (shown in box). **B)** And **C)** The residues of all superposed structures involved in shifting of L3 loop are shown (same color scheme was used). His39 and Ser40 shifted  $\sim 2.5\text{\AA}$  sideward in metal-free state of S38A CLas-ZnuA2. The interactions are shown as broken lines.

In metal-free state of S38A CLas-ZnuA2, the main-chain NH of Ala38 makes water mediated interaction with main-chain oxygen of Asp247, direct interactions with main-chain oxygen of Asn36 and side-chain of Asp37. The main-chain oxygen of Ala38 interacts with side chain OH of Tyr 68. The main-chain oxygen of Asn36 also makes water-mediated interaction with Asp247 of C-lobe (Fig. 2.3A). In metal-free state of wild-type CLas-ZnuA2, the main-chain NH and side chain of Ser38, the side-chain of Asp37 and main chain oxygen of Asn36 interact with Asp247 through three water molecules. The main-chain NH of Ser38 also interacts with side-chain of Asp37. The interaction of OH of Tyr68 happens only with side-chain OG and not main-chain oxygen of Ser38. The main-chain oxygen rather interacts with Ser40, Tyr41 and Thr67 (Fig. 2.3B). The metal-binding in S38A CLas-ZnuA2 showed a rather strong H-bond ( $2.6\text{\AA}$  from  $2.9\text{\AA}$  in metal-free-state) between main-chain oxygen of Ala38 and side-chain OH of Tyr68. The NH of

Ala38 makes interactions with Asp37 and water interacting directly with Asp37. The side-chain of Asp37, through two water molecules, makes interaction with main-chain oxygen and side-chain of Asp247. The interactions shown by Asn36 in metal-free state are lost on metal-binding in S38A CLas-ZnuA2 (Fig. 2.3C). In contrast, metal-binding in wild-type CLas-ZnuA2 results in direct interaction of main-chain oxygen of Asp247 with one of the alternate conformations of side-chain of Ser38. The main chain oxygen and other alternate conformation of side-chain of Ser38 make interaction with Tyr68. The interactions of main-chain oxygen of Ser38 are lost in metal-bound state. There is also a water mediated interaction between Asp247 and Ser38 and main-chain oxygen of Asn36. Asp37 only interacts with NH of Ser38 in metal-bound state of wild-type protein (Fig. 2.3D).

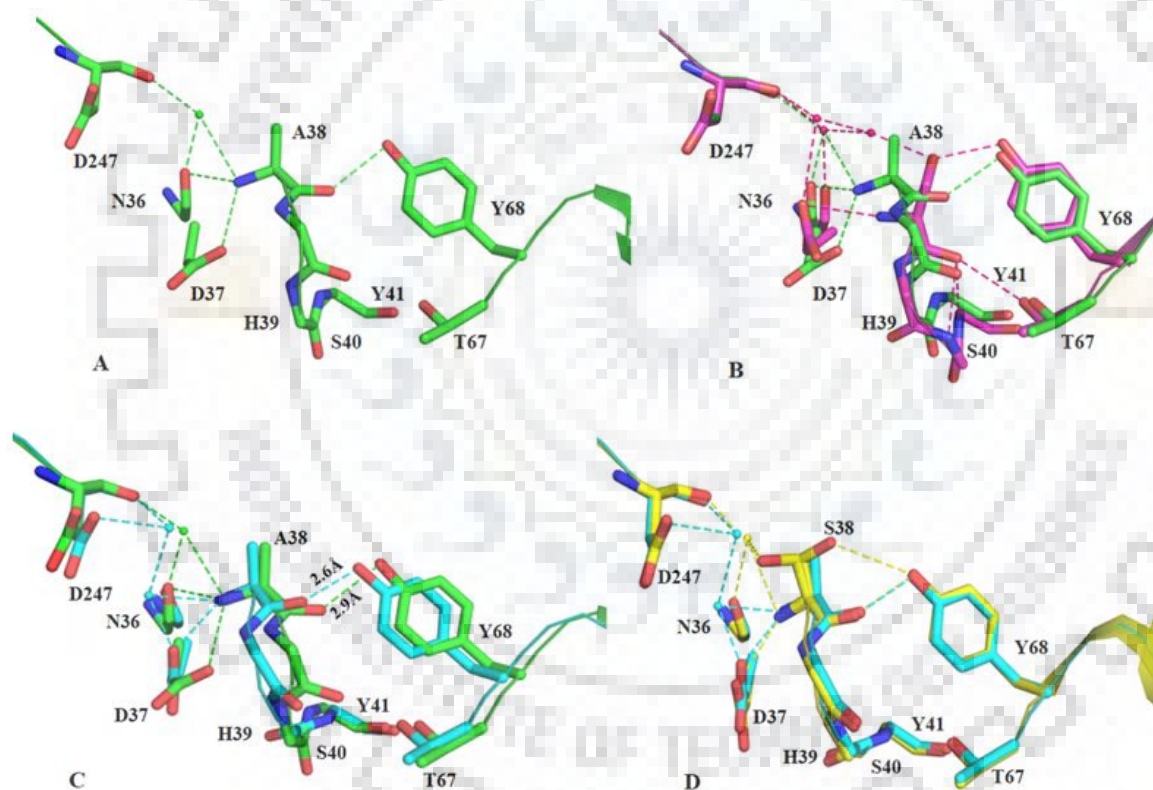


**Fig. 2.3. The comparison of interactions of residues Ser/Ala38 and Asp247 between wild-type and S38A CLas-ZnuA2.** A) In metal-free S38A CLas-ZnuA2 (green), the main-chain Ala38 forms water mediated interaction with main-chain oxygen of Asp247, direct interactions with main-chain oxygen of Asn36 and side-chain of Asp37. The main-chain oxygen of Ala38 interacts with side-chain OH of Tyr68. B) The superposition of metal-free state of S38A CLas-ZnuA2



(green) with wild-type CLas-ZnuA2 (pink) shows loss of main-chain interaction of Ala38 with Ser40, Tyr41, Thr67 and side-chain interaction with Tyr68 in S38A CLas-ZnuA2. **C)** The superposition of metal-free (green) and metal-bound (cyan) states of S38ACLas-ZnuA2 reveals the presence of strong hydrogen bond network in metal-bound state. The interactions of Asn36 were lost after metal binding. **D)** The superposition of metal-bound states of S38ACLas-ZnuA2 and wild-type CLas-ZnuA2 shows loss of direct interaction of side-chain of Ala38 with main-chain oxygen of Asp247 and Tyr68 after mutation. The interactions are shown as broken lines.

There were notable changes in interactions of metal coordinating residues with second shell residues and water as compared to wild-type metal-free and metal-bound structures of CLas-ZnuA2. In S38A CLas-ZnuA2, one of the metal coordinating residues His39 on L3 directly interacts with Glu66 (L5) whereas this interaction is water mediated in metal-free CLas-ZnuA2. His39 interacts with one water molecule only in S38A CLas-ZnuA2 as compared to wild-type structure where it forms additional H-bond with Tyr41 and three water molecules. Side-chain of His106, metal coordinating residue on L7, interacts with side-chain of Asn104 (L7) in metal-free state of S38A CLas-ZnuA2 while it is absent in metal-free wild-type CLas-ZnuA2. An interaction of main -chain of His106 with main-chain of Asn104 (L7) was observed in metal-bound state of S38A CLas-ZnuA2 but it was absent in wild-type CLas-ZnuA2. His106 interacts with Gly173 (L11) in present structure but absent in wild-type CLas-ZnuA2. The interaction of Glu172 side chain (metal coordinating residue on strand E) with Asn193 N<sup>δ2</sup> (L12), present in wild-type metal-free state of CLas-ZnuA2, is lost in metal-free state of S38A CLas-ZnuA2. Asn193 (L12) interacts with Glu172 (strand E) in metal-bound states of both wild-type CLas-ZnuA2 and S38A CLas-ZnuA2 with distances of 3.45 Å and 3.35Å respectively (Fig. 2.4A and B). The metal coordinating residue Asp247 on L16 interacts with 5 water molecules only, whereas in wild-type CLas-ZnuA2, it interacts with Thr223 (L14) and seven water molecule. The water mediated interaction was observed between Asp247 and Ala38 at the opening of the cleft have been described above.

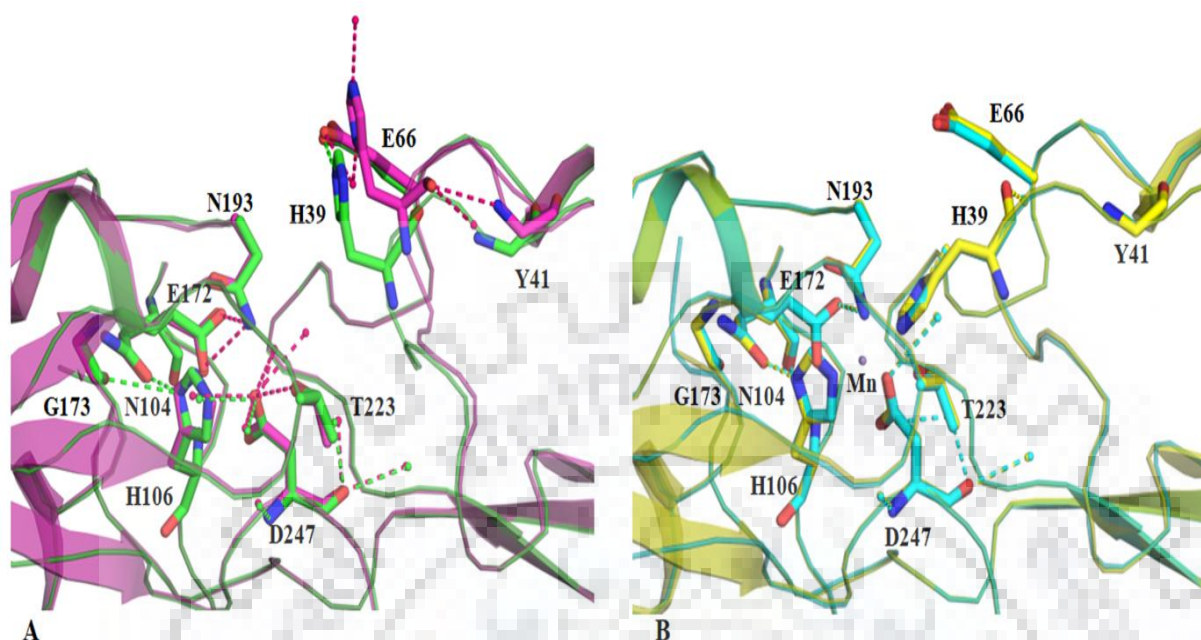


**Fig. 2.4:** The comparison of interactions involving metal coordinating residues in S38A CLas-ZnuA2 and wild-type CLas-ZnuA2 in **A)** metal-free (green-mutant; pink-wild-type) and **B)** metal-bound states (cyan-mutant; yellow-wild-type). The interactions are shown as broken lines.

There are major alterations in interactions between and within secondary structure elements as compared to wild-type metal-free and metal-bound forms. These include, i) Ser9 (strand A) showed alternate conformations in metal-free and metal-bound states of S38A mutant whereas only metal-bound state of wild-type showed alternate conformation. The alternate conformations led to a change in interactions between wild-type CLas-ZnuA2 and mutant forms. In wild-type protein, it interacts with main-chain of Gly15 (3.35Å), whereas in metal-free mutant form one conformation interacts with Thr30 (strand B), Gly15(helix a) and Thr29(strand B) and other conformation interacts with main-chain of Gly15 (3.41Å) only, ii) Ser40 (L3) interacts with Asp37 (L3) in the present structure but this interaction is absent in the wild-type CLas-ZnuA2, additionally, an interaction of main-chain of Asp37 with main-chain of Tyr41(L3) is observed in metal-free state of S38A CLas-ZnuA2 but not in wild-type CLas-ZnuA2, iii) Glu66 O<sup>ε1</sup> (L5) interacts with His63 N<sup>δ1</sup> (L5) in present structure while this interaction is water mediated in wild-type CLas-ZnuA2; the distance between His63 N<sup>δ1</sup> and Glu102 O<sup>ε1</sup> (L7) is 2.61 Å in metal-free wild-type CLas-ZnuA2, while in metal-free state of mutant, this distance is higher (3.41Å),



iv) A water mediated interaction between Met69 (helix c) and Phe72 (helix c) was observed in metal-free S38A CLas-ZnuA2 but not in metal-free state of wild-type CLas-ZnuA2, v) Thr73 (L6) shows two alternate conformations in metal-free S38A CLas-ZnuA2 but no additional interaction was observed whereas no alternate conformation was observed in wild-type CLas-ZnuA2. In metal-bound state of S38A CLas-ZnuA2, Thr73 (L6) shows two alternate conformation with one conformation interacting with Lys70 (helix c) and other with Asn74 (L6). No alternate conformation of Thr73 was observed in metal-bound state of wild-type CLas-ZnuA2 and it only interacts with Lys70, vi) Thr83 (strand D) interacts with Asp86 (L7) in metal-free state of wild-type CLas-ZnuA2 while it is absent in the metal-free state of present structure. Asp86 (L7) shows two alternate conformation in metal-bound S38A CLas-ZnuA2, one interacts with Gly87 (L7) and other interacts with Thr83 (strand D) whereas no alternate conformation was observed in metal-bound wild-type CLas-ZnuA2 and it only interacts with Thr83, vii) Ser94 (L7) makes interaction with side chain of Ser101 (L7) in metal-free wild-type CLas-ZnuA2 while it is lost in present structure where it interacts with Asp96. In metal-bound state of S38A CLas-ZnuA2, Ser94 (L7) shows two alternate conformation, both interacting with main chain Asp96 (L7) with distances 2.56 Å and 3.16 Å, Additionally one conformation interacts with Ser101 with distance 2.85 Å. In metal-bound state of CLas-ZnuA2, no alternate conformation for Ser101 was observed and it interacts with side-chain of Asp96 and Ser101(L7) with distances 2.81 Å and 3.20 Å respectively, viii) Ser131 (L8) interacts with Asp129 (helix d) and one water molecule in wild-type CLas-ZnuA2 while Ser131 interacts with 4 water molecules only in metal-free S38A CLas-ZnuA2, ix) Arg157 (helix d') shows two alternate conformations and broken density in metal-free S38A CLas-ZnuA2 with one conformation interacting with Asp272 (helix h) and Phe275 (helix h) mediated through a water molecule whereas no alternate conformation and interaction was observed in metal-free wild-type CLas-ZnuA2. Arg157 (helix d') shows two alternate conformation in metal-bound states of both wild-type and S38A CLas-ZnuA2, one conformation of both interacts with Asp272(L16) with distances 3.26 Å and 3.12 Å in wild-type and S38A CLas-ZnuA2 respectively, x) Glu159 O<sup>ε1</sup> (helix d') interacts with Arg166 N<sup>h1</sup> (L10) and Arg166 N<sup>h2</sup> of distances 3.15 Å and 3.26 Å respectively in wild-type CLas-ZnuA2 metal-free state whereas, Glu159 O<sup>ε1</sup> interacts with Arg166 N<sup>h1</sup> of distance 2.53 Å in mutant metal free S38A CLas-ZnuA2. Glu159 O<sup>ε1</sup> (helix d') interacts with Arg166 N<sup>h1</sup> (L10) and Arg166 N<sup>h2</sup> of distances 2.93 Å and 2.86 Å respectively, in wild-type CLas-ZnuA2 metal bound state whereas, Glu159 O<sup>ε1</sup> interacts with Arg166 N<sup>h1</sup> of distance 2.44 Å and one water molecule in mutant metal-bound S38A CLas-ZnuA2, xi) one of the

most important water mediated interaction was observed in between side-chain of Glu180 (helix e) and main-chain of Asn89 (L7) in both wild-type CLas-ZnuA2 and S38A CLas-ZnuA2 in metal-free state. The Glu180 shows alternate conformation in metal-free state of S38A CLas-ZnuA2 and both conformation interact with Asp181 (helix e) mediated through water. The Glu180 (helix e) shows alternate conformation in both wild-type and mutant metal-bound CLas-ZnuA2, one conformation interacts with Asn89 (L7) through water in both wild and mutant metal-bound states but with shorter distances in metal-bound S38A CLas-ZnuA2 and other conformation interacts with Asp181 (helix e) through water in wild-type metal-bound CLas-ZnuA2 whereas it is absent in mutant metal-bound S38A CLas-ZnuA2, xii) Ser186 (strand F) shows two alternate conformations in mutant metal-free S38A CLas-ZnuA2, one conformation interacts with Phe168 (strand E) mediated through water and additionally a water mediated interaction was also observed with Val176 (helix e), whereas, it directly interacts with Phe168 and no alternate conformation was observed in wild metal-free CLas-ZnuA2. Ser186 (strand F) shows alternate conformation in both wild-type and mutant metal bound S38A CLas-ZnuA2, it directly interacts with Phe168 (strand E) in wild metal-bound CLas-ZnuA2 whereas it is water mediated in mutant metal-bound CLas-ZnuA2, xiii) Asn193 (L12) makes interaction with both alternate conformations of Arg198 (L12) while no interaction and alternate conformations were observed in wild-type CLas-ZnuA2 and it interacts with Ser194. Asn193 (L12) interacts with Arg198 (L12) in mutant metal-bound S38A CLas-ZnuA2 while it is absent in wild metal-bound state of CLas-ZnuA2. Asn193 (L12) interacts with Glu172 (strand E) in metal-bound state of both wild-type CLas-ZnuA2 and S38A CLas-ZnuA2 of distances 3.45 Å and 3.35 Å respectively (Fig. 2.5A and B). xiv) Arg211 (helix f) interacts with Asn237 (helix g) in present structure whereas in wild-type CLas-ZnuA2 it is interacting with one water molecule only. Ser212 (helix f) shows two alternate conformation in mutant metal-free S38A CLas-ZnuA2 one conformation interacts with His213 and other conformation interacts with Asn208 (helix f) whereas, in wild-type CLas-ZnuA2, no alternate conformation was observed and it only interacts with Asn208; Ser212 (helix f) shows two alternate conformations in mutant metal-bound S38A CLas-ZnuA2, one interacts with Asn208 and other do not interact, whereas in wild metal-bound CLas-ZnuA2, no alternate conformations was observed but interacting with His213 (helix f) and Gln209 (helix f), xv) 253Asp (L16) shows two alternate conformations in mutant metal-bound S38A CLas-ZnuA2, no alternate conformation was observed in wild-type CLas-ZnuA2 but interacting with Lys251 (L16) whereas it was lost in mutant metal-bound S38A CLas-ZnuA2, xvi) Thr273 (helix h) shows two alternate conformations in mutant

metal-bound S38A CLas-ZnuA2, it interacts with Ile270 (helix h) whereas no alternate conformation and interaction was observed in wild metal- bound CLas-ZnuA2.

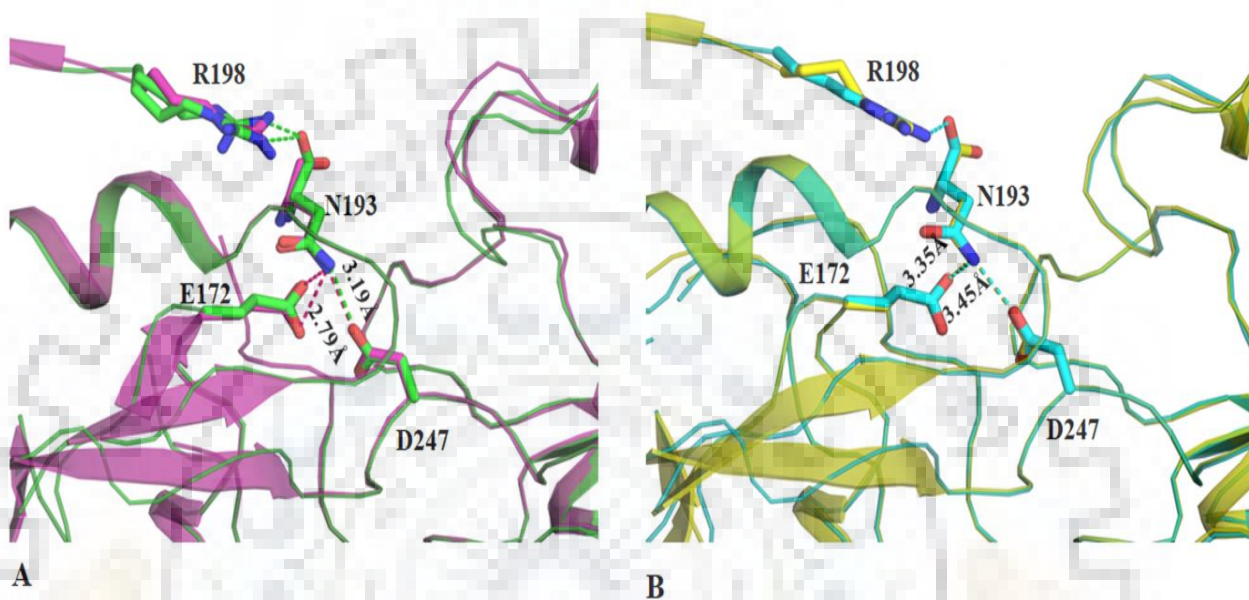


**Fig. 2.5:** The comparison of the interaction involving residues Asn193, Glu172 and Arg198 of S38A CLas-ZnuA2 and wild-type CLas-ZnuA2 are shown in **A)** metal-free (green-mutant; pink-wild-type) and **B)** metal-bound states (cyan-mutant; yellow-wild-type). The interactions are shown as broken lines. In metal-free state, the loss of interaction between Asn193 and Glu172 and higher distance between Asn193 and Asp247 was observed in S38A CLas-ZnuA2 along with additional interactions with both conformations of Arg198. In metal-bound state, Asn193 interacts with both conformation of Arg198 in S38A CLas-ZnuA2.

xvii) Ile147(helix d'), Arg148(helix d'), Ile158(helix d') , Ile192 (L12), Leu260 (helix h) and Val271 (helix h) shows two alternate conformations in mutant metal-free S38A CLas-ZnuA2 but no additional interaction was observed whereas no alternate conformation was observed in wild-type metal-free CLas-ZnuA2. The detailed list of all interactions and bond distances as compared to wild type protein is given in Table 2.3 and 2.4.

**Table 2.3: Comparison of Exclusive interactions of Metal-free S38A CLas-ZnuA2 and wild-type CLas-ZnuA2. The distance <math><3.5\text{\AA}</math> is considered as interaction.**

	Residue	Atom	Location in secondary structure	Residue	Atom	Location in secondary structure	Metal- free S38 CLas- ZnuA2	Wild- type Metal- free CLas- ZnuA2	Distance ( $\text{\AA}$ )
Main chain- Main chain	Tyr 41	N	L3	His 39	O	L3	-	+	3.24
	Tyr 41	N	L3	Asp 37	O	L3	+	-	3.27
	Gln 42	N	L3	Ser 40	O	L3	-	+	3.39
	Val 43	N	L3	Tyr 41	O	L3	-	+	3.41
	His 106	N	L7	Asn 104	O	L7	+	-	3.40
	Ile 121	N	helix d	Glu 119	O	helix d	+	-	3.39
Side chain- side chain	Thr30	OG1	strand B	Ser 9	OG	strand A	+	-	3.25
	His39	NE2	L3	Glu66	OE2	L5	+	-	2.64
	His63	ND1	L5	Glu66	OE1	L5	+	-	3.49
	His39	ND1	L3	Ser194	OG	L12	+	-	2.45
	Ser 40	OG	L3	Asp37	OD1	L3	+	-	3.12
	Thr83	OG1	Strand D	Asp 86	OD 1	L7	-	+	2.77
	Asn104	OD1	L7	His106	ND1	L7	+	-	2.67
	Arg 211	NH1	helix f	Asn 237	OD1	helix g	+	-	3.24
	Thr223	OG1	L14	Asp 247	OD2	L16	-	+	3.49
Main chain – side chain	Ser40	N	L3	Asp 37	OD1	L3	+	-	2.83
	Ser40	N	L3	Thr 67	OG1	L5	-	+	3.17
	Thr 67	OG1	L5	His 39	O	L3	+	-	3.06

	Thr 79	OG1	L6	Asp 55	O	L4	-	+	3.37
	Thr 112	N	helix d	Ser 110	OG	helix d	+	-	3.38
	Ser 150	OG	helix d'	Lys 146	O	helix d'	-	+	3.35
	Ser 186	OG	strand F	Phe 168	O	strand E	-	+	3.11
	Arg198	NH2	L12	Asn193	O	L12	+	-	3.43
	Arg 211	NH1	helix f	Thr 236	O	helix g	-	+	2.93

**Table 2.4: Comparison of interactions of Mn-bound S38A CLas-ZnuA2 and wild -type CLas-ZnuA2. The distance <math><3.5\text{\AA}</math> is considered as interaction.**

	Residue	Atom	Location in secondary structure	Residue	Atom	Location in secondary structure	Mn- bound S38A CLas- ZnuA2	Wild- type Mn- bound CLas- ZnuA2	Distance ( $\text{\AA}$ )
Main chain - Main chain	Asn 36	N	L3	Ala34	O	L3	+	-	3.47
	Ala46	N	L3	Thr44	O	L3	+	-	3.43
	His 106	N	L7	Asn 104	O	L7	+	-	3.44
Side Chain - Side	Thr268	N	helix h	Ser 266	N	helix h	+	-	3.47
	Asp272	N	helix h	Lys269		helix h	+	-	3.41
	His 39	NE2	L3	His 106	NE2	L7	+	-	3.45

Chain	Ser 110	OG	helix d	Asn 113	ND2	helix d	+	-	3.47
	Arg 211	NH1	helix f	Asn237	OD1	helix g	+	-	3.23
Main chain-side chain	Arg 211	NH1	helix f	Thr 236	O	helix g	+	-	3.38
	His 213	ND1	helix f	Gln 209	O	helix f	+	-	3.12

### 2.3.1.2. Crystal structure of Y68F CLas-ZnuA2

#### 2.3.1.2.1. Quality of the model

The crystal structure of Y68F CLas-ZnuA2 has been determined in metal-free state and intermediate state of metal-binding to 1.8 Å resolutions. The refinement data statistics in Table 2. 2 show that both models are well refined with excellent stereochemistry and crystallographic R factor values. The overall electron density in both states is well defined except for the three N-terminal residues and two loop regions. The residues 95-99 and 194-197 showed weak electron density in metal-free state and residues 95-99 and 194-197 had no electron density in intermediate form of metal-binding. The N-terminal residues and some residues in loop regions (residues 98-99, 196-197 in metal-free form, and residues 95-99, 194-197 in intermediate form) were not included in the models.

The final model of metal-free Y68F CLas-ZnuA2 consist of 268 amino acid residues, 337 waters, 4 glycerol molecules , 3 sulphate ions and 3 acetate ions. Of the 268 residues, 12 residues (Ser9, Ser45, Thr73, Asn89, Ile147, Arg148, Ile158, Gln227, Glu235, Leu260, Val271 and Thr273) have been refined with alternate conformations. The final model of metal-bound state of Y68F CLas-ZnuA2 consist of 263 amino acid residues, one metal ion, 374 water, 8 glycerol molecules, 14 acetate ions and 1 sulphate ion. Of the 263 residues, 8 residues (Ser9, Ile13, Ser45, Glu145, Arg157, Ile158, Glu180 and Ser186.) have been refined with alternate conformation and



one residue with partial occupancy (His 39 with occupancy of 0.6). The metal ion was modelled as Mn(II) (refined to 0.6 occupancy).

### **2.3.1.2.2. Overall structure and its comparison with wild-type CLas-ZnuA2**

The overall structure of Y68F CLas-ZnuA2 is similar to the previously reported wild-type CLas-ZnuA2 [113]. It consists of a pair of N- and C-terminal domains linked through a long rigid linker helix. The superposition of metal-free and metal-bound Y68F CLas-ZnuA2 with corresponding wild-type CLas-ZnuA2 forms gave r.m.s.d values of 0.39 Å and 0.26 Å respectively.

However, there are significant differences in length of parallel  $\beta$ -sheets in C-domain of metal bound state of Y68F CLas-ZnuA2 as compared to previously reported wild-type CLas-ZnuA2. The C-domain is made of shortened parallel  $\beta$ -sheets (residues 167-169, 185-187, 217-221, 239-244 form strands E-H in metal bound state of Y68F CLas-ZnuA2 as shown in Fig. 2.6 while, no differences were observed in metal-free state of Y68F CLas-ZnuA2. The N-terminal domain is made of four parallel  $\beta$ -sheets (residues 6-11, 27-32, 56-59, 80-83 form strands A-D) of similar length in both state of metal-free and metal-bound state of Y68F CLas-ZnuA2 as compared to metal-free and metal bound state of wild-type CLas-ZnuA2. There are no major differences in number and length of helices in Y68F CLas-ZnuA2. Each domain is made of four helices (residues 12-23, 44-54, 69-72 and 110-129 forms a-d in N-domain and residues 175-183, 199-213, 226-237 and 258-275 forms helices e-h in C-domain) in both metal free and metal bound state of Y68F CLas-ZnuA2.

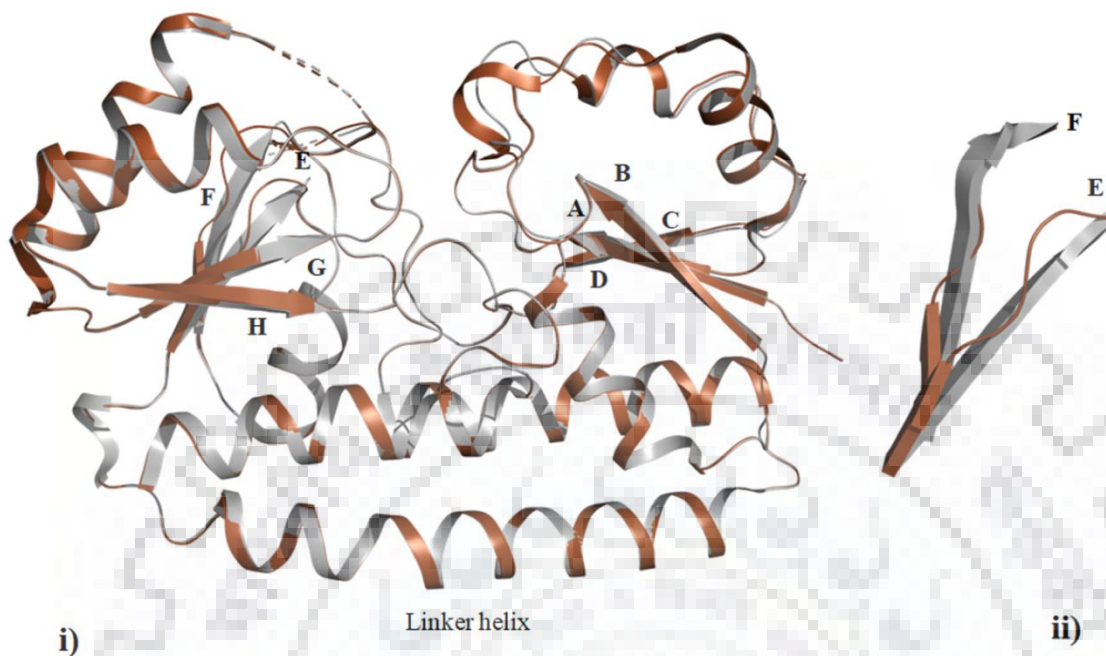


**Fig. 2.6: Superposition of Y68F CLas-ZnuA2 with wild-type CLas-ZnuA2** i) The superposition of metal-bound states of Y68F CLas-ZnuA2 (brown) and wild-type CLas-ZnuA2 (grey) (PDBID: 4CL2). (ii) The variation in secondary structure elements in C-domain.

The overall architecture and positions of metal-binding residues in metal binding cleft of Y68F CLas-ZnuA2 are comparable to wild-type CLas-ZnuA2. The metal-bound form of Y68F CLas-ZnuA2 exhibited a partial metal-bound state. The Y68F mutation resulted in notable differences at the opening of the metal-binding cleft. The L3 architecture remains unchanged and no sideward shift of L3 like S38A CLas-ZnuA2 was observed in metal-free state. Similar to metal-free wild-type CLas-ZnuA2, main-chain oxygen of Ser38 in Y68F CLas-ZnuA2 interacts with Ser40, Tyr41 and Thr67 but the side-chain interaction between Ser38 and Y68 present in wild-type structure is lost in Y68F CLas-ZnuA2. The network of four water molecules, present at the opening of the cleft between N- and C-domain in Y68F CLas-ZnuA2, mediates interactions between Asp247 and Ser38, Asp37 and Asn36 (Fig. 2.7A). In metal-free state of wild-type CLas-ZnuA2, the same interactions were mediated through three water molecules and the side-chain of Asp247 was not involved in any interaction in contrast to Y68F CLas-ZnuA2 where water mediated interaction is observed (Fig. 2.7B). In metal-bound form of Y68F CLas-ZnuA2, the

inward shift of L3 is not complete to bring His39 within coordinating distance with metal. This partial inward shift of L3 results in a water mediated interaction among side-chain of Ser38, main-chain of Asp247 and side-chain of one of the alternate conformations of His39. Also, main-chain oxygen of Ser38 interacts with Ser40 in Y68F CLas-ZnuA2 whereas all the interactions of main-chain Ser38 in metal-free state are lost in metal-bound form in wild-type protein (Fig. 2.7C and D).

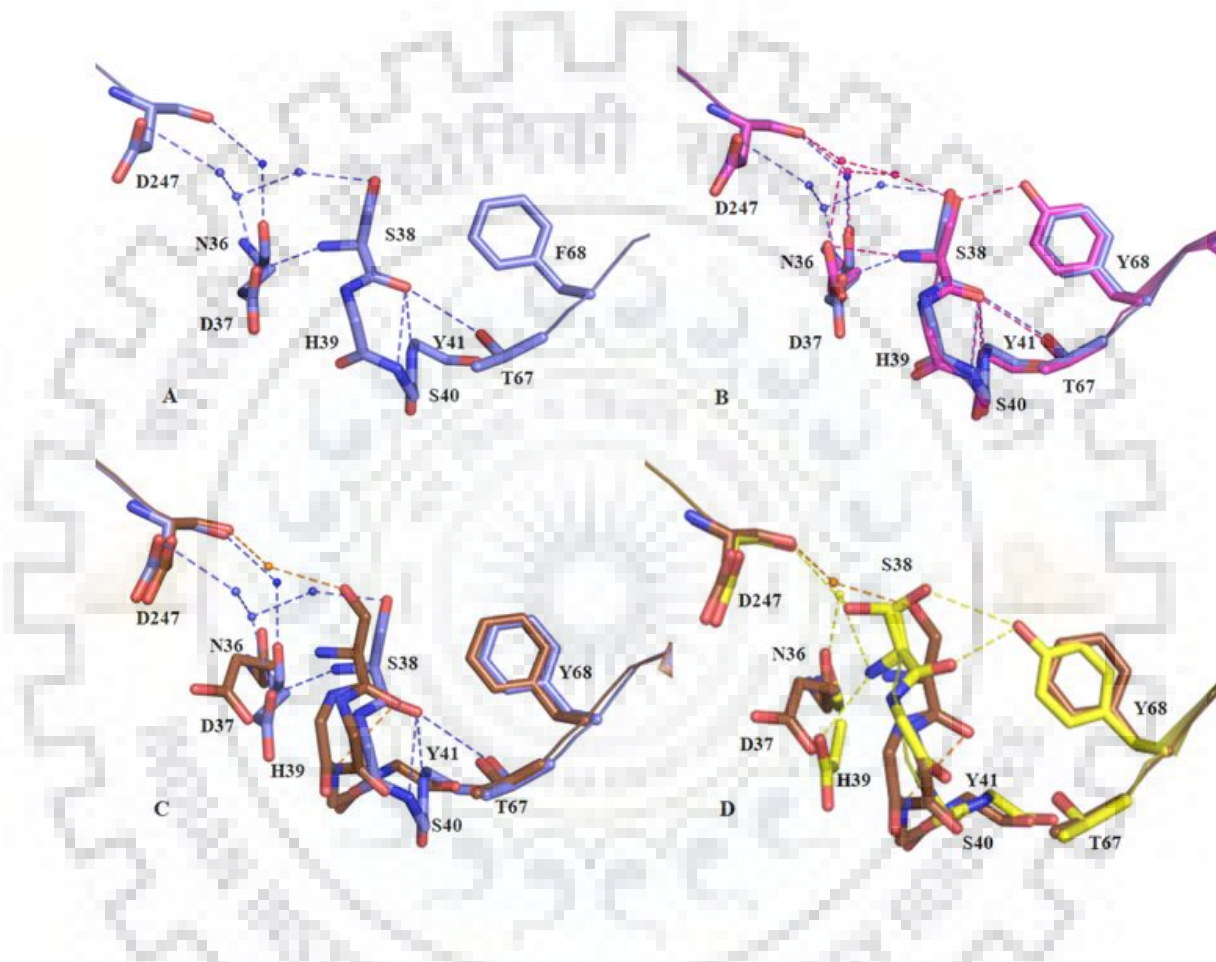


**Fig. 2.7: The comparison of interaction of residues Tyr/Phe68 and Asp247 between wild-type and Y68F CLas-ZnuA2.** **A)** In metal-free Y68F CLas-ZnuA2 (blue), the side-chain Ser38 forms water mediated interaction with Asn36, Asp37 and Asp247. The main-chain Ser38 interacts with Ser40, Tyr41 and Thr67. **B)** The superposition of metal-free state of Y68F CLas-ZnuA2 (blue) with wild-type CLas-ZnuA2 (pink) shows loss of side-chain interaction of Ser38 with Phe68. **C)** The superposition of metal-free (blue) and metal-bound (brown) states of Y68F CLas-ZnuA2 reveals the loss of main-chain interaction of Ser38 with Ser40, Tyr41 and Thr67 in metal-bound state. The water mediated side-chain interaction of Ser38 with Asn36 and Asp37 were lost after metal binding. **D)** The superposition of metal-bound states of Y68F CLas-ZnuA2 and wild-type CLas-ZnuA2 shows loss of direct interaction of Ser38 with Phe68 after mutation. The interactions are shown as broken lines.

The differences in interactions of metal coordinating residues with second shell residues and water as compared to wild-type structures were observed. A water mediated interaction was observed between His39 (L3) and Leu64 (L5) in metal-free Y68F CLas-ZnuA2 whereas it is absent in metal-free wild-type CLas-ZnuA2. In metal-bound form of Y68F CLas-ZnuA2, main-chain of Ser38 (L3) interacts with Ser40 only and a water mediated interaction was observed between Asp247 (L16) and Ser38 (L3). His39 (L3) has been refined with two alternate conformations with partial occupancy of 0.6 and 0.4 in metal-bound Y68F CLas-ZnuA2. A break in electron density was also observed in His39 side-chain along with main-chain and between Ser40 and Tyr41 (Fig. 2.8).

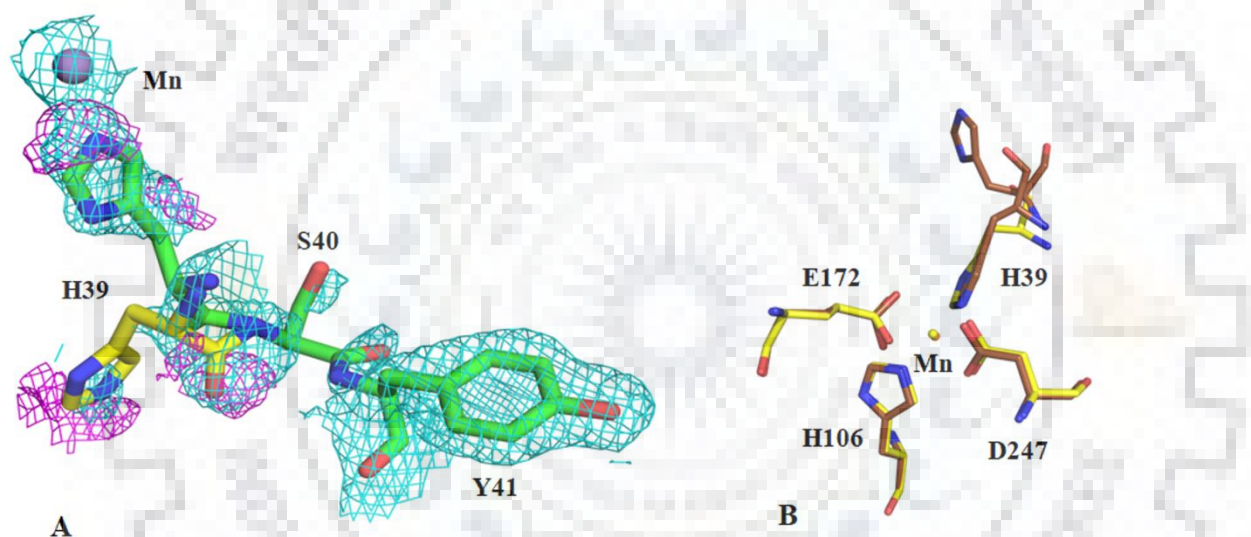


**Fig. 2.8: The electron density map** **A)** The electron density shown around residues in L3 in metal-bound state of Y68F CLas-ZnuA2. The  $2F_o - F_c$  map (cyan) and  $F_o - F_c$  map (magenta) were shown for His39 exhibiting two alternate conformations with partial occupancy of 0.6 and 0.4 and broken density for side-chain. The break in electron density between Ser40 and Tyr41 is also observed. **B)** The superposition of metal coordinating residues of metal-bound states of both Y68F CLas-ZnuA2 and wild-type CLas-ZnuA2 are shown in brown and yellow respectively.

The side-chain of His106 one of the metal coordinating residues on L7, interacts with side-chain of Asn104 (L7) in metal-free state of Y68F CLas-ZnuA2 while it is absent in metal-free wild-type



CLas-ZnuA2. The side-chain of metal coordinating residue Glu172 ( $O^{\epsilon 1}$  and  $O^{\epsilon 2}$ ) on strand E interacts with Asn193  $N^{\delta 2}$  (L12) in metal-free wild-type CLas-ZnuA2 whereas in Y68F CLas-ZnuA2 Asn193 interacts with only Glu172  $O^{\epsilon 1}$ . Asp247 interacts with Thr223 (L14) and seven water molecules in wild-type CLas-ZnuA2 whereas, interaction of Asp247 with Thr223 and two waters are lost in present structure. In metal bound Y68F CLas-ZnuA2, Asn193  $N^{\delta 2}$  and  $O^{\delta 1}$  (L12) interacts with Glu172  $O^{\epsilon 2}$  (2.85 Å and 3.22Å) whereas, in wild metal bound CLas-ZnuA2, Asn193  $N^{\delta 2}$  interacts with Glu172  $O^{\epsilon 2}$  of distance 3.45 Å only (Fig.2. 9A and B).

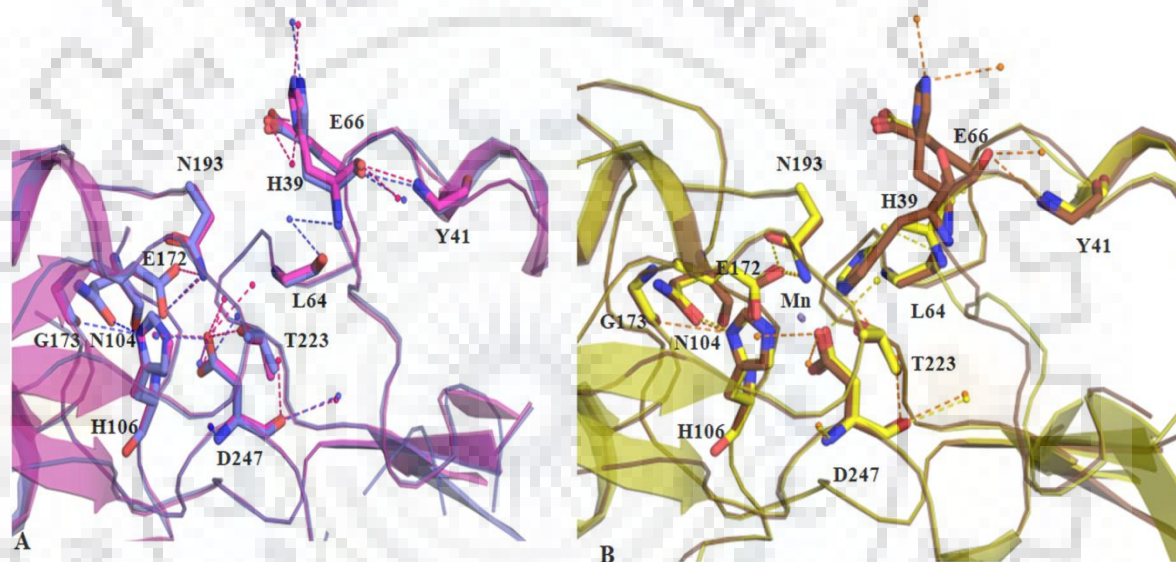


**Fig. 2.9: The comparison of interaction of metal coordinating residues of Y68F CLas-ZnuA2 with wild-type CLas-ZnuA2 in A) metal-free and B) metal-bound state. The metal-free and metal-bound states of Y68F CLas-ZnuA2 are shown as blue and brown color while those of wild-type CLas-ZnuA2 as pink and yellow color respectively.**

The comparison of Y68F CLas-ZnuA2 and CLas-ZnuA2 structure revealed a number of differences in interactions between and within the secondary structure elements. These include, i) Ser9 (strand A) has been refined with two alternate conformations in metal-free state of Y68F CLas-ZnuA2 where one conformation interacts with Thr18 (helix a) and Gly15 (helix a) and other conformation interacts with Thr29 (strand B), Thr30 (strand B) and Gly15 (helix a) whereas no alternate conformation for Ser9 was observed and it only interacts with Gly15 in wild-type metal-

free CLas-ZnuA2. In all metal-bound states Ser 9 (strand A) showed alternate conformation. In metal-bound Y68F CLas-ZnuA2, one conformation interacts with Gly15 (helix a) and Thr30 (strand B) whereas, in wild-type metal-bound CLas-ZnuA2, one conformation interacts with Gly15 (helix a), Thr30 (strand B) and Thr29 (strand B) and other interacts with Gly15 (helix a) and Thr18 (helix a) ii) Ile13 (helix a) shows two alternate conformation in both wild-type and mutant metal-bound state of CLas-ZnuA2 but no alternate conformation was observed in intermediate form of CLas-ZnuA2 and no additional interaction was observed in mutant metal-bound state of CLas-ZnuA2, iii) Ser 45 (helix b) has been refined with three alternate conformations in metal-free state of Y68F CLas-ZnuA2 whereas no alternate conformation was observed in wild-type metal-free state of CLas-ZnuA2 and no additional interaction was observed, iv) His 63 N<sup>δ1</sup> (L5) interacts with Glu102 O<sup>ε1</sup> (L7) within distance of 2.61 Å in metal-free CLas-ZnuA2 while in metal-free Y68F CLas-ZnuA2, it interacts with higher distance (2.98 Å). His 63 N<sup>δ1</sup> (L5) interacts with Glu102 O<sup>ε1</sup> (L7) in intermediate and metal-bound state of CLas-ZnuA2 of distances 3.23 Å and 3.08 Å respectively, while in mutant metal-bound state of Y68F CLas-ZnuA2, it interacts with slightly higher distance 3.37 Å, v) Thr73 (L6) shows two alternate conformation in mutant metal-free Y68F CLas-ZnuA2, both conformation interact with Lys70 (helix c) of distances 3.40 Å and 2.43 Å and no alternate conformation was observed in wild-type metal-free CLas-ZnuA2 and it interact with 70Lys (helix c) of distance 3.30 Å. A water mediated interaction in between Met69 (helix c) and Phe72 (helix c) was observed in metal-free Mutant Y68F- CLas-ZnuA2 whereas it is absent in wild-type metal-free State of CLas-ZnuA2, vi) Ser94(L7) make interaction with side-chain of Ser101 (L7) in both wild (3.12 Å) and mutant metal-free state Y68F CLas-ZnuA2 (2.45 Å) although distance is shorter in mutant Y68-CLas-ZnuA2, vii) Asp129 (helix d) interacts with Asn132 (helix d') in wild-type and mutant metal-free CLas-ZnuA2 having distances 2.88 Å and 2.68 Å respectively. Glu145 (helix d') shows two alternate conformations in mutant metal-bound Y68-CLas-ZnuA2, where one interacts with Arg148 (helix d') and other conformation makes interaction with Arg141 (helix d') while no alternate conformation of Glu145 was observed in intermediate and metal-bound CLas-ZnuA2 here it only interacts with Arg148, viii) Glu235 (helix g) shows two alternate conformation in mutant metal-free Y68F CLas-ZnuA2, it interacts with Gln231 (2.60 Å) whereas no alternate conformation was observed in wild-type CLas-ZnuA2 and it interacts with Gln231 (helix g) (2.49 Å), ix) Arg157 (helix d') interacts with Asp272 (helix h) in mutant metal-free Y68F-CLas-ZnuA2 whereas it was absent in wild-type metal-free state of CLas-ZnuA2. Two alternate conformation of Arg157 (helix d') were also observed and one



conformation interacts with Asp 272 (helix h) of distance 2.82 Å in mutant metal bound Y68F-CLas-ZnuA2 which is lesser than the interaction in wild metal-bound CLas-ZnuA2 (3.26Å) and 3.13Å in intermediate CLas-ZnuA2, x) Glu159 O<sup>ε1</sup> ( helix d') interacts with Arg166 N<sup>h1</sup> (L10 ) and Arg166 N<sup>h2</sup> of distances 3.15Å and 3.26Å respectively in wild-type CLas-ZnuA2 metal-free state whereas, Glu159 O<sup>ε1</sup> interacts with Arg166 N<sup>h1</sup> of distance 2.53Å in mutant metal-free state of Y68F- CLas-ZnuA2. Glu159 O<sup>ε1</sup> ( helix d') interacts with Arg166 N<sup>h1</sup> and Arg166 N<sup>h2</sup>(L10) of distances 3.32Å, 2.90Å and 2.93Å and 2.86Å respectively, in intermediate and wild-type metal-bound CLas-ZnuA2 whereas, Glu159 O<sup>ε1</sup> interacts with Arg166 N<sup>h2</sup> of distance 2.59Å in mutant metal- bound state of Y68F CLas-ZnuA2, xi) Asn89 (L7) shows two alternate conformations and one conformation of Asn89 interacts with Pro90 in mutant metal-free state of Y68F- CLas-ZnuA2 and No water mediated interaction was observed in between side-chain of Glu180 and main- chain of Asn89 (L7) in mutant metal-free Y68F CLas-ZnuA2, xii) A water mediated interaction was observed in between Glu180 (helix e) and Asn89 (L7) in all wild, intermediate and mutant metal-bound state of CLas-ZnuA2, xiii) Thr273 (helix h) shows two alternate conformation in mutant metal-free Y68F CLas-ZnuA2, and it interacts with Lys269 (helix h) mediated through water whereas it was not observed in wild-type metal-free CLas-ZnuA2, xiv) Ile147 (helix d'), Arg148 (helix d'), Ileu158 (helix d'), Gln227 (helix f), Leu260 (helix h) and Val271 (helix h) shows two alternate conformations in mutant metal-free Y68F CLas-ZnuA2 but no additional interaction was observed whereas no alternate conformation was observed in wild-type metal- free CLas-ZnuA2. Thr156 (helix d') form H-bond with Pro153 (helix d') in both wild-type and mutant metal-bound CLas-ZnuA2 of distance 3.45Å and 3.39Å respectively, whereas it is absent in intermediate CLas-ZnuA2; Ser45 (helix b) and Ser186 (strand F) shows two alternate conformations in all, wild-type metal-bound, intermediate and mutant metal-bound Y68F CLas-ZnuA2 but no additional interaction was observed whereas no alternate conformation was observed in wild-type metal-free CLas-ZnuA2. Ile158 (helix d') shows two alternate conformations in metal-bound Y68F CLas-ZnuA2 and intermediate CLas-ZnuA2 but no alternate conformation was observed in wild-type CLas-ZnuA2 and no additional interaction was observed. A detailed list of all the interactions and bond distances as compared to wild-type protein is given in Table 2.5 and 2.6.

**Table 2.5 : Comparison of interactions of Metal-free Y68F CLas-ZnuA2 and wild-type CLas-ZnuA2. The distance <3.5Å is considered as interaction.**

	Residue	Atom	Location in secondary structure	Residue	Atom	Location in secondary structure	Metal- free Y68F CLas- ZnuA2	Wild- type Metal- free CLas- ZnuA2	Distance (Å)
Main chain -Main chain	Ala 46	N	helix b	Thr 44	O	helix b	+	-	3.41
	Leu 56	N	strand C	Val 6	O	strand A	-	+	3.39
	Phe 72	N	helix c	Lys 70	O	helix c	-	+	3.45
	His 106	N	L7	Asn 104	O	L7	+	-	3.43
	Ile121	N	helix d	Glu119	O	helix d	+	-	3.37
	Thr 156	N	helix d'	Pro 153	O	helix d'	-	+	3.23
	Leu125	N	helix d	Arg122	O	O helix d	+	-	3.41
Side chain -side chain	Thr30	OG1	strand B	Ser 9	OG	strand A	+	-	3.30
	Tyr 41	OH	L3	Asp 47	OD1	helix b	+	-	3.49
	Asn104	OD1	L7	His 106	ND1	L7	+	-	2.61
	His 106	NE2	L7	Glu 172	OE1	strand E	+	-	3.06
	Ser 110	OG	helix d	Asn 113	ND2	helix d	-	+	3.43
	Arg 211	NH1	helix f	Asn 237	OD1	helix g	+	-	2.98
	Thr223	OG1	L14	Asp 247	OD2	L16	-	+	3.49
Main Chain- side chain	Ser 9	OG	strand A	Thr 29	O	strand B	+	-	2.92
	Gly 15	N	helix a	Ser 9	OG	strand A	+	-	3.16
							+	-	3.37

	His 106	ND1	L7	Gly 173	O	L11			
	Thr 112	N	helix d	Ser 110	OG	helix d	+	-	3.42
	Arg 166	NH2	L10	Phe 182	O	helix e	+	-	3.15
	Arg198	NH1	L12	Asn193	O	L3)	+	-	2.21
	Ser 212	OG	helix f	Asn 208	O	helix f)	-	+	2.64
	Glu 221	OE2	helix g	Phe 219	O	strand G	-	+	3.33
	Ser 239	OG	strand H	Lys 216	O	L13	-	+	3.43
	Tyr 240	OH	strand H	Gly 242	O	strand H	-	+	3.32

**Table 2.6: Comparison of interactions of Metal-bound Y68F CLas-ZnuA2 and wild -type CLas-ZnuA2. The distance <math><3.5\text{\AA}</math> is considered as interaction.**

	Residue	Atom	Location in secondary structure	Residue	Atom	Location in secondary structure	Mn- bound Y68F CLas- ZnuA2	Wild - type Mn- bound CLas- ZnuA2	Distance ( $\text{\AA}$ )
Main Chain- Main Chain	Ser38	N	L3	Asn 36	O	L3	-	+	3.48
	Ser40	N	L3	Asp37	O	L3	-	+	3.4
	Ser40	N	L3	Ser38	O	L3	+	-	3.25
	Tyr41	N	L3	Asp37	O	L3	+	-	3.37
	Tyr41	N	L3	His39	O	L3	+	-	3.34
	Ala46	N	helix b	Thr44	O	helix b	+	-	3.5
Side chain - Side chain	Thr18	OG1	helix a	Ser 9	OG	strand A	-	+	3.45
	His63	ND1	L5	Glu66	OE1	L5	-	+	3.3
	Arg141	NH1	helix d'	Glu145	OE1	helix d'	+	-	2.84

	Thr170	OG1	Strand E	Cys174	SG	L11	+	-	3.98
	Thr223	OG1	L14	Asp37	OD1	L3	+	-	3.34
	Thr223	OG1	L14	Asn 193	ND2	L12	+	-	3.45
Main Chain-Side Chain	Asn36	ND2	L3	Glu33	O	L3	+	-	2.78
	Ser38	OG	L3	Asp247	O		-	+	3.46
	Ser40	OG	L3	Asp37	O	L3	+	-	3.49
	Tyr41	OH	L3	Leu31	O	Strand B	+	-	3.4
	Tyr68	OH		Ser38	O	L3	-	+	2.93
	Thr73	OG1	L6	Lys 70	O	helix c	-	+	3.19
	His106	ND1	L7	Gly 173	O	L11	+	-	3.4
	Arg 198	NH1	L12	Asn193	O	L12	+	-	3.13

### 2.3.2. Circular dichroism

Thermal studies were carried out using circular dichroism technique in the similar manner as reported previously [254]. Far UV circular dichroism (wavelength range 200-250nm) for metal-free-states was performed in the absence and presence of different concentrations of  $MnCl_2$  and  $ZnCl_2$  (10  $\mu$ m, 500 $\mu$ m, 1mM and 10mM) at an increasing temperature range (20-70°C). Efforts to record the data below 205nm was not successful because of excessive noise. CD-spectra of metal-free S38A CLas-ZnuA2 and Y68F CLas-ZnuA2 showed negative peaks around 208 nm and 222nm similar to wild-type CLas-ZnuA2 (Fig. 2.10).

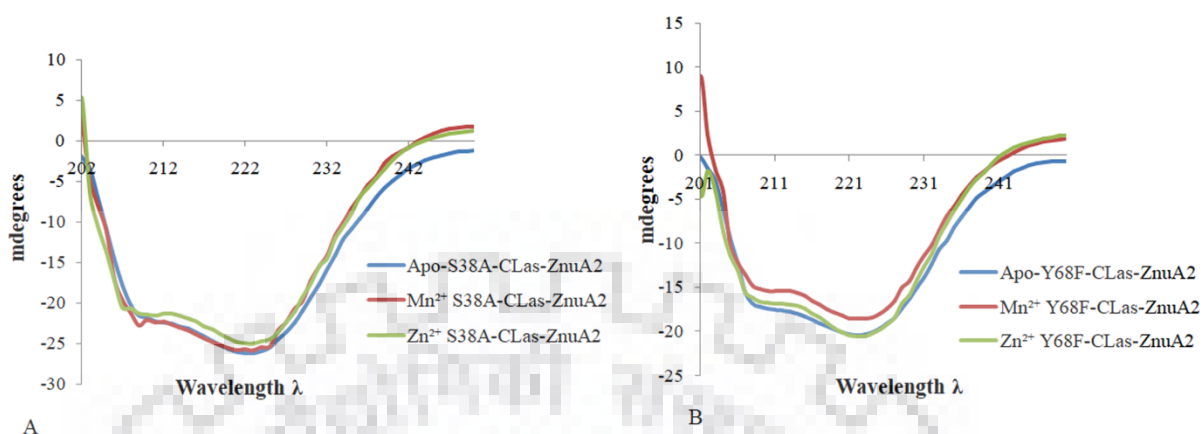


**Fig. 2.10: The comparison of CD spectra of A) metal-free S38A CLas-ZnuA2, Mn<sup>2+</sup>-bound, Zn<sup>2+</sup>-bound CLas-ZnuA2, and B) metal-free Y68F CLas-ZnuA2, Mn<sup>2+</sup>-bound, Zn<sup>2+</sup>-bound CLas-ZnuA2 showing almost similar secondary structure and conformation. The metal-free Mn<sup>2+</sup>-bound, Zn<sup>2+</sup>-bound states are shown in blue, dark red and green respectively.**

On increasing temperature, both metal-free mutants began to unfold at 45°C similar to wild-type CLas-ZnuA2. On addition of MnCl<sub>2</sub> to 50, 100 and 1000 fold, the unfolding temperature of both mutant protein was increased to 60 °C, 65°C and 70°C respectively (similar to wild-type CLas-ZnuA2) (Table 2.7, Fig. 2.11 and Fig. 2.13). Upon addition of 10 fold of ZnCl<sub>2</sub>, both mutant proteins remained stable up to 60°C similarly observed in wild-type CLas-ZnuA2. Further addition of 50 and 100 fold ZnCl<sub>2</sub> in S38A CLas-ZnuA2 increased the unfolding temperature to 65°C, however, addition of 1000 fold ZnCl<sub>2</sub> destabilized the protein (Table 2.7 and Fig. 2.12). In case of Y68F CLas-ZnuA2, addition of ZnCl<sub>2</sub> up to 50 fold increased the temperature of unfolding to 65°C, however, further addition of ZnCl<sub>2</sub> resulted in protein destabilization (Table 2.7 and Fig. 2.14).

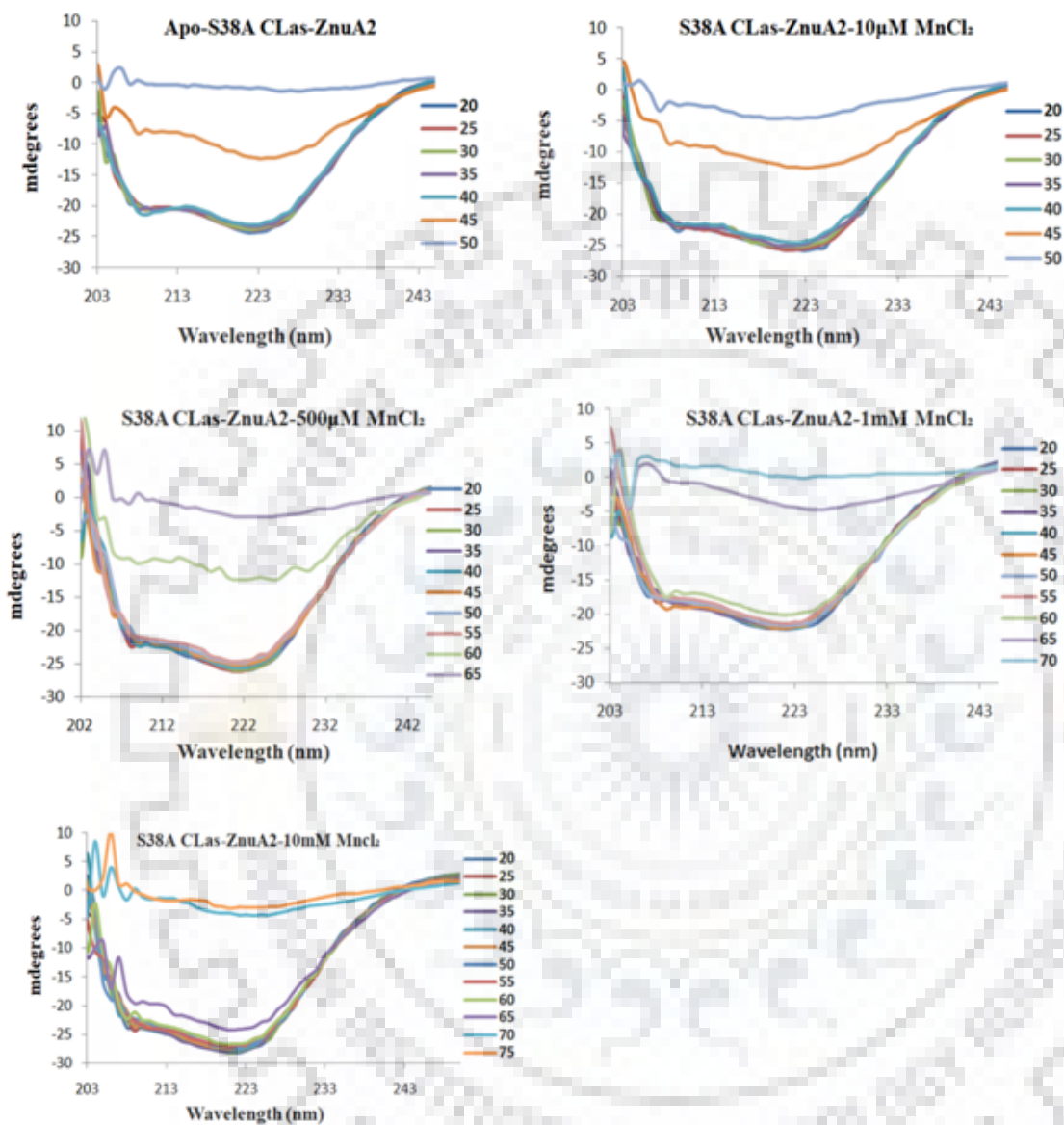


**Fig. 2.11:** CD spectra showing differences in temperature of unfolding of Apo S38A CLas-ZnuA2 and after adding MnCl<sub>2</sub> in different concentrations. Concentrations of MnCl<sub>2</sub> added were 10  $\mu$ M (1:1), 500  $\mu$ M (1:50), 1 mM (1:100) and 10mM (1:1000).



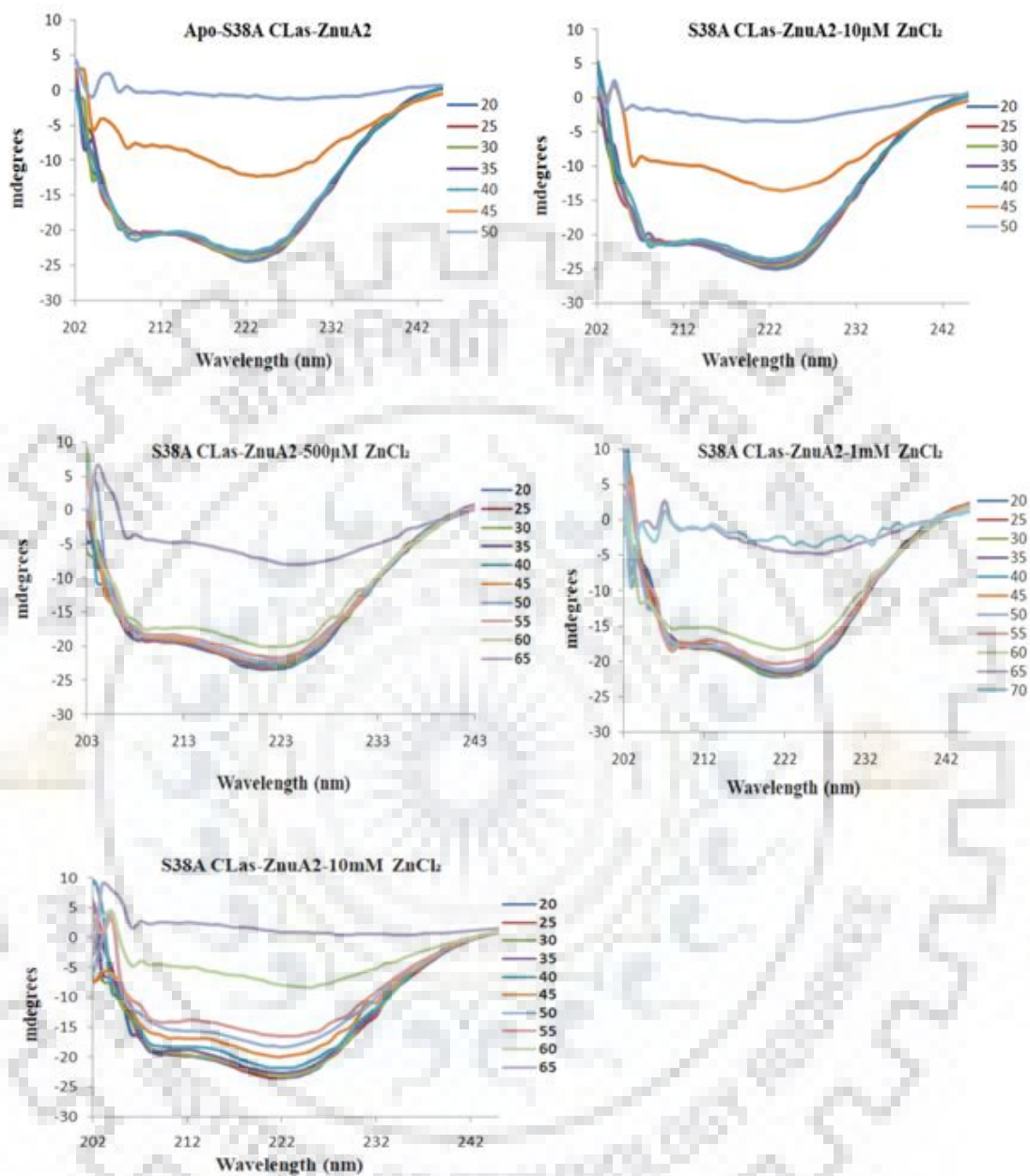


**Fig.2.12:** CD spectra showing differences in temperature of unfolding of Apo S38A CLas-ZnuA2 and after adding ZnCl<sub>2</sub> in different concentrations. Concentrations of ZnCl<sub>2</sub> added were 10 µM (1:1), 500 µM (1:50), 1 mM (1:100) and 10mM (1:1000).

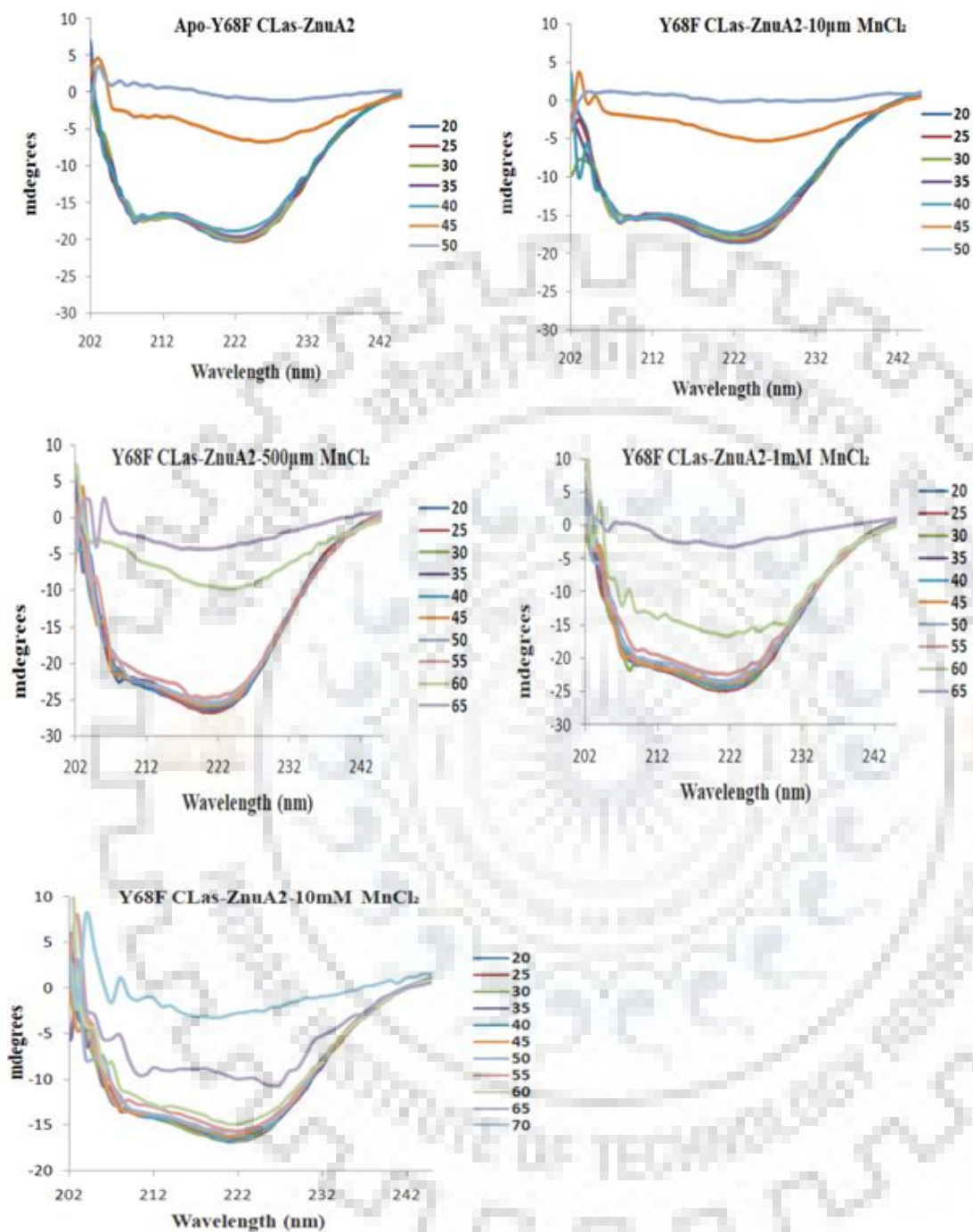


**Fig. 2.13:** CD spectra showing differences in temperature of unfolding of Apo Y68F CLas-ZnuA2 and after adding MnCl<sub>2</sub> in different concentrations. Concentrations of MnCl<sub>2</sub> added were 10 μM (1:1), 500 μM (1:50), 1 mM (1:100) and 10mM (1:1000).

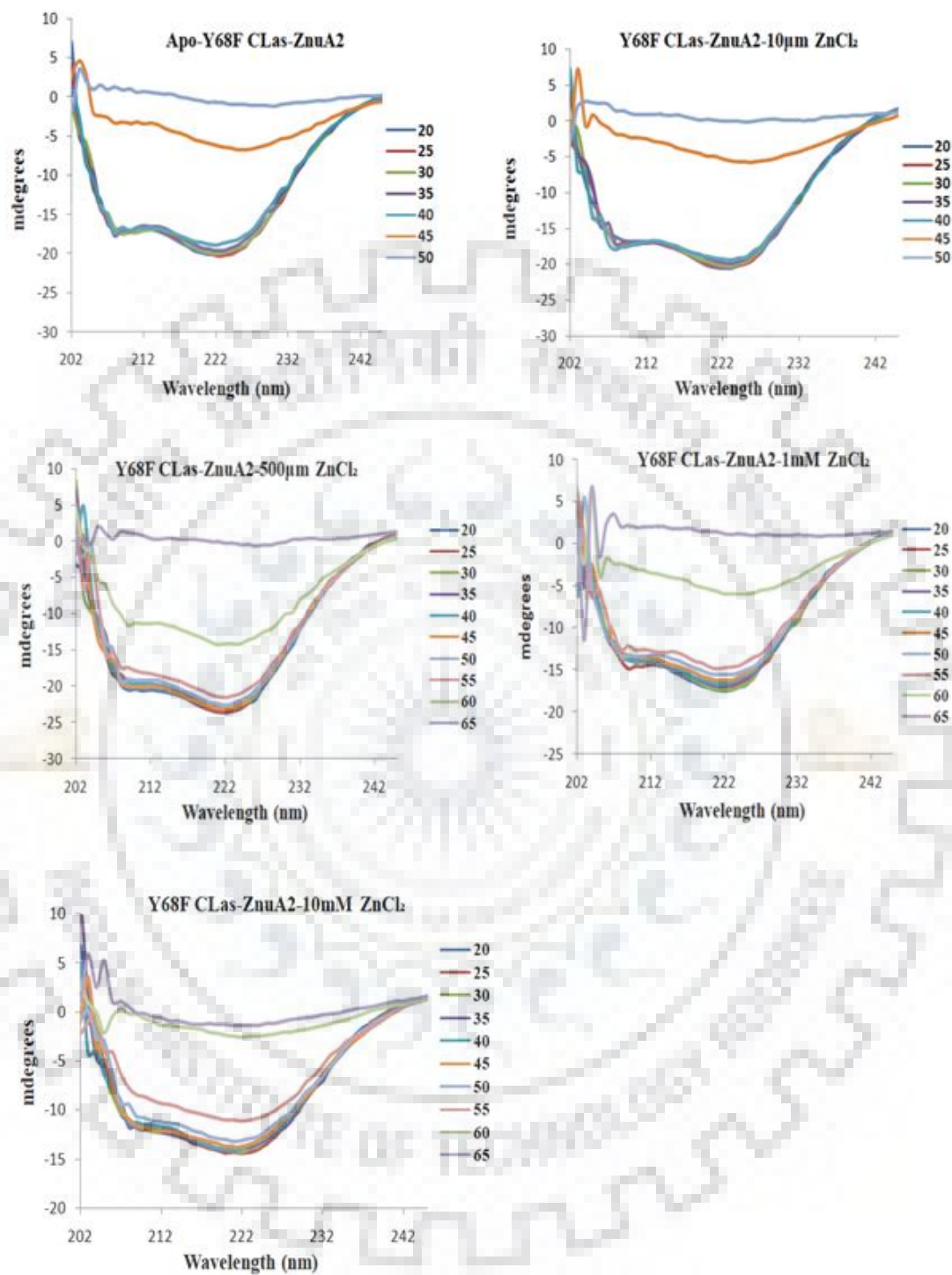


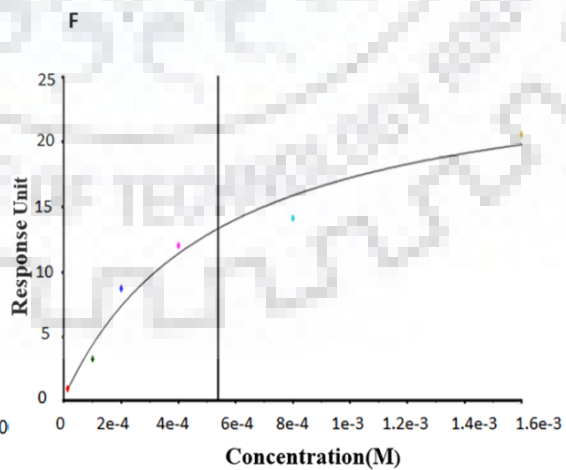
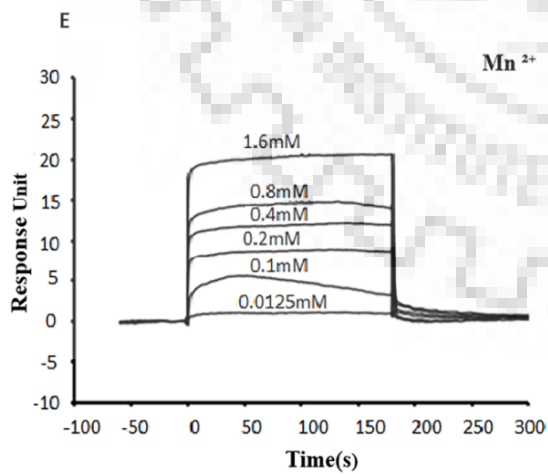
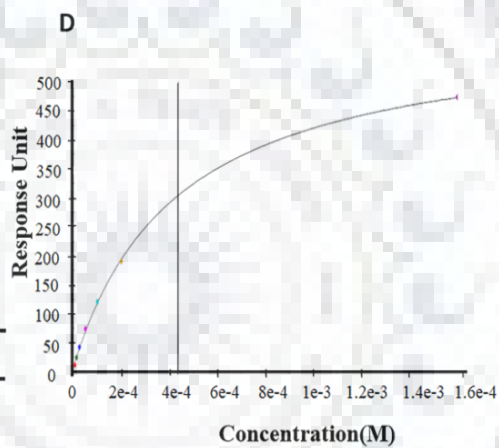
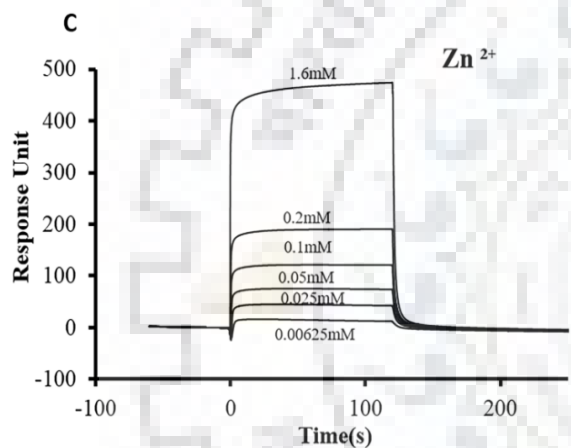
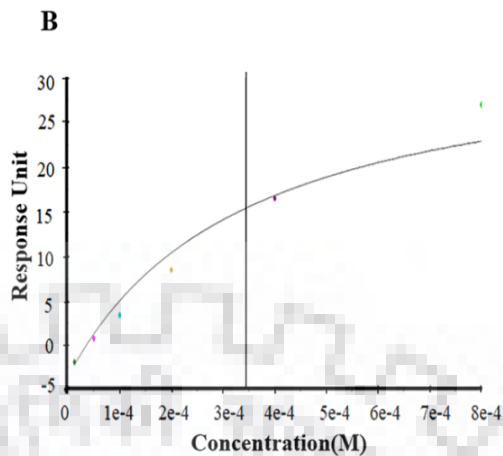
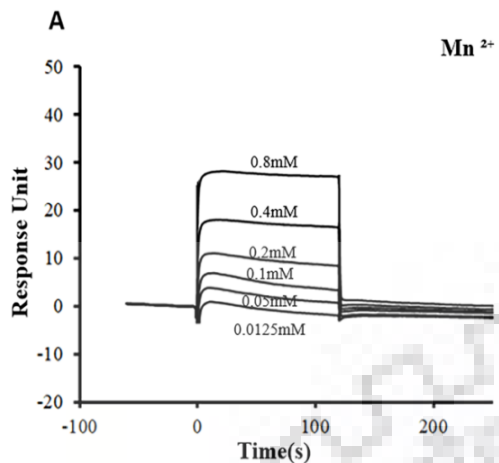
**Fig. 2.14:** CD spectra showing differences in temperature of unfolding of Apo Y68F CLas-ZnuA2 and after adding ZnCl<sub>2</sub> in different concentrations. Concentration of ZnCl<sub>2</sub> added were 10 µM (1:1), 500 µM (1:50), 1 mM (1:100) and 10mM (1:1000).

**Table2.7 : Effect of Metal ions concentration on Temperature of unfolding of Mutants CLas-ZnuA2 Protein.**

<b>Mutant protein + metal ions</b>	<b>Temperature of unfolding</b>	<b>Protein : metal</b>
<b>Apo S38A CLas-ZnuA2</b>	45 <sup>0</sup> C	None
<b>Apo + 10μM MnCl<sub>2</sub></b>	45 <sup>0</sup> C	1:1
<b>Apo + 500μM MnCl<sub>2</sub></b>	60 <sup>0</sup> C	1:50
<b>Apo + 1mM MnCl<sub>2</sub></b>	65 <sup>0</sup> C	1:100
<b>Apo + 10mM MnCl<sub>2</sub></b>	70 <sup>0</sup> C	1:1000
<b>Apo + 10μM ZnCl<sub>2</sub></b>	45 <sup>0</sup> C	1:1
<b>Apo + 500μM ZnCl<sub>2</sub></b>	65 <sup>0</sup> C	1:50
<b>Apo + 1mM ZnCl<sub>2</sub></b>	65 <sup>0</sup> C	1:100
<b>Apo + 10mM ZnCl<sub>2</sub></b>	60 <sup>0</sup> C	1:1000
<b>Apo Y68F CLas-ZnuA2</b>	45 <sup>0</sup> C	None
<b>Apo + 10μM MnCl<sub>2</sub></b>	45 <sup>0</sup> C	1:1
<b>Apo + 500μM MnCl<sub>2</sub></b>	60 <sup>0</sup> C	1:50
<b>Apo + 1mM MnCl<sub>2</sub></b>	65 <sup>0</sup> C	1:100
<b>Apo + 10mM MnCl<sub>2</sub></b>	70 <sup>0</sup> C	1:1000
<b>Apo + 10μM ZnCl<sub>2</sub></b>	45 <sup>0</sup> C	1:1
<b>Apo + 500μM ZnCl<sub>2</sub></b>	65 <sup>0</sup> C	1:50
<b>Apo + 1mM ZnCl<sub>2</sub></b>	60 <sup>0</sup> C	1:100
<b>Apo + 10mM ZnCl<sub>2</sub></b>	60 <sup>0</sup> C	1:1000

### 2.3.3. Surface plasmon resonance

Binding experiment of S38A CLas-ZnuA2 and Y68F CLas-ZnuA2 to  $Mn^{2+}$  and  $Zn^{2+}$  ions has been carried out using surface plasmon resonance technique in a similar manner as reported previously for wild-type CLas-ZnuA2 [254]. Binding affinity of both  $Mn^{2+}$  and  $Zn^{2+}$  to the immobilized S38A CLas-ZnuA2 and Y68F CLas-ZnuA2 proteins were determined separately. Analysis was done using BIAcore T200 evaluation software version 2.0 using model 1:1 binding. The response curves generated for  $Mn^{2+}$  and  $Zn^{2+}$  binding to S38A CLas-ZnuA2 and Y68F CLas-ZnuA2 are shown in Fig. 2.15. Steady state response level has also been shown for  $Mn^{2+}$  and  $Zn^{2+}$  concentration. The  $K_D$  values calculated for binding of  $Mn^{2+}$  and  $Zn^{2+}$  to S38A CLas-ZnuA2 and Y68F CLas-ZnuA2 were comparable to the already reported  $K_D$  values for wild-type CLas-ZnuA2 ( $3.7 \times 10^{-4} M$  for  $Mn^{2+}$  and  $4.3 \times 10^{-4} M$  for  $Zn^{2+}$ ). The  $K_D$  values calculated for  $Mn^{2+}$  and  $Zn^{2+}$  binding to S38A CLas-ZnuA2 were  $3.4 \times 10^{-4} M$  and  $4.3 \times 10^{-4} M$  respectively and the  $K_D$  values for Y68F CLas-ZnuA2 for  $Mn^{2+}$  and  $Zn^{2+}$  were  $5.4 \times 10^{-4} M$ ,  $6.5 \times 10^{-4} M$  respectively. The results indicate that there is a very slight increase in metal binding affinity for S38A CLas-ZnuA2 and a slight decrease in binding affinity in case of Y68F CLas-ZnuA2.





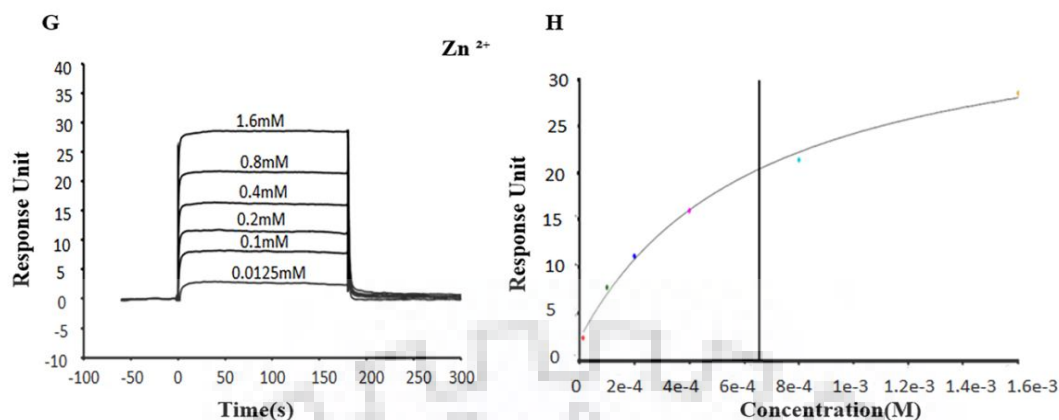


**Fig. 2.15:** SPR sensogram showing S38A Clas-ZnuA2 and Y68F Clas-ZnuA2 interaction with  $Mn^{+2}$  and  $Zn^{+2}$ . A, C, E and G represent the curves showing the binding of 100  $\mu$ M immobilized S38A Clas-ZnuA2 and Y68F Clas-ZnuA2 with  $MnCl_2$  and  $ZnCl_2$  between concentrations 0.0125mM-1.6mM in presence of 10mM sodium cacodylate buffer pH 7.0 respectively. B, D, F and H indicate representative graph showing plot of response Req against concentration of  $Mn^{+2}$  and  $Zn^{+2}$  injected. Vertical line crossing the plot represents the equilibrium constant  $K_D$  calculated (concentration at which half of binding site is saturated).

#### 2.3.4. Aggregation effect of mutation

AGGRESCAN program calculates the average aggregation propensity of sequence (a3vSA), number of hot spots (nHS) and normalized aggregation propensity (Na4vSS). The change in value of normalized Na4vSS is the indicator of change in aggregation properties of sequence due to mutations. The comparison of AGGRESCAN output results (Table 2.8 and Fig. 2.16) of all mutants Pro153Ala, Glu159Ala, Pro153Ala/Glu159Ala and Asn193Ala CLas-ZnuA2 protein with wild-type CLas-ZnuA2 indicate the tendency of mutation to promote the aggregation.

**Table 2.8: Comparison of different AGGRESCAN parameters for CLas-ZnuA2, P153A CLas-ZnuA2, E159ACLas-ZnuA2 , P153A&E159A CLas-ZnuA2 and N193ACLas-ZnuA2.**

<b>Sequence Name</b>	<b>CLas-ZnuA2</b>	<b>P153A CLas-ZnuA2</b>	<b>E159A CLas-ZnuA2</b>	<b>P153A&amp;E159A CLas-ZnuA2</b>	<b>N193ACLas-ZnuA2</b>
a3v Sequence Average (a3vSA):	-0.005	-0.004	0	0.001	-0.001
Number of Hot Spots (nHS):	10	11	10	11	10
Normalized nHS for 100 residues (NnHS):	3.636	4	3.636	4	3.636
Area of the profile Above Threshold (AAT):	42.171	42.461	42.599	42.92	42.617
Total Hot Spot Area (THSA):	39.016	40.595	39.016	41.053	39.297
Total Area (TA):	3.095	3.393	4.471	4.769	4.361
Normalized a4v Sequence Sum for 100 residues (Na4vSS):	-0.8	-0.7	-0.3	-0.2	-0.4



**Fig. 2.16: Hot spot area graphics. Hot spot areas plot for A) Wild CLas-ZnuA2 protein B) P153A CLa-ZnuA2 protein C) P153A&E159A CLas-ZnuA2 protein. Change in the hot spot area plot caused by mutation in CLas-ZnuA2 protein can be seen from sequence 150-160 in B)P153A CLas-ZnuA2 and B) P153A&E159A CLas-ZnuA2 protein.**

## 2.4. Discussion

The subtle internal communications in structure, during metal-binding and release, through intricate network of interactions play an important role in cluster A-I family proteins. The effect of alteration in single amino acid on this intricate network of interactions is key highlight of the present study. The studies on CLas-ZnuA2 mutants, in present work, highlighted the importance of some of the critical residues present in different secondary structure elements apart from metal coordinating residues in cluster A-I family proteins. The amino acid residues mutated were carefully selected considering their importance in structure and function of CLas-ZnuA2 as revealed from the crystal structures in metal-free, intermediate state of metal-binding and metal-bound states. The Ser38 (S38A) on L3 and Tyr68 (Y68F) on helix c were chosen as they play an important role in evolved mechanism of metal-binding and release in CLas-ZnuA2. The Pro153 (P153A) on linker helix was selected as the presence of a proline results in relatively higher bending and rigidity of the linker helix in CLas-ZnuA2 as compared to related Mn-specific proteins. The Glu159 (E159A) was mutated alone as well in combination with P153A as it is involved in making interactions at the C-terminal end of the curved linker helix in CLas-ZnuA2. The unfolding at C-terminal end of linker helix is observed in PsaA (Mn-binding protein from *Streptococcus pneumonia*) but not in CLas-ZnuA2. The fact that except for the S38A and Y68F mutations, site-directed mutagenesis resulted in destabilization and subsequently degradation of protein indicated a major disturbance in otherwise fine-tuned structure. The bioinformatics analysis of amino acid sequences after single mutations revealed the generation of hot spot in P153A CLas-ZnuA2 and P153A/E159A CLas-ZnuA2. An increase in the values of normalized average aggregation propensity in all mutations indicate that the protein is highly susceptible to destabilization and degradation. The results indicated that the divergence and development of different mechanisms and specificities of this group of proteins seem to have been perfected in long course of evolution and any change in critical residues may have a substantial effect on structure and function.

The importance of network of interactions between and within different secondary structure elements which maintains the overall architecture is demonstrated from the high resolution crystal structures, in both metal-free and metal-bound-states, of S38A CLas-ZnuA2 and Y68F CLas-ZnuA2. The disruption and therefore alterations in network of interactions through internal

communications was quite evident in both metal-free and metal-bound forms of mutant structures. The single amino acid change affected the whole structure in terms of interactions and secondary structure elements. Also, the effect of two single mutations was quite different demonstrating the role of each amino acid in intricate balance. Due to S38A mutation in S38A CLas-ZnuA2, the interaction between side chains of Ser38 and Tyr68 is disrupted and an inward/sideward shift of part of the L3 is observed. In wild-type CLas-ZnuA2, comparatively a larger inward shift towards metal-binding site is observed on metal-binding where alternate conformations of Ser38 interact with Tyr68 and Asp247. This sliding of Ser38 inwards during metal-binding disrupts all the interactions of main-chain oxygen in metal-free state and brings it in hydrogen bonding distance to side-chain of Tyr68 in wild-type CLas-ZnuA2. It is to be noted that the inward shift of part of L3 observed in S38A CLas-ZnuA2 in metal-free state occurs only on metal-binding in presence of high metal-ion concentration in wild-type CLas-ZnuA2. The mutation of S38A demonstrated that the sliding of Ser38 present on restrained L3 during metal-binding is part of the metal-binding mechanism for this low metal-binding affinity protein. The mutation to Ala leads to disruption of that mechanism along with disruption of intricate network of interactions affecting the overall fine-tuned structure. The role of Y68, on which Ser38 slides through, during metal-binding and release was demonstrated from the detailed analysis Y68F CLas-ZnuA2 structure in metal-free and metal-bound states. The Y68F mutation completely abolished any interaction between mutated Phe68 and Ser38 and therefore the interplay of interactions during metal-binding and release. No inward shift of part of L3 and change in interactions of main-chain oxygen of Ser38, like S38A CLas-ZnuA2, were observed in metal-free state of Y68F CLas-ZnuA2. It showed almost similar structure as wild-type CLas-ZnuA2, although now only three interactions restrained L3 as compared to wild-type structure. The role of interaction between Y68 and S38 was quite evident where only partially closed metal-bound state was observed for Y68F CLas-ZnuA2, even after soaking the crystals in very high concentration of metal-ion like wild-type and S38A CLas-ZnuA2. A relatively smaller inward shift of L3 towards metal-binding cleft as compared to wild-type CLas-ZnuA2 results in disruption of direct interaction of Ser38 side-chain with main-chain of Asp247 (coordinating residue on L16). Rather, a water mediated interaction of Ser38 and one of the alternate conformations of His39 (one of the coordinating residues) with Asp247 is observed. Also, the main-chain interactions of Ser38 are not completely disrupted unlike wild-type CLas-ZnuA2 on metal-binding. These disruptions in interactions at the opening of the metal-binding cleft involving N- and C-domains are relayed through internal communications and showed-up as

distortions in otherwise fine-tuned structure. Another important indicator of relatively less stability of mutant structures was increased number of alternate conformations for amino acid residues. There are 14 and 12 alternate conformations in metal-free states of S38A CLas-ZnuA2 and Y68F CLas-ZnuA2 respectively as compared to metal-free wild-type CLas-ZnuA2 where no alternate conformations were observed. The metal-free wild-type CLas-ZnuA2 is therefore considered as most stable and preferred state as compared to metal-bound form where the presence of high number of amino acid residues, particularly in L3, in alternate conformations was observed. Likewise, 20 alternate conformations in metal-bound state of S38A CLas-ZnuA2 as compared to 7 alternate conformations in wild-type CLas-ZnuA2 indicated less stable structure. However, Y68F CLas-ZnuA2 showed less number of alternate conformations in metal-bound form depicting rather a relatively stable form as compared to metal-free state.

The disturbance in subtle internal communication between secondary structure elements, due to a single amino acid mutation, is demonstrated through alterations in intricate balance of interactions. The effect is, quite interestingly, different for two mutants signifying their roles in overall architecture and mechanism. Some of the notable alterations in interactions between different secondary structure elements in both mutant structures as compared to wild-type protein included: i) L3 and L5 where S38A mutation resulted in direct interaction between metal coordinating residue His39 (L3) and Glu66 (L5) as compared to a water mediated interaction in CLas-ZnuA2 and no interaction was observed after Y68F mutation, ii) L5 and L7 where a rather weak interaction between His63 (L5) and Glu102 (L7) in metal-free S38A CLas-ZnuA2 (3.4 Å) was observed as compared to wild-type metal-free (2.6 Å) and metal-bound (3.08 Å) CLas-ZnuA2 signifying the loosening of interaction between L5 in N-domain and L7 at the interface of two domains. The loosening of interaction in metal-free Y68F CLas-ZnuA2 (2.98 Å) was relatively smaller as compared to S38A CLas-ZnuA2 signifying the difference in effects of two mutants (Fig. 2.17A, B and C). However, partially metal-bound state of Y68F CLas-ZnuA2 showed slightly higher bond distance (3.37 Å) as compared to intermediate state of metal-binding (3.23 Å) and metal-bound state (3.08 Å) of wild-type CLas-ZnuA2. The role of this interaction where a high mobility of Glu102 is evident from broken and poorly defined electron density for side-chain in only intermediate state in wild-type CLas-ZnuA2 and, iii) L7 and strand D where interaction between Asp86 (L7) and Thr83 (strand D) is absent in metal-free and metal-bound states of S38A CLas-ZnuA2 but present in metal-free states of CLas-ZnuA2 and no interaction was observed in



Y68F CLas-ZnuA2, iv) L7 and helix e where a water mediated interaction between one of the alternate conformations of Glu180 (helix e) and main chain of Asn89 (L7) and additionally a water mediated interactions were also observed between both conformation of Asp180 (helix e) and Asp181 (helix e) in metal-free states of S38A CLas-ZnuA2. The metal-free CLas-ZnuA2 makes similar interaction with Asn89 (L7) but does not show any alternate conformation for Glu180. In metal-bound states, the alternate conformations of Glu180 in CLas-ZnuA2, S38A CLas-ZnuA2 and Y68F CLas-ZnuA2 showed similar water mediated interaction but with shorter bond lengths for S38A CLas-ZnuA2. In metal-free states of Y68F CLas-ZnuA2, Glu180 does not show alternate conformation and interaction with Asn89 while Asn89 shows alternate conformation and one conformation makes interaction with Pro90 (L7). v) Strand F with strand E and helix e where Ser186 (strand F) shows two alternate conformations in metal-free S38A CLas-ZnuA2, one conformation interacts with Phe168 (strand E) mediated through water and additionally a water mediated interaction was also observed with Val176 (helix e), whereas, it directly interacts with Phe168 and no alternate conformation was observed in wild metal free CLas-ZnuA2. Ser186 (strand F) shows alternate conformation in both wild-type and mutant metal-bound S38A CLas-ZnuA2, it directly interacts with Phe168 (strand E) in wild-type metal-bound CLas-ZnuA2 whereas it is water mediated in mutant metal-bound CLas-ZnuA2, while no alternate conformation and direct interaction of Ser186 with Phe168 was observed in metal-free state of Y68F CLas-ZnuA2 and Ser186 shows two alternate conformation in metal-bound state of Y68F CLas-ZnuA2 where one conformation directly interacts with Phe168 additionally, water mediated interactions with Phe168, Thr170 (strand E) and Leu187 (strand F) vi) Strand E and L12 where Asn193 (L12) interacts with Glu172 (strand E) in wild-type metal-free state of CLas-ZnuA2 whereas it is lost in metal-free S38A CLas-ZnuA2. Asn193 (L12) makes interaction with both alternate conformations of Arg198 (L12) while no interaction and alternate conformations were observed in wild-type CLas-ZnuA2 and it interacts with Ser194. Asn193 (L12) interacts with Arg198 (L12) in mutant metal-bound S38A CLas-ZnuA2 while it is absent in wild-type metal-bound state of CLas-ZnuA2. Asn193 N<sup>δ2</sup> (L12) interacts with Glu172 O<sup>ε2</sup> (strand E) in metal-bound state of both wild-type and S38A CLas-ZnuA2 of distances 3.45 Å and 3.35 Å respectively, while in metal-free state of Y68F CLas-ZnuA2, Asn193 interacts with Glu172 and one alternate conformation of Arg198 and Asn193 N<sup>δ2</sup> and O<sup>δ1</sup> interacts with Glu172 O<sup>ε2</sup> of distances 2.85 Å and 3.22 Å respectively, and additionally makes interaction with one conformation of Arg198 in metal bound state of Y68F CLas-ZnuA2.

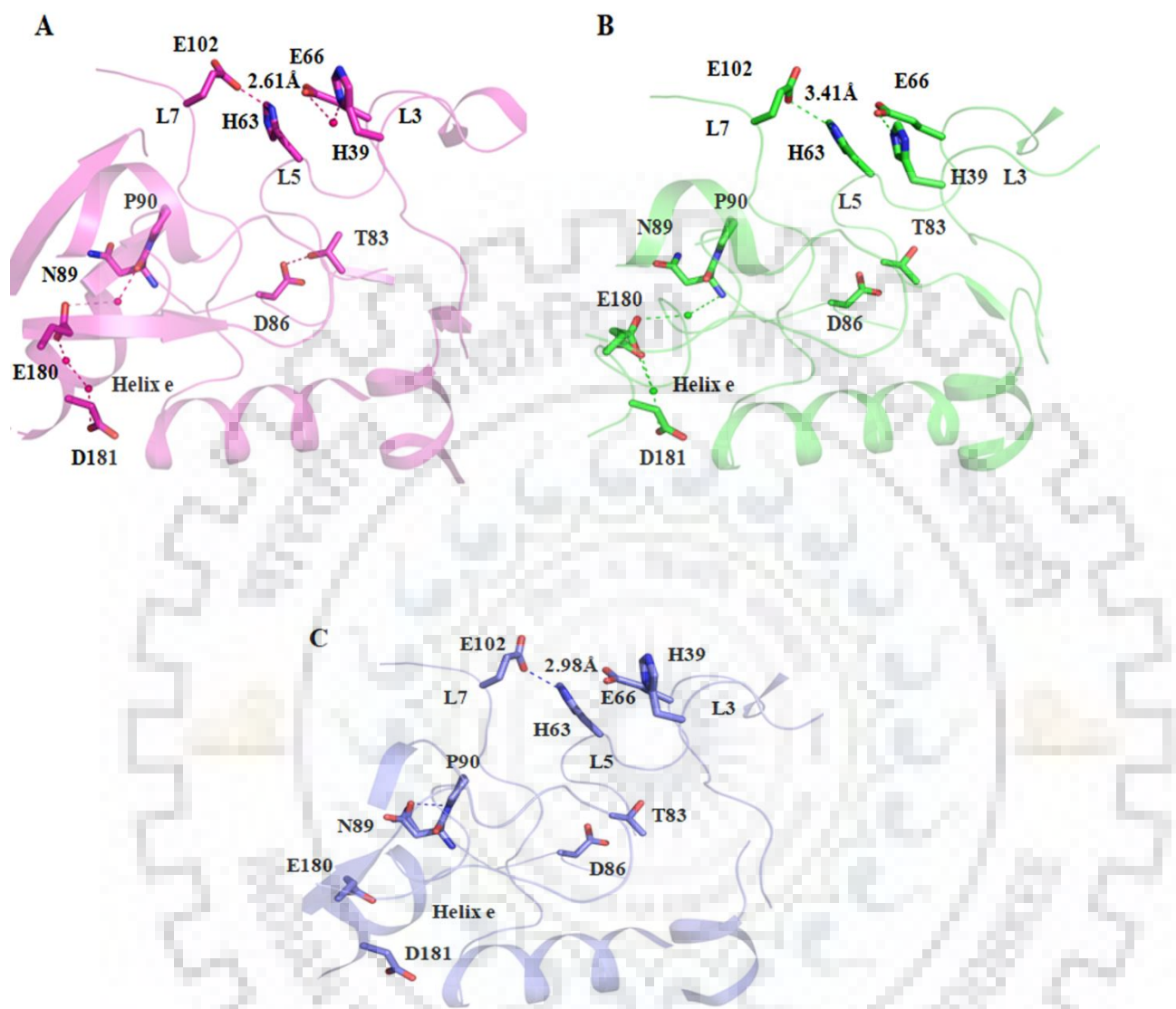


**Fig. 2.17:** The comparison of interactions between L3, L5, L7 and Helix e are shown in metal-free state of A) wild-type CLas-ZnuA2, B) S38A CLas-ZnuA2, and C) Y68F CLas-ZnuA2.

## 2.5. Conclusion

In conclusions, the high resolution crystal structures of two CLas-ZnuA2 mutants demonstrated the role of critical residues, apart from primary metal-binding residues, in preserving the intricate network of interactions important for structure and function of the protein. Both S38A and Y68F mutations in CLas-ZnuA2 resulted in the notable alterations in the network of interactions which might affect the mechanism of action of the protein. The C-domain of S38A CLas-ZnuA2 and Y68F CLas-ZnuA2 are made up of shortened  $\beta$ -sheets in metal-free state and metal bound states respectively, while no differences was observed in metal-bound S38A CLas-ZnuA2 and metal free Y68F CLas-ZnuA2.

The S38A mutation in CLas-ZnuA2 showed major changes in structure and interactions at domain interface in loop L3 at the opening of metal-binding cleft. The metal-free state of S38A CLas-ZnuA2 showed major sideward shift of part of L3 including residue 36-43 as compared to metal-free wild-type CLas-ZnuA2, where L3 is displaced away from metal-binding cleft exhibiting an open conformation. This shift seems to be due to change in the interaction between Ser38 and Tyr68. In wild-type CLas-ZnuA2, side chain of Ser38 and Tyr68 forms hydrogen bond, while after mutation of Ser to Ala, this particular hydrogen bond ceases to exist and now the Tyr68 form hydrogen bond with main chain oxygen of Ala38. The inward shift of part of L3 observed in S38A CLas-ZnuA2 in metal-free state occurs only on metal-binding in presence of high metal-ion concentration in wild-type CLas-ZnuA2. The mutation of S38A demonstrated that the sliding of Ser38 present on restrained L3 during metal-binding is part of the metal-binding mechanism for this low metal-binding affinity protein. The mutation to Ala leads to disruption of that mechanism along with disruption of intricate network of interactions affecting the overall fine-tuned structure. The Y68F mutation completely abolished any interaction between mutated Phe68 and Ser38 and therefore the interplay of interactions during metal-binding and release. No sideward shift of part of L3 and change in interactions of main-chain oxygen of Ser38, like S38A CLas-ZnuA2, were observed in metal-free state of Y68F CLas-ZnuA2. It showed almost similar structure as wild-type CLas-ZnuA2. There were notable changes in interactions of metal coordinating residues with second shell residues and water as compared to wild-type metal-free and metal-bound structures of CLas-ZnuA2. Although the thermal and binding affinity studies did not show significant change as compared to wild-type CLas-ZnuA2 may be due to very low metal-binding affinities, which can be

explained by mutation in PsaA protein. In this, two disulphide bonds were engineered at the C-terminal helix and studied that cross-linking resulted in the significant decrease in the binding capacity of the Cys-mutant PsaA for  $Mn^{2+}$  and  $Zn^{2+}$ . However, P153A, E159A, P153A/E159A and N193A mutations in CLas-ZnuA2 resulted in destabilization and degradation suggests the major disturbance of internal communication in fine-tuned structure.



## CHAPTER 3

# CLONING OF *ZnuA1* FROM *CANDIDATUS LIBERIBACTER ASIATICUS* AND STRUCTURE BASED IDENTIFICATION OF INHIBITORS AGAINST *ZnuA1*

---

### 3.1. Introduction

Huanglongbing (HLB), also known as citrus greening, is one of the most destructive diseases of citrus, causing substantial losses in citrus fruit production throughout the world [255]. HLB is related with three species of phloem-limited, gram-negative fastidious  $\alpha$ - proteobacteria: ‘*Candidatus Liberibacter asiaticus*’ (Las), ‘*Ca. L. africanus*’ (Laf) and ‘*Ca. L. americanus*’ [146, 267, 268]. Of the three species, *Ca. L. asiaticus* is widely distributed and most virulent strain. It is transmitted by Asian citrus psyllid (*Diaphorina citri* Kuwayama) [169]. HLB symptoms include blotchy chlorosis /mottling of leaves, yellow shoot, stunted growth, vein corking, and fruits are small, green, lopsided and contain aborted seeds [269]. HLB is difficult to manage, and currently, no cure is available for infected trees. The recommended control strategy is to chemically control the psyllids and removal of the infected trees [270]. In this study, CLas-ZnuA1, first, of the two gene clusters of Znu system, protein was selected as a target for virtual screening and molecular docking to identify the compounds against the *Candidatus Liberibacter asiaticus*.

Uptake of the metal ion is critical for vitality and growth of bacteria in the atmosphere as well as within the host [271]. Among transition metal, Zinc is essential for the various biological process since it is used as cofactors for a very wide number of enzymes and proteins involved in DNA replication, cell wall synthesis and oxidative stress management [25]. Additionally, it is bound to several proteins involved in the gene expression management, [272], RNA polymerase [273], tRna synthetases [274].  $Zn^{2+}$  metal ions sequestration or uptake is possible through bacterial ABC-metal ions transport system, belongs to the Cluster A-1 family of solute binding protein. This system comprises three proteins; ZnuA, ZnuB, and ZnuC. ZnuB is integrated into the membrane, ZnuC is an ATPase component of ABC transporter system and, ZnuA is a soluble periplasmic component which efficiently captures the Zn(II) in the cellular compartment and delivers to the membrane permease whose opening is regulated by channel ATPase.

Prior microbial pathogenesis studies stated that bacteria compete with their host for Zn (II). In spite of the apparent abundance of Zn in the host cell, most of the zinc is tightly bound to proteins, only picomolar range is available for infectious bacteria [272]. Therefore, bacteria must produce high-affinity importer for growth and multiplication in the host. Notably, it becomes clear that ZnuABC transporter play a major role in bacteria pathogenicity as evidence by series of investigation that its disruption dramatically reduced the pathogenicity and colonization of host in various bacteria. Bacterial pathogen which has been shown to critically dependent on ZnuABC to infect their hosts such as *Salmonella enterica* [141, 142], pathogenic *E. coli* strains [138, 140] and *Campylobacter jejuni* [275].

Several crystal structure have been described for metal-free state and metal-bound closed forms for Zinc transporting SBPs belongs to Cluster A-family [66, 93, 99, 113]. An overall structural organization consists of two sandwich domain connected through a long backbone of linker  $\alpha$ -helix running across the two domains. The inter-domain cleft comprises the metal binding site. Thus, affecting the binding process of Zinc metal ion by identifying small molecule inhibitor at the metal binding site will intrude the function of CLas-ZnuA1 and thus stop the uptake of metal ion, and this could lead to the discovery of potent antibacterial agent against the pathogenic bacteria.

In the present study, CLas-ZnuA1 gene has been cloned. Homology modeling was used for the prediction of the 3-dimensional structure of CLas-ZnuA1 for the screening of novel lead compound through virtual screening from the ZINC database. 50 molecules were screened fulfilled the Lipinski rule of five. Out of 50, 10 molecules were showing maximum binding affinity. Molecular docking program, AutoDock Tools and AutoDock Vina showed that 5 compounds having more binding affinity score as compared to reference molecule RDS51(PDB ID: 4BBP). In order to better understand the stable behaviour of the CLas-ZnuA1-inhibitor(s) complexes, complexes were subjected to molecular dynamics (MD) simulation and molecular mechanic/Poisson-Boltzmann surface area (MMPBSA) binding free energy calculations. This newer approach will be helpful in designing the antibacterial agent against pathogenic bacteria CLA to control the spreading of Huanglongbing disease in the citrus world.



## 3.2. Material & Method

### 3.2.1. Cloning and expression of CLas-ZnuA1

Isolation of genomic DNA of CLA from HLB infected sweet orange plants (*Citrus sinensis*) was performed at Nagpur, Maharashtra. CLas ZnuA1 gene (CLIBASIA\_03020) encoding protein of 272 amino acids lacking signal peptide was amplified using specific forward (ZnuA1 F; 5'- AAT ACA TAT GGG TTC TTT GCA AGT GGT TGT CTC -3' ) and reverse (5'- GGT ACT CGA GTC AAC AGT TCT TAG CTA TTG AAT TAG AC -3') primers with NdeI and XhoI restriction sites respectively. The 50  $\mu$ L of PCR amplification mixture had 5 $\mu$ L of 5X reaction buffer, 1 $\mu$ L of dNTP mixture (each dNTP, 2.5 mmol/ $\mu$ L), 1 $\mu$ L of each primer (20 pmol/ $\mu$ L), 2  $\mu$ L of the template DNA (100 ng/ $\mu$ L) and 0.5 $\mu$ L of Taq DNA polymerase enzyme (New England BioLabs, USA). The Thermocycler program was set as initial denaturation occurred at 94°C for 4 min trailed by 32 cycles at 94°C for 45 s, at 58°C for 45 s, at 72°C for 90 s, and further final extension was at 72°C for 10 min and finally stored at 4°C. Further, purification of PCR product was done using QIAquick Gel Extraction Kit (QIAGEN, Germany). The restricted amplicon was ligated in restricted pET-28c and transformed in *E. coli* XL1-Blue cells and sequenced from Eurofins Scientific India Pvt Ltd, Bengaluru, India. The recombinant expression vector pET-28c having CLas-ZnuA1 insert was transformed into freshly prepared *E. Coli* BL21 DE3 host cells for expression in the presence of antibiotics; kanamycin (30  $\mu$ g/ml) and chloramphenicol (35  $\mu$ g/ml). Expression was tried to optimize using the different concentration of IPTG (0.1-1.0mM) at different temperatures (16-37 °C).

### 3.2.2. Sequence analysis

Initially, BLAST tool was used for sequence search at the NCBI website ([www.ncbi.nlm.nih.gov](http://www.ncbi.nlm.nih.gov)). SignalP 3.0 server was used for prediction of putative signal peptide [276]. The ProtParam (<http://web.expasy.org/protparam/>), an expasy tool was used for determination of Physico-chemical properties, such as GRAVY (grand average of hydropathy), aliphatic index (AI), extinction coefficients, isoelectric point (pI), and molecular weight. Multiple sequence alignment was performed by Clustal Omega web server (<http://www.ebi.ac.uk/Tools/msa/clustalo/>) with default parameters and sequence similarity was rendered by Esprict 3.0 (<http://esprict.ibcp.fr/ESPrict/ESPrict/>) [277, 278]. Phylogenetic

analysis was made using MEGA X program from the alignment of amino acid utilizing the Maximum Parsimony method [279-281]. The validation of the tree branch was examined by the bootstrap test (500 replicates).

### **3.2.3. Homology modeling and Structure validation**

Homology model of CLas-ZnuA1 was built by using Phyre2 involving four steps: fold assignment, sequence alignment, model building and model refinement [282]. The refinement of the disordered loop regions of the model was performed using ModLoop program [283]. Swiss PDB Viewer 4.10 has been utilized for the energy minimization of the predicted model [284]. Structure analysis validation server, PROCHECK was used to check the quality of the predicted model [261]. The Figure of the model was prepared using Chimera [265].

### **3.2.4. Virtual screening**

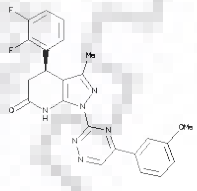
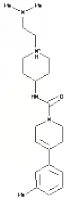
Drug like molecules were retrieved from ZINC DATABASE (<http://zinc.docking.org>), further energy minimization and changed to pdbqt format using Open Babel in PyRx 0.8 for virtual screening [285-287]. All the retrieved compounds were subjected for molecular docking against the Zn binding site of modeled protein by using PyRx 0.8 along with AutoDock Vina [286]. The grid for molecular docking calculations was centered on Zn binding site of the CLas-ZnuA1 protein. An online tool SWISSADME was used to check the molecular properties i.e. Lipinski rule of five of the screened ligand subsets [288, 289]. This rule states that most “drug-like” molecules exhibit molecular weight  $\leq 500$  Da,  $\log P \leq 5$ , number of hydrogen bond donors  $\leq 5$ , and number of hydrogen bond acceptors  $\leq 10$ .

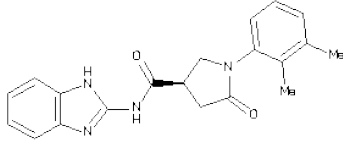
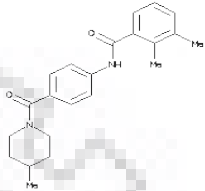
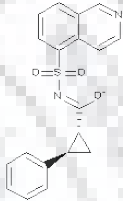
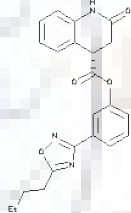
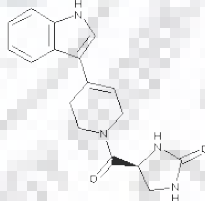
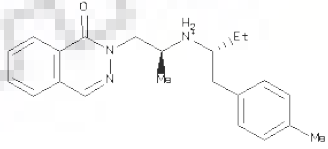
### **3.2.5. Molecular docking**

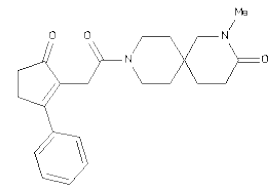
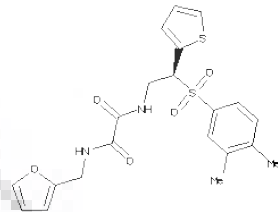
AutoDock was used to carry out the docking of screened compounds with modeled CLas-ZnuA1 protein. AutoDock uses a semi-empirical free energy force field to determine the binding free energy of ligands to protein receptor. AutoDock Tools 4.2.6 was used to add the explicit hydrogen molecules and associated Kollman charges (8.028) to the receptor molecule and saved in pdbqt format [290]. 10 compounds used for docking with model are: ZINC15670529, ZINC92774705, ZINC06510089, ZINC79841324, ZINC69594834, ZINC67523096, ZINC89866566, ZINC90938461, ZINC91444996 and ZINC9104096. Already reported RDS51

(PDB ID: 4BBP) which showed concomitant binding with Zn(II) in *SeZnuA* was used as positive control [97]. RDS51 was docked with CLas-ZnuA1 and compared with binding affinity scores of CLas-ZnuA1-inhibitor complexes. The chemical name and structure of all compounds are shown in Table. 3.1 and 3.2. Gasteiger charges were added to the ligand and saved in pdbqt format. The torsional degrees of freedom of ligand molecule were specified by ligand flexibility. AutoGrid 4 was utilized to generate the grid map with a spacing of 0.375 Å. The grid for the molecular docking was created by selecting the key residue involved in the binding of Zn to CLas-ZnuA1. The dimension and centre point coordinates of the grid box were set as 60 Å x 60 Å x 60 Å and 46.958, -16.172, -4.658 respectively. Lamarckian genetic algorithm was used for molecular docking. Default parameters were used for docking; only total GA runs number was increased from 10 to 100. The highest binding affinity pose was studied along with interactions. PyMol protein viewer tool was used for structural analysis and visualization of the protein [264]. Molecular docking interactions figures were prepared using PyMol and Maestro [291].

**Table 3.1: Chemicals name and structures of selected compounds from the ZINC database.**

S.No	Compound ID	Chemical name	Structure
1.	ZINC15670529	(4R)-4-(2,3-difluorophenyl)-1-[5-(3-methoxyphenyl)-1,2,4-triazin-3-yl]-3-methyl-5,7-dihydro-4H-pyraz	
2.	ZINC92774705	N-[1-(2-dimethylaminoethyl)-4-piperidyl]-4-(m-tolyl)-3,6-dihydro-2H-pyridine-1-carboxamide	

3.	ZINC06510089	N-(1H-benzoimidazol-2-yl)-1-(2,3-dimethylphenyl)-5-oxo-pyrrolidine-3-carboxamide	
4.	ZINC79841324	2,3-dimethyl-N-[4-(4-methylpiperidine-1-carbonyl)phenyl]benzamide	
5.	ZINC69594834	1R,2R)-N-(5-isoquinolylsulfonyl)-2-phenyl-cyclopropanecarboxamide	
6.	ZINC67523096	3-(5-butyl-1,2,4-oxadiazol-3-yl)phenyl	
7.	ZINC89866566	(4S)-4-[4-(1H-indol-3-yl)-3,6-dihydro-2H-pyridine-1-carbonyl]imidazolidin-2-one	
8.	ZINC90938461	2-[(2S)-2-[[[(1R)-1-(p-tolylmethyl)propyl]amino]propyl]phthalazin-1-one	

9.	ZINC91444996	4-methyl-9-[2-(5-oxo-2-phenyl-cyclopenten-1-yl)acetyl]-4,9-diazaspiro[5.5]undecan-3-one	
10.	ZINC9104096	N-[2-(3,4-dimethylphenyl)sulfonyl-2-(2-thienyl)ethyl]-N'-(2-furylmethyl)oxamide	

**Table 3.2: Chemicals formulae of selected compounds from ZINC database.**

S.No.	Compound ID	Chemical formula
1.	ZINC15670529	C23H18F2N6O2
2.	ZINC92774705	C22H35N4O
3.	ZINC06510089	C20H20N4O2
4.	ZINC79841324	C22H26N2O2
5.	ZINC69594834	C19H15N2O3S
6.	ZINC67523096	C22H21N3O4
7.	ZINC89866566	C17H18N4O2
8.	ZINC90938461	C22H28N3O

9.	ZINC91444996	C23H28N2O3
10.	ZINC9104096	C21H22N2O5S2

### 3.2.6. Molecular dynamics simulation

The binding stability and dynamics of CLas-ZnuA1-RDS51 and CLas-ZnuA1-inhibitors complexes at the atomistic level were studied by Molecular dynamic simulation. The simulation studies were carried out using GROMOS96 43a1 force field in Gromacs 5.1.4 suite on ubuntu based LINUX workstation [292, 293]. The topology files of the small molecules (RDS51, ZINC15670529, ZINC92774705, ZINC06510089, ZINC79841324, and ZINC69594834) were generated using PRODRG [294]. The protein complexes were solvated in a cubic box of volume 716.31 nm<sup>3</sup> with 1nm marginal radii using SPC (simple point charges) model and counter ions (Na<sup>+</sup>) were added to neutralize the system [295]. To minimize the steric clashes, energy minimization was performed by utilizing algorithm; steepest descent for 5000 iteration steps and cut off was kept up to 1000 kJmol<sup>-1</sup>. Two different equilibration phases were carried out for 5,00,000 steps. The first phase of equilibration includes the constant number of particles, volume and temperature (NVT) for 1ns. Further, the second phase of equilibration involved the constant number of particles, pressure, and temperature (NPT) at 300K, for each step of 2fs. Covalent bond constraints were done using the LINCS algorithm. Coulomb interaction and Lennard- jones were calculated within a cut off radius of 1.4 nm. Particle Mesh Ewald (PME) with 1.6Å Fourier grid spacing was used for calculation of Long-range electrostatics [296]. A modified Berendsen temperature coupling method, V-rescale was used to regulate the internal temperature of the box. NPT equilibration was maintained using Parrinello- Rahman pressure coupling method. The molecular dynamics simulation run of 20 ns was performed with a time step of 2 fs. The RMSD (Root Mean Square Deviation), RMSF (Root Mean Square Fluctuation), Hydrogen bonds were determined using g\_rms, g\_rmsf, and g\_hbond respectively, within the GROMACS suite [292]. A roughly measurement of compact factor and solvent accessible surface area (SASA) of protein was estimated using g\_gyrate tool and gmx\_sasa during simulation.



### 3.2.7. MMPBSA binding free energy calculation

The Binding free energy of CLas-ZnuA1- RDS51 and CLas-ZnuA1- Inhibitor(s) complexes was calculated using g\_mmpbsa tool [297]. This software employs the Molecular Mechanic/Poisson-Boltzmann Surface Area (MMPBSA) method for calculation of the binding free energy of interaction between protein-inhibitor(s) complexes. This tool determines the Molecular mechanic's potential energy (Van derWaals interaction + electrostatic) and solvation free energy (polar + non polarsolvation energies). Average of these energy terms indicates the binding energy. In the present work, the snapshots for every 10 ps for last 5 ns i.e. between 15 ns to 20 ns were collected and predicted the binding energy.

## 3.3. Results

### 3.3.1. Cloning and expression of CLas-ZnuA1

The CLA genomic DNA was isolated from the infected citrus plant at NRCC Nagpur. The presence of genomic DNA was confirmed by PCR amplification of 16S rDNA of 1160 bp fragment using primers OI1/OI2c [298]. Directional cloning of the CLas-ZnuA1 gene lacking signal peptide from *Candidatus Liberibacter asiaticus* was performed using restriction digestion. Correct insert size of 816 bp was obtained after PCR amplification and restriction digestion (Fig. 3.1). The sequencing result confirms the correct frame of the insert with no mutation. The recombinant expression vector pET-28c having CLas-ZnuA1 insert was transformed in the *E.coli* BL21 host cells. Different strategies like lowering the expression temperature, changing the IPTG concentration, expression time and different concentration of urea to solubilise the protein were tried but all remained unsuccessful.



**Fig. 3.1: Agarose gel electrophoresis confirming the positive clones.** Lane1 : PCR amplification from the pET-28c plasmid containing CLas-ZnuA1 gene (816bp), Lane2 : restriction digestion of pET-28c containing CLas-ZnuA1, Lane3: 100bp DNA ladder.

### 3.3.2. Bioinformatics analysis of CLas-ZnuA1

#### 3.3.2.1. Prediction of the signal peptide

CLas-ZnuA1 protein sequence (294 amino acids) showed the presence of 21 residues long signal peptide at the N-terminal end as predicted by SignalP 3.0server (Figure 3.2). The nucleotide sequence coding this signal peptide has not been included for cloning.

#### 3.3.2.2. Physico-chemical parameters

Analysis of Different physico-chemical properties using Protparam tool revealed that CLas-ZnuA1 protein has 22920 extinction coefficient, 103.24 aliphatic index, -0.044 grand average of hydrophobicity. The CLas-ZnuA1 protein containing 272 amino acid residues was estimated to have a molecular mass of 30843.72 and isoelectric pH at 6.40.

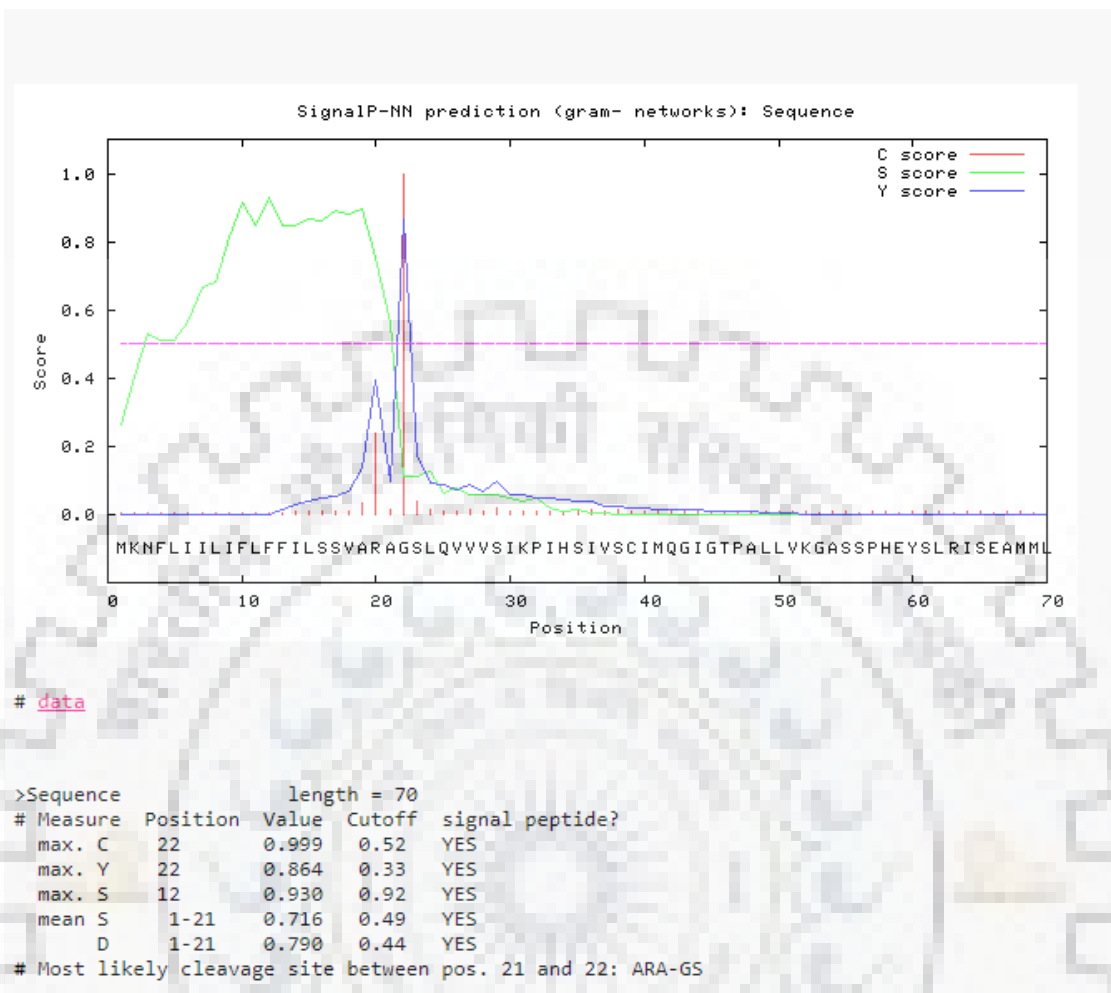


**Figure 3.2: Prediction of the signal sequence in CLas-ZnuA1.** The Signal peptide of length 21 residues (residue 1-21) in the CLas-ZnuA1 sequence as predicted by SignalP 3.0 server.

### 3.3.2.3. Model building and structure validation

The 3-dimensional structure of CLas-ZnuA1 was predicted using Phyre2.0 and Swiss PDB viewer has been used for energy minimization of the predicted model (Fig. 3.3).

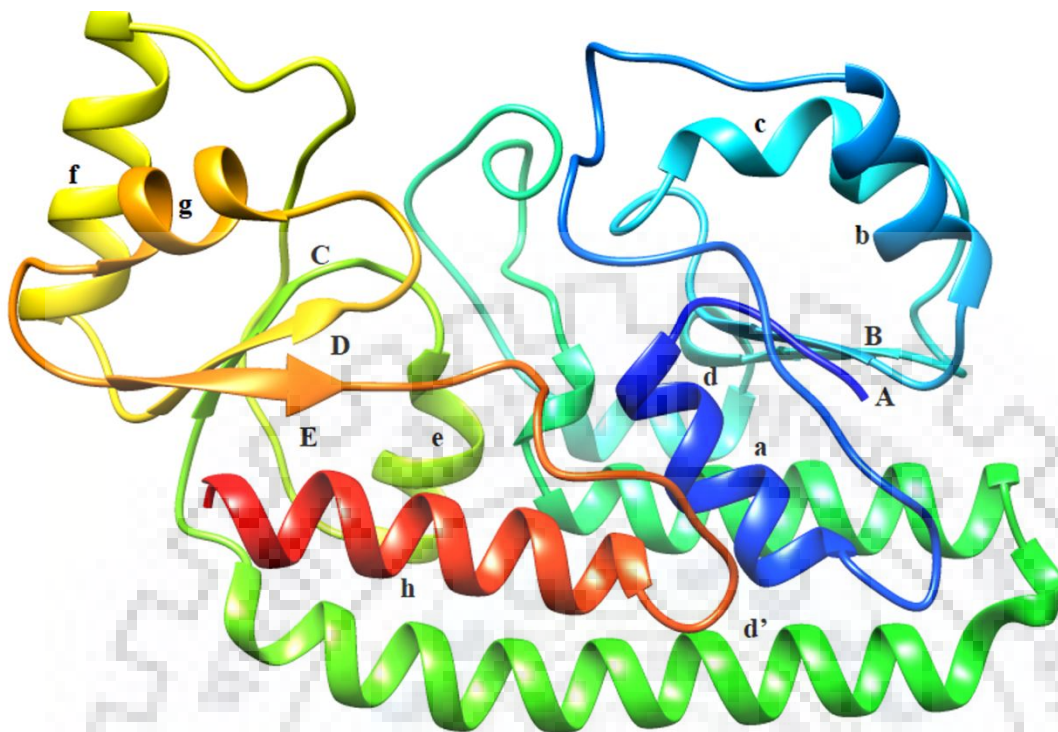


**Fig.3.3:** Cartoon representation of the predicted model of CLas-ZnuA1.  $\beta$ - Strands designated as A-E;  $\alpha$ -helix as a-h (CLas-ZnuA2 nomenclature).

#### 3.3.2.4.Amino acid sequence similarity search by NCBI-BLAST

A sequence similarity search of CLas-ZnuA1 amino acid sequence using NCBI-BLAST search engine in non-redundant (NR) and Protein Data Bank (PDB) databases showed homology to metal-transporting solute binding proteins (SBPs) of TroA like superfamily as classified by NCBI's Conserved Domain Database (CDD). These proteins belong to Cluster A-I family of substrate binding proteins.

When searched against NR database, CLas-ZnuA1 showed maximum sequence similarity to *Candidatus Liberibacter africanus* (69%) and *Candidatus Liberibacter solanacearum* (63%). Other proteins which shared similarity belong to families Rhizobiaceae, Phyllobacteriaceae, Comamonadaceae and Rhodospirillaceae. When searched against PDB database, CLas-ZnuA1 showed maximum sequence similarity to SBPs of Cluster A-1 family including *Salmonella enterica* ZnuA (31%), *Escherichia coli* ZnuA (30%), *Streptococcus pneumoniae* PsaA (27%) and

*Synechocystis* ZnuA (26%). All of the above proteins are involved in binding to Mn, Zn, and Fe. Fig. 3.4. Multiple sequence alignment of CLas-ZnuA1 with the related SBPs *Salmonella enterica* ZnuA, *Escherichia coli* ZnuA *Streptococcus pneumoniae* PsaA (27%) and *Synechocystis* ZnuA of Cluster A-1 family are shown in the Fig. 3.5. MSA showed conserved residues in the related SBPs present in the PDB blast database. These proteins are involved in uptake of Mn, Zn or Fe.

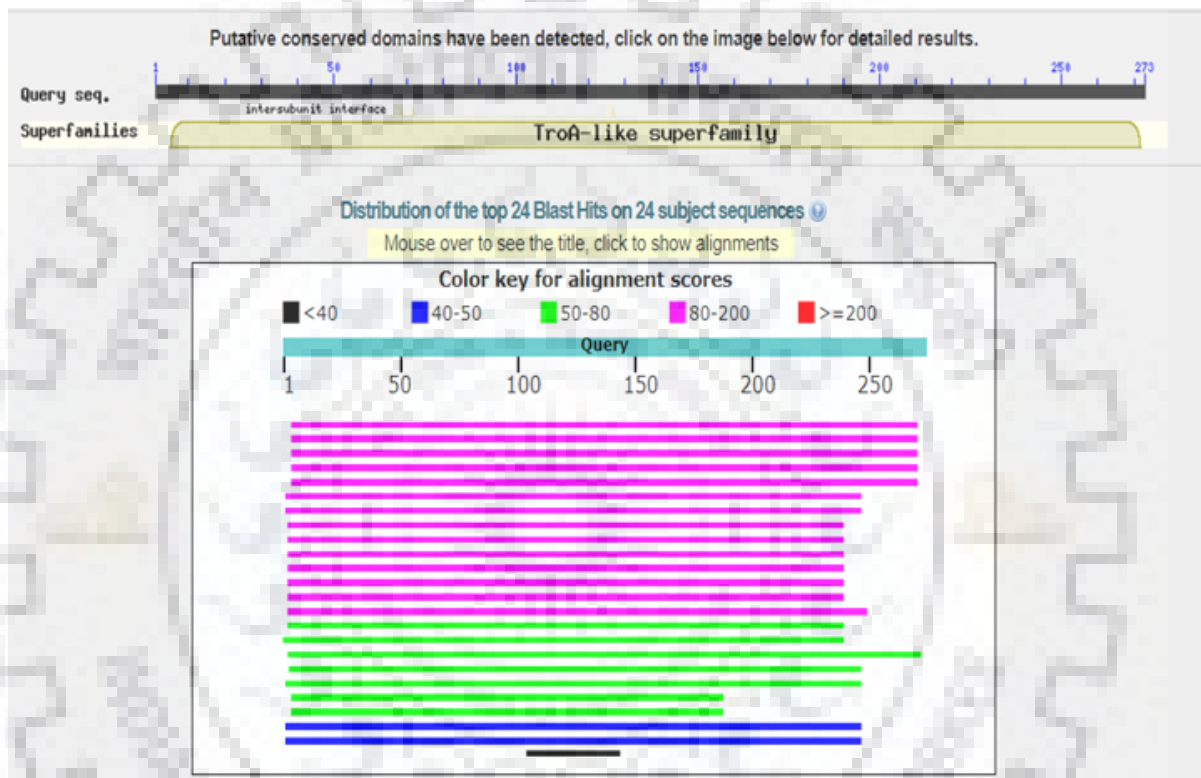


**Fig. 3.4: Sequence similarity search of CLas-ZnuA1 using NCBI BLAST search tool.** Significant similar proteins (maximum 31%) were found in PDB database which belong to Cluster A-I family and involve in divalent metal ion transport.

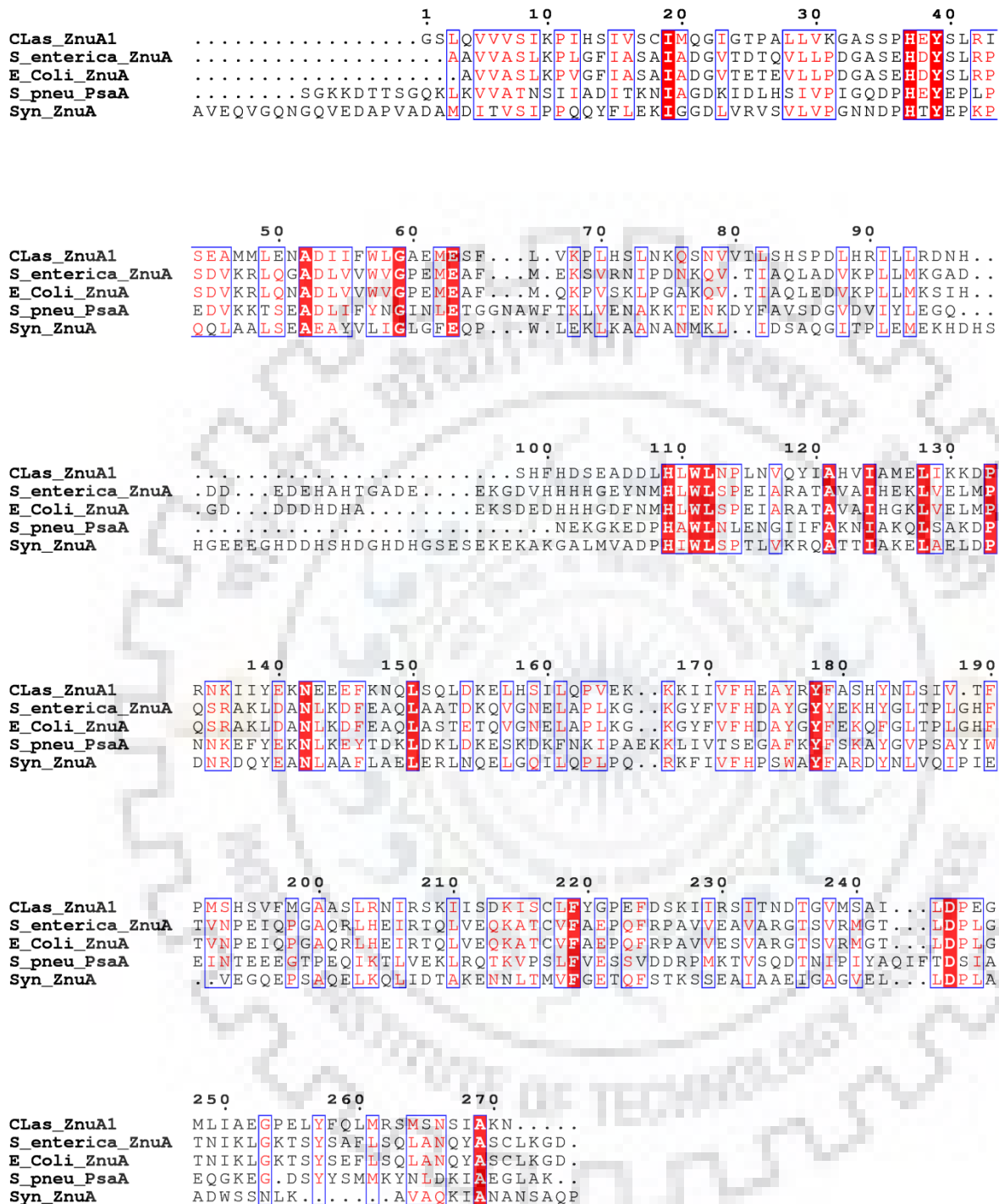


**Fig. 3.5:** Multiple sequence alignment of CLas-ZnuA1 with other related SBPs of cluster A-1 using Clustal Omega web server. The available sequences of Cluster A-1 SBPs in protein data bank, involved in uptake of Mn, Zn or Fe were aligned.



The phylogenetic analysis of related Cluster A-I proteins present in NR database and PDB database is shown in the Fig. 3.6. It includes the protein from NR database and proteins specific for Mn/Fe and Zn specific binding.

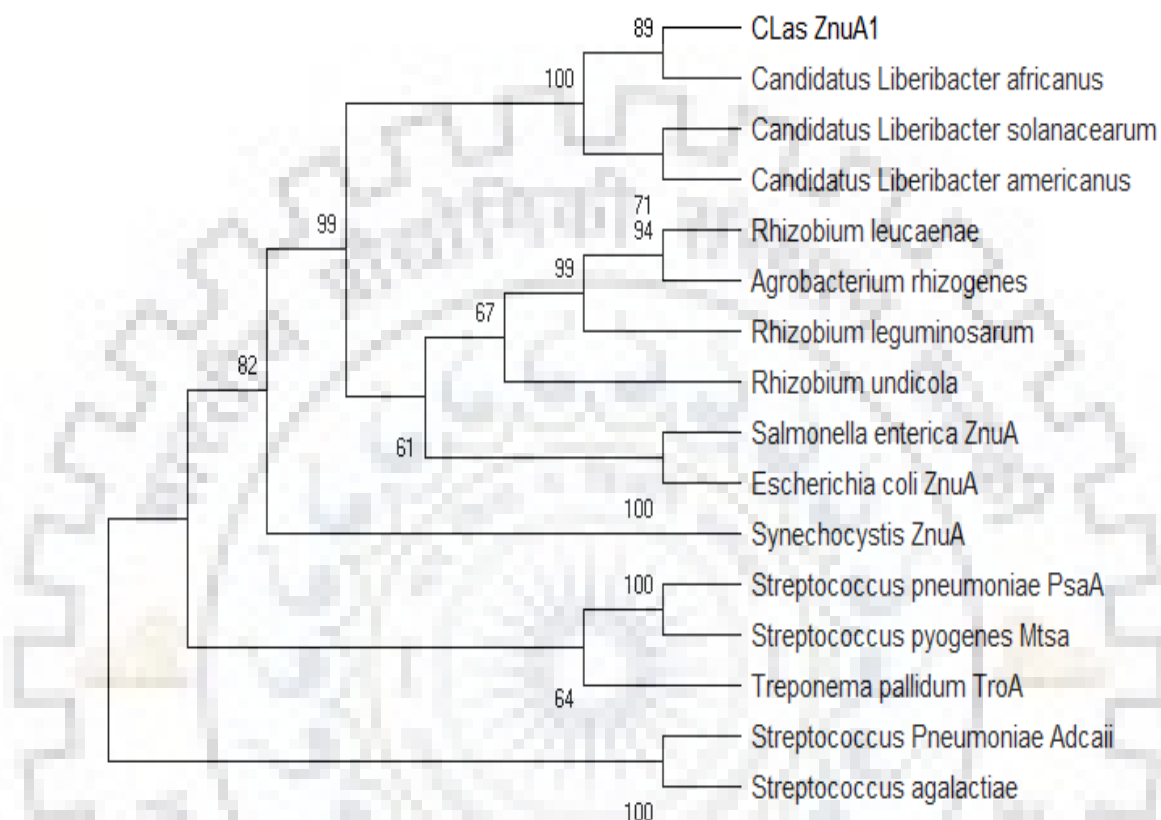


**Fig. 3.6:** Phylogenetic tree of CLas-ZnuA1 and related proteins present in the PDB database and NR database constructed by the maximum parsimony method. The percentage of replicate trees in which the associated taxa clustered together in the bootstrap test (500 replicates) is shown next to the branches. This includes the protein from NR database and PDB database, involved in uptake of Mn, Zn and Fe metal ions. The numbers above and below the branch points indicate the confidence levels for the relationship of the paired sequences as determined by bootstrap statistical analysis. The tree is drawn to scale, with branch lengths measured in the number of substitutions per site.

Ramachandran plot generated by PROCHECK, depicted that 92.7% residues are in the core region, 5.7% residues are in the allowed region, and 1.6% residues are in generously allowed and no residues are in the disallowed region (Fig. 3.7).

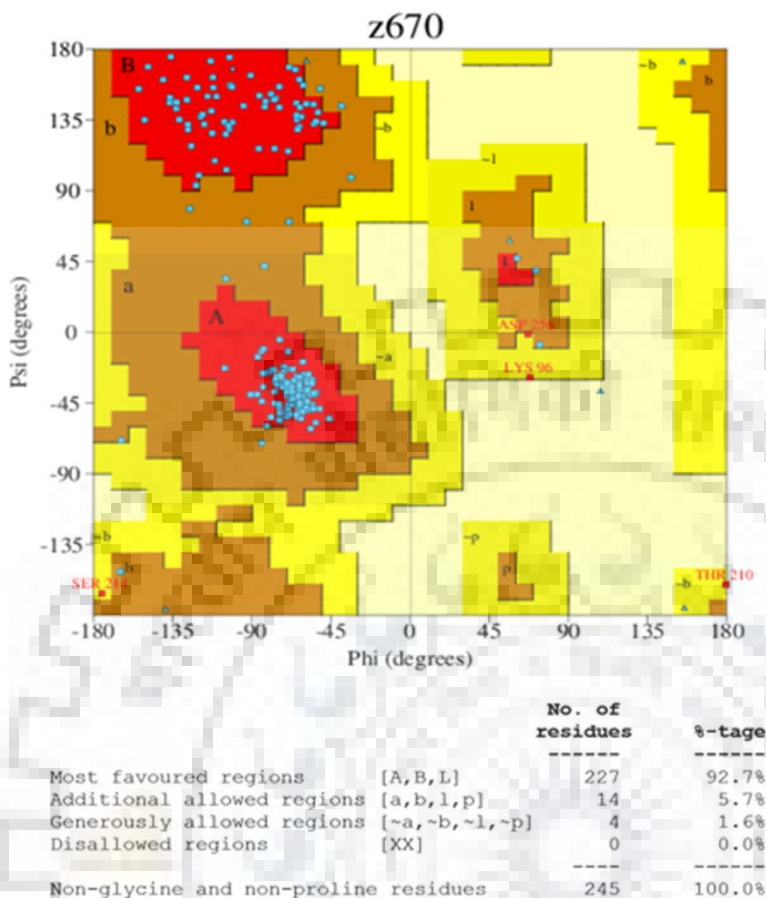


**Fig. 3.7:** Ramachandran plot of CLas-ZnuA1 model, showing the distribution of amino acid based on psi and phi angles using PROCHECK tool.

### 3.3.3. Virtual screening

Drug like compounds in sdf format were retrieved from ZINC database, have been used for virtual screening of model utilizing molecular docking program Auto Dock Vina in PyRx 0.8 [286], and it generates the nine distinct poses of each ligand. Molecular Docking of RDS51 with AutoDock Vina shows -8.7 kcal/ mole, and interaction of residue in binding site His122 and His130. Top 50 compounds were selected by virtual screening showed binding to the active site of the CLas-ZnuA1 protein. The higher binding affinity of screened lead molecules as compared to the reference (RDS51) indicates that they would bind more efficiently into the binding site of CLas-ZnuA1. For evaluation of physico-chemical properties, 50 molecules were sequentially

selected based on Lipinski's rule of five criteria [289]. Out of 50 hits, 10 molecules were chosen on the basis of the maximum binding affinities. The physico-chemical properties of the selected 10 molecules are shown in Table 3.3. But prior to moving further analysis, the binding of these molecules with CLAs- ZnuA1 were cross-checked through another molecular docking program.

**Table 3.3.**

**Lipinski's Rule of Five**

**Physico-chemical properties (molecular weight, LogP, H-bond donor, H-bond acceptor) of all selected ZINC IDs fulfilling the Lipinski rule of five ( $\log P \leq 5$ , molecular weight  $\leq 500$  Da, number of hydrogen bond acceptors  $\leq 10$ , and number of hydrogen bond donors  $\leq 5$ ).**

S.No.	Compounds	Molecular weight (g/mol)	LogP	H-bond donor	H-bond acceptor	Lipinski Drug-likeness
1.	ZINC15670529	448.42	3.38	1	8	Yes; 0 violation
2.	ZINC92774705	371.54	4.14	2	2	Yes; 0 violation
3.	ZINC06510089	348.40	2.02	2	3	Yes; 0 violation
4.	ZINC79841324	350.45	3.40	1	2	Yes; 0 violation
5.	ZINC69594834	351.40	2.36	0	5	Yes; 0 violation
6.	ZINC67523096	391.42	3.62	1	6	Yes; 0 violation
7.	ZINC89866566	310.35	1.81	3	2	Yes; 0 violation
8.	ZINC90938461	350.48	3.27	1	2	Yes; 0 violation
9.	ZINC91444996	380.48	3.18	0	3	Yes; 0

						violation
10.	ZINC9104096	446.54	2.94	2	5	Yes; 0 violation

### 3.3.4. Molecular docking

AutoDock 4.2.6 was utilized for the comparative docking study of RDS51 and potent molecule full filling the Lipinski rule of five criteria. Overall, AutoDock Tools and AutoDock Vina result shows that 5 compounds exhibit more binding affinity as compared to RDS51. Fig. 3.8 shows the electrostatic potential view of selected compounds in the binding site of CLas-ZnuA1.

Molecular docking binding affinities and interactions analysis are shown in Table 3.4. Docking results reveal that five molecules exhibit higher binding affinities in range of -11.13 to -8.71 kcal/mol as compared to RDS51 (-8.03 kcal/mol). RDS51, ZINC92774705 and ZINC69594834 show hydrogen bonding interactions with His122 and His130 as shown in Fig. 3.9. However, other molecules ZINC15670529, ZINC06510089, ZINC79841324 also interact with His122 and founded in the vicinity of His130.

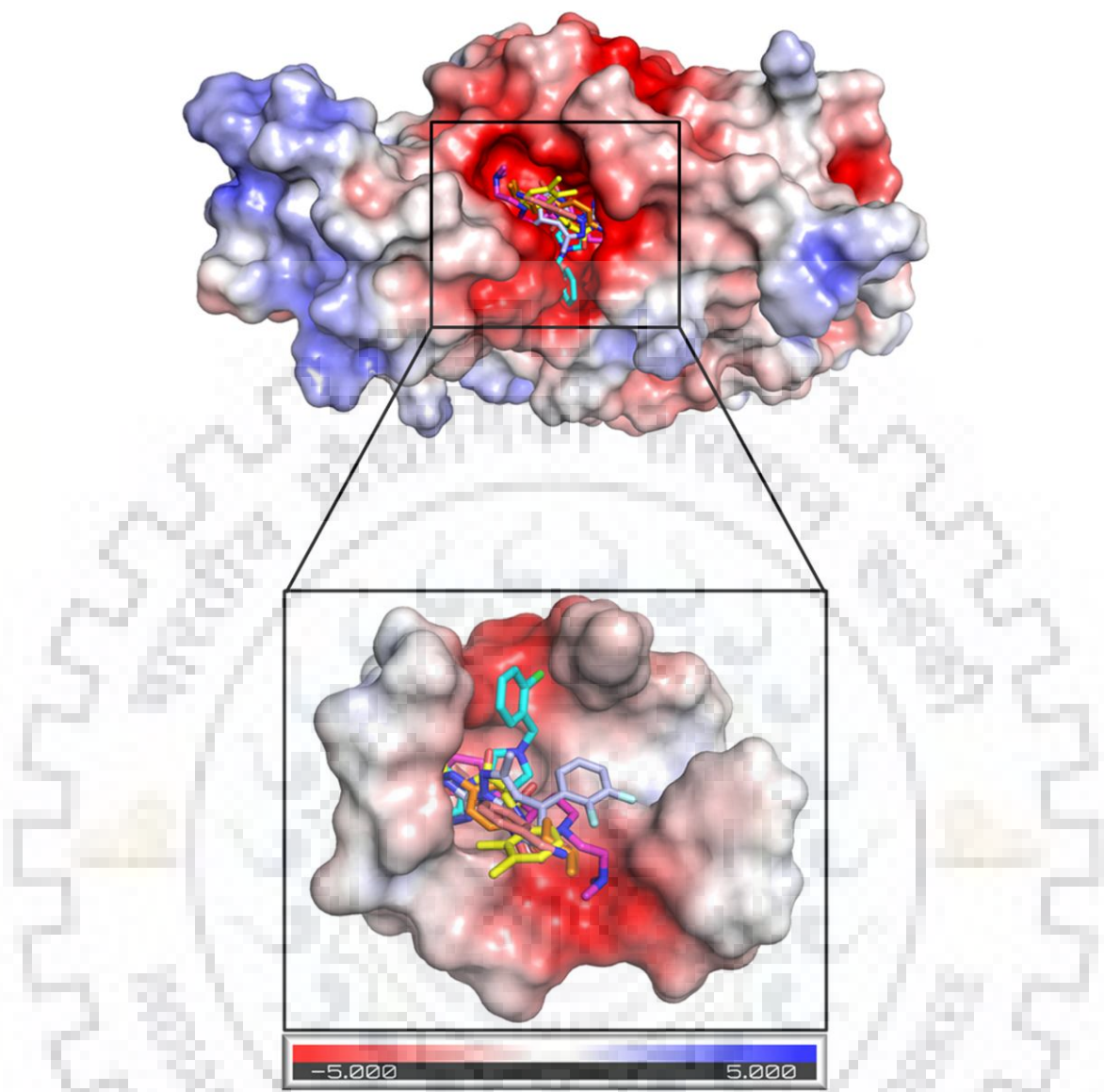
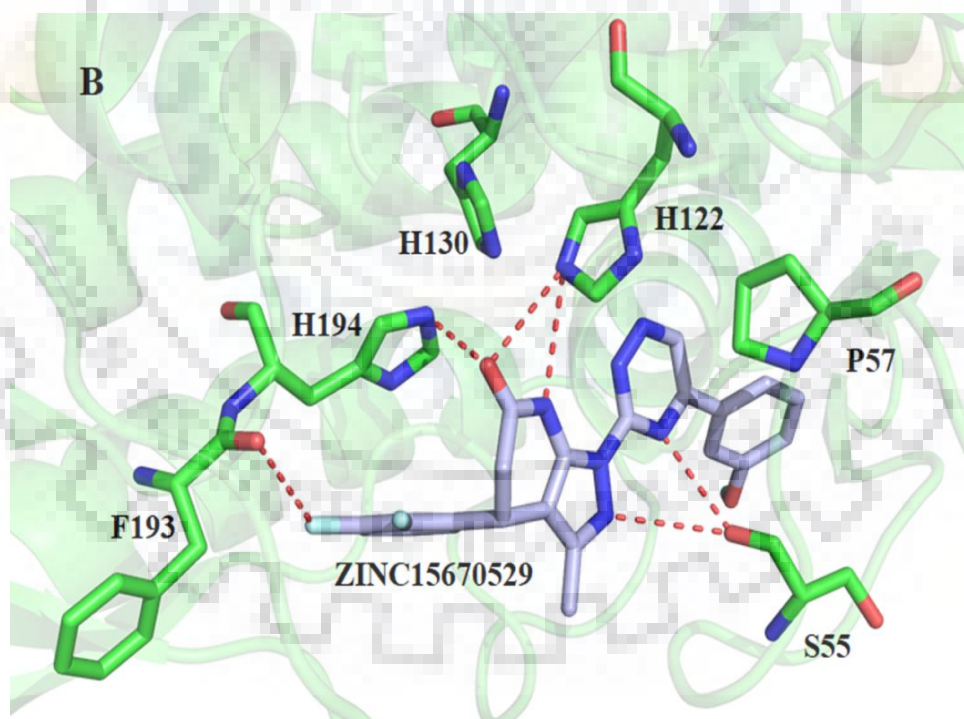
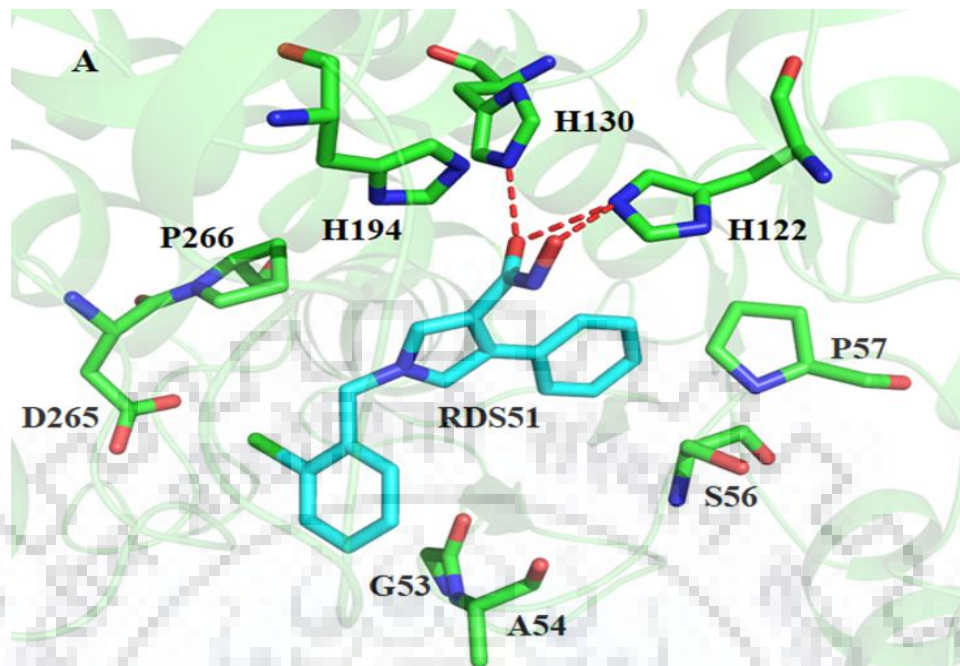


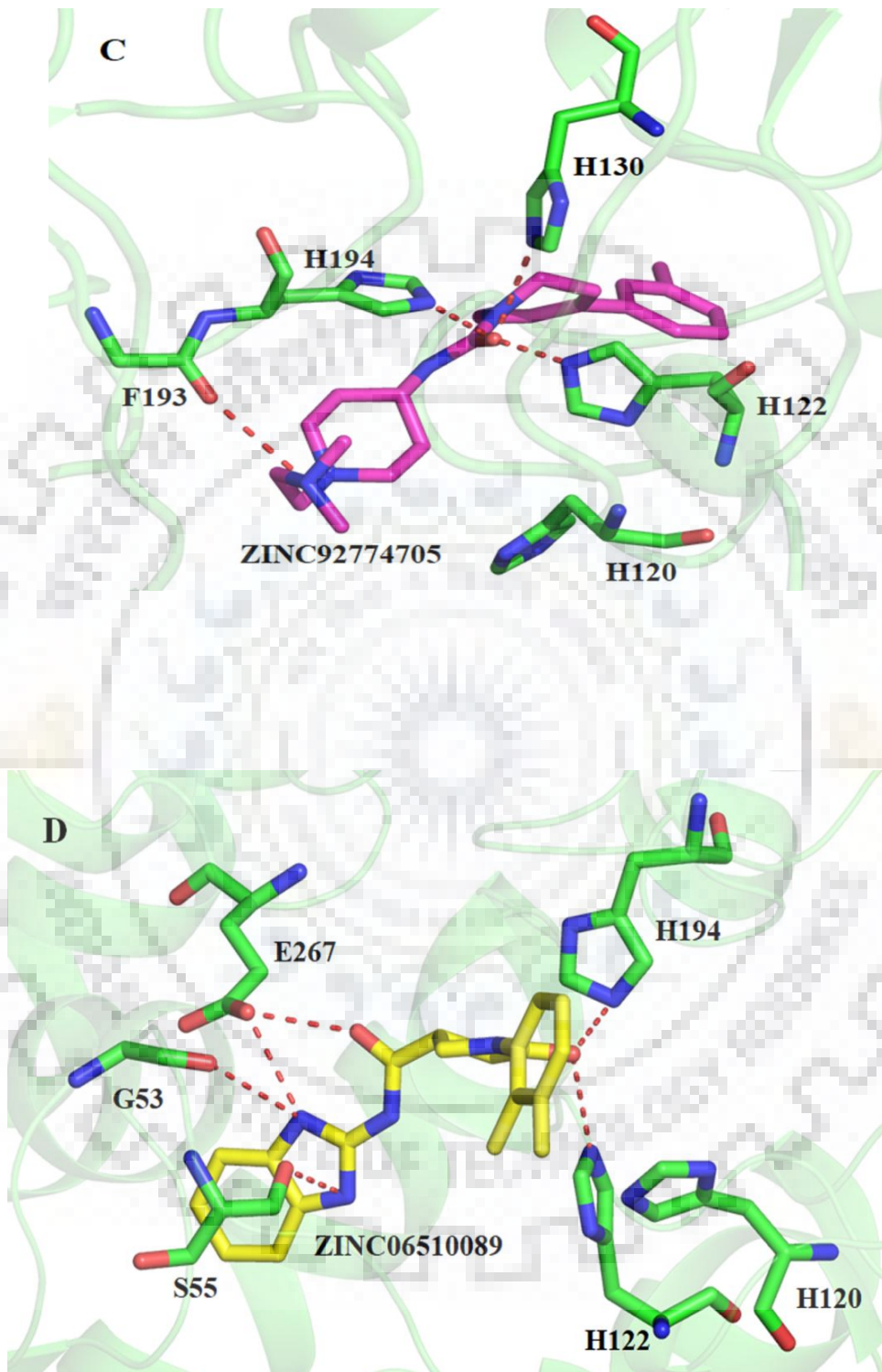
**Fig. 3.8: Electrostatic potential surface view of CLas-ZnuA1 protein.** Zoom window shows the binding pocket with RDS51(cyan), ZINC15670529 (light blue), ZINC92774705 (magenta), ZINC06510089 (yellow), ZINC79841324 (orange) and ZINC69594834 (light red).

**Table 3.4: A detailed summary of the docking binding affinities (kcal/mol) of selected compounds using two different software's (AutoDock Vina and AutoDock) and hydrogen bonding interaction of the CLas-ZnuA1-RDS51 complex and CLas -ZnuA1- inhibitor(s) complexes.**

S.No.	Compounds	AutoDock Vina Binding affinity (kcal/mol)	AutoDock Binding affinity (kcal/mol)	Interacting residues
1.	RDS51	-8.7	-8.03	His122, His130
2.	ZINC15670529	-10.2	-11.13	Ser55, His122, , Phe193, His194
3.	ZINC92774705	-9.1	-10.34	His122, His130, Phe193, His194
4.	ZINC06510089	-9.1	-9.33	Gly53, Ser55, His122,His194,Glu267
5.	ZINC79841324	-9.0	9.49	Ser55, His122, His194
6.	ZINC69594834	-8.9	-8.71	His122, His130, His194







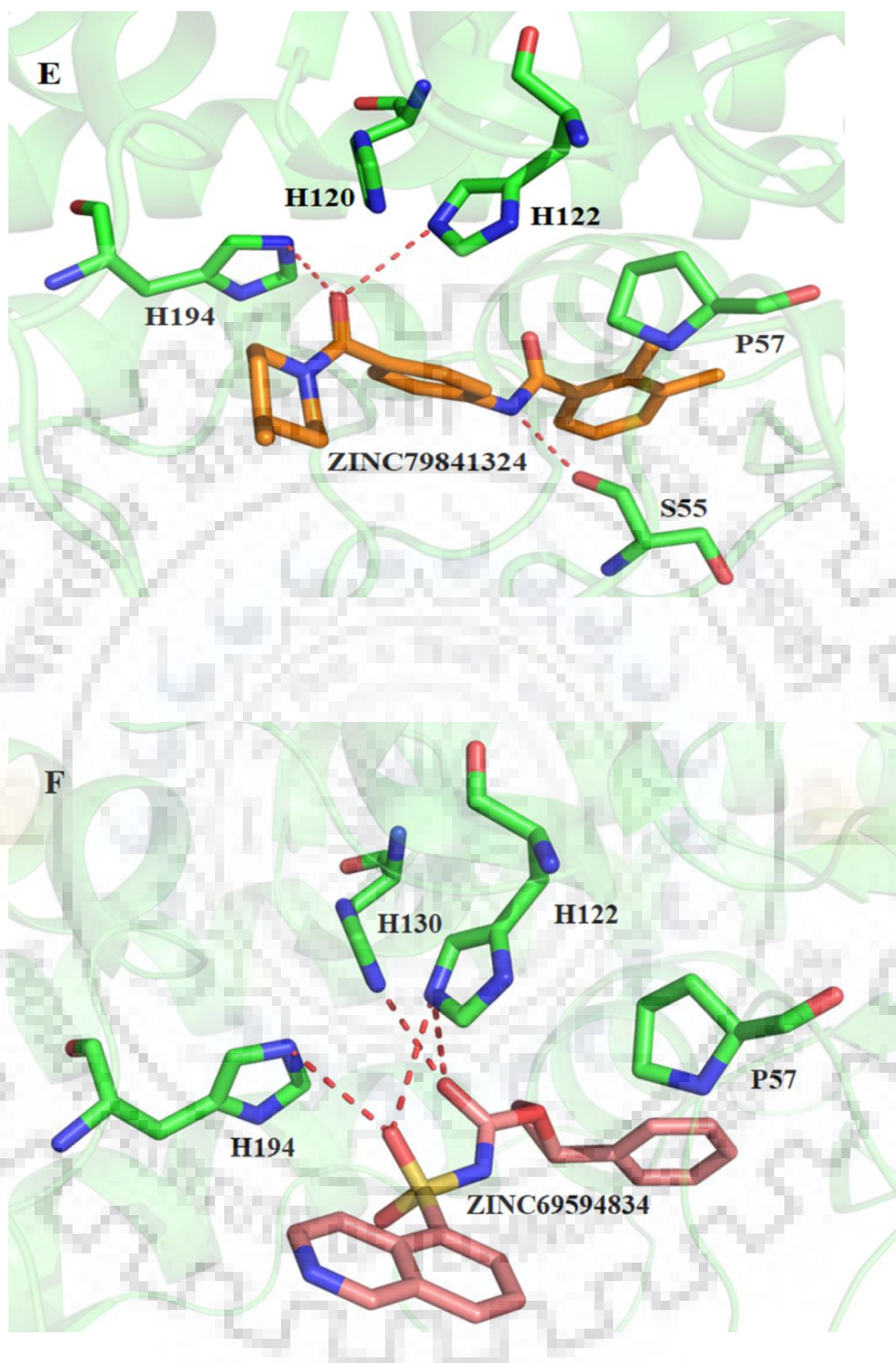


**Fig. 3.9: Docking interaction analysis of A) CLas-ZnuA1-RDS51 (cyan) and CLas-ZnuA1 with B) ZINC15670529 (light blue), C) ZINC92774705 (magenta), D) ZINC06510089 (yellow), E) ZINC79841324 (orange) and F) ZINC69594834 (light red) complexes. Interacting residues of CLas- ZnuA1 are shown in sticks colored by atom type, carbon in green, nitrogen in blue and oxygen in red. The interactions are shown as broken red lines.**

### 3.3.5. Molecular dynamics simulation

Molecular dynamics (MD) simulations were performed to understand the variation occurring in the protein-ligand system at atomistic level and articulate on the stability of the protein-ligand complex in the dynamic environment. The MD simulations have been carried out in order to explore the dynamic movement intricate during binding of inhibitors to CLas-ZnuA1. In the present study, we investigated the various molecular simulation results such as RMSD, RMSF, radius of gyration (Rg), SASA, hydrogen bond formation and length distribution throughout the simulation.

#### 3.3.5.1. Root mean square deviation (RMSD)

The dynamic stability and conformation variation existing in the C $\alpha$  backbone of the CLas-ZnuA1- RDS51 complex and CLas-ZnuA1 inhibitor(s) were studied by monitoring the RMSD of the sampled structure during the simulation. RMSD plot indicates that most of the protein-ligand complexes attained equilibrium at 9 ns and system found to be stable up to 20 ns, during the MD simulation as shown in Fig. 3.10A. The comparison of the average RMSD values of the CLas-ZnuA1-inhibitor(s) complexes with the reference CLas-ZnuA1-RDS51 complex is shown in Table 3.5. The RMSD values show fluctuation within the range of 0.24 nm to 0.38 nm for all complexes. RMSD plots suggested that there is no large changes were observed in the C $\alpha$  backbone RMSD arrangement patterns of the CLas-ZnuA1-inhibitor(s) complexes as compared to CLas-ZnuA1-RDS51 complex. Ligand RMSD of inhibitor(s) and RDS51 is shown in Fig. 3.10B.



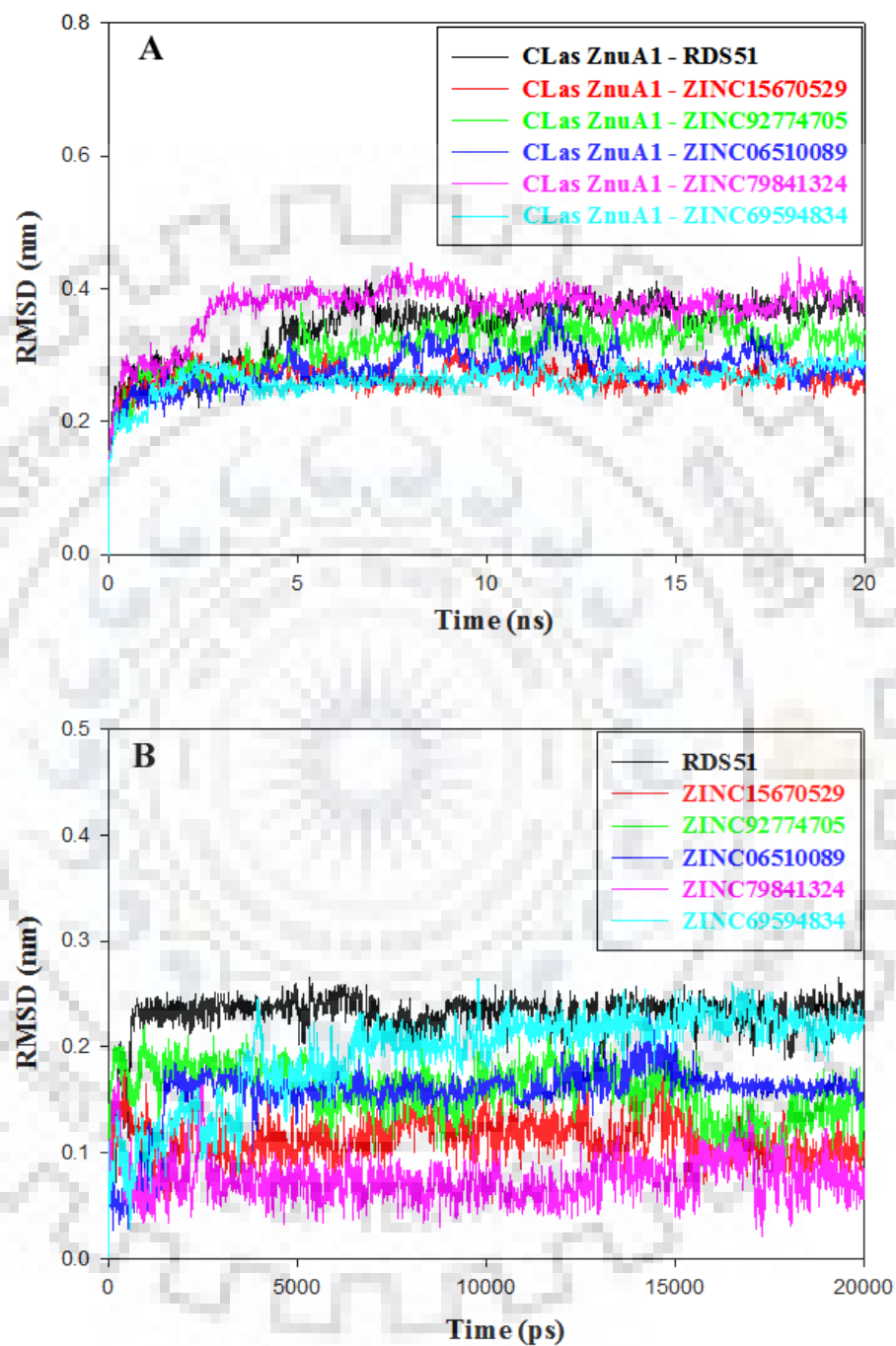


**Fig. 3.10: Root mean square deviation of protein-inhibitor(s) complexes and inhibitor(s) only.** RMSD plots showing; A) CLas-ZnuA1- RDS51 and CLas-ZnuA1- inhibitor(s) complexes, B) reference RDS51(black) and inhibitors: ZINC15670529 (red) , ZINC92774705 (green) , ZINC06510089 (blue), ZINC79841324 (pink) and ZINC69594834 (cyan) for 20 ns MD simulation.

All the inhibitors show less RMSD as compared to the RDS51 (0.25 nm) which clearly suggested that binding of inhibitor(s) are more static and stable as compared to RDS51. Overall RMSD, results show that the binding of inhibitor(s) at the binding site of CLas-ZnuA1 was stable and do not affect the stability of C $\alpha$  backbone of protein.

**Table 3.5: Average values of RMSD , RMSF, radius of gyration, SASA and intra-H bond of CLas ZnuA1-RDS51 complex and CLas-ZnuA1- inhibitor(s) complexes.**

S.No.	Compounds	Average Protein RMSD (nm)	Average ligand RMSD (nm)	Average RMSF (nm)	Average Radius of gyration(nm)	Average SASA (nm) <sup>2</sup>	Intra-H bond numbers
1.	RDS51	0.34	0.23	0.17	1.95	131.37	1307
2.	ZINC15670529	0.27	0.11	0.13	1.89	132.04	1310.6
3.	ZINC92774705	0.31	0.16	0.13	1.90	134.92	1309.3
4.	ZINC06510089	0.28	0.16	0.15	1.89	134.63	1314.6
5.	ZINC79841324	0.37	0.07	0.12	1.87	132.26	1316.2
6.	ZINC69594834	0.26	0.19	0.12	1.94	131.24	1312.1



### 3.3.5.2. Root mean square fluctuation (RMSF)

RMSF calculates the flexibility of the backbone of protein after fitting to the frame of reference. It refers to the fluctuation occur in the C $\alpha$  atoms from its average position throughout the molecular simulation. Generally, the high RMSF values indicate the loosely organized loops, while less flexibility was shown by secondary structural elements in the protein. Here, we determined the residue mobility for each protein-ligand complex and plotted against the amino acid residues number according to MD simulation trajectory. The RMSF fluctuation profiles of CLas-ZnuA1-inhibitors complexes were almost comparable to CLas-ZnuA1-RDS51 complex as shown in Fig. 3.11. The Average RMSF of CLas-ZnuA1-inhibitors are in the range of 0.11 nm to 0.15 nm while the average RMSF value of CLas-ZnuA1-RDS51 is 0.16 nm as shown in Table 3.5. Therefore, the overall results of RMSF showed that the inhibitors were well fitted in the binding cavity of CLas-ZnuA1 and do not much fluctuate in the CLas-ZnuA1 cavity.

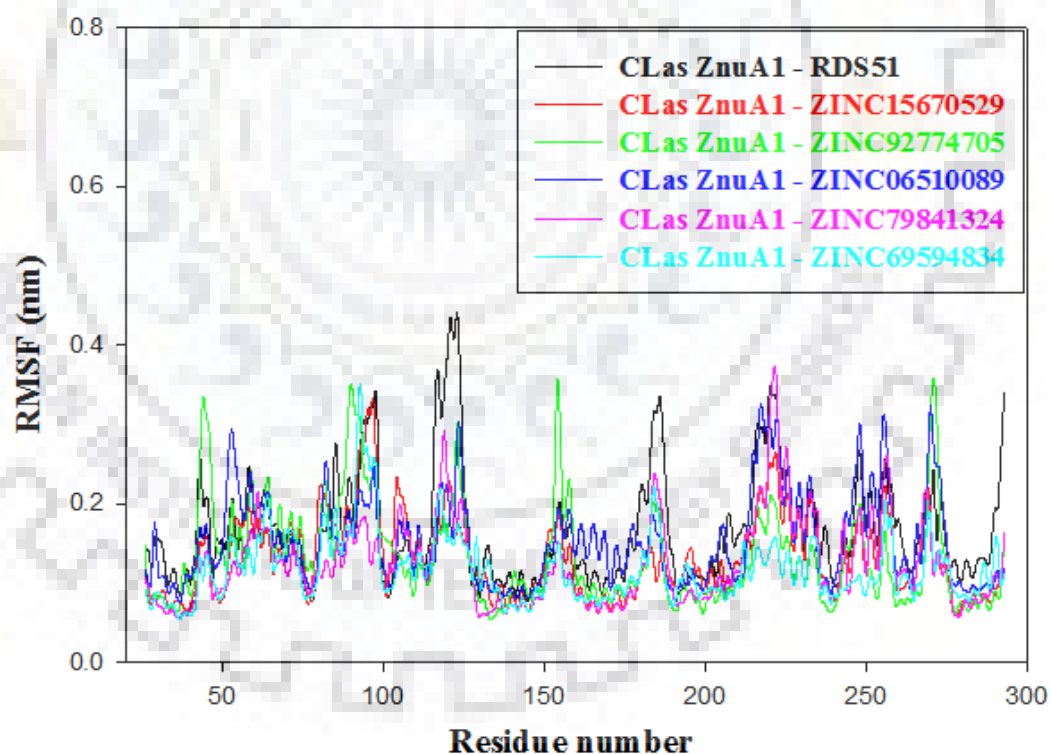


**Fig. 3.11: Root mean square fluctuation profiles of CLas-ZnuA1- RDS51 (black) and CLas ZnuA1- ZINC15670529 (red) , CLas-ZnuA1- ZINC92774705 (green) , CLas-ZnuA1- ZINC06510089 (blue), CLas-ZnuA1- ZINC79841324 (pink) and CLas-ZnuA1- ZINC69594834 (cyan) inhibitor(s) complexes during 20 ns MD simulation.**

### 3.3.5.3. Radius of gyration (Rg)

Radius of gyration (Rg) demonstrated the overall compactness of the protein throughout molecular dynamics. It is the distance between the centre of mass of all atoms of protein and its terminal in a particular time interval. The less variation in the value of Rg indicates a stably folded protein. The plot of variation in value of Rg versus time is represented in Fig. 3.12. The overall result suggested the compactness of CLas-ZnuA1-inhibitor(s) complexes is comparable to CLas-ZnuA1-RDS51 complex (Table 3.5). It also explains that secondary structure is packed compactly in case of CLas- ZnuA1-inhibitor(s) and thus forms stable complexes.

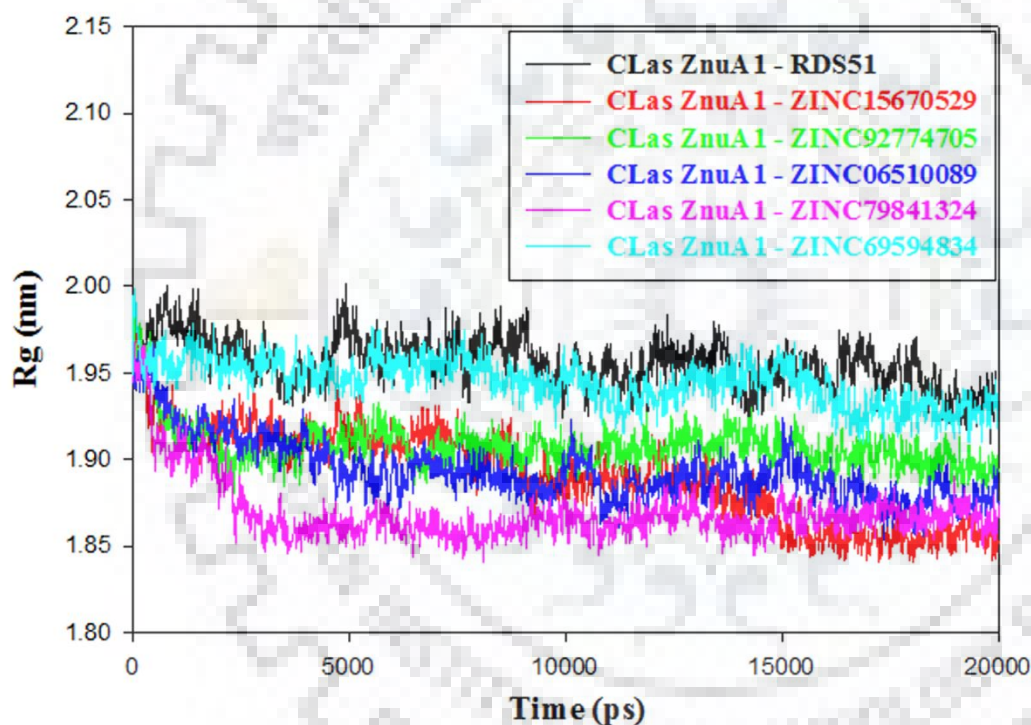


**Fig. 3.12:** Radius of gyration of CLas-ZnuA1-RDS51(black) and CLas-ZnuA1-ZINC15670529 (red) , CLas-ZnuA1- ZINC92774705 (green) , CLas-ZnuA1- ZINC06510089 (blue), CLas-ZnuA1- ZINC79841324 (pink) and CLas-ZnuA1- ZINC69594834 (cyan) inhibitor(s) complexes during 20 ns MD simulation.

### 3.3.5.4. Solvent accessible surface area (SASA)

SASA displayed the probe of the centre of the solvent molecule as it rolls over the van der Waals surface of the receptor molecule. SASA of a protein decreases with increment in compactness of protein, so a change in SASA can predict the change in the structure of a protein. SASA plot of CLas-ZnuA1-inhibitor(s) complexes is similar to CLas-ZnuA1-RDS51 complexes represented in Fig. 3.13. An overall result of SASA suggests the stable complex formation of the CLas-ZnuA1- inhibitor(s) (Table 3.5).

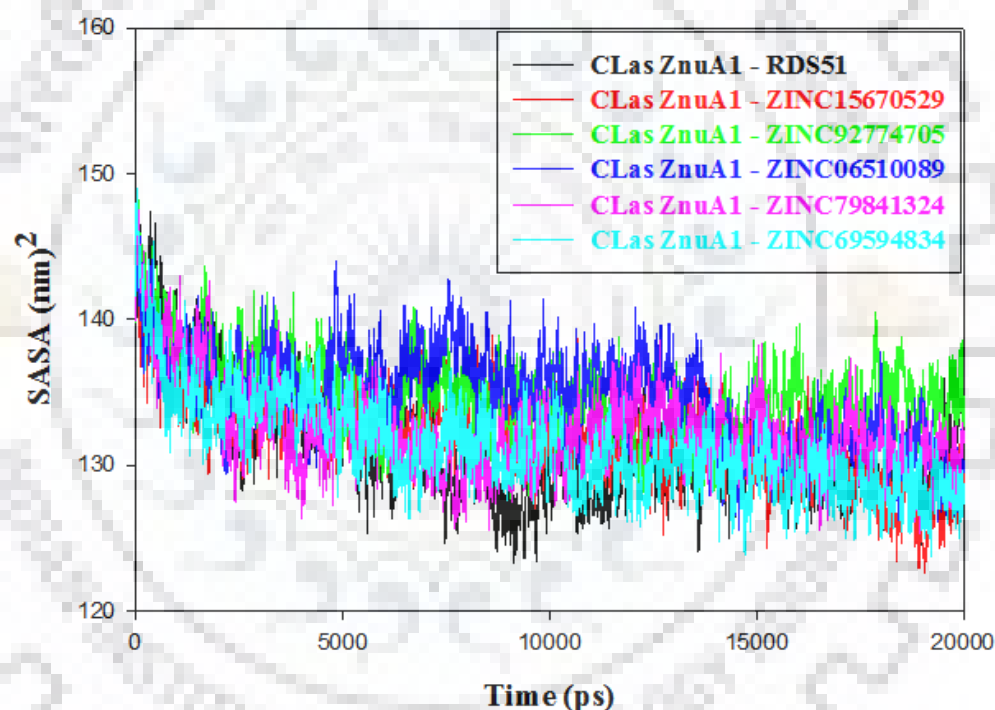


**Fig. 3.13:** Solvent accessible surface area profiles of CLas-ZnuA1- RDS51(black) and CLas-ZnuA1- ZINC15670529 (red) , CLas-ZnuA1- ZINC92774705 (green) , CLas-ZnuA1- ZINC06510089 (blue), CLas-ZnuA1- ZINC79841324 (pink) and CLas-ZnuA1- ZINC69594834 (cyan) inhibitor(s) complexes during 20 ns MD simulation.

### 3.3.5.5. Hydrogen bond analysis

Hydrogen atom covalently attached to an electronegative atom can form hydrogen bonds within the molecule or with other electronegative atoms. Hydrogen bond was generated within a range of  $3.5\text{\AA}$  between acceptor and donor. The `g_hbond` of GROMACS utility was used to investigate the number and distribution of hydrogen bond in the CLas-ZnuA1- inhibitors and CLas-ZnuA1-RDS51 complexes in order to calculate the system stability through the molecular simulation period of 20ns. Intra-molecular hydrogen plot in CLas-ZnuA1-RDS51 and CLas-ZnuA1-inhibitor(s) complexes is shown in Fig. 3.14A. The average number of intra-molecular hydrogen bonds formed in CLas-ZnuA1-RDS51 and CLas-ZnuA1-inhibitor(s) are shown in Table 3.5. The average number of intra-molecular results shows that CLas-ZnuA1- inhibitor(s) complex are in the range of 1309 to 1316 while complex of CLas-ZnuA1 - RDS51 has 1307. Inter-molecular hydrogen bonding result shows that CLas-ZnuA1-inhibitor(s) complexes possessed the minimum of four hydrogen bonds during the MD simulation as represented in Fig. 3.14B. The distribution of hydrogen bond lengths suggested the CLas- ZnuA1-inhibitor(s) complexes form hydrogen bond from high to low affinity which is related to CLas-ZnuA1-RDS51 complex as represented in Fig. 3.14C. Overall, hydrogen bonds results show that the binding of inhibitors results in stable complexes as compared to RDS51.

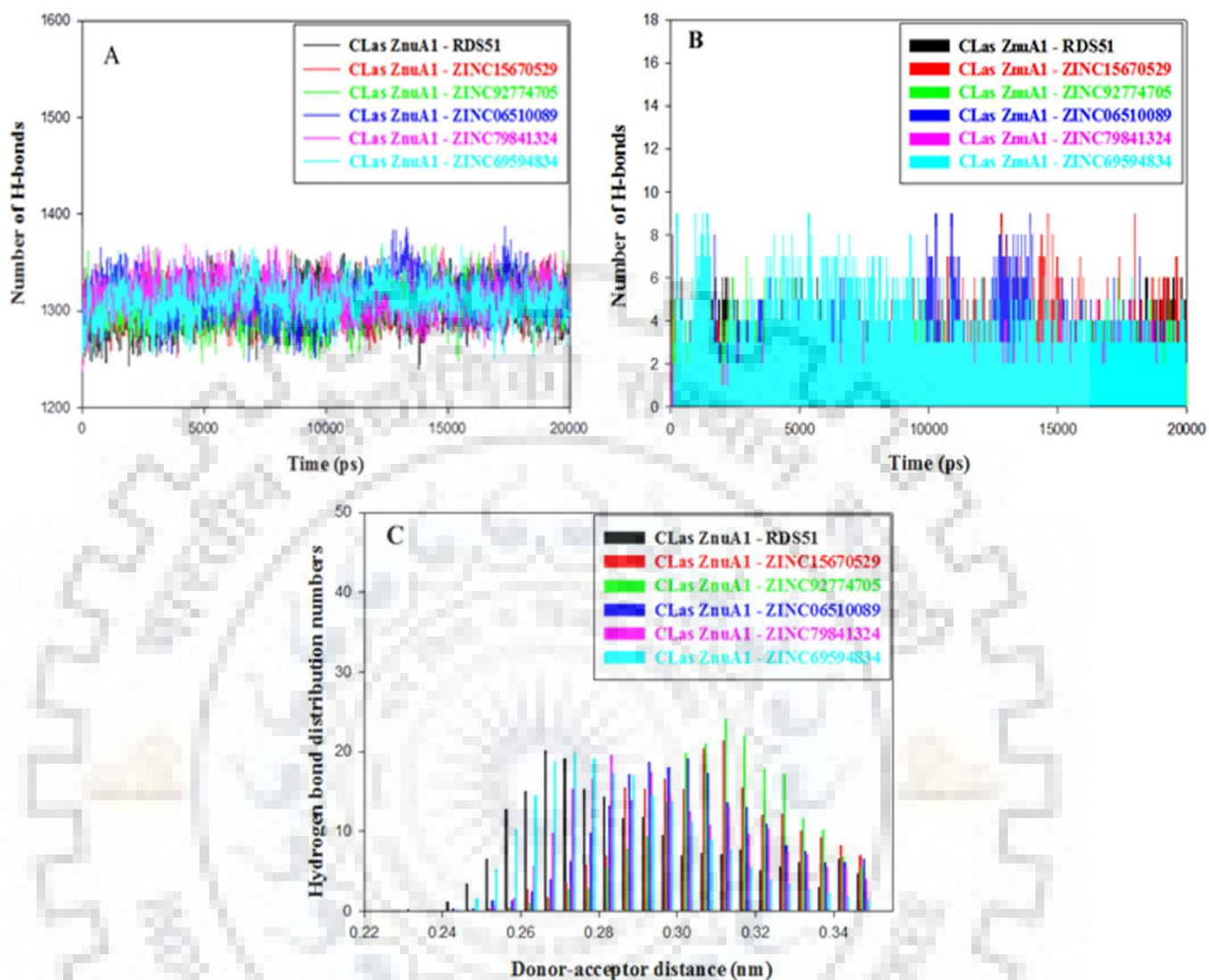


Fig. 3.14: Hydrogen bond analysis of CLas-ZnuA1-RDS51(black) and CLas-ZnuA1-ZINC15670529 (red) , CLas-ZnuA1-ZINC92774705(green) ,CLas-ZnuA1-ZINC06510089 (blue), CLas-ZnuA1-ZINC79841324 (pink) and CLas-ZnuA1-ZINC69594834 (cyan) inhibitor(s) complexes. Hydrogen bonding plots of: A) intramolecular hydrogen bonding, B) intermolecular hydrogen bonding, C) Distribution of Hydrogen bonding during 20 ns MD simulation.

### 3.3.5.6. MMPBSA binding free energy calculation

The quantitative estimation of binding potential of the ligand was determined using free binding energy calculation analysis. The binding free energies of all complexes were calculated using MMPBSA. MMPBSA uses the trajectories of 15 ns to 20 ns of all complexes for determination of the binding energy of the complexes. The results indicate the binding energy of CLas-ZnuA1 inhibitor(s) complexes show higher binding energy than CLas-ZnuA1-RDS51 as represented in Table 3.6. The binding free energy clearly shows that CLas-ZnuA1-inhibitors complexes were stable. It confirms that these inhibitors bind efficiently in the active site of CLas-ZnuA1 and block the Zn metal binding to the CLas-ZnuA1 protein.





**Table 3.6: Binding free energies calculation of CLas-ZnuA1-RDS51 complex and CLas-ZnuA1-inhibitor(s) complexes by MMPBSA.**

S NO	Compound	Van der Waals energy (kJ/mol)	Electrostatic energy (kJ/mol)	Polar solvation energy (kJ/mol)	SASA energy (kJ/mol)	Binding energy (kJ/mol)
1.	RDS51	-273.141 +/- 0.589	-7.190 +/- 0.517	137.181 +/- 0.863	-12.542 +/- 0.191	-155.706 +/- 0.662
2.	ZINC15670529	-252.916 +/- 0.546	-33.802 +/- 0.543	103.653 +/- 0.632	-34.986 +/- 0.181	-218.052 +/- 0.621
3.	ZINC92774705	-179.291 +/- 11.148	-31.777 +/- 3.618	33.909 +/- 8.069	-14.501 +/- 0.353	-191.366 +/- 7.289
4.	ZINC06510089	-219.980 +/- 0.703	-40.165 +/- 0.360	94.788 +/- 0.641	-18.456 +/- 0.039	-183.853 +/- 0.760
5.	ZINC79841324	-201.041 +/- 0.545	-6.740 +/- 0.483	51.157 +/- 0.493	-17.281 +/- 0.055	-173.896 +/- 0.548
6.	ZINC69594834	-109.349 +/- 3.819	-188.295 +/- 6.462	163.146 +/- 10.133	-26.553 +/- 0.422	-161.167 +/- 1.566

### 3.4. Discussion

For decades, the control and management of the HLB disease caused by *Candidatus* species is limited to chemically control psyllids, and removal of infected trees [299]. However, these efforts have not been able to completely eradicate the HLB disease. An approach of chemotherapy in conjunction with thermotherapy could be beneficial for HLB control, and extension of the life of fruit production of the citrus tree infected with HLB [300, 301]. Structural based virtual screening and molecular docking method have been used to discover the potent molecule to initiate synthesis of effective antimicrobial compounds [302, 303]. Molecular docking and simulations studies were utilized to predict the efficiency of binding of the ligand with macromolecules [304, 305]. In this study, we report the homology modeling of CLas-ZnuA1 and further virtual screening and simulation study to identify the novel potent antimicrobial compound(s).

The present study reports the successful search of novel compounds might be able to inhibit the CLA growth by interfering with the activity of ZnuA, a periplasmic component of ZnuABC, involved in the binding to Zn metal. The identified compounds might be suggested to affect the CLA vitality and specifically target the periplasmic component of ZnuABC transporter system, ZnuA1 (CLas-ZnuA1). This protein was selected as target, because its inactivation dramatically reduces pathogenicity and colonization of host by CLA as well as other Gram-negative bacteria [141, 306].

CLas-ZnuA1 gene *Candidatus* Liberibacter asiaticus was cloned and followed by computational analysis. The three dimensional model of CLas-ZnuA1 consists of five  $\beta$ -strands and eight  $\alpha$ -helices connecting through loops. The Ramachandran plot analysis ensures the reliability and quality of the Model. Furthermore, this valid model was used for virtual screening of drug-like molecules.

Virtual screening can provide a valuable contribution to the discovery of novel compound(s); various software's have been designed for this purpose [307]. In several projects of drug discovery, the virtual screening technology has been a powerful contributor to search the new molecule on the basis of the model and their binding site residue [307, 308]. The predicted binding site of CLas-ZnuA1 was the target for virtual screening to evaluate the binding affinity of the inhibitor(s). The top identified 50 novel compounds were fulfilling the Lipinski rule of five

criteria. Out of 50, 10 compound(s) were showing the maximum binding affinity. The comparative study of selected potent compounds was made using another molecular docking program Auto Dock 4.2.6. The Result of molecular docking showed that five compounds ZINC15670529, ZINC92774705, ZINC06510089, ZINC79841324, and ZINC69594834 exhibit more binding affinities as compared to RDS51. ZINC92774705 and ZINC69594834 forms hydrogen bonding with His122, His130 and His194 additionally, ZINC92774705 interacts with Phe193. Both make hydrophobic interaction with Ile30, Pro57, Phe86, and Trp132. Also, ZINC92774705 interacts with Leu49, Val51, Met83, Phe193, Met213, and Phe245 through hydrophobic interaction. ZINC15670529, ZINC06510089 and ZINC79841324 form hydrogen bonding with Ser55, His122 and His194, moreover ZINC15670529 interacts with Phe193 and, ZINC06510089 interacts with Gly53 and Glu267. ZINC15670529, ZINC06510089, and ZINC79841324 interacts with Ile30, Val51, Pro57, Phe86 through hydrophobic interaction, additionally, ZINC15670529 interacts with Leu59, Met83, Trp132, Tyr197, Phe193, Phe245 and both showed hydrophobic interaction with Ala54 whereas, in comparison to these compound(s) reference molecule RDS51 forms only, hydrogen bond with residue His122 and His130, and make hydrophobic interaction with Ala54, Pro57, Met83, Pro243, Pro266 and Met269 ( Fig. 3.9, Fig.3.15 and Table 3.4). The comparison of binding energies indicates the higher strength of binding interaction of these selected compounds than reference molecule RDS51 (Table 3.4).

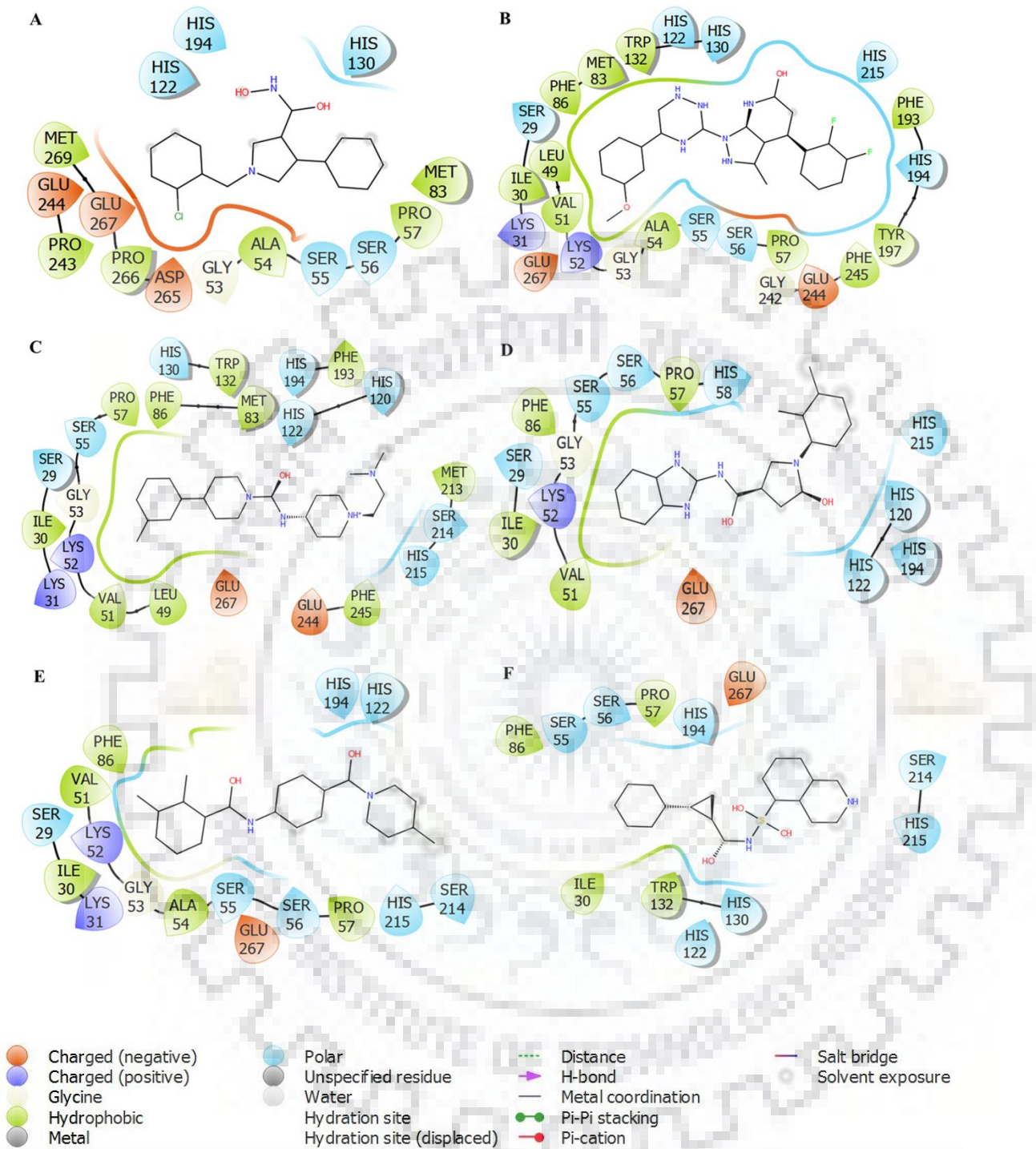


**Fig. 3.15:** Pictographic representation of interaction involved in binding of RDS51 and inhibitor(s) to CLas-ZnuA1 using Maestro 11.2. Hydrophobic, charged positive residues, charged negative residues and polar residues are shown in green color, blue color, orange color and cyan color, respectively.

To understand the structural and conformational variation, protein-ligand complexes were subjected to molecular dynamics simulation. The overall RMSD value revealed that CLAs-ZnuA1-inhibitor(s) was forming stable complexes. All the predicted inhibitor(s) showed less RMSD value as compared to RDS51 (0.25 nm) indicated the static and stable binding of inhibitor(s) to CLAs-ZnuA1 protein. The overall value of RMSF concluded that all the predicted inhibitor(s) were well established in the CLAs-ZnuA1 protein cavity without causing much fluctuation in the protein-ligand complex. The less variation in the value of the radius of gyration of CLAs-ZnuA1-inhibitor(s) as compared to CLAs-ZnuA1 - RDS51 complex suggested that the protein is compactly packed and maintaining the rigidity of the CLAs-ZnuA1-inhibitor(s) complexes.

Further, SASA and hydrogen bonding results also reveal that protein-inhibitor(s) complexes maintain the stability as compared to protein-RDS51 complex.

An increase in the binding free energies of all the inhibitor(s) related to RDS51, obtained from MMPBSA estimation, indicating the ability of the screened novel compound(s) to bind to the cavity of CLAs-ZnuA1 more efficiently. From molecular dynamics analysis, we concludes that, all the inhibitors were suggested to be a novel potent molecule(s) to block the binding of Zn(II) in the active site of CLAs-ZnuA1 protein and affect the sequestration or uptake of Zn metal ion by this protein, thus interferes the activity of ZnuABC transporter system.

### **3.5. Conclusion**

In conclusion, ZnuA1, a periplasmic component of the ZnuABC transport system, involved in the capture of Zn in Gram-negative bacteria like CLA, may be a good target in search of potent antibacterial agents. In silico-analysis such as structure-based virtual screening was carried out to identify the potent ZnuA1 inhibitors of CLA. Out of 50 screened compounds, 10 molecules showing good binding affinity fulfilling the Lipinski rule of five. The molecular docking was used to analyse the interaction of screened compounds with the CLAs-ZnuA1. Molecular docking studies showed the higher docking binding affinity in comparison to positive control RDS51. Five molecules were selected for further analyze on the basis of comparison of the binding affinity energy of the AutoDock Tools and AutoDock Vina. The minimization studies confirm that all the selected compounds ZINC15670529, ZINC92774705, ZINC06510089, ZINC79841324, and ZINC69594834 bind to the CLAs-ZnuA1 more efficiently and inhibit the binding of Zn and

subsequently, affect the activity of ZnuABC transport system in CLA. All of the above findings suggested that the selected compounds might be good inhibitors of CLAs-ZnuA1 protein. Thus, we feel that these selected novel lead compounds provide a path for further innovation and development of antimicrobial compounds against CLA. In Future, biochemical characterization and in-vitro assays will help to confirm the binding of screened inhibitors with CLAs-ZnuA1.





## CHAPTER 4

# CLONING AND STRUCTURE BASED IDENTIFICATION OF INHIBITORS AGAINST Esbp FROM *CANDIDATUS LIBERIBACTER ASIATICUS*

---

### 4.1.Introduction

Citrus Greening (huanglongbing) is a widespread, extremely destructive citrus plant disease. HLB is associated with three species of unculturable, phloem-limited, fastidious  $\alpha$ -proteobacteria; *Candidatus Liberibacter asiaticus* (Las), '*Ca. L. africanus*' (Laf) and '*Ca. L. americanus*'. [146, 267, 268]. It is transmitted by Asian citrus psyllid (*Diaphorina citri* Kuwayama) [169]. Out of three, Las is the most virulent and widely distributed. HLB disease symptoms include blotchy chlorosis and /or mottling of leaves: stunted growth: malformed fruits and finally death [146]. This disease is difficult to manage and to the date, there is no strategies developed which can eradicate it completely. The only recommended control strategy is to remove the infected plant and chemically control the psyllids [299]. In this study, CLas-Esbp was used as a target for virtual screening and molecular docking program to identify the compounds against the *Candidatus Liberibacter asiaticus*.

Metal ions are vital components of the biological system. Iron is an essential nutrient required for survival of the most of the living organisms [309]. Because of its versatile coordination properties and tunable oxidation-reduction state, it is an essential element in several chemical reactions needed for the survival of microorganism in an oxygen environment [310]. Iron is the fourth most abundant element found in the earth's crust, and due to extremely less solubility of  $\text{Fe}^{3+}$  ( $\sim 10^{-18}$  M) at neutral pH, it's not readily available to the microorganism. It is the major component of a wide number of enzymes including ribonucleotide reductase and cytochromes. It is present in proteins used in metabolic processes from dioxygen transport and energy transducing pathways to hydrogen and nitrogen fixation [311]. However, reduced  $\text{Fe}^{2+}$  is highly soluble, which can increase the generation of highly reactive free radical by Fenton chemistry. These toxic free radicals specifically damage the membrane lipids by initiating the unsaturated bonds formation, decrease the fluidity of membrane and promote cell lysis. Therefore, it becomes necessary that

living system balance the chemical atmosphere of iron. For many microbial pathogens, it is a restricted factor for colonization and infection [312].

Most of the living system has developed an exclusive system for sequestration, transport, and storage of this essential trace element to retain in a non-toxic state. In response to the matter of iron inadequacy, Gram-negative pathogenic microorganisms have developed a range of various high-affinity iron uptake systems for survival. One strategy through which bacteria can overcome the problem of iron scarcity is the synthesis of small iron chelators termed as “siderophores” [313, 314].

Most of the siderophores are produced by large multienzyme synthases that show resemblance to the fatty acid synthases of eukaryotes [315-317]. Once siderophores are delivered within the bacterial cell, iron is discharged from siderophores and reduction of siderophore-bound  $Fe^{3+}$  to  $Fe^{2+}$  was carried out by the action of enzymes [318]. This  $Fe^{2+}$  can be directly assimilated into metalloenzymes, or if it is in excess, can be stored in bacterioferritin or in the associated Dps proteins [319]. An alternate of iron uptake system, also used by Gram-negative bacteria has been found in many human and veterinary diseases causing microorganism [320, 321]. These bacteria consist of an outer membrane receptor which directly involved in acquisition of iron from transferrin and/or lactoferrin. Further transport across the membrane is facilitated by the ATP-binding cassette (ABC-type) transport system. This system works by using the solute binding protein (SBPs) to capture the molecule and deliver the substrate for translocation by transmembrane domain of ABC transporter powered by the hydrolysis of ATP by nucleotide binding domain of the membrane [35]. This transport system refers to the superfamily of ATP-binding cassette transporters which includes a large range of import and export system exist in prokaryotes and eukaryotes [13]. Therefore, affecting the binding process of iron by identifying the small molecule inhibitor at the metal binding site will interrupt the function of CLas-Esbp and thus inhibit the iron uptake process, and this strategy could be used in the discovery of antimicrobial agent against the pathogenic microorganism.

In the present study, CLas-Esbp gene was cloned and further studied by *in-silico* analysis. Homology modeling was used to predict the 3-dimensional structure of CLas-Esbp. Drug-like molecules were retrieved from the ZINC database and used for virtual screening. 50 molecules were screened and checked on the basis of Lipinski rule of five. On the basis of Molecular docking

program, AutoDock Tools and AutoDock Vina, we selected the 3 molecules, having maximum binding affinity score. In order to better understand the stable behaviour of the protein-ligand complex(s), complex(s) were subjected to molecular dynamics (MD) simulation and molecular mechanic/Poisson-Boltzmann Surface Area (MMPBSA) was employed for binding free energy calculation. This approach is providing an idea in designing the antimicrobial agent against pathogenic bacteria CLA to manage the spreading of HLB in citrus orchids.

## **4.2. Material & Method**

### **4.2.1. Cloning and expression of CLAs-Esbp**

The genomic DNA of CLA was isolated from infected sweet orange (*Citrus sinensis*) at NRCC Nagpur, Maharashtra. CLAs-Esbp gene (CLIBASIA\_02250) encoding protein of 166 amino acids lacking signal sequence was amplified using the forward primer ESBP FP- 5'- AAT ACA TAT GAC GGA AAA TAC TAC CAA ATA TTT GAC -3' and reverse primer ESBP RP- 5'- AAT ACT CGA GCT ATC GCT TGT ATT TGG TC -3' with Nde1 and Xho1 site respectively. The 50 µl PCR amplification mixture had 5µL of 5X reaction buffer, 1µL of dNTP mixture (each dNTP, 2.5 mmol/µL), 1µL of each primer (20 pmol/µL), 2 µL of the template DNA (100 ng/µL) and 0.5µL of Taq DNA polymerase enzyme (New England BioLabs, USA). The PCR program was set as; initial denaturation at 94°C for 4 min followed by 30 cycles at 94°C for 45 s, at 59°C for 45 s, at 72°C for 90 s, and final extension for 10 min at 72°C and stored at 4°C. The amplified product was purified by using QIAquick Gel Extraction Kit (QIAGEN, Germany). The restricted amplicon was ligated in restricted pET-28c and transformed in *E.Coli* XL1-Blue cells and sequenced from Eurofins Scientific India Pvt Ltd, Bengaluru, India. The recombinant CLAs-Esbp was transformed in the *E.coli* BL21 host cells for expression of the protein in the presence of antibiotics; kanamycin (30 µg/ml) and chloramphenicol (35 µg/ml). Overexpression was tried to optimize using the different concentration of IPTG (0.1-1.0mM) and at different temperature (16-37 °C).

### **4.2.2. Sequence analysis**

Initially, BLAST tool was used for sequence search at NCBI web site ([www.ncbi.nlm.nih.gov](http://www.ncbi.nlm.nih.gov)). SignalP 3.0 server was used for the prediction of putative signal peptide sequence [276]. An ExPASy tool, ProtParam (<http://web.expasy.org/protparam/>) was used for

determination of Physico-chemical properties such as GRAVY (grand average of hydropathy), aliphatic index (AI), extinction coefficients, isoelectric point (pI), and molecular weight.

#### **4.2.3. Homology modeling and Structure validation**

Three-dimensional structure of CLas-Esbp was built by using Phyre 2.0 [282]. ModLoop program was used for the refinement of disorder region of the model [283]. Swiss PDB viewer 4.10 has been used for energy minimization of the predicted model [284]. PROCHECK, validation server was used to check the quality of the predicted model [261]. The picture of the model was made by using Chimera [265].

#### **4.2.4. Virtual screening**

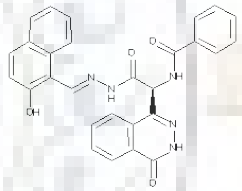
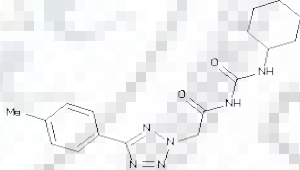
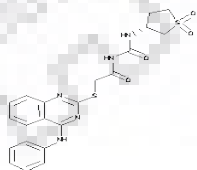
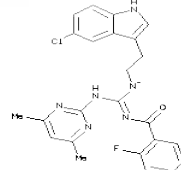
Drug-like molecules were retrieved from the ZINC DATABASE (<http://zinc.docking.org>), further minimization of the energy was done. All molecules were converted into pdbqt format using Open Babel in PyRx 0.8 for virtual screening [265, 286, 287]. All the retrieved molecules were undergone for docking against the binding site of the modeled protein by employing PyRx 0.8 along with AutoDock Vina [286]. SWISSADME, an online tool was used to check the molecular properties of the screened molecules subsets [288]. These subsets must be in the range of Lipinski rule of five criteria [289]. This rule suggests the most “drug-like” molecules must exhibit molecular weight  $\leq 500$  Da,  $\log P \leq 5$ , number of hydrogen bond donors  $\leq 5$ , and number of hydrogen bond acceptors  $\leq 10$ .

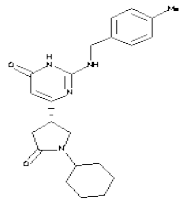
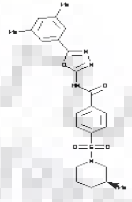
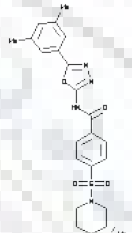
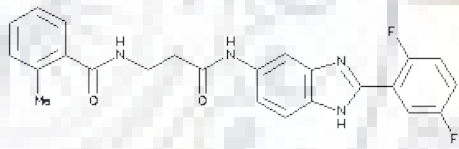
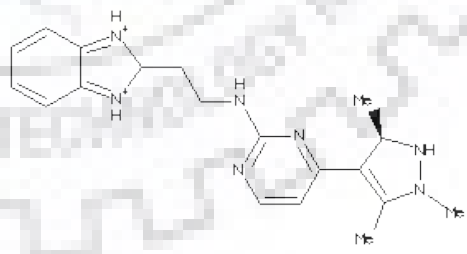
#### **4.2.5. Molecular docking**

AutoDock was used to perform the docking of the screened molecules with modeled CLas-Esbp protein. AutoDock employs a semi-empirical free energy force field to calculate the binding free energy of ligand to receptor, protein molecule. AutoDock Tools 4.2.6 was utilized to add the explicit hydrogen molecules and associated Kollman charges (14.016) to the receptor molecule and saved in pdbqt format [290]. 10 molecules used for docking with protein are: ZINC03143779, ZINC05491830, ZINC08750867, ZINC14671545, ZINC19210425, ZINC36682252, ZINC36682254, ZINC48279035, ZINC63868855 and ZINC86208064. The chemical name and structure of all molecules are shown in Table 4.1 Before saved in pdbqt format, Gasteiger charges

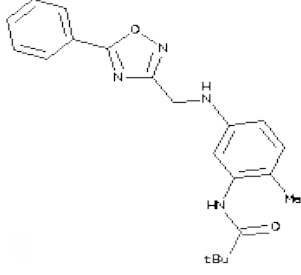
were added to the ligand. The torsional degrees of freedom of ligand molecule were specified by the flexibility of the ligand. AutoGrid 4 was utilized to generate the grid map with a spacing of 0.375 Å. The dimension and centre point coordinates of the grid box were set as 50 Å x 50 Å x 50 Å and 28.548, 30.477, 14.424 respectively. Lamarckian genetic algorithm was adopted for the molecular docking program. Docking was performed with default parameters, except total GA runs number which was increased from 10 to 100. The maximum binding affinity pose was studied along with interactions. PyMol protein viewer tool was used for structural analysis and visualization of the protein [264]. Molecular docking interactions figures were prepared using PyMol and Maestro [322].

**Table 4.1: Chemical name and structure of selected compounds from ZINC database.**

S.No.	Compound ID	Chemical name	Structure
1.	ZINC03143779	N-[(1S)-2-[(N'E)-N'-[(2-hydroxy-1-naphthyl)methylene]hydrazino]-2-keto-1-(4-keto-3H-phthalazin-1-yl)]	
2.	ZINC05491830	N-(cyclohexylcarbonyl)-2-[5-(p-tolyl)tetrazol-2-yl]-acetamide	
3.	ZINC08750867	N-[(1,1-dioxothiolan-3-yl)carbonyl]-2-[4-phenylimino-3H-quinazolin-2-yl]sulfanyl]acetamide	
4.	ZINC14671545	(NZ)-N-[[2-(5-chloro-1H-indol-3-yl)ethylamino]-[(4,6-dimethylpyrimidin-2-yl)amino]methylene]-2-fluor	

5.	ZINC19210425	(4S)-1-cyclohexyl-4-[6-hydroxy-2-(p-tolylmethylamino)pyrimidin-4-yl]pyrrolidin-2-one	
6.	ZINC36682252	N-[5-(3,5-dimethylphenyl)-1,3,4-oxadiazol-2-yl]-4-[[[(3S)-3-methyl-1-piperidyl]sulfonyl]benzamide	
7.	ZINC36682254	N-[5-(3,5-dimethylphenyl)-1,3,4-oxadiazol-2-yl]-4-[[[(3R)-3-methyl-1-piperidyl]sulfonyl]benzamide	
8.	ZINC48279035	N-[3-[[2-(2,5-difluorophenyl)-1H-benzimidazol-5-yl]amino]-3-oxo-propyl]-2-methyl-benzamide	
9.	ZINC63868855	N-[2-(2H-benzimidazol-2-yl)ethyl]-4-[(5R)-2,3,5-trimethyl-1,5-dihydropyrazol-4-yl]pyrimidin-2-amine	



10.	ZINC86208064	2,2-dimethyl-N-[2-methyl-5-[(5-phenyl-1,2,4-oxadiazol-3-yl)methylamino]phenyl]propanamide	
-----	--------------	---	---

#### 4.2.6. Molecular dynamics simulation

Molecular dynamics simulation was performed to study the binding stability and dynamics of CLas- Esbp-inhibitor complex(s) at an atomistic level. The simulation studies were carried out using GROMOS96 43a1 force field in Gromacs 5.1.4 suite on ubuntu based LINUX workstation [292, 293]. The topology files of the small molecules (ZINC03143779, ZINC05491830, and ZINC19210425) were created by using PRODRG [323]. The protein complexes were solvated in a cubic box of volume 719.49 nm<sup>3</sup> with 1nm marginal radii using SPC (simple point charges) model and counter ions were added to neutralize the system [295]. To reduce the steric clashes, energy minimization was done using algorithm; Two different equilibration phases were carried out for 5,00,000 steps. The first phase of equilibration includes a constant number of particles, volume and temperature (NVT) for 1ns. Further, second phase of equilibration involved constant number of particles, pressure, and temperature (NPT) at 300K, for each step of 2fs. LINCS algorithm was used to constraints the covalent bond. Coulomb interaction and Lennard- jones were determined within a cut off radius of 1.4 nm. Particle Mesh Ewald (PME) with 1.6Å Fourier grid spacing was used for determination of Long- range electrostatics [296]. A modified Berendsen temperature coupling method, V-rescale was used to control the internal temperature of the box. Parrinello-Rahman pressure coupling method was used to maintain the NPT equilibration. The molecular dynamics simulation run of 30 ns was performed with a time step of 2 fs. The RMSD (Root Mean Square Deviation), RMSF (Root Mean Square Fluctuation), Hydrogen bonds were determined using *g\_rms*, *g\_rmsf*, and *g\_hbond* respectively, within the GROMACS suite [292]. A roughly measurement of the compact factor and solvent accessible surface area (SASA) of protein was estimated using *g\_gyrate* tool and *gmx\_sasa* during simulation.

#### 4.2.7. MMPBSA binding free energy calculation

The binding energy,  $\Delta G_{\text{bind}}$ , was calculated using the following equation, from the free energy of the receptor-ligand complex ( $G_{\text{rlc}}$ ) with respect to the unbound receptor ( $G_{\text{rec}}$ ) and ligand ( $G_{\text{lig}}$ ):

$$\Delta G_{\text{bind}} = G_{\text{rlc}} - (G_{\text{rec}} + G_{\text{lig}})$$

On the basis of the complete thermodynamic cycle, MMPBSA permits the calculation of binding free energy, including ligand and protein desolvation energies. The binding energy includes the average of potential energy in the vacuum, polar-solvation energy, and non-polar solvation energy, respectively. `g_mmpbsa` tool was used for determining the binding energy of the protein-ligand complexes [293]. In the present work, the snapshots for every 10 ps for last 5 ns were collected and predicted the binding energy.

### 4.3. Results

#### 4.3.1. Cloning and expression of CLas-Esbp

The presence of CLA genome was confirmed by PCR amplification of 16S rDNA bp fragment using primers OI1/OI2c [298]. Cloning of the CLas-Esbp gene without signal peptide from *Candidatus Liberibacter asiaticus* was performed by using restriction digestion. The correct size of 498bp was obtained after PCR amplification and restriction digestion (Fig. 4.1). Further, the sequencing result confirms the correct frame of the insert and no mutation. The recombinant expression vector pET-28c having CLas-Esbp insert was transformed in the freshly prepared competent *E.coli* BL21 host cells. Various approaches like decreasing the expression temperature, changing the IPTG concentration, expression time and different concentration of urea to obtain the protein in soluble were tried but all efforts remained unsuccessful.

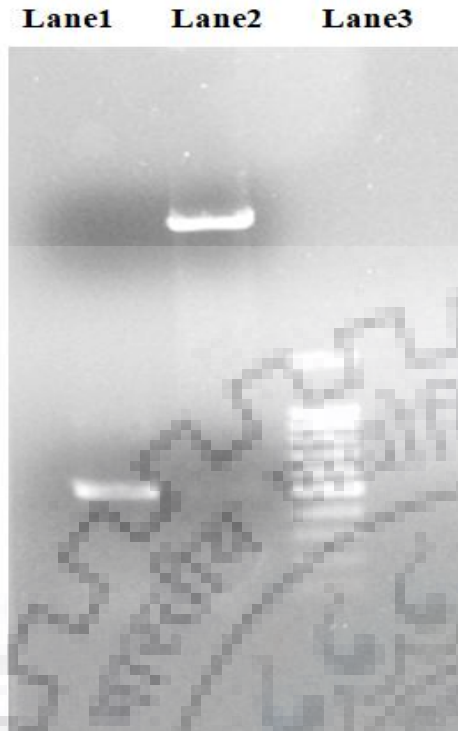


**Fig. 4.1: Agarose gel electrophoresis confirming the positive clones.** Lane 1 : PCR amplification from pET-28c plasmid containing CLas-Esbp gene (498bp) , Lane2 : restriction digestion of pET-28c containing CLas-Esbp, Lane3 : 100bp DNA ladder.

### 4.3.2. Bioinformatic analysis

#### 4.3.2.1. Prediction of the signal peptide

CLas-Esbp protein sequence showed (195 amino acids) presence of 21 residues long signal peptide sequence at the N-terminal end as predicted by SignalP 3.0 server (Fig. 4.2). The nucleotide sequence coding this signal peptide has not been included for cloning.

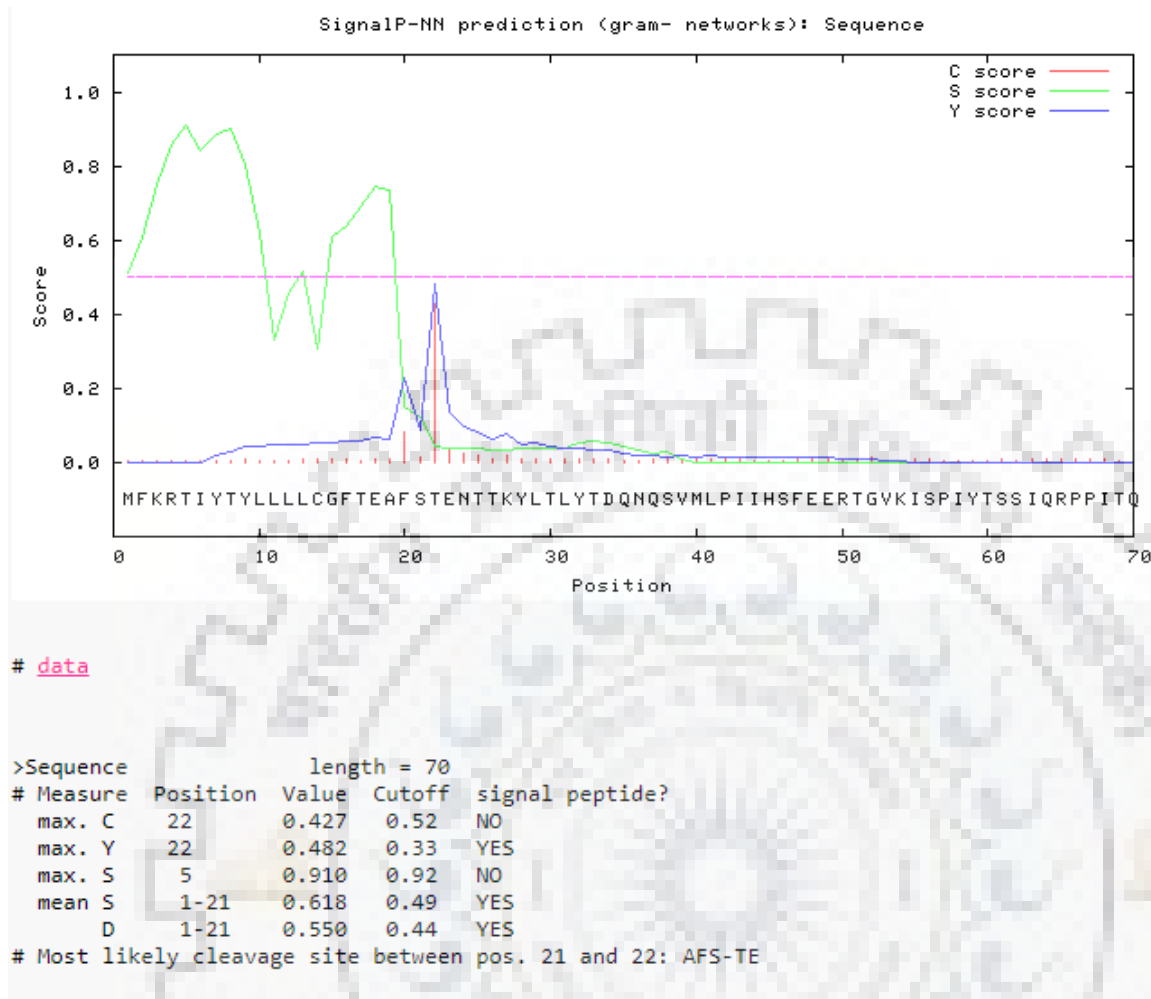


**Fig. 4.2: Prediction of the signal sequence in CLas-Esbp.** Signal peptide of length 21 residues (residue 1-21) in the CLas-Esbp sequence as predicted by SignalP 3.0 server.

#### 4.3.2.2. Amino acid sequence similarity search by NCBI-BLAST

A sequence similarity search of CLas-Esbp amino acid sequence using NCBI-BLAST search engine in non-redundant (NR) and Protein Data Bank (PDB) databases showed homology to periplasmic solute binding proteins of type 2 superfamily as classified by NCBI's Conserved Domain Database (CDD). These proteins belong to ABC transporter substrate-binding protein.

When searched against NR database, CLas-Esbp shared maximum sequence identity to iron ABC transporter substrate-binding protein from *Rhizobium rhizosphaerae* (31%). Other protein which shares similarity belongs to families Micromonosporaceae, Streptomycetaceae and

Hyphomicrobiaceae. When searched against PDB blast containing known structures, CLas-Esbp shared sequence identity to iron binding protein YfuA from *Yersinia enterocolitica* (24 %) and iron free SfuA from *Serratia marcescens* (22%) (Fig. 4.3).

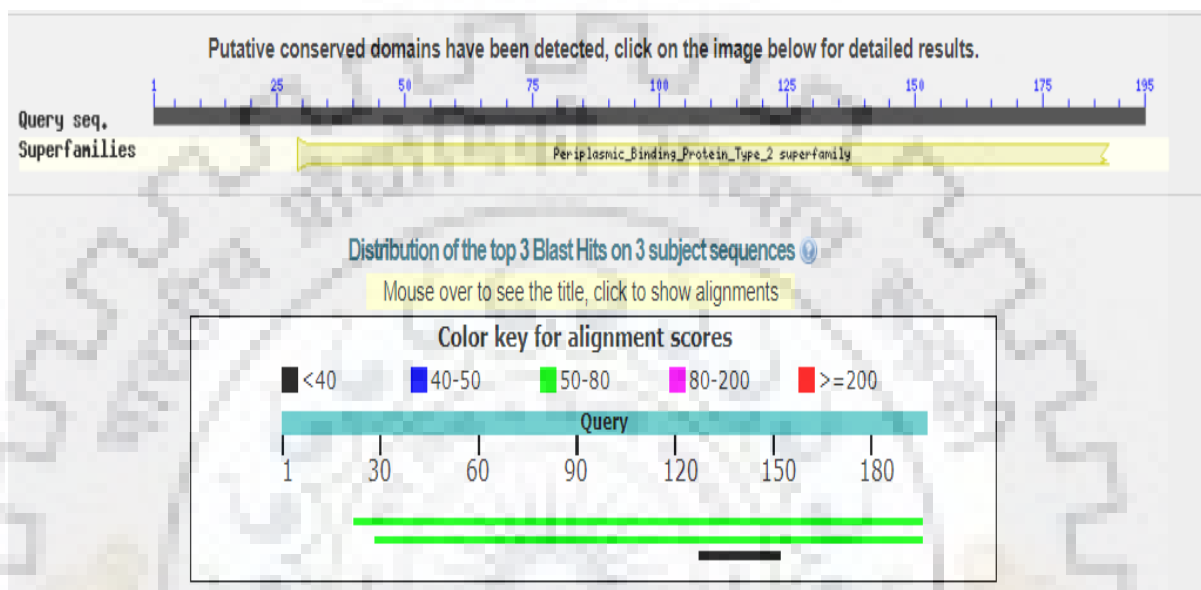


**Figure 4.3:** Sequence similarity search of CLas-Esbp using NCBI BLAST search tool.

#### 4.3.2.3. Physico-chemical parameters

The Physico-chemical properties were analyzed by using an ExPASy tool, ProtParam which reveals that CLas-Esbp protein has 11460 extinction coefficient, 99.82 aliphatic index, -0.369 grand average of hydropathicity. The CLas-Esbp protein containing 166 amino acid residues was estimated to have a molecular mass of 19047.13 Da and isoelectric pH at 9.79.

#### 4.3.2.4. Model building and structure validation

Phyre 2.0 server was used for prediction of the 3-dimensional structure and further energy minimization was done by using Swiss PDB viewer (Fig. 4.4.).

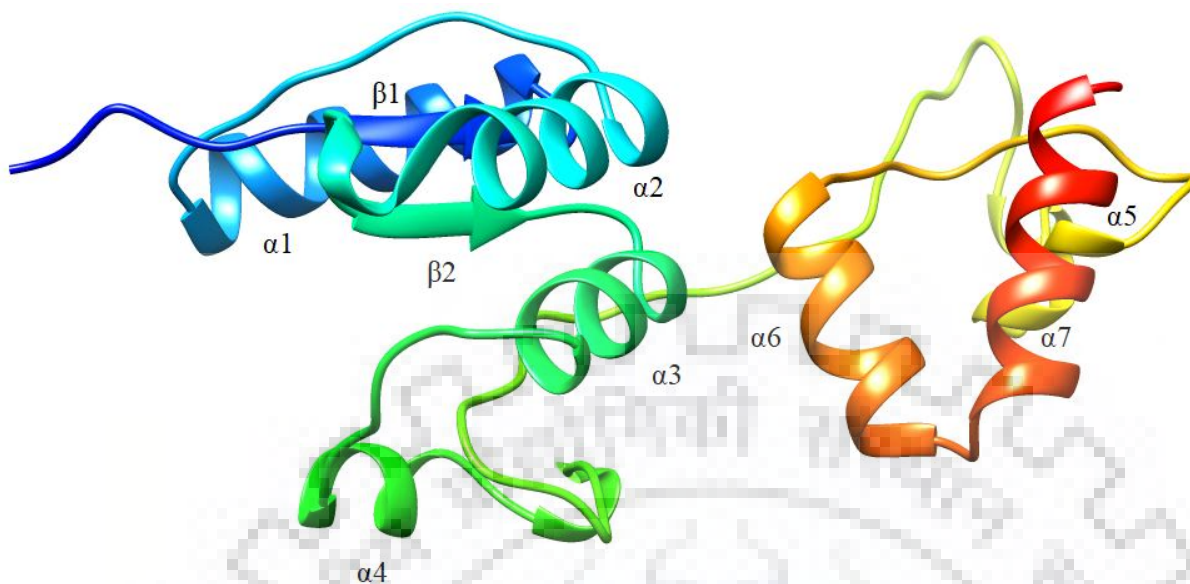


**Fig. 4.4:** Cartoon representation of the 3-dimensional model of the CLas- Esbp protein.

The Ramachandran plot analysis was performed using PROCHECK which depicts the 87.3 % residues are in the core region, 11.3 % residues are in the allowed region, and 1.3 % residues are in generously allowed and no residues are in the disallowed region (Fig. 4.5).



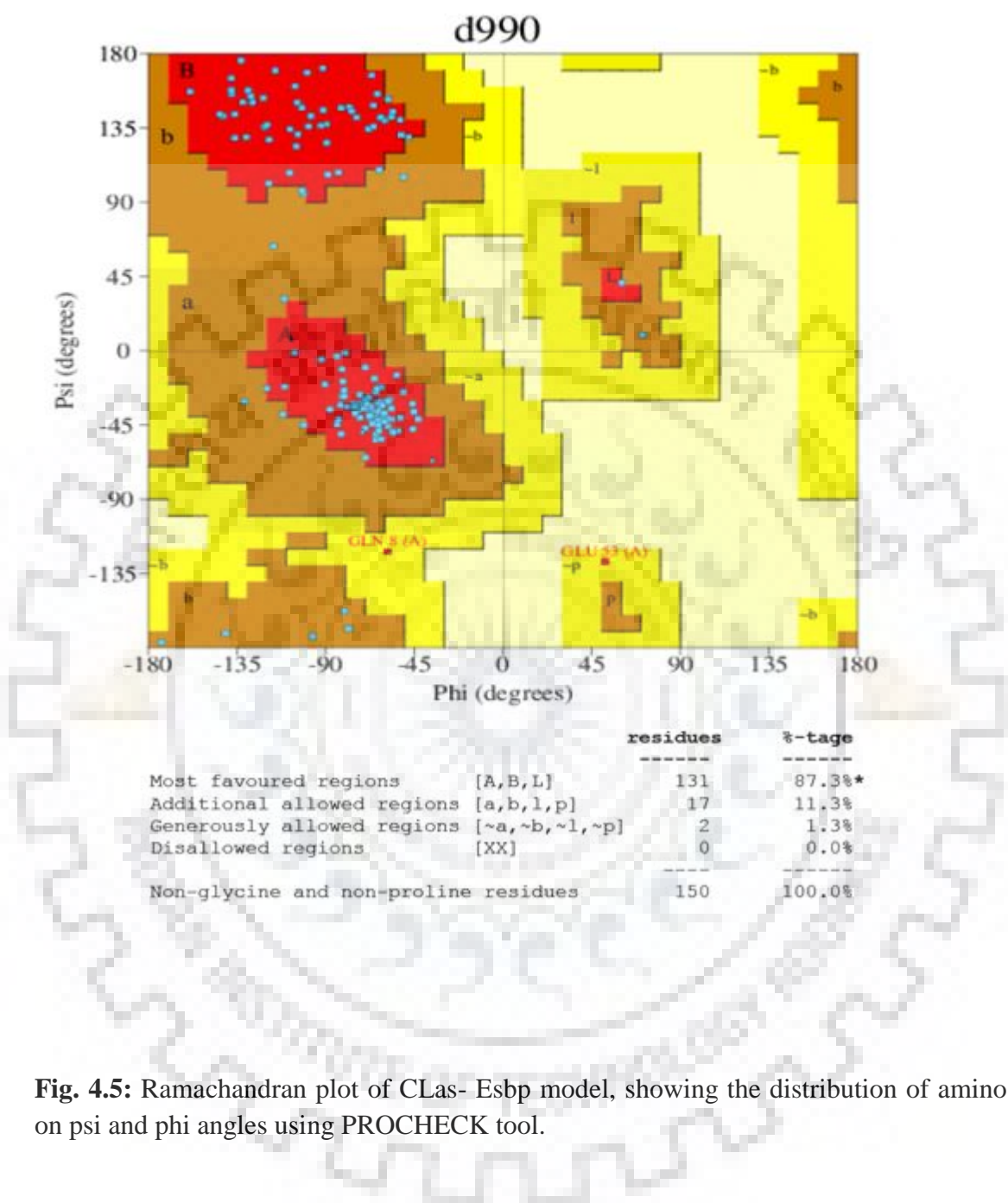


**Fig. 4.5:** Ramachandran plot of CLas- Esbp model, showing the distribution of amino acid based on psi and phi angles using PROCHECK tool.

### 4.3.3. Virtual screening

ZINC database was used for the retrieval of the drug-like molecules in the sdf format, which have been used for the virtual screening of the predicted structure by using molecular docking program, Auto Dock Vina in PyRx 0.8 [286]. Each ligand was generated in nine distinct

poses. Top 50 molecules were chosen by the virtual screening which showed the binding with CLas-Esbp protein. An online tool, SWISSADME was used for evaluation of the physico-chemical properties which showed that all molecules were found to be in the range of the Lipinski's rule of five criteria [289]. The physico-chemical properties of selected 10 molecules are shown in Table 4.2. The top 10 molecules based on the maximum binding affinity, were selected for further analysis. However, to achieve the docking accuracy, binding of the all selected molecules with the CLas-Esbp was checked through another molecular docking program.

**Table 4.2: Physico-chemical properties (molecular weight, LogP, H-bond donor, H-bond acceptor) of all selected ZINC IDs fulfilling the Lipinski rule of five ( $\log P \leq 5$ , molecular weight  $\leq 500$  Da, number of hydrogen bond acceptors  $\leq 10$ , and number of hydrogen bond donors  $\leq 5$ ).**

S.No.	Compounds	Molecular weight (g/mol)	LogP	H-bond donor	H-bond acceptor	Lipinski Druglikeness
1.	ZINC03143779	491.50	2.50	4	6	Yes; 0 violation
2.	ZINC05491830	342.40	1.84	2	5	Yes; 0 violation
3.	ZINC08750867	471.55	2.33	3	6	Yes; 0 violation
4.	ZINC14671545	463.91	3.24	2	6	Yes; 0 violation
5.	ZINC19210425	380.48	3.17	2	3	Yes; 0 violation
6.	ZINC36682252	454.54	3.45	1	7	Yes; 0 violation
7.	ZINC36682254	454.54	3.70	1	7	Yes; 0 violation
8.	ZINC48279035	434.44	2.44	3	5	Yes; 0 violation
9.	ZINC63868855	351.45	3.13	4	3	Yes; 0

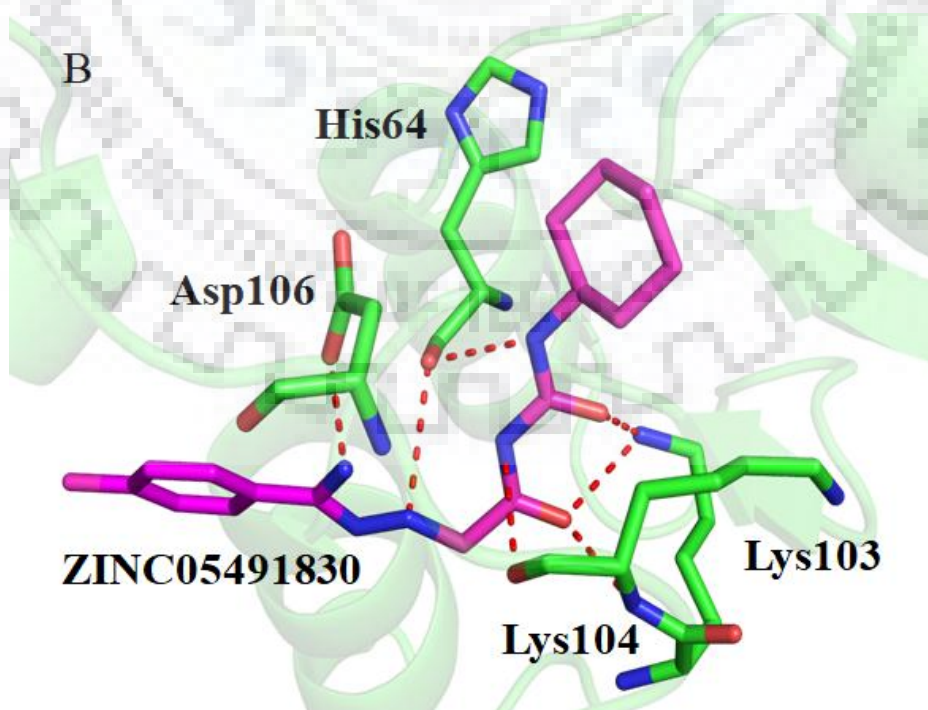
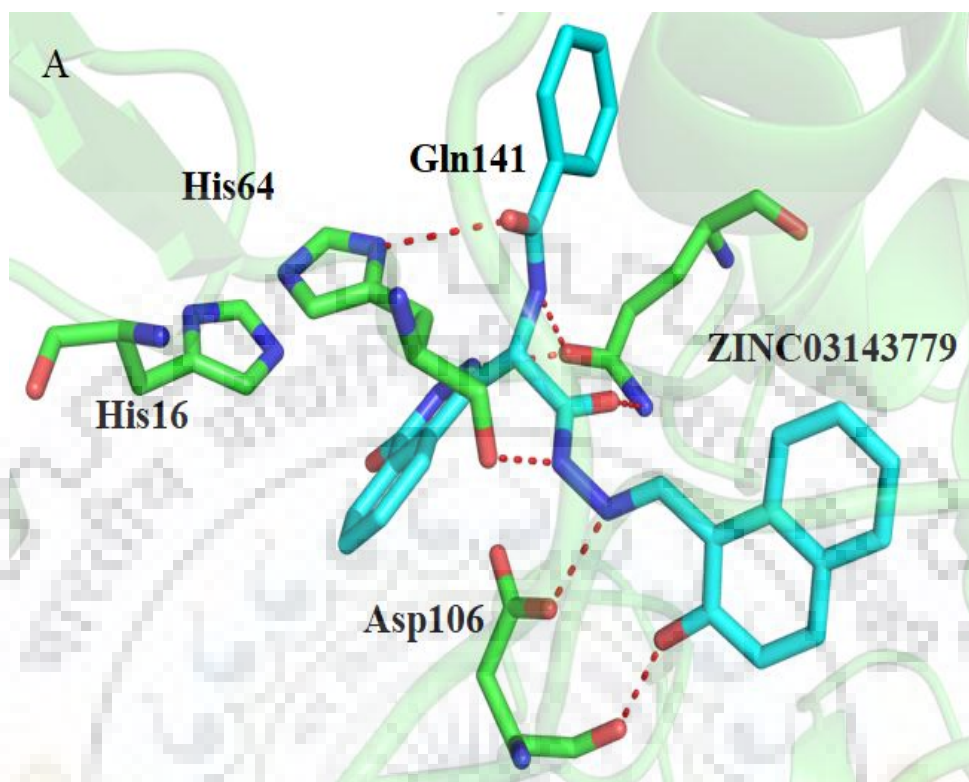
						violation
10.	ZINC86208064	364.44	3.62	2	4	Yes; 0 violation

#### 4.3.4. Molecular docking

Molecular docking program Autodock 4.2.6 was used to perform the docking study of the selected novel molecule fulfilling the range of the Lipinski rule of five criteria. 3 molecules were further selected on the basis of the comparison of the binding affinity energy, showed by AutoDock Tools and AutoDock Vina. Molecular docking binding affinities and interactions analysis are shown in Table 4.3. Docking analysis revealed that the three molecules lie in the range of -9.8 to -9.3 kcal/mol of binding affinity energy. (Fig. 4.6).

**Table 4.3: A detailed summary of the docking binding affinities (kcal/mol) of selected compounds using two different software's (AutoDock Vina and AutoDock) and hydrogen bonding interaction of the CLas-Esbp- inhibitor(s) complexes.**

S.No.	Compounds	AutoDock Vina Binding affinity (kcal/mol)	AutoDock Binding affinity (kcal/mol)	Interacting residues
1.	ZINC03143779	-8.3	-9.8	His16, His64, Asp106, Gln141
2.	ZINC05491830	-8.1	-9.3	His 64, Lys103, Lys104,Asp106
5.	ZINC19210425	-8.5	-9.5	His64, Lys104,Asp106



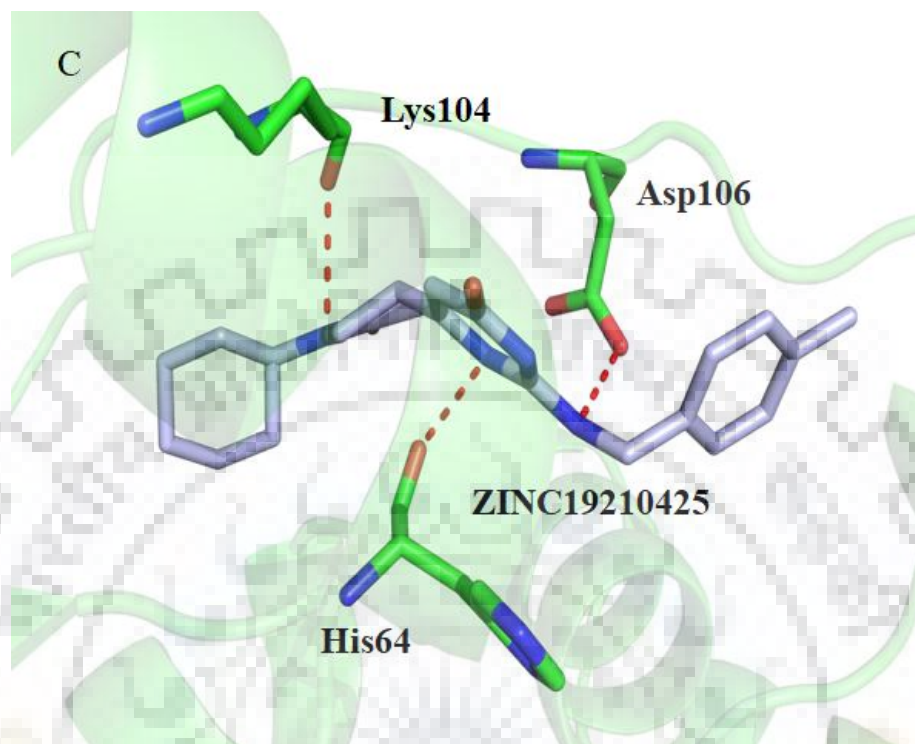


**Fig.4.6:** Docking interaction analysis of CLas-Esbp with A) ZINC03143779 (cyan), B) ZINC05491830 (magenta), C) ZINC19210425 (light blue) complexes. Interacting residues of CLas-Esbp are shown in sticks colored by atom type, carbon in green, nitrogen in blue and oxygen in red. The interactions are shown as broken red lines.

#### 4.3.5. Molecular dynamic simulation

Molecular dynamics simulation studies were carried out in order to better understand the variation occurring in the protein-ligand system at atomistic level and focused on the stability of the complex in the dynamic environment. The MD simulations were performed to explore the dynamics intricate during binding of molecules to the CLas-Esbp protein. In the present chapter, we examined the various molecular simulation results including RMSD, RMSF, radius of gyration (Rg), SASA, hydrogen bond formation and length distribution throughout the simulation.

#### 4.3.5.1. Root mean square deviation (RMSD)

RMSD represents the dynamic stability and conformation changes occur in C $\alpha$  backbone of the CLAs- Esbp inhibitor(s) complexes during simulation. RMSD plot showed that most of the protein-ligand complexes acquired equilibrium at 19s and system was found to be stable up to 30s during the molecular dynamic simulation as shown in the Fig. 4.7. The average RMSD values of the CLAs-Esbp inhibitor(s) are shown in Table 4.4. No large changes were observed in the C $\alpha$  backbone RMSD arrangement patterns of the CLAs-Esbp- inhibitor(s) complexes. Ligand RMSD of the inhibitors is shown in the Fig. 4.7. Overall RMSD study suggested that the binding of the small molecule(s) at the binding site of the CLAs-Esbp were found to be stable and do not affect the stability of the C $\alpha$  backbone of protein.

**Table 4.4: Average values of RMSD, RMSF, radius of gyration, SASA and intra-H bond of CLAs Esbp- inhibitor(s) complexes.**

S.No.	Compounds	Average Protein RMSD (nm)	Average ligand RMSD (nm)	Average RMSF (nm)	Average Radius of gyration(nm)	Average SASA (nm) <sup>2</sup>
1.	ZINC03143779	0.32	0.10	0.12	1.7	106.46
2.	ZINC05491830	0.30	0.13	0.11	1.8	103.66
3.	ZINC19210425	0.28	0.18	0.11	1.7	105.15



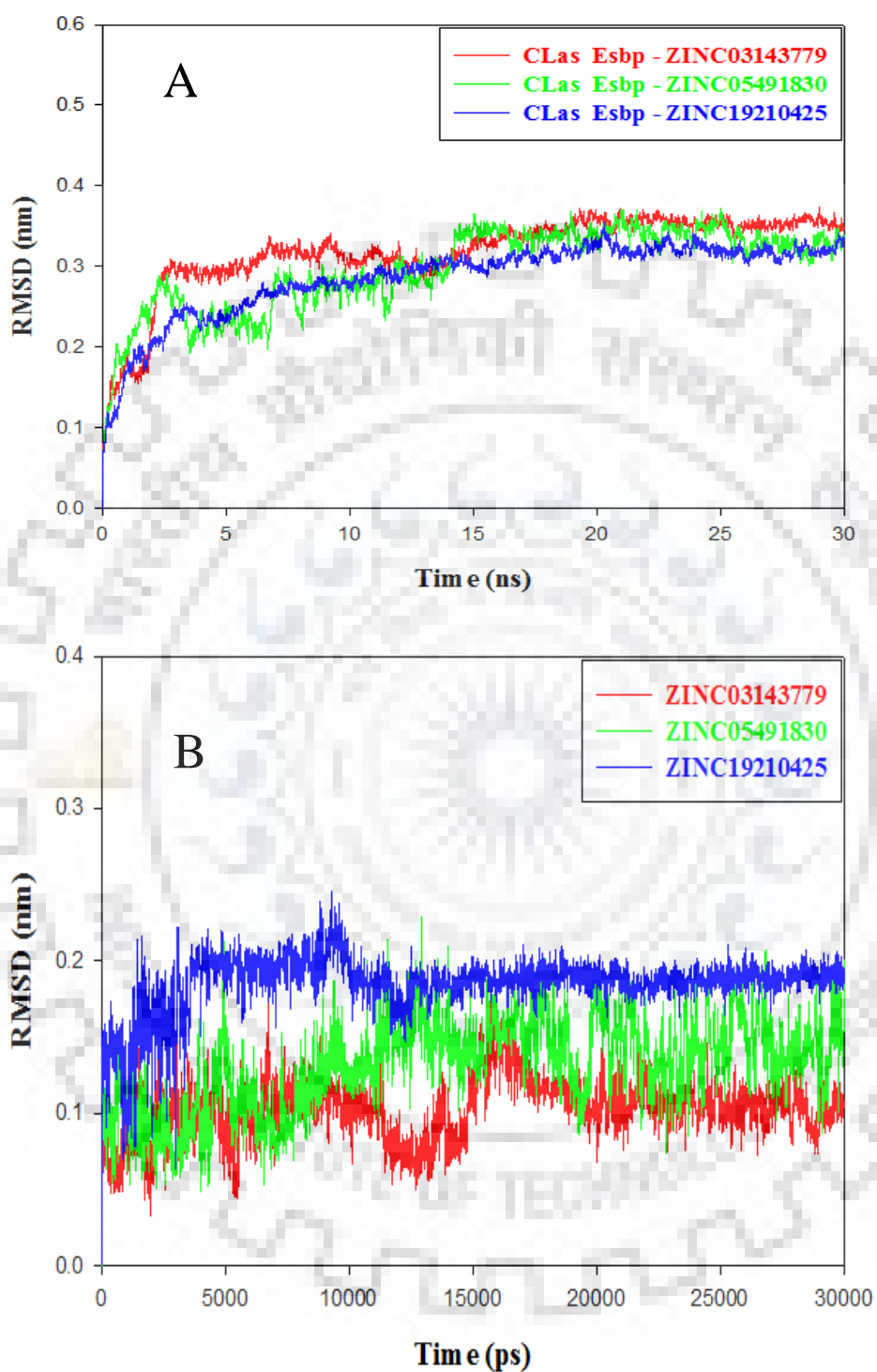


**Fig. 4.7: Root mean square deviation of protein-inhibitor(s) complexes and inhibitor(s) only.** RMSD plots showing; A) CLas-Esbp inhibitor(s) complexes, B) inhibitors: ZINC03143779 (red) , ZINC05491830 (green) and ZINC19210425 (blue), for 30 ns MD simulation.

#### 4.3.5.2. Root mean square fluctuation (RMSF)

The flexibility of the backbone of protein was determined by monitoring the RMSF of the sample structure. It refers to the fluctuation of the C $\alpha$  atom coordinates from its average position throughout the simulation. Usually, the high RMSF values indicate the loosely organized loops while secondary elements in the protein represent the less flexibility. In the present work, we calculated the residue mobility for each protein-ligand complex and plotted against the amino acid residues number according to MD simulation trajectory. The RMSF plot of CLas-Esbp-inhibitor(s) complexes is shown in Fig. 4.8. Results revealed that all three CLas-Esbp-ZINC03143779, CLas-Esbp- ZINC05491830 and CLas-Esbp-ZINC19210425 complexes were stable. The average RMSF values of the CLas-Esbp- inhibitor(s) are shown in Table 4.4. The overall study implies that all the inhibitor(s) molecules were well fitted in the binding site of the CLas-Esbp and forming a static and stable complex with CLas-Esbp protein.

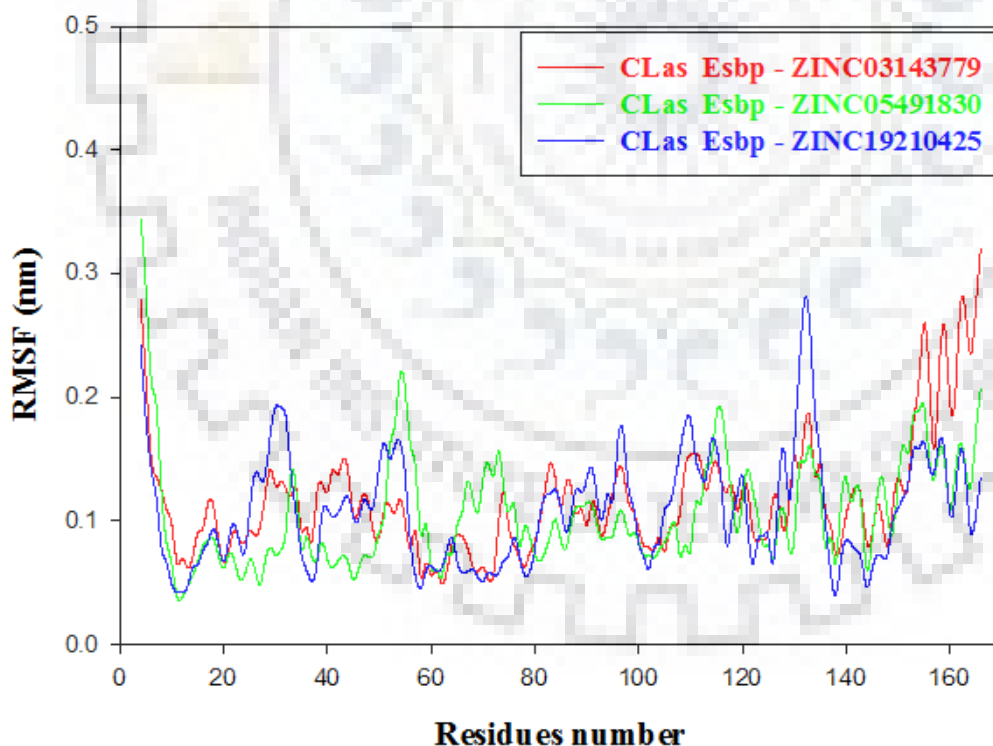


**Fig. 4.8: Root mean square fluctuation profiles of CLas-Esbp- ZINC03143779 (red) ,CLas-Esbp- ZINC05491830 (green) and CLas-Esbp- ZINC19210425 (blue) inhibitor(s) complexes during 30 ns MD simulation.**

### 4.3.5.3. Radius of gyration (Rg)

The overall compactness of the protein structure during the simulation was demonstrated by Radius of gyration (Rg). It is the distance between the center of mass of all atoms of protein and its terminal in a particular time interval. Generally, a stable folded protein structure maintains relatively less variation in the Rg value which calculates its dynamic stability. The plot of variation in the value of Rg versus time is represented in Fig. 4.9. The overall result revealed the compactness of the CLas-Esbp- inhibitor(s) complexes (Table 4.4). It also suggested that the secondary structural element is compactly packed in the CLas-Esbp- inhibitors and therefore forms stable complexes.

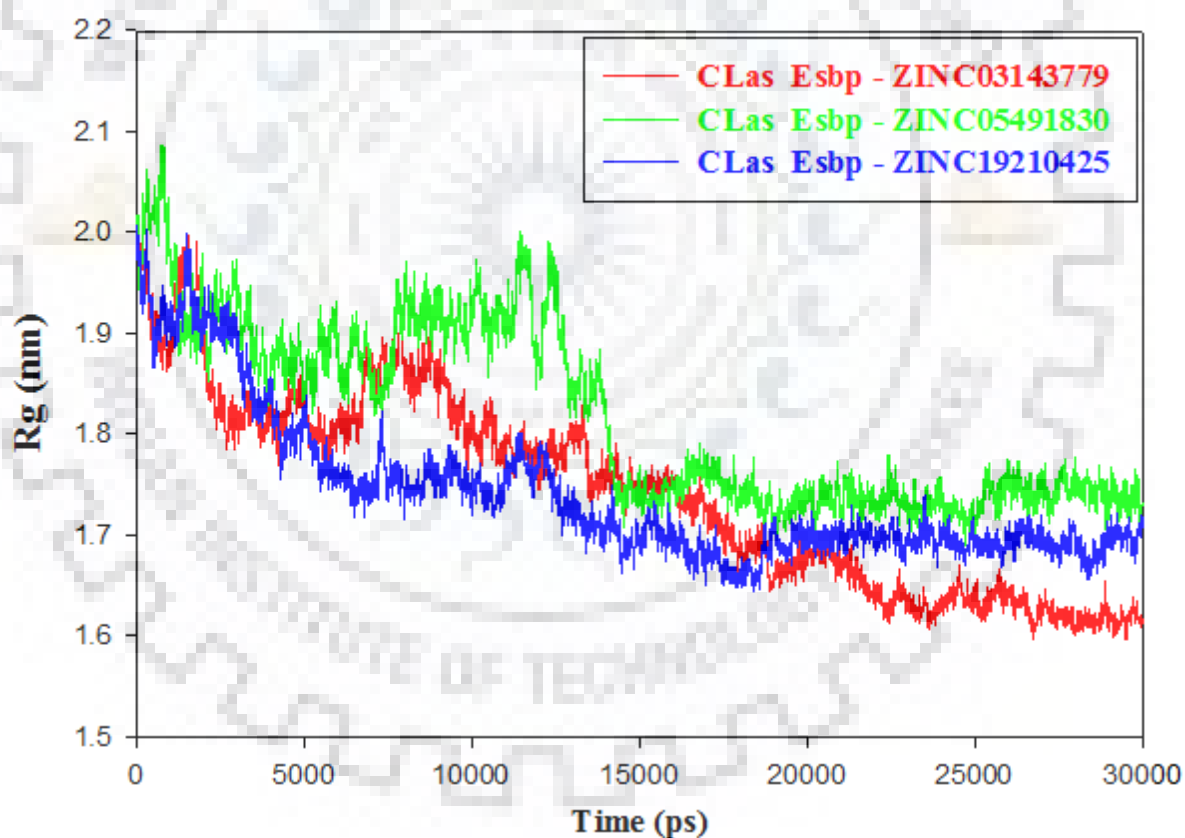


**Fig. 4.9:** Radius of gyration of CLas-Esbp- ZINC03143779 (red) , CLas-Esbp- ZINC05491830 (green) and CLas-Esbp- ZINC19210425 (blue) inhibitor(s) complexes during 30 ns MD simulation.

#### 4.3.5.4.Solvent accessible surface area (SASA)

Solvent accessible surface area (SASA) calculates the area of the solute which can interact with the solvent molecule through Van der Waals forces. SASA of a protein decreases with increment in compactness of protein, so a change in SASA can predict the change in the structure of a protein. The result of SASA suggests the stable complex formation of the CLas-Esbp with ZINC03143779, ZINC05491830, and ZINC19210425. Solvent accessible surface area profiles of CLas-Esbp-inhibitor(s) complexes are shown in the Fig. 4.10.

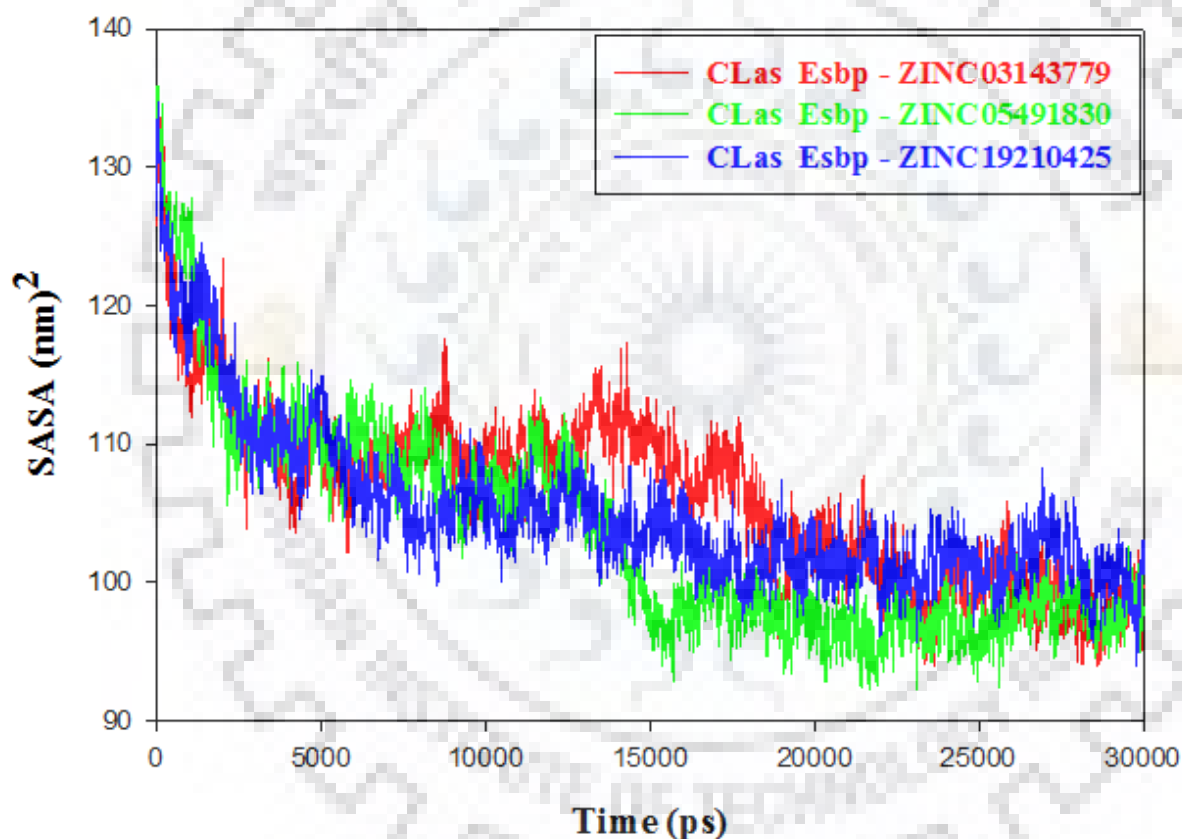


**Fig. 4.10:** Solvent accessible surface area profiles of of CLas-Esbp- ZINC03143779 (red) , CLas-Esbp- ZINC05491830 (green) and CLas-Esbp- ZINC19210425 (blue) inhibitor(s) complexes during 30 ns MD simulation.

#### 4.3.5.5. Hydrogen bond analysis

Hydrogen atom covalently attached to an electronegative atom can form hydrogen bonds within molecules or with other electronegative atoms. Hydrogen bond was generated within a range of 3.5Å between acceptor and donor. The g\_hbond of the GROMACS utility was used to find out the number and distribution of hydrogen bond in the CLas-Esbp- inhibitors complexes in order to explore the system stability through the molecular dynamic simulation period of 30ns. Inter-molecular hydrogen bonding result shows that CLas-Esbp -inhibitor(s) complexes possessed the minimum of four hydrogen bonds during the MD simulation as represented in Fig. 4.11A. The distribution of hydrogen bond length indicates the CLas-Esbp inhibitor complexes form hydrogen bond from high to low affinity as shown in Fig. 4.11B. The hydrogen bond results showed that all small molecules were efficiently bounded with the CLas-Esbp protein.



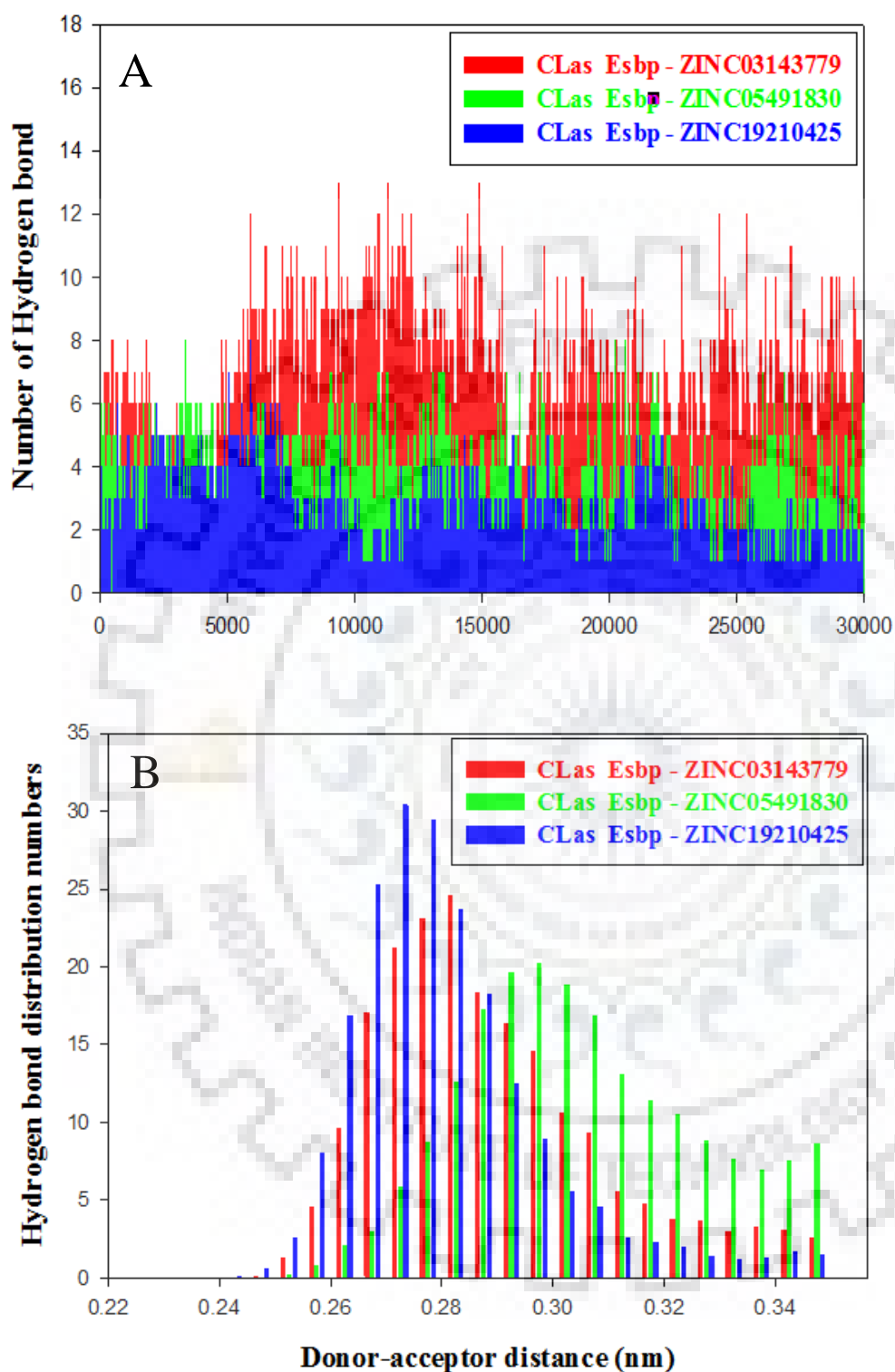


**Fig. 4.11: Hydrogen bond analysis of CLas-Esbp- ZINC03143779 (red) , CLas-Esbp- ZINC05491830 (green) and CLas-Esbp- ZINC19210425 (blue) inhibitor(s) complexes. A)intermolecular hydrogen bonding and B) Distribution of the Hydrogen bond during 30 ns MD simulation.**



#### 4.3.6. MMPBSA binding free energy calculation

The binding free energy calculation analysis was used for the quantitative estimation of the binding potential of the ligand. The binding free energies of all the protein-ligand complex(s) were determined using MMPBSA, a utility within GROMACS. It uses the trajectories of 25 ns to 30 ns of all protein-ligand complex(s) for determination of the binding energy of the complex(s). The results of MMPBSA are represented in Table 4.5. The binding free energy analysis showed that CLas-Esbp- inhibitor(s) complex(s) were stable. It confirms that selected small molecules ZINC03143779, ZINC05491830, and ZINC19210425 can bind efficiently at the binding site of CLas-Esbp protein.



**Table 4.5: Binding free energies calculation of CLas Esbp-inhibitor(s) complexes by MMPBSA.**

S.N O.	Compound	Van der Waals energy (kJ/mol)	Electrostatic energy (kJ/mol)	Polar solvation energy (kJ/mol)	SASA energy (kJ/mol)	Binding energy (kJ/mol)
1.	ZINC03143779	-90.000 +/- 0.361	-20.955 +/- 0.037	6.281 +/- 2.310	0.176 +/- 0.223	-105.452 +/- 2.715
2.	ZINC05491830	-119.426 +/- 4.300	-45.675 +/- 10.909	54.018 +/- 16.423	-2.038 +/- 0.500	-112.758 +/- 1.396
3.	ZINC19210425	-100.000 +/- 0.214	-1.678 +/- 0.014	-12.308 +/- 2.457	-0.254 +/- 0.191	-114.064 +/- 2.688

#### 4.4. Discussion

Huanglongbing (HLB) is a serious destructive disease of the citrus world [148]. It becomes difficult to effectively control with chemical compounds because CLas bacterium resides in the phloem as well as the presence of barrier of plant cuticle. However, several studies have reported many compounds which possess antimicrobial activity against HLB [239, 241, 324]. But to date, no compounds have been used commercially to control the HLB disease. There is no control strategy to control HLB disease in the field due to lack of HLB resistance cultivars, the fast rate of disease spreading and our inability to control the psyllids vector [325, 326]. Structural based virtual screening and molecular docking method have been used to discover the potent molecule to initiate synthesis of effective antimicrobial compounds. Molecular docking and simulations studies were utilized to predict the efficiency of binding of the ligand with macromolecules [303]. Here, we used the homology modeling for determining the 3-dimensional structure of CLas-Esbp protein and structure-based virtual screening to identify the novel potent antimicrobial compound(s) further simulation study to confirm the stability of the protein-inhibitor(s) complexes.

The present chapter focused on the successful search of novel potent compounds which might be able to inhibit the CLA growth by interferes the activity of Esbp which is an extracellular solute binding protein involved in binding to Fe metal. The identified compounds were suggested to affect the CLA vitality and survival by specifically inhibit the activity of Esbp protein.

The present study involves the cloning of Esbp from *Candidatus Liberibacter asiaticus* followed by computational analysis. The 3-dimensional model of CLas-Esbp consists of two  $\beta$ -strands and seven  $\alpha$ -helices connecting through loops. The Ramachandran plot analysis ensures the reliability and quality of the Model. And, this valid model was used for virtual screening of drug-like molecules.

Virtual screening can provide a valuable contribution to the discovery of novel compound(s); various software's have been designed for this purpose. In several projects of drug discovery, the virtual screening technology has been a powerful contributor to search the new molecule on the basis of the model and their binding site residue [307].

The predicted binding site of the CLas-Esbp was the target for virtual screening of the different compounds retrieved from the ZINC database and binding affinities of the compounds

were evaluated. Top 50 compounds were screened, fulfilling the Lipinski rule of five criteria. Out of 50, 10 molecules were selected on the basis of maximum binding affinity. Further, the comparative study of the selected small molecules was made with another molecular docking program Auto Dock 4.2.6. Molecular docking result show that three compounds ZINC03143779, ZINC05491830 and ZINC19210425 shows maximum binding affinity. ZINC03143779 forms hydrogen bond with His16, His64, Asp106 and Gln141, and interacts with Leu66, Pro67, and Pro143 through hydrophobic interaction. ZINC05491830 makes hydrogen bond with His64, Lys103, and Lys104 and Asp106, and interacts with Ile15, Leu66, Ile102, Pro143 and VAL147 hydrophobically. ZINC19210425 interacts with His64, Lys104 and Asp106 through hydrogen bonding and forms hydrophobic interaction with Ile15, Leu66, Ile102, Ala105 and Met139 (Fig. 4.6 and Fig. 4.12). A detailed summary of docking interaction is shown in Table 4.3.

To explore the structural and conformational variation, protein-ligand complexes were subjected to the molecular dynamic simulation. The overall RMSD result suggested that all three CLas-Esbp-ZINC03143779, CLas-Esbp- ZINC05491830 and CLas-Esbp-ZINC19210425 was forming stable complexes. The overall results of RMSF indicate that all the predicted small molecule inhibitors were found to be established in the cavity of the protein and binding of the inhibitors to the protein is static.

The less variation in the value of radius of gyration suggested that protein is compactly packed and binding of inhibitors do not affect the rigidity of the protein. SASA and hydrogen bonding analysis also support the stable binding of the small molecules to the protein.

The results of MMPBSA indicate that ZINC03143779, ZINC05491830 and ZINC19210425 inhibitors bind to the CLas-Esbp protein efficiently. Molecular dynamics study concludes that all three selected potent novel small molecules might be suggested to inhibit the activity of the Esbp protein of *Candidatus Liberibacter asiaticus*.

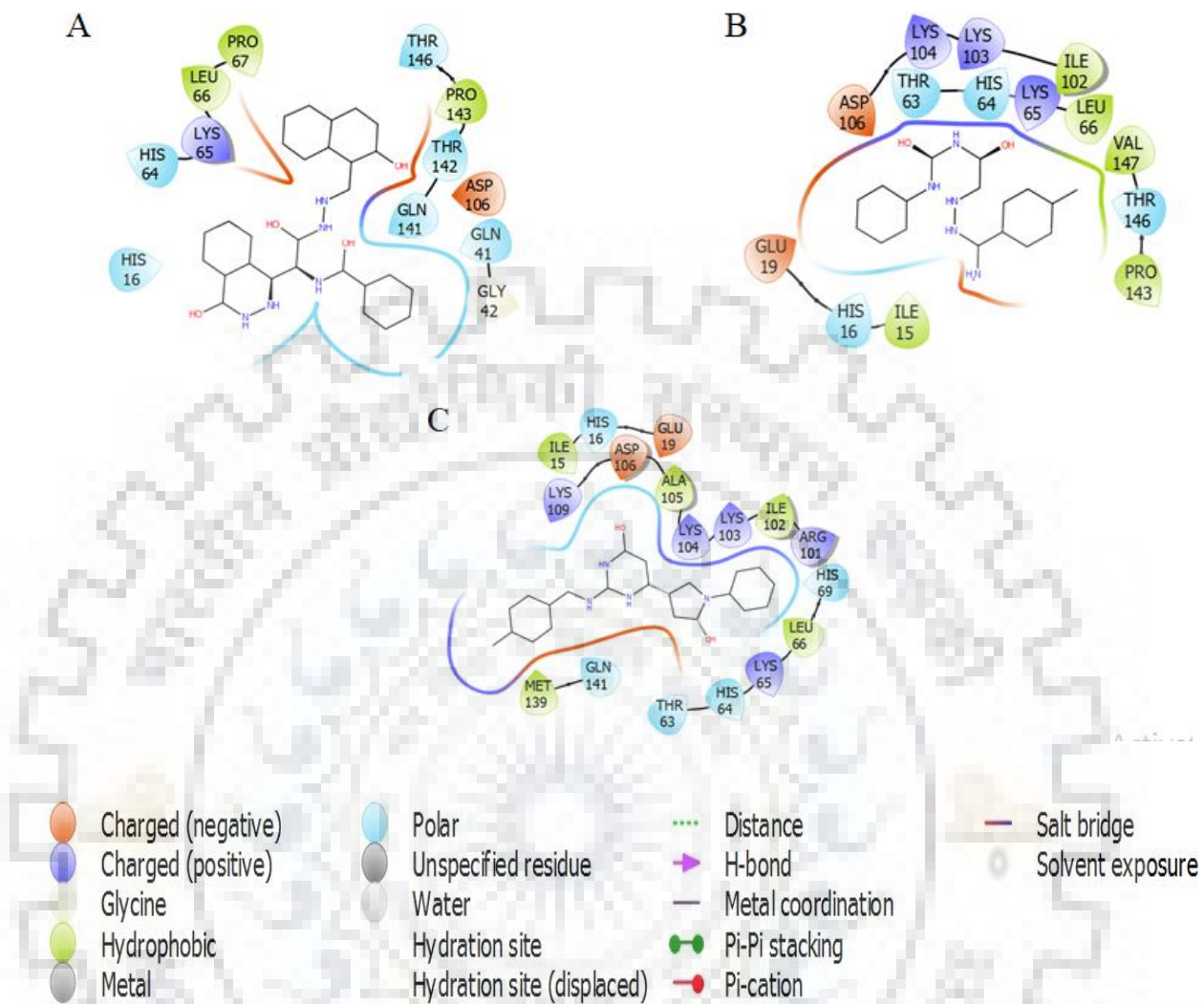


**Fig. 4.12:** Pictographic representation of interaction involved in binding of inhibitor(s) to CLAs-Esbp using Maestro 11.2. Hydrophobic, charged positive residues, charged negative residues and polar residues are shown in green color, blue color, orange color and cyan color, respectively.

#### 4.5. Conclusion

Citrus Huanglongbing is the most destructive disease of the citrus world. There are no control strategies to completely eradicate this disease. The effective strategy to control the HLB is to development of the inhibitors molecules against the CLA proteins which are critical for bacterial survival. Esbp, the extracellular solute binding protein might be suggested as a potential target protein in search of antimicrobial agents against the *Candidatus Liberibacter asiaticus*. Structure-based method was implied to identify the novel small molecules which can inhibit the activity of the CLAs-Esbp protein. For this, 3-dimension model of CLAs-Esbp was predicted and used for virtual screening of small molecules retrieved from ZINC database. 50 molecules were screened, fulfilling the range of Lipinski rule of five criteria. Out of 50 molecules, 10 were selected on the basis of maximum binding affinity score. The molecular docking was carried out to analyze the molecular interaction of the compounds with the protein. 3 molecules were selected for further analysis on the basis of comparison of the binding affinity energy showed by AutoDock Tools and AutoDock Vina. The minimization study confirms that the identified compounds ZINC03143779, ZINC05491830 and ZINC19210425 forming stable complexes with the CLAs-Esbp protein and inhibits the activity of Esbp protein of CLA. All of the above studied suggested that all the identified compounds might be good inhibitors of the Esbp protein of *Candidatus Liberibacter asiaticus*. This study provides a new pathway in the development of the antibacterial agents against the *Candidatus Liberibacter asiaticus*.



## REFERENCES

- [1] K. Singh, F. Ahmad, V.K. Singh, K. Kayastha, A.M. Kayastha, Purification, biochemical characterization and Insilico modeling of  $\alpha$ -amylase from *Vicia faba*, *Journal of Molecular Liquids*, 234 (2017) 133-141.
- [2] A. Kumari, V. Singh, J. Fitter, T. Polen, A. Kayastha, Purification, characterization and sequential similarity of conserved and catalytic amino acid residues, *Phytochemistry*, 71 (2010) 1657-1666.
- [3] T.J. Bourret, S. Porwollik, M. McClelland, R. Zhao, T. Greco, H. Ischiropoulos, A. Vázquez-Torres, Nitric oxide antagonizes the acid tolerance response that protects *Salmonella* against innate gastric defenses, *PLoS One*, 3 (2008) e1833.
- [4] Y. Pazy, A.C. Wollish, S.A. Thomas, P.J. Miller, E.J. Collins, R.B. Bourret, R.E. Silversmith, Matching biochemical reaction kinetics to the timescales of life: structural determinants that influence the autodephosphorylation rate of response regulator proteins, *Journal of molecular biology*, 392 (2009) 1205-1220.
- [5] R. Zhao, E.J. Collins, R.B. Bourret, R.E. Silversmith, Structure and catalytic mechanism of the *E. coli* chemotaxis phosphatase CheZ, *Nature Structural and Molecular Biology*, 9 (2002) 570.
- [6] A. Sette, J. Sidney, B.D. Livingston, J.L. Dzuris, C. Crimi, C.M. Walker, S. Southwood, E.J. Collins, A.L. Hughes, Class I molecules with similar peptide-binding specificities are the result of both common ancestry and convergent evolution, *Immunogenetics*, 54 (2003) 830-841.
- [7] S.R. Meena, S.P. Gangwar, A.K. Saxena, Purification, crystallization and preliminary X-ray crystallographic analysis of the ATPase domain of human TAP in nucleotide-free and ADP-, vanadate-and azide-complexed forms, *Acta Crystallographica Section F: Structural Biology and Crystallization Communications*, 68 (2012) 655-658.
- [8] K.P. Locher, Structure and mechanism of ATP-binding cassette transporters, *Philosophical Transactions of the Royal Society B: Biological Sciences*, 364 (2009) 239.
- [9] T. Mohammadi, V. Van Dam, R. Sijbrandi, T. Vernet, A. Zapun, A. Bouhss, M. Diepeveen-de Bruin, M. Nguyen-Distèche, B. De Kruijff, E. Breukink, Identification of

- FtsW as a transporter of lipid-linked cell wall precursors across the membrane, *The EMBO journal*, 30 (2011) 1425-1432.
- [10] M.K. Rawal, M.F. Khan, K. Kapoor, N. Goyal, S. Sen, A.K. Saxena, A.M. Lynn, J.D. Tyndall, B.C. Monk, R.D. Cannon, Insight into pleiotropic drug resistance ATP-binding cassette pump drug transport through mutagenesis of Cdr1p transmembrane domains, *Journal of Biological Chemistry*, 288 (2013) 24480-24493.
- [11] J. Kang, J.-U. Hwang, M. Lee, Y.-Y. Kim, S.M. Assmann, E. Martinoia, Y. Lee, PDR-type ABC transporter mediates cellular uptake of the phytohormone abscisic acid, *Proceedings of the National Academy of sciences*, 107 (2010) 2355-2360.
- [12] M. Lee, Y. Choi, B. Burla, Y.-Y. Kim, B. Jeon, M. Maeshima, J.-Y. Yoo, E. Martinoia, Y. Lee, The ABC transporter AtABCB14 is a malate importer and modulates stomatal response to CO<sub>2</sub>, *nature cell biology*, 10 (2008) 1217.
- [13] C.F. Higgins, ABC transporters: from microorganisms to man, *Annual review of cell biology*, 8 (1992) 67-113.
- [14] R.P.-A. Berntsson, S.H. Smits, L. Schmitt, D.-J. Slotboom, B. Poolman, A structural classification of substrate-binding proteins, *FEBS letters*, 584 (2010) 2606-2617.
- [15] C.F. Higgins, K.J. Linton, The ATP switch model for ABC transporters, *Nature Structural and Molecular Biology*, 11 (2004) 918.
- [16] T. van der Heide, B. Poolman, ABC transporters: one, two or four extracytoplasmic substrate-binding sites?, *EMBO reports*, 3 (2002) 938-943.
- [17] A.E. Senior, M.K. Al-Shawi, I.L. Urbatsch, The catalytic cycle of P-glycoprotein, *FEBS letters*, 377 (1995) 285-289.
- [18] Z.E. Sauna, I.-W. Kim, K. Nandigama, S. Kopp, P. Chiba, S.V. Ambudkar, Catalytic Cycle of ATP Hydrolysis by P-Glycoprotein: Evidence for Formation of the E<sub>o</sub>S Reaction Intermediate with ATP- $\gamma$ -S, a Nonhydrolyzable Analogue of ATP, *Biochemistry*, 46 (2007) 13787-13799.
- [19] A. Siarheyeva, R. Liu, F.J. Sharom, Characterization of an Asymmetric Occluded State of P-glycoprotein with Two Bound Nucleotides IMPLICATIONS FOR CATALYSIS, *Journal of Biological Chemistry*, 285 (2010) 7575-7586.
- [20] J. Chen, Molecular mechanism of the Escherichia coli maltose transporter, *Current opinion in structural biology*, 23 (2013) 492-498.

- [21] M.L. Oldham, J. Chen, Snapshots of the maltose transporter during ATP hydrolysis, *Proceedings of the National Academy of Sciences*, 108 (2011) 15152-15156.
- [22] V.M. Korkhov, S.A. Mireku, K.P. Locher, Structure of AMP-PNP-bound vitamin B 12 transporter BtuCD–F, *Nature*, 490 (2012) 367.
- [23] K.P. Locher, A.T. Lee, D.C. Rees, The E. coli BtuCD structure: a framework for ABC transporter architecture and mechanism, *Science*, 296 (2002) 1091-1098.
- [24] O. Lewinson, A.T. Lee, K.P. Locher, D.C. Rees, A distinct mechanism for the ABC transporter BtuCD–BtuF revealed by the dynamics of complex formation, *Nature Structural and Molecular Biology*, 17 (2010) 332.
- [25] R. M Counago, C. A McDevitt, M. P Ween, B. Kobe, Prokaryotic substrate-binding proteins as targets for antimicrobial therapies, *Current drug targets*, 13 (2012) 1400-1410.
- [26] F. Husada, G. Gouridis, R. Vietrov, G.K. Schuurman-Wolters, E. Ploetz, M. de Boer, B. Poolman, T. Cordes, Watching conformational dynamics of ABC transporters with single-molecule tools, *Biochemical Society Transactions*, 43 (2015) 1041-1047.
- [27] K. Hollenstein, D.C. Frei, K.P. Locher, Structure of an ABC transporter in complex with its binding protein, *Nature*, 446 (2007) 213.
- [28] H. Pinkett, A. Lee, P. Lum, K. Locher, D. Rees, An inward-facing conformation of a putative metal-chelate-type ABC transporter, *Science*, 315 (2007) 373-377.
- [29] R.J. Dawson, K.P. Locher, Structure of a bacterial multidrug ABC transporter, *Nature*, 443 (2006) 180.
- [30] R.J. Dawson, K.P. Locher, Structure of the multidrug ABC transporter Sav1866 from *Staphylococcus aureus* in complex with AMP-PNP, *FEBS letters*, 581 (2007) 935-938.
- [31] N.S. Kadaba, J.T. Kaiser, E. Johnson, A. Lee, D.C. Rees, The high-affinity E. coli methionine ABC transporter: structure and allosteric regulation, *Science*, 321 (2008) 250-253.
- [32] J. Kim, S. Wu, T.M. Tomasiak, C. Mergel, M.B. Winter, S.B. Stiller, Y. Robles-Colmanares, R.M. Stroud, R. Tampé, C.S. Craik, Subnanometre-resolution electron cryomicroscopy structure of a heterodimeric ABC exporter, *Nature*, 517 (2015) 396.
- [33] V. Srinivasan, A.J. Pierik, R. Lill, Crystal structures of nucleotide-free and glutathione-bound mitochondrial ABC transporter Atm1, *Science*, 343 (2014) 1137-1140.

- [34] K. Xu, M. Zhang, Q. Zhao, F. Yu, H. Guo, C. Wang, F. He, J. Ding, P. Zhang, Crystal structure of a folate energy-coupling factor transporter from *Lactobacillus brevis*, *Nature*, 497 (2013) 268.
- [35] K. Hollenstein, R.J. Dawson, K.P. Locher, Structure and mechanism of ABC transporter proteins, *Current opinion in structural biology*, 17 (2007) 412-418.
- [36] K.S. Chaturvedi, J.P. Henderson, Pathogenic adaptations to host-derived antibacterial copper, *Frontiers in cellular and infection microbiology*, 4 (2014) 3.
- [37] A.G. Vitreschak, D.A. Rodionov, A.A. Mironov, M.S. Gelfand, Regulation of riboflavin biosynthesis and transport genes in bacteria by transcriptional and translational attenuation, *Nucleic acids research*, 30 (2002) 3141-3151.
- [38] A. Gutiérrez-Preciado, A.G. Torres, E. Merino, H.R. Bonomi, F.A. Goldbaum, V.A. García-Angulo, Extensive identification of bacterial riboflavin transporters and their distribution across bacterial species, *PLoS One*, 10 (2015) e0126124.
- [39] K.J. Tanaka, S. Song, K. Mason, H.W. Pinkett, Selective substrate uptake: The role of ATP-binding cassette (ABC) importers in pathogenesis, *Biochimica et Biophysica Acta (BBA)-Biomembranes*, (2017).
- [40] S.C. Andrews, A.K. Robinson, F. Rodríguez-Quñones, Bacterial iron homeostasis, *FEMS microbiology reviews*, 27 (2003) 215-237.
- [41] R. Tam, M. Saier, Structural, functional, and evolutionary relationships among extracellular solute-binding receptors of bacteria, *Microbiological reviews*, 57 (1993) 320-346.
- [42] M.-H. Charon, L.-F. Wu, C. Piras, K. de Pina, M.-A. Mandrand-Berthelot, J.C. Fontecilla-Camps, Crystallization and preliminary X-ray diffraction study of the nickel-binding protein NikA of *Escherichia coli*, *Journal of molecular biology*, 243 (1994) 353-355.
- [43] C.B. Felder, R.C. Graul, A.Y. Lee, H.-P. Merkle, W. Sadee, The Venus flytrap of periplasmic binding proteins: an ancient protein module present in multiple drug receptors, *AAps pharmsci*, 1 (1999) 7-26.
- [44] J. Marvin, E. Corcoran, N. Hattangadi, J. Zhang, S. Gere, H. Hellinga, The rational design of allosteric interactions in a monomeric protein and its applications to the construction of biosensors, *Proceedings of the National Academy of Sciences*, 94 (1997) 4366-4371.
- [45] D. Maglott, J. Ostell, K.D. Pruitt, T. Tatusova, Entrez Gene: gene-centered information at NCBI, *Nucleic acids research*, 39 (2010) D52-D57.

- [46] R.P.-A. Berntsson, Structure and function of substrate-binding proteins of ABC-transporters, University of Groningen, (2010).
- [47] S. Gonin, P. Arnoux, B. Pierru, J. Lavergne, B. Alonso, M. Sabaty, D. Pignol, Crystal structures of an extracytoplasmic solute receptor from a TRAP transporter in its open and closed forms reveal a helix-swapped dimer requiring a cation for  $\alpha$ -keto acid binding, *BMC structural biology*, 7 (2007) 11.
- [48] C. Mulligan, E.R. Geertsma, E. Severi, D.J. Kelly, B. Poolman, G.H. Thomas, The substrate-binding protein imposes directionality on an electrochemical sodium gradient-driven TRAP transporter, *Proceedings of the National Academy of Sciences*, 106 (2009) 1778-1783.
- [49] L.T. Rosa, M.E. Bianconi, G.H. Thomas, D.J. Kelly, Tripartite ATP-Independent Periplasmic (TRAP) Transporters and Tripartite Tricarboxylate Transporters (TTT): From Uptake to Pathogenicity, *Frontiers in Cellular and Infection Microbiology*, 8 (2018).
- [50] M.B. Neiditch, M.J. Federle, A.J. Pompeani, R.C. Kelly, D.L. Swem, P.D. Jeffrey, B.L. Bassler, F.M. Hughson, Ligand-induced asymmetry in histidine sensor kinase complex regulates quorum sensing, *Cell*, 126 (2006) 1095-1108.
- [51] K.S. Misono, Natriuretic peptide receptor: structure and signaling, *Molecular and cellular biochemistry*, 230 (2002) 49-60.
- [52] N. Armstrong, E. Gouaux, Mechanisms for activation and antagonism of an AMPA-sensitive glutamate receptor: crystal structures of the GluR2 ligand binding core, *Neuron*, 28 (2000) 165-181.
- [53] M. Lewis, G. Chang, N.C. Horton, M.A. Kercher, H.C. Pace, M.A. Schumacher, R.G. Brennan, P. Lu, Crystal structure of the lactose operon repressor and its complexes with DNA and inducer, *Science*, 271 (1996) 1247-1254.
- [54] A.M. Friedman, T.O. Fischmann, T.A. Steitz, Crystal structure of lac repressor core tetramer and its implications for DNA looping, *Science*, 268 (1995) 1721-1727.
- [55] M.A. Schumacher, K.Y. Choi, H. Zalkin, R.G. Brennan, Crystal structure of LacI member, PurR, bound to DNA: minor groove binding by alpha helices, *Science*, 266 (1994) 763-770.
- [56] G.H. Scheepers, J.A. Lycklama a Nijeholt, B. Poolman, An updated structural classification of substrate-binding proteins, *FEBS letters*, 590 (2016) 4393-4401.



- [57] M.H. Saier Jr, V.S. Reddy, D.G. Tamang, Å. Västermark, The transporter classification database, *Nucleic acids research*, 42 (2013) D251-D258.
- [58] M.H. Saier Jr, V.S. Reddy, B.V. Tsu, M.S. Ahmed, C. Li, G. Moreno-Hagelsieb, The transporter classification database (TCDB): recent advances, *Nucleic acids research*, 44 (2015) D372-D379.
- [59] M.H. Saier Jr, M.R. Yen, K. Noto, D.G. Tamang, C. Elkan, The transporter classification database: recent advances, *Nucleic acids research*, 37 (2008) D274-D278.
- [60] B. Wang, M. Dukarevich, E.I. Sun, M.R. Yen, M.H. Saier, Membrane porters of ATP-binding cassette transport systems are polyphyletic, *Journal of Membrane Biology*, 231 (2009) 1.
- [61] M.H. Saier, A functional-phylogenetic classification system for transmembrane solute transporters, *Microbiology and Molecular Biology Reviews*, 64 (2000) 354-411.
- [62] W. Saurin, E. Dassa, Sequence relationships between integral inner membrane proteins of binding protein-dependent transport systems: Evolution by recurrent gene duplications, *Protein Science*, 3 (1994) 325-344.
- [63] J.-P. Claverys, A new family of high-affinity ABC manganese and zinc permeases, *Research in microbiology*, 152 (2001) 231-243.
- [64] A. Dintilhac, J.-P. Claverys, The *adc* locus, which affects competence for genetic transformation in *Streptococcus pneumoniae*, encodes an ABC transporter with a putative lipoprotein homologous to a family of streptococcal adhesins, *Research in microbiology*, 148 (1997) 119-131.
- [65] K. Fukami-Kobayashi, Y. Tateno, K. Nishikawa, Domain dislocation: a change of core structure in periplasmic binding proteins in their evolutionary history<sup>1</sup>, *Journal of molecular biology*, 286 (1999) 279-290.
- [66] Y.-H. Lee, R.K. Deka, M.V. Norgard, J.D. Radolf, C.A. Hasemann, *Treponema pallidum* TroA is a periplasmic zinc-binding protein with a helical backbone, *Nature Structural and Molecular Biology*, 6 (1999) 628.
- [67] J.S. Klein, O. Lewinson, Bacterial ATP-driven transporters of transition metals: physiological roles, mechanisms of action, and roles in bacterial virulence, *Metallomics*, 3 (2011) 1098-1108.
- [68] A.I. Graham, S. Hunt, S.L. Stokes, N. Bramall, J. Bunch, A.G. Cox, C.W. McLeod, R.K. Poole, Severe zinc depletion of *Escherichia coli* roles for high affinity zinc binding by



- ZinT, zinc transport and zinc-independent proteins, *Journal of Biological Chemistry*, 284 (2009) 18377-18389.
- [69] V.G. Lewis, M.P. Ween, C.A. McDevitt, The role of ATP-binding cassette transporters in bacterial pathogenicity, *Protoplasma*, 249 (2012) 919-942.
- [70] J.C. Fenno, A. Shaikh, G. Spatafora, P. Fives-Taylor, The *fimA* locus of *Streptococcus parasanguis* encodes an ATP-binding membrane transport system, *Molecular microbiology*, 15 (1995) 849-863.
- [71] H.F. Jenkinson, Cell surface protein receptors in oral streptococci, *FEMS microbiology letters*, 121 (1994) 133-140.
- [72] P.E. Kolenbrander, R.N. Andersen, N. Ganeshkumar, Nucleotide sequence of the *Streptococcus gordonii* PK488 coaggregation adhesin gene, *scaA*, and ATP-binding cassette, *Infection and immunity*, 62 (1994) 4469-4480.
- [73] V.V. Bartsevich, H. Pakrasi, Molecular identification of an ABC transporter complex for manganese: analysis of a cyanobacterial mutant strain impaired in the photosynthetic oxygen evolution process, *The EMBO journal*, 14 (1995) 1845-1853.
- [74] A. Dintilhac, G. Alloing, C. Granadel, J.P. Claverys, Competence and virulence of *Streptococcus pneumoniae*: *Adc* and *PsaA* mutants exhibit a requirement for Zn and Mn resulting from inactivation of putative ABC metal permeases, *Molecular microbiology*, 25 (1997) 727-739.
- [75] V. Tedde, R. Rosini, C.L. Galeotti, Zn<sup>2+</sup> Uptake in *Streptococcus pyogenes*: Characterization of *adcA* and *lmb* Null Mutants, *PloS one*, 11 (2016) e0152835.
- [76] B.F. Weston, A. Brenot, M.G. Caparon, The metal homeostasis protein, *Lsp*, of *Streptococcus pyogenes* is necessary for acquisition of zinc and virulence, *Infection and immunity*, 77 (2009) 2840-2848.
- [77] N.S. Jakubovics, A.W. Smith, H.F. Jenkinson, Expression of the virulence-related *Sca* (Mn<sup>2+</sup>) permease in *Streptococcus gordonii* is regulated by a diphtheria toxin metalloregressor-like protein *ScaR*, *Molecular microbiology*, 38 (2000) 140-153.
- [78] C. Linke, T.T. Caradoc-Davies, P.G. Young, T. Proft, E.N. Baker, The laminin-binding protein *Lbp* from *Streptococcus pyogenes* is a zinc receptor, *Journal of bacteriology*, 191 (2009) 5814-5823.

- [79] P. Raganathan, B. Spellerberg, K. Ponnuraj, Structure of laminin-binding adhesin (Lmb) from *Streptococcus agalactiae*, *Acta Crystallographica Section D: Biological Crystallography*, 65 (2009) 1262-1269.
- [80] A.J. Messenger, R. Barclay, Bacteria, iron and pathogenicity, *Biochemistry and Molecular Biology Education*, 11 (1983) 54-63.
- [81] L.D. Palmer, E.P. Skaar, Transition Metals and Virulence in Bacteria, *Annual Review of Genetics*, 50 (2016) 67-91.
- [82] M.I. Hood, E.P. Skaar, Nutritional immunity: transition metals at the pathogen–host interface, *Nature Reviews Microbiology*, 10 (2012) 525.
- [83] L.D. Palmer, E.P. Skaar, Transition metals and virulence in bacteria, *Annual review of genetics*, 50 (2016) 67-91.
- [84] D.G. Kehres, A. Janakiraman, J.M. Slauch, M.E. Maguire, SitABCD is the alkaline Mn<sup>2+</sup> transporter of *Salmonella enterica* serovar Typhimurium, *Journal of bacteriology*, 184 (2002) 3159-3166.
- [85] J. Kelliher, T. Kehl-Fie, Competition for manganese at the host–pathogen interface, *Progress in molecular biology and translational science*, Elsevier, Place Published, 2016, pp. 1-25.
- [86] E. Boyer, I. Bergevin, D. Malo, P. Gros, M. Cellier, Acquisition of Mn (II) in addition to Fe (II) is required for full virulence of *Salmonella enterica* serovar Typhimurium, *Infection and immunity*, 70 (2002) 6032-6042.
- [87] C.M. Litwin, S. Calderwood, Role of iron in regulation of virulence genes, *Clinical microbiology reviews*, 6 (1993) 137-149.
- [88] S.A. Moore, B.F. Anderson, C.R. Groom, M. Haridas, E.N. Baker, Three-dimensional structure of diferric bovine lactoferrin at 2.8 Å resolution<sup>11</sup>Edited by D. Rees, *Journal of Molecular Biology*, 274 (1997) 222-236.
- [89] S. Sharma, J. Jasti, J. Kumar, A.K. Mohanty, T.P. Singh, Crystal Structure of a Proteolytically Generated Functional Monoferric C-lobe of Bovine Lactoferrin at 1.9Å Resolution, *Journal of Molecular Biology*, 331 (2003) 485-496.
- [90] E.N. Baker, H.M. Baker, A structural framework for understanding the multifunctional character of lactoferrin, *Biochimie*, 91 (2009) 3-10.
- [91] H.M. Baker, E.N. Baker, Lactoferrin and Iron: structural and dynamic aspects of binding and release, *Biometals*, 17 (2004) 209-216.

- [92] K.R. Hazlett, F. Rusnak, D.G. Kehres, S.W. Bearden, C.J. La Vake, M.E. La Vake, M.E. Maguire, R.D. Perry, J.D. Radolf, The *Treponema pallidum* tro operon encodes a multiple metal transporter, a zinc-dependent transcriptional repressor, and a semi-autonomously expressed phosphoglycerate mutase, *Journal of Biological Chemistry*, 278 (2003) 20687-20694.
- [93] M.C. Lawrence, P.A. Pilling, V.C. Epa, A.M. Berry, A.D. Ogunniyi, J.C. Paton, The crystal structure of pneumococcal surface antigen PsaA reveals a metal-binding site and a novel structure for a putative ABC-type binding protein, *Structure*, 6 (1998) 1553-1561.
- [94] E. Permyakov, *Metalloproteomics*, John Wiley & Sons, Place Published, 2009.
- [95] M.M. Harding, Small revisions to predicted distances around metal sites in proteins, *Acta Crystallographica Section D: Biological Crystallography*, 62 (2006) 678-682.
- [96] E. Thomas Yukl, *The Cluster A-I Solute-Binding Proteins*, Place Published, 2017.
- [97] A. Ilari, L. Pescatori, R. Di Santo, A. Battistoni, S. Ammendola, M. Falconi, F. Berlutti, P. Valenti, E. Chiancone, *Salmonella enterica* serovar Typhimurium growth is inhibited by the concomitant binding of Zn (II) and a pyrrolyl-hydroxamate to ZnuA, the soluble component of the ZnuABC transporter, *Biochimica et Biophysica Acta (BBA)-General Subjects*, 1860 (2016) 534-541.
- [98] A. Ilari, F. Alaleona, P. Petrarca, A. Battistoni, E. Chiancone, The X-ray structure of the zinc transporter ZnuA from *Salmonella enterica* discloses a unique triad of zinc-coordinating histidines, *Journal of molecular biology*, 409 (2011) 630-641.
- [99] B.R. Chandra, M. Yogavel, A. Sharma, Structural analysis of ABC-family periplasmic zinc binding protein provides new insights into mechanism of ligand uptake and release, *Journal of molecular biology*, 367 (2007) 970-982.
- [100] H. Li, G. Jogl, Crystal structure of the zinc-binding transport protein ZnuA from *Escherichia coli* reveals an unexpected variation in metal coordination, *Journal of molecular biology*, 368 (2007) 1358-1366.
- [101] L.A. Yatsunyk, J.A. Easton, L.R. Kim, S.A. Sugarbaker, B. Bennett, R.M. Brece, I.I. Vorontsov, D.L. Tierney, M.W. Crowder, A.C. Rosenzweig, Structure and metal binding properties of ZnuA, a periplasmic zinc transporter from *Escherichia coli*, *JBIC Journal of Biological Inorganic Chemistry*, 13 (2008) 271-288.

- [102] S. Banerjee, B. Wei, M. Bhattacharyya-Pakrasi, H.B. Pakrasi, T.J. Smith, Structural determinants of metal specificity in the zinc transport protein ZnuA from *Synechocystis* 6803, *Journal of molecular biology*, 333 (2003) 1061-1069.
- [103] B. Wei, A.M. Randich, M. Bhattacharyya-Pakrasi, H.B. Pakrasi, T.J. Smith, Possible regulatory role for the histidine-rich loop in the zinc transport protein, ZnuA, *Biochemistry*, 46 (2007) 8734-8743.
- [104] B. Zheng, Q. Zhang, J. Gao, H. Han, M. Li, J. Zhang, J. Qi, J. Yan, G.F. Gao, Insight into the interaction of metal ions with TroA from *Streptococcus suis*, *PLoS One*, 6 (2011) e19510.
- [105] Y.-H. Lee, M.R. Dorwart, K.R. Hazlett, R.K. Deka, M.V. Norgard, J.D. Radolf, C.A. Hasemann, The crystal structure of Zn (II)-free *Treponema pallidum* TroA, a periplasmic metal-binding protein, reveals a closed conformation, *Journal of bacteriology*, 184 (2002) 2300-2304.
- [106] P. Ragunathan, D. Sridaran, A. Weigel, S. Shabayek, B. Spellerberg, K. Ponnuraj, Metal binding is critical for the folding and function of laminin binding protein, Lmb of *Streptococcus agalactiae*, *PloS one*, 8 (2013) e67517.
- [107] V. Rukhman, R. Anati, M. Melamed-Frank, N. Adir, The MntC crystal structure suggests that import of Mn<sup>2+</sup> in cyanobacteria is redox controlled, *Journal of molecular biology*, 348 (2005) 961-969.
- [108] M. Kanteev, N. Adir, Arginine 116 stabilizes the entrance to the metal ion-binding site of the MntC protein, *Acta Crystallographica Section F: Structural Biology and Crystallization Communications*, 69 (2013) 237-242.
- [109] R.M. Couñago, M.P. Ween, S.L. Begg, M. Bajaj, J. Zuegg, M.L. O'mara, M.A. Cooper, A.G. McEwan, J.C. Paton, B. Kobe, Imperfect coordination chemistry facilitates metal ion release in the Psa permease, *Nature chemical biology*, 10 (2014) 35.
- [110] S.L. Begg, B.A. Eijkelkamp, Z. Luo, R.M. Couñago, J.R. Morey, M.J. Maher, Y.O. Cheryl-lynn, A.G. McEwan, B. Kobe, M.L. O'Mara, Dysregulation of transition metal ion homeostasis is the molecular basis for cadmium toxicity in *Streptococcus pneumoniae*, *Nature communications*, 6 (2015) 6418.
- [111] C.A. McDevitt, A.D. Ogunniyi, E. Valkov, M.C. Lawrence, B. Kobe, A.G. McEwan, J.C. Paton, A molecular mechanism for bacterial susceptibility to zinc, *PLoS pathogens*, 7 (2011) e1002357.

- [112] E. Loisel, L. Jacquamet, L. Serre, C. Bauvois, J.L. Ferrer, T. Vernet, A.M. Di Guilmi, C. Durmort, AdcAII, a new pneumococcal Zn-binding protein homologous with ABC transporters: biochemical and structural analysis, *Journal of molecular biology*, 381 (2008) 594-606.
- [113] N. Sharma, P. Selvakumar, S. Bhose, D.K. Ghosh, P. Kumar, A.K. Sharma, Crystal structure of a periplasmic solute binding protein in metal-free, intermediate and metal-bound states from *Candidatus Liberibacter asiaticus*, *Journal of structural biology*, 189 (2015) 184-194.
- [114] X. Sun, H.M. Baker, R. Ge, H. Sun, Q.-Y. He, E.N. Baker, Crystal structure and metal binding properties of the lipoprotein MtsA, responsible for iron transport in *Streptococcus pyogenes*, *Biochemistry*, 48 (2009) 6184-6190.
- [115] M. Handali, D.P. Neupane, H. Roychowdhury, E.T. Yukl, Transcriptional regulation, metal binding properties and structure of Pden1597, an unusual zinc transport protein from *Paracoccus denitrificans*, *Journal of Biological Chemistry*, 290 (2015) 11878-11889.
- [116] D.C. Desrosiers, Y.C. Sun, A.A. Zaidi, C.H. Eggers, D.L. Cox, J.D. Radolf, The general transition metal (Tro) and Zn<sup>2+</sup> (Znu) transporters in *Treponema pallidum*: analysis of metal specificities and expression profiles, *Molecular microbiology*, 65 (2007) 137-152.
- [117] K. Guan, J.E. Dixon, Protein tyrosine phosphatase activity of an essential virulence determinant in *Yersinia*, *Science*, 249 (1990) 553-556.
- [118] A. Koul, A. Choidas, M. Treder, A.K. Tyagi, K. Drlica, Y. Singh, A. Ullrich, Cloning and characterization of secretory tyrosine phosphatases of *Mycobacterium tuberculosis*, *Journal of Bacteriology*, 182 (2000) 5425-5432.
- [119] A.K. Saxena, K. Singh, H.-P. Su, M.M. Klein, A.W. Stowers, A.J. Saul, C.A. Long, D.N. Garboczi, The essential mosquito-stage P25 and P28 proteins from *Plasmodium falciparum* form tile-like triangular prisms, *Nature Structural and Molecular Biology*, 13 (2006) 90.
- [120] P. Gupta, M. Kumar Singh, P. Singh, M. Tiwari, R. Kumar Dhaked, Antibodies against recombinant shiga toxin subunit B neutralize shiga toxin toxicity in HeLa cells, *Protein and peptide letters*, 17 (2010) 774-781.
- [121] C. Frolet, M. Beniazza, L. Roux, B. Gallet, M. Noirclerc-Savoye, T. Vernet, A.M. Di Guilmi, New adhesin functions of surface-exposed pneumococcal proteins, *BMC microbiology*, 10 (2010) 190.



- [122] H. Bora, S. Garg, P. Sen, D. Kumar, P. Kaur, R.H. Khan, Y.D. Sharma, Plasmodium vivax tryptophan-rich antigen PvTRAg33. 5 contains alpha helical structure and multidomain architecture, PLoS One, 6 (2011) e16294.
- [123] S.P. Gangwar, S.R. Meena, A.K. Saxena, Cloning, purification, crystallization and preliminary X-ray analysis of ESX-1-secreted protein regulator (EspR) from Mycobacterium tuberculosis, Acta Crystallographica Section F: Structural Biology and Crystallization Communications, 67 (2011) 83-86.
- [124] U. Jayaramaiah, N. Singh, S. Thankappan, A.K. Mohanty, P. Chaudhuri, V.P. Singh, V.K. Nagaleekar, Proteomic analysis and identification of cell surface-associated proteins of Clostridium chauvoei, Anaerobe, 39 (2016) 77-83.
- [125] R.K. Dhaked, M.K. Singh, P. Singh, P. Gupta, Botulinum toxin: bioweapon & magic drug, The Indian journal of medical research, 132 (2010) 489.
- [126] M. Kumar Singh, R. Kumar Dhaked, P. Singh, P. Gupta, L. Singh, Characterization of LC-HCC fusion protein of botulinum neurotoxin type A, Protein and peptide letters, 18 (2011) 295-304.
- [127] G. Weiss, P.L. Carver, Role of divalent metals in infectious disease susceptibility and outcome, Clinical Microbiology and Infection, 24 (2018) 16-23.
- [128] K.M. Papp-Wallace, M.E. Maguire, Manganese transport and the role of manganese in virulence, Annu. Rev. Microbiol., 60 (2006) 187-209.
- [129] L.J. McAllister, H.J. Tseng, A.D. Ogunniyi, M.P. Jennings, A.G. McEwan, J.C. Paton, Molecular analysis of the psa permease complex of Streptococcus pneumoniae, Molecular microbiology, 53 (2004) 889-901.
- [130] M.J. Horsburgh, S.J. Wharton, A.G. Cox, E. Ingham, S. Peacock, S.J. Foster, MntR modulates expression of the PerR regulon and superoxide resistance in Staphylococcus aureus through control of manganese uptake, Molecular microbiology, 44 (2002) 1269-1286.
- [131] R. Janulczyk, S. Ricci, L. Björck, MntABC is important for manganese and iron transport, oxidative stress resistance, and virulence of Streptococcus pyogenes, Infection and immunity, 71 (2003) 2656-2664.
- [132] K.H. Lim, C.E. Jones, R.N. Vanden Hoven, J.L. Edwards, M.L. Falsetta, M.A. Apicella, M.P. Jennings, A.G. McEwan, Metal binding specificity of the MntABC permease of



- Neisseria gonorrhoeae* and its influence on bacterial growth and interaction with cervical epithelial cells, *Infection and immunity*, 76 (2008) 3569-3576.
- [133] S. Paik, A. Brown, C.L. Munro, C.N. Cornelissen, T. Kitten, The *sloABCR* operon of *Streptococcus mutans* encodes an Mn and Fe transport system required for endocarditis virulence and its Mn-dependent repressor, *Journal of bacteriology*, 185 (2003) 5967-5975.
- [134] P.J.W. Schreur, J.M. Rebel, M.A. Smits, J.P. van Putten, H.E. Smith, *TroA* of *Streptococcus suis* is required for manganese acquisition and full virulence, *Journal of bacteriology*, 193 (2011) 5073-5080.
- [135] C. Andreini, I. Bertini, G. Cavallaro, G.L. Holliday, J.M. Thornton, Metal ions in biological catalysis: from enzyme databases to general principles, *JBIC Journal of Biological Inorganic Chemistry*, 13 (2008) 1205-1218.
- [136] J.E. Coleman, Zinc enzymes, *Current opinion in chemical biology*, 2 (1998) 222-234.
- [137] L. Bayle, S. Chimalapati, G. Schoehn, J. Brown, T. Vernet, C. Durmort, Zinc uptake by *Streptococcus pneumoniae* depends on both *AdcA* and *AdcAII* and is essential for normal bacterial morphology and virulence, *Molecular microbiology*, 82 (2011) 904-916.
- [138] R. Gabbianelli, R. Scotti, S. Ammendola, P. Petrarca, L. Nicolini, A. Battistoni, Role of *ZnuABC* and *ZinT* in *Escherichia coli* O157: H7 zinc acquisition and interaction with epithelial cells, *BMC microbiology*, 11 (2011) 36.
- [139] T.S. Gunasekera, A.H. Herre, M.W. Crowder, Absence of *ZnuABC*-mediated zinc uptake affects virulence-associated phenotypes of uropathogenic *Escherichia coli* CFT073 under Zn (II)-depleted conditions, *FEMS microbiology letters*, 300 (2009) 36-41.
- [140] M. Sabri, S. Houle, C.M. Dozois, Roles of the extraintestinal pathogenic *Escherichia coli* *ZnuACB* and *ZupT* zinc transporters during urinary tract infection, *Infection and immunity*, 77 (2009) 1155-1164.
- [141] S. Ammendola, P. Pasquali, C. Pistoia, P. Petrucci, P. Petrarca, G. Rotilio, A. Battistoni, High-affinity Zn<sup>2+</sup> uptake system *ZnuABC* is required for bacterial zinc homeostasis in intracellular environments and contributes to the virulence of *Salmonella enterica*, *Infection and immunity*, 75 (2007) 5867-5876.
- [142] S. Campoy, M. Jara, N. Busquets, A.M.P. de Rozas, I. Badiola, J. Barbé, Role of the high-affinity zinc uptake *znuABC* system in *Salmonella enterica* serovar typhimurium virulence, *Infection and immunity*, 70 (2002) 4721-4725.

- [143] M. Bajaj, S.K. Mamidyala, J. Zuegg, S.L. Begg, M.P. Ween, Z. Luo, J.X. Huang, A.G. McEwan, B. Kobe, J.C. Paton, Discovery of novel pneumococcal surface antigen A (PsaA) inhibitors using a fragment-based drug design approach, *ACS chemical biology*, 10 (2015) 1511-1520.
- [144] S. Ahuja, L. Rougé, D.L. Swem, J. Sudhamsu, P. Wu, S.J. Russell, M.K. Alexander, C. Tam, M. Nishiyama, M.A. Starovasnik, Structural analysis of bacterial ABC transporter inhibition by an antibody fragment, *Structure*, 23 (2015) 713-723.
- [145] A. Batool, Y. Iftikhar, S. Mughal, M. Khan, M. Jaskani, M. Abbas, I. Khan, Citrus Greening Disease—A major cause of citrus decline in the world—A Review, *Hort. Sci.(Prague)*, 34 (2007) 159-166.
- [146] J.M. Bové, Huanglongbing: a destructive, newly-emerging, century-old disease of citrus, *Journal of plant pathology*, (2006) 7-37.
- [147] J.d. Graca, Citrus greening disease, *Annual Review of Phytopathology*, 29 (1991) 109-136.
- [148] T.R. Gottwald, Current epidemiological understanding of citrus huanglongbing, *Annual review of phytopathology*, 48 (2010) 119-139.
- [149] S. Capoor, Decline of citrus trees in India, *Bull Natl Inst Sci India*, 24 (1963) 48-64.
- [150] J.H. Burke, The commercial citrus regions of the world, *The citrus industry*, 1 (1967) 40-189.
- [151] P. Obergolzer, D. Von Standen, W. Basson, Greening disease of sweet orange in South Africa, *International Organization of Citrus Virologists Conference Proceedings (1957-2010)*, 1965.
- [152] X.Y. Zhao, Citrus yellow shoot disease (huanglongbing) in China—a Review, *Proc. Int. Citriculture*, 1981, ICI Japan, Shimizu, Japan, 1 (1982) 466-469.
- [153] K.-H. Lin, Observations on yellow shoot of Citrus. Etiological studies of yellow shoot of Citrus, *Acta Phytopathologica Sinica*, 2 (1956).
- [154] G. Beattie, P. Broadbent, H-5 Huanglongbing: its possible origins, collaborative research in Southeast Asia, and developing incursion management plans for Australia, (2005).
- [155] H.A. Lee, The relation of stocks to mottled leaf of citrus trees, *Philippine Jour. Sci*, 18 (1921) 85-95.
- [156] N. FURUYA, K. MATSUKURA, K. TOMIMURA, M. OKUDA, S.-i. MIYATA, T. IWANAMI, Bibliography of citrus greening disease and its vectors attached with indices and a critical review on the ecology of the vectors and their control *Bibliography of citrus*

- greening disease and its vectors attached with indices and a critical review on the ecology of the vectors and their control 161, 1990, *Journal of general plant pathology*, 76 (2010) 122-131.
- [157] B. Aubert, M. Garnier, D. Guillaumin, B. Herbagyandono, L. Setiobudi, F. Nurhadi, Greening, a serious threat for the citrus productions of the Indonesian archipelago. Future prospects of integrated control, *Fruits (France)*, (1985).
- [158] G. Beattie, P. Holford, D. Mabblerley, A. Haigh, R. Bayer, P. Broadbent, Aspects and insights of Australia-Asia collaborative research on huanglongbing, *Proceedings of the international workshop for the prevention of citrus greening disease in severely infected areas*, Ministry of Agriculture, Forestry and Fisheries Tokyo, 2006.
- [159] D. Teixeira, C. Saillard, C. Couture, E. Martins, N. Wulff, P. Yamamoto, S. Eveillard-Jagoueix, A. Ayres, J. Bové, *Candidatus Liberibacter americanus*, agent of huanglongbing disease of citrus in Sao Paulo State, Brasil: distribution and quantification of the liberibacter in leaves of an affected sweet orange tree as determined by conventional PCR, nested PCR and quantitative, real time PCR, *Mol. Cell. Probes*.(DOI 10.1016/j. mcp. 2007.12. 2006), (2008).
- [160] D. Lafleche, J.M. Bové, Mycoplasmes dans les agrumes atteints de " greening", de " stubborn" ou de maladies similaires, *Fruits*, 25 (1970) 455-465.
- [161] M. Garnier, J. Bové, ORGANISM ASSOCIATED WITH CITRUS GREENING DISEASE IS PROBABLY A MEMBER OF SCHIZOMYCETES, *ZENTRALBLATT FUR BAKTERIOLOGIE MIKROBIOLOGIE UND HYGIENE SERIES A-MEDICAL MICROBIOLOGY INFECTIOUS DISEASES VIROLOGY PARASITOLOGY*, GUSTAV FISCHER VERLAG VILLENANG 2, D-07745 JENA, GERMANY, 1978, pp. 221-222.
- [162] M. Garnier, N. Danel, J. Bové, Aetiology of citrus greening disease, *Annales de l'Institut Pasteur/Microbiologie*, Elsevier, 1984, pp. 169-179.
- [163] M. Garnier, S. Jagoueix-Eveillard, P.R. Cronje, H.F. Le Roux, J.M. Bove, Genomic characterization of a liberibacter present in an ornamental rutaceous tree, *Calodendrum capense*, in the Western Cape Province of South Africa. Proposal of '*Candidatus Liberibacter africanus subsp. capensis*', *International Journal of Systematic and Evolutionary Microbiology*, 50 (2000) 2119-2125.
- [164] D. Teixeira, C. Saillard, S. Eveillard, J. Danet, A. Ayres, J. Bové, A new liberibacter species, *Candidatus Liberibacter americanus sp. nov.*, is associated with citrus

- huanglongbing (greening disease) in São Paulo State, Brazil, International Organization of Citrus Virologists Conference Proceedings (1957-2010), 2005.
- [165] F. Coletta, E. Carlos, L. Lotto, F. Luciane, K. Alves, M. Pereira, M. Machado, Prevalence of *Candidatus Liberibacter* spp. in HLB-diseased citrus plants in São Paulo State, Brazil, Proceedings of the Seventeenth International Organization of Citrus Virologists, 22-26 October 2007, Adana, Turkey, (2010) 110-115.
- [166] R. McClean, Greening or blotchy-mottle disease of citrus, *Phytophylactica*, 2 (1970) 177-194.
- [167] H. Schneider, Anatomy of greening-diseased sweet orange shoots, *Phytopathology*, 58 (1968) 1155-1160.
- [168] D.G. Hall, M.L. Richardson, E.D. Ammar, S.E. Halbert, Asian citrus psyllid, *Diaphorina citri*, vector of citrus huanglongbing disease, *Entomologia Experimentalis et Applicata*, 146 (2013) 207-223.
- [169] S.E. Halbert, K.L. Manjunath, Asian citrus psyllids (Sternorrhyncha: Psyllidae) and greening disease of citrus: a literature review and assessment of risk in Florida, *Florida entomologist*, 87 (2004) 330-353.
- [170] C. Xu, Y. Xia, K. Li, C. Ke, Further study of the transmission of citrus huanglongbin by a psyllid, *Diaphorina citri* Kuwayama, International Organization of Citrus Virologists Conference Proceedings (1957-2010), 1988.
- [171] E.-D. Ammar, J.E. Ramos, D.G. Hall, W.O. Dawson, R.G. Shatters Jr, Acquisition, replication and inoculation of *Candidatus Liberibacter asiaticus* following various acquisition periods on huanglongbing-infected citrus by nymphs and adults of the Asian citrus psyllid, *PloS one*, 11 (2016) e0159594.
- [172] M. Moll, Electron microscope evidence that citrus psylla (*Trioza erytreae*) is a vector of greening disease in South Africa, *Phytophylactica*, 5 (1973) 41-44.
- [173] R.S. Mann, J.G. Ali, S.L. Hermann, S. Tiwari, K.S. Pelz-Stelinski, H.T. Alborn, L.L. Stelinski, Induced release of a plant-defense volatile ‘deceptively’ attracts insect vectors to plants infected with a bacterial pathogen, *PLoS pathogens*, 8 (2012) e1002610.
- [174] T.H. Hung, S.C. Hung, C.N. Chen, M.H. Hsu, H.J. Su, Detection by PCR of *Candidatus Liberibacter asiaticus*, the bacterium causing citrus huanglongbing in vector psyllids: application to the study of vector–pathogen relationships, *Plant Pathology*, 53 (2004) 96-102.

- [175] G.A. Thompson, A.J. Van Bel, Phloem: Molecular cell biology, systemic communication, biotic interactions, John Wiley & Sons, Place Published, 2012.
- [176] N. Killiny, F. Hijaz, I. El-Shesheny, S. Alfaress, S.E. Jones, M.E. Rogers, Metabolomic analyses of the haemolymph of the Asian citrus psyllid *Diaphorina citri*, the vector of huanglongbing, *Physiological Entomology*, 42 (2017) 134-145.
- [177] J. Tamesse, J. Messi, Factors influencing the population dynamics of the African citrus psyllid *Trioza erythrae* Del Guercio (Hemiptera: Triozidae) in Cameroon, *International Journal of Tropical Insect Science*, 24 (2004) 213-227.
- [178] V. Baranwal, S. Majumder, Y. Ahlawat, R. Singh, A novel approach for simultaneous detection of Citrus yellow mosaic virus and Citrus greening bacterium by multiplex polymerase chain reaction, (2005).
- [179] M. Okuda, M. Matsumoto, Y. Tanaka, S. Subandiyah, T. Iwanami, Characterization of the *tuf B-sec E-nus G-rpl KAJL-rpo B* gene cluster of the citrus greening organism and detection by loop-mediated isothermal amplification, *Plant Disease*, 89 (2005) 705-711.
- [180] M. Nageswara-Rao, M. Ireya, S.M. Garnsey, S. Gowda, Candidate gene makers for *Candidatus Liberibacter asiaticus* for detecting citrus greening disease, *Journal of biosciences*, 38 (2013) 229-237.
- [181] S. Sankaran, J.M. Maja, S. Buchanon, R. Ehsani, Huanglongbing (citrus greening) detection using visible, near infrared and thermal imaging techniques, *Sensors*, 13 (2013) 2117-2130.
- [182] A. Pourreza, W.S.D. Lee, E. Raveh, Y. Hong, H.-J. Kim, Identification of citrus greening disease using a visible band image analysis, 2013 Kansas City, Missouri, July 21-July 24, 2013, American Society of Agricultural and Biological Engineers, 2013, pp. 1.
- [183] Y. Duan, L. Zhou, D.G. Hall, W. Li, H. Doddapaneni, H. Lin, L. Liu, C.M. Vahling, D.W. Gabriel, K.P. Williams, Complete genome sequence of citrus huanglongbing bacterium, '*Candidatus Liberibacter asiaticus*' obtained through metagenomics, *Molecular Plant-Microbe Interactions*, 22 (2009) 1011-1020.
- [184] H.L. Tyler, L.F. Roesch, S. Gowda, W.O. Dawson, E.W. Triplett, Confirmation of the sequence of '*Candidatus Liberibacter asiaticus*' and assessment of microbial diversity in Huanglongbing-infected citrus phloem using a metagenomic approach, *Molecular Plant-Microbe Interactions*, 22 (2009) 1624-1634.



- [185] S.A. Lee, L.A. Gallagher, M. Thongdee, B.J. Staudinger, S. Lippman, P.K. Singh, C. Manoil, General and condition-specific essential functions of *Pseudomonas aeruginosa*, *Proceedings of the National Academy of Sciences*, 112 (2015) 5189-5194.
- [186] N.A. Moran, Microbial minimalism: genome reduction in bacterial pathogens, *Cell*, 108 (2002) 583-586.
- [187] A. Bhattacharyya, S. Stilwagen, G. Reznik, H. Feil, W.S. Feil, I. Anderson, A. Bernal, M. D'Souza, N. Ivanova, V. Kapratl, Draft sequencing and comparative genomics of *Xylella fastidiosa* strains reveal novel biological insights, *Genome research*, 12 (2002) 1556-1563.
- [188] P. Cotter, V. Chepuri, R. Gennis, R. Gunsalus, Cytochrome o (cyoABCDE) and d (cydAB) oxidase gene expression in *Escherichia coli* is regulated by oxygen, pH, and the *fnr* gene product, *Journal of bacteriology*, 172 (1990) 6333-6338.
- [189] C.W. Rice, W.P. Hempfling, Oxygen-limited continuous culture and respiratory energy conservation in *Escherichia coli*, *Journal of bacteriology*, 134 (1978) 115-124.
- [190] A.L. Davidson, E. Dassa, C. Orelle, J. Chen, Structure, function, and evolution of bacterial ATP-binding cassette systems, *Microbiology and Molecular Biology Reviews*, 72 (2008) 317-364.
- [191] M.E. Garrido, M. Bosch, R. Medina, M. Llagostera, A.M. Pérez de Rozas, I. Badiola, J. Barbé, The high-affinity zinc-uptake system *znuACB* is under control of the iron-uptake regulator (*fur*) gene in the animal pathogen *Pasteurella multocida*, *FEMS microbiology letters*, 221 (2003) 31-37.
- [192] A.P. Pugsley, The complete general secretory pathway in gram-negative bacteria, *Microbiological reviews*, 57 (1993) 50-108.
- [193] J.D. Reddy, S.L. Reddy, D.L. Hopkins, D.W. Gabriel, TolC is required for pathogenicity of *Xylella fastidiosa* in *Vitis vinifera* grapevines, *Molecular plant-microbe interactions*, 20 (2007) 403-410.
- [194] V. Koronakis, J. Eswaran, C. Hughes, Structure and function of TolC: the bacterial exit duct for proteins and drugs, *Annual review of biochemistry*, 73 (2004) 467-489.
- [195] P. Delepelaire, Type I secretion in gram-negative bacteria, *Biochimica et Biophysica Acta (BBA) - Molecular Cell Research*, 1694 (2004) 149-161.
- [196] J. Fan, C. Chen, Q. Yu, R.H. Brlansky, Z.G. Li, F.G. Gmitter, Comparative iTRAQ proteome and transcriptome analyses of sweet orange infected by "Candidatus *Liberibacter asiaticus*", *Physiologia plantarum*, 143 (2011) 235-245.



- [197] C.C. Nwugo, H. Lin, Y. Duan, E.L. Civerolo, The effect of 'Candidatus Liberibacter asiaticus' infection on the proteomic profiles and nutritional status of pre-symptomatic and symptomatic grapefruit (*Citrus paradisi*) plants, *BMC plant biology*, 13 (2013) 59.
- [198] P. Trivedi, U.S. Sagaram, J.-S. Kim, R.H. Brlansky, M.E. Rogers, L.L. Stelinski, C. Oswalt, N. Wang, Quantification of viable *Candidatus Liberibacter asiaticus* in hosts using quantitative PCR with the aid of ethidium monoazide (EMA), *European journal of plant pathology*, 124 (2009) 553-563.
- [199] J. Fan, C. Chen, R. Brlansky, F. Gmitter Jr, Z.G. Li, Changes in carbohydrate metabolism in *Citrus sinensis* infected with 'Candidatus *Liberibacter asiaticus*', *Plant pathology*, 59 (2010) 1037-1043.
- [200] J. Fan, C. Chen, Q. Yu, A. Khalaf, D.S. Achor, R.H. Brlansky, G.A. Moore, Z.-G. Li, F.G. Gmitter Jr, Comparative transcriptional and anatomical analyses of tolerant rough lemon and susceptible sweet orange in response to 'Candidatus *Liberibacter asiaticus*' infection, *Molecular plant-microbe interactions*, 25 (2012) 1396-1407.
- [201] E.-J. Koh, L. Zhou, D.S. Williams, J. Park, N. Ding, Y.-P. Duan, B.-H. Kang, Callose deposition in the phloem plasmodesmata and inhibition of phloem transport in citrus leaves infected with "Candidatus *Liberibacter asiaticus*", *Protoplasma*, 249 (2012) 687-697.
- [202] A. Gómez-Cadenas, J. Mehouchi, F.R. Tadeo, E. Primo-Millo, M. Talon, Hormonal regulation of fruitlet abscission induced by carbohydrate shortage in citrus, *Planta*, 210 (2000) 636-643.
- [203] U. Albrecht, K.D. Bowman, Gene expression in *Citrus sinensis* (L.) Osbeck following infection with the bacterial pathogen *Candidatus Liberibacter asiaticus* causing Huanglongbing in Florida, *Plant Science*, 175 (2008) 291-306.
- [204] W. Li, Q. Cong, J. Pei, L.N. Kinch, N.V. Grishin, The ABC transporters in *Candidatus Liberibacter asiaticus*, *Proteins: Structure, Function, and Bioinformatics*, 80 (2012) 2614-2628.
- [205] R. Rosales, J.K. Burns, Phytohormone changes and carbohydrate status in sweet orange fruit from Huanglongbing-infected trees, *Journal of Plant Growth Regulation*, 30 (2011) 312-321.
- [206] P. Sharma, D. Dube, A. Singh, B. Mishra, N. Singh, M. Sinha, S. Dey, P. Kaur, D.K. Mitra, S. Sharma, Structural basis of recognition of pathogen-associated molecular patterns and

- inhibition of proinflammatory cytokines by camel peptidoglycan recognition protein, *Journal of Biological Chemistry*, 286 (2011) 16208-16217.
- [207] M. Orozco-Cardenas, C.A. Ryan, Hydrogen peroxide is generated systemically in plant leaves by wounding and systemin via the octadecanoid pathway, *Proceedings of the National Academy of Sciences*, 96 (1999) 6553-6557.
- [208] H. Zou, S. Gowda, L. Zhou, S. Hajeri, G. Chen, Y. Duan, The destructive citrus pathogen, 'Candidatus *Liberibacter asiaticus*' encodes a functional flagellin characteristic of a pathogen-associated molecular pattern, *PLoS One*, 7 (2012) e46447.
- [209] L. Van Loon, P. Bakker, C. Pieterse, Systemic resistance induced by rhizosphere bacteria, *Annual review of phytopathology*, 36 (1998) 453-483.
- [210] L. Sticher, B. Mauch-Mani, Métraux, JP, Systemic acquired resistance, *Annual review of phytopathology*, 35 (1997) 235-270.
- [211] S. Van Wees, J. Glazebrook, Loss of non-host resistance of *Arabidopsis NahG* to *Pseudomonas syringae* pv. *phaseolicola* is due to degradation products of salicylic acid, *The Plant Journal*, 33 (2003) 733-742.
- [212] P. Trivedi, Y. Duan, N. Wang, Huanglongbing, a systemic disease, restructures the bacterial community associated with citrus roots, *Applied and environmental microbiology*, 76 (2010) 3427-3436.
- [213] P. Trivedi, Z. He, J.D. Van Nostrand, G. Albrigo, J. Zhou, N. Wang, Huanglongbing alters the structure and functional diversity of microbial communities associated with citrus rhizosphere, *The ISME journal*, 6 (2012) 363.
- [214] S. Zhang, Z. Flores-Cruz, L. Zhou, B.-H. Kang, L.A. Fleites, M.D. Gooch, N.A. Wulff, M.J. Davis, Y.-P. Duan, D.W. Gabriel, 'Ca. *Liberibacter asiaticus*' carries an excision plasmid prophage and a chromosomally integrated prophage that becomes lytic in plant infections, *Molecular plant-microbe interactions*, 24 (2011) 458-468.
- [215] S.Y. Folimonova, C.J. Robertson, S.M. Garnsey, S. Gowda, W.O. Dawson, Examination of the responses of different genotypes of citrus to Huanglongbing (citrus greening) under different conditions, *Phytopathology*, 99 (2009) 1346-1354.
- [216] Q. Yan, A. Sreedharan, S. Wei, J. Wang, K. Pelz-Stelinski, S. Folimonova, N. Wang, Global gene expression changes in *Candidatus Liberibacter asiaticus* during the transmission in distinct hosts between plant and insect, *Molecular plant pathology*, 14 (2013) 391-404.

- [217] A. Schmidtchen, I.M. Frick, E. Andersson, H. Tapper, L. Björck, Proteinases of common pathogenic bacteria degrade and inactivate the antibacterial peptide LL-37, *Molecular microbiology*, 46 (2002) 157-168.
- [218] B. Basu, S.K. Apte, A novel serralyisin metalloprotease from *Deinococcus radiodurans*, *Biochimica et Biophysica Acta (BBA)-Proteins and Proteomics*, 1784 (2008) 1256-1264.
- [219] R. Belas, J. Manos, R. Suvanasuthi, *Proteus mirabilis* ZapA metalloprotease degrades a broad spectrum of substrates, including antimicrobial peptides, *Infection and immunity*, 72 (2004) 5159-5167.
- [220] M.T. Leonard, J.R. Fagen, A.G. Davis-Richardson, M.J. Davis, E.W. Triplett, Complete genome sequence of *Liberibacter crescens* BT-1, *Standards in genomic sciences*, 7 (2012) 271.
- [221] J.A. Stoebner, S.M. Payne, Iron-regulated hemolysin production and utilization of heme and hemoglobin by *Vibrio cholerae*, *Infection and immunity*, 56 (1988) 2891-2895.
- [222] E. Gouaux,  $\alpha$ -Hemolysin from *Staphylococcus aureus*: an archetype of  $\beta$ -barrel, channel-forming toxins, *Journal of structural biology*, 121 (1998) 110-122.
- [223] M. Kube, B. Schneider, H. Kuhl, T. Dandekar, K. Heitmann, A.M. Migdoll, R. Reinhardt, E. Seemüller, The linear chromosome of the plant-pathogenic mycoplasma 'Candidatus *Phytoplasma mali*', *Bmc Genomics*, 9 (2008) 306.
- [224] E.L. Chin, D.O. Mishchuk, A.P. Breksa, C.M. Slupsky, Metabolite signature of Candidatus *Liberibacter asiaticus* infection in two citrus varieties, *Journal of agricultural and food chemistry*, 62 (2014) 6585-6591.
- [225] A.M. Slisz, A.P. Breksa III, D.O. Mishchuk, G. McCollum, C.M. Slupsky, Metabolomic analysis of citrus infection by 'Candidatus *Liberibacter*' reveals insight into pathogenicity, *Journal of proteome research*, 11 (2012) 4223-4230.
- [226] S. Tian, L. Lu, J.M. Labavitch, S.M. Webb, X. Yang, P.H. Brown, Z. He, Spatial imaging of Zn and other elements in Huanglongbing-affected grapefruit by synchrotron-based micro X-ray fluorescence investigation, *Journal of experimental botany*, 65 (2014) 953-964.
- [227] G.-c. Fan, Y.-l. Xia, X.-j. Lin, H.-q. Hu, X.-d. Wang, C.-q. Ruan, L.-m. Lu, B. Liu, Evaluation of thermotherapy against Huanglongbing (citrus greening) in the greenhouse, *Journal of Integrative Agriculture*, 15 (2016) 111-119.
- [228] F. Joubert, P. Stassen, The effect of time of pruning on yield, fruit size and greening disease incidence of Valencia citrus trees, *Neltropika Bulletin*, (2000) 28-31.

- [229] S. Ruilin, W. Rujian, C. Qingying, Increasing the survival rate of shoot-tip grafting (STG) and its application in production of disease-free citrus seedlings, *Fujian Journal of Agricultural Sciences*, 5 (1990) 20-26.
- [230] N.X. Binh, N.D. Lam, Use of technical means of intensive farming to improve fruit productivity of orange orchard slightly injured by greening disease in Ha Giang Province, *Science and Technology Journal of Agriculture and Rural Development*, (2004).
- [231] N.B. Ve, N.T.M. Chau, The effects of foliar application of (SO<sub>4</sub>Zn+ SO<sub>4</sub>Mn) on the symptom of Greening disease of Cam Mat and Quyt Duong at the immature tree stage of growing and levels of disease, *Science and Technology Journal of Agriculture and Rural Development*, (2004).
- [232] A.S. Marsh, Use of Curry Leaf (*Murraya koenigii*) and Volkamer Lemon (*Citrus volkameriana*) as Potential Trap Crops for the Asian Citrus Psyllid (*Diaphorina citri*) in a Commercial Citrus Grove, California State Polytechnic University, Pomona, 2017.
- [233] J.A. Qureshi, M.E. Rogers, D.G. Hall, P.A. Stansly, Incidence of invasive *Diaphorina citri* (Hemiptera: Psyllidae) and its introduced parasitoid *Tamarixia radiata* (Hymenoptera: Eulophidae) in Florida citrus, *Journal of Economic Entomology*, 102 (2009) 247-256.
- [234] S. Subandiyah, T. Iwanami, S. Tsuyumu, H. Ieki, Comparison of 16S rDNA and 16S/23S intergenic region sequences among citrus greening organisms in Asia, *Plant disease*, 84 (2000) 15-18.
- [235] W. Hu, F. Kuang, Z. Lu, N. Zhang, T. Chen, Killing effects of an isolated *Serratia marcescens* KH-001 on *Diaphorina citri* via lowering the endosymbiont numbers, *Frontiers in microbiology*, 9 (2018).
- [236] A. Martinez, D. Nora, A. Armedilla, Suppression of symptoms of citrus greening disease in the Philippines by treatment with tetracycline antibiotics, *Plant Disease Reporter*, 54 (1970) 1007-1009.
- [237] T. Nariani, S. Ghosh, D. Kumar, S. Raychaudhuri, S. Viswanath, Detection and possibilities of therapeutic control of the greening disease of citrus caused by mycoplasma, *Proc. Indian Nat. Acad. B*, 1975, pp. 334-339.
- [238] H. Shokrollah, T. Lee Abdullah, K. Sijam, S.N.A. Abdullah, Identification of physical and biochemical characteristic of mandarin (*Citrus reticulata*) fruit infected by huanglongbing (HLB), *Australian Journal of Crop Science*, 5 (2011) 181.

- [239] M. Zhang, Y. Duan, L. Zhou, W.W. Turechek, E. Stover, C.A. Powell, Screening molecules for control of citrus huanglongbing using an optimized regeneration system for 'Candidatus Liberibacter asiaticus'-infected periwinkle (*Catharanthus roseus*) cuttings, *Phytopathology*, 100 (2010) 239-245.
- [240] M. Zhang, C.A. Powell, L. Zhou, Z. He, E. Stover, Y. Duan, Chemical compounds effective against the citrus Huanglongbing bacterium 'Candidatus Liberibacter asiaticus' in planta, *Phytopathology*, 101 (2011) 1097-1103.
- [241] M. Zhang, C.A. Powell, Y. Guo, M.S. Doud, Y. Duan, A graft-based chemotherapy method for screening effective molecules and rescuing huanglongbing-affected citrus plants, *Phytopathology*, 102 (2012) 567-574.
- [242] M.T. Guarnieri, B.S. Blagg, R. Zhao, A high-throughput TNP-ATP displacement assay for screening inhibitors of ATP-binding in bacterial histidine kinases, *Assay and drug development technologies*, 9 (2011) 174-183.
- [243] M.T. Guarnieri, L. Zhang, J. Shen, R. Zhao, The Hsp90 inhibitor radicicol interacts with the ATP-binding pocket of bacterial sensor kinase PhoQ, *Journal of molecular biology*, 379 (2008) 82-93.
- [244] M. Kumar, S. Sharma, A. Srinivasan, T.P. Singh, P. Kaur, Structure-based in-silico rational design of a selective peptide inhibitor for thymidine monophosphate kinase of mycobacterium tuberculosis, *Journal of Molecular Modeling*, 17 (2011) 1173-1182.
- [245] D. Dube, V. Periwal, M. Kumar, S. Sharma, T.P. Singh, P. Kaur, 3D-QSAR based pharmacophore modeling and virtual screening for identification of novel pteridine reductase inhibitors, *Journal of Molecular Modeling*, 18 (2012) 1701-1711.
- [246] M. Serrano, V. Gonzalez, S. Ray, M.D. Chavez, M. Narayan, Identification of Structure-Stabilizing Interactions in Enzymes: A Novel Mechanism to Impact Enzyme Activity, *Cell Biochemistry and Biophysics*, 76 (2018) 59-71.
- [247] P. Kabiraj, J.E. Marin, A. Varela-Ramirez, E. Zubia, M. Narayan, Ellagic acid mitigates SNO-PDI induced aggregation of Parkinsonian biomarkers, *ACS chemical neuroscience*, 5 (2014) 1209-1220.
- [248] L. Redecke, K. Nass, D.P. DePonte, T.A. White, D. Rehders, A. Barty, F. Stellato, M. Liang, T.R. Barends, S. Boutet, Natively inhibited *Trypanosoma brucei* cathepsin B structure determined by using an X-ray laser, *Science*, 339 (2013) 227-230.



- [249] V.V. Balaev, A.A. Lashkov, A.G. Gabdulkhakov, M.V. Dontsova, A.S. Mironov, C. Betzel, A.M. Mikhailov, Three-dimensional structures of unligated uridine phosphorylase from *Yersinia pseudotuberculosis* at 1.4 Å resolution and its complex with an antibacterial drug, *Crystallography Reports*, 60 (2015) 525-531.
- [250] A.A. Lashkov, S.E. Sotnichenko, I.I. Prokofiev, A.G. Gabdulkhakov, I.I. Agapov, A.A. Shtil, C. Betzel, A.S. Mironov, A.b.M. Mikhailov, X-ray structure of *Salmonella typhimurium* uridine phosphorylase complexed with 5-fluorouracil and molecular modelling of the complex of 5-fluorouracil with uridine phosphorylase from *Vibrio cholerae*, *Acta Crystallographica Section D: Biological Crystallography*, 68 (2012) 968-974.
- [251] J. Drebes, M. Künz, B. Windshügel, A.G. Kikhney, I.B. Müller, R.J. Eberle, D. Oberthür, H. Cang, D.I. Svergun, M. Perbandt, Structure of ThiM from Vitamin B1 biosynthetic pathway of *Staphylococcus aureus*—insights into a novel pro-drug approach addressing MRSA infections, *Scientific reports*, 6 (2016) 22871.
- [252] C.M. Vahling-Armstrong, H. Zhou, L. Benyon, J.K. Morgan, Y. Duan, Two plant bacteria, *S. meliloti* and *Ca. Liberibacter asiaticus*, share functional *znuABC* homologues that encode for a high affinity zinc uptake system, *PLoS One*, 7 (2012) e37340.
- [253] C.F. Higgins, "ABC transporters: physiology, structure and mechanism" an overview, *Res Microbiol*, 152 (2001) 205-210.
- [254] N. Sharma, P. Selvakumar, G. Saini, A. Warghane, D.K. Ghosh, A.K. Sharma, Crystal structure analysis in Zn<sup>2+</sup>-bound state and biophysical characterization of CLas-ZnuA2, *Biochimica et Biophysica Acta (BBA)-Proteins and Proteomics*, 1864 (2016) 1649-1657.
- [255] J. Da Graça, L. Korsten, *Citrus huanglongbing: Review, present status and future strategies*, *Diseases of fruits and vegetables volume I*, Springer, Place Published, 2004, pp. 229-245.
- [256] A. Vagin, A. Teplyakov, MOLREP: an automated program for molecular replacement, *Journal of applied crystallography*, 30 (1997) 1022-1025.
- [257] P. Emsley, K. Cowtan, Coot: model-building tools for molecular graphics, *Acta Crystallographica Section D: Biological Crystallography*, 60 (2004) 2126-2132.
- [258] P. Emsley, B. Lohkamp, W.G. Scott, K. Cowtan, Features and development of Coot, *Acta Crystallographica Section D: Biological Crystallography*, 66 (2010) 486-501.



- [259] G.N. Murshudov, A.A. Vagin, E.J. Dodson, Refinement of macromolecular structures by the maximum-likelihood method, *Acta Crystallographica Section D: Biological Crystallography*, 53 (1997) 240-255.
- [260] M. Winn, M. Isupov, G.N. Murshudov, Use of TLS parameters to model anisotropic displacements in macromolecular refinement, *Acta Crystallographica Section D: Biological Crystallography*, 57 (2001) 122-133.
- [261] R.A. Laskowski, M.W. MacArthur, D.S. Moss, J.M. Thornton, PROCHECK: a program to check the stereochemical quality of protein structures, *Journal of applied crystallography*, 26 (1993) 283-291.
- [262] V.B. Chen, W.B. Arendall, J.J. Headd, D.A. Keedy, R.M. Immormino, G.J. Kapral, L.W. Murray, J.S. Richardson, D.C. Richardson, MolProbity: all-atom structure validation for macromolecular crystallography, *Acta Crystallographica Section D: Biological Crystallography*, 66 (2010) 12-21.
- [263] E. Krissinel, K. Henrick, Secondary-structure matching (SSM), a new tool for fast protein structure alignment in three dimensions, *Acta Crystallographica Section D: Biological Crystallography*, 60 (2004) 2256-2268.
- [264] W.L. DeLano, The PyMOL molecular graphics system, <http://www.pymol.org>, (2002).
- [265] E.F. Pettersen, T.D. Goddard, C.C. Huang, G.S. Couch, D.M. Greenblatt, E.C. Meng, T.E. Ferrin, UCSF Chimera—a visualization system for exploratory research and analysis, *Journal of computational chemistry*, 25 (2004) 1605-1612.
- [266] O. Conchillo-Solé, N.S. de Groot, F.X. Avilés, J. Vendrell, X. Daura, S. Ventura, AGGREGSCAN: a server for the prediction and evaluation of "hot spots" of aggregation in polypeptides, *BMC bioinformatics*, 8 (2007) 65.
- [267] M. Garnier, J. Bové, C. Cronje, G. Sanders, L. Korsten, H. Le Roux, Presence of "Candidatus *Liberibacter africanus*" in the Western Cape province of South Africa, *International Organization of Citrus Virologists Conference Proceedings (1957-2010)*, 2000.
- [268] D.d.C. Texeira, J. Ayres, E. Kitajima, L. Danet, S. Jagoueix-Eveillard, C. Saillard, J. Bové, First report of a huanglongbing-like disease of citrus in São Paulo State, Brazil and association of a new *Liberibacter* species, "Candidatus *Liberibacter americanus*", with the disease, *Plant Disease*, 89 (2005) 107-107.

- [269] R. Brlansky, K. Chung, M. Rogers, 2006 Florida citrus pest management guide: Huanglongbing (citrus greening), UF/IFAS Extension, (2012).
- [270] E.E. Grafton-Cardwell, L.L. Stelinski, P.A. Stansly, Biology and management of Asian citrus psyllid, vector of the huanglongbing pathogens, *Annual Review of Entomology*, 58 (2013) 413-432.
- [271] K.J. Waldron, N.J. Robinson, How do bacterial cells ensure that metalloproteins get the correct metal?, *Nature Reviews Microbiology*, 7 (2009) 25.
- [272] M. Cerasi, S. Ammendola, A. Battistoni, Competition for zinc binding in the host-pathogen interaction, *Frontiers in cellular and infection microbiology*, 3 (2013) 108.
- [273] M. Scrutton, C. Wu, D. Goldthwait, The presence and possible role of zinc in RNA polymerase obtained from *Escherichia coli*, *Proceedings of the National Academy of Sciences*, 68 (1971) 2497-2501.
- [274] W.T. Miller, K.A. Hill, P. Schimmel, Evidence for a "cysteine-histidine box" metal-binding site in an *Escherichia coli* aminoacyl-tRNA synthetase, *Biochemistry*, 30 (1991) 6970-6976.
- [275] L.M. Davis, T. Kakuda, V.J. DiRita, A *Campylobacter jejuni* *znuA* orthologue is essential for growth in low-zinc environments and chick colonization, *Journal of bacteriology*, 191 (2009) 1631-1640.
- [276] T.N. Petersen, S. Brunak, G. von Heijne, H. Nielsen, SignalP 4.0: discriminating signal peptides from transmembrane regions, *Nature methods*, 8 (2011) 785.
- [277] X. Robert, P. Gouet, Deciphering key features in protein structures with the new ENDscript server, *Nucleic acids research*, 42 (2014) W320-W324.
- [278] F. Sievers, A. Wilm, D. Dineen, T.J. Gibson, K. Karplus, W. Li, R. Lopez, H. McWilliam, M. Remmert, J. Söding, Fast, scalable generation of high-quality protein multiple sequence alignments using Clustal Omega, *Molecular systems biology*, 7 (2011) 539.
- [279] J. Felsenstein, Confidence limits on phylogenies: an approach using the bootstrap, *Evolution*, 39 (1985) 783-791.
- [280] M. Nei, S. Kumar, *Molecular evolution and phylogenetics*, Oxford university press, Place Published, 2000.
- [281] S. Kumar, G. Stecher, M. Li, C. Knyaz, K. Tamura, MEGA X: Molecular Evolutionary Genetics Analysis across Computing Platforms, *Molecular biology and evolution*, 35 (2018) 1547-1549.

- [282] L.A. Kelley, S. Mezulis, C.M. Yates, M.N. Wass, M.J. Sternberg, The Phyre2 web portal for protein modeling, prediction and analysis, *Nature protocols*, 10 (2015) 845.
- [283] A. Fiser, A. Sali, ModLoop: automated modeling of loops in protein structures, *Bioinformatics*, 19 (2003) 2500-2501.
- [284] K. Arnold, L. Bordoli, J. Kopp, T. Schwede, The SWISS-MODEL workspace: a web-based environment for protein structure homology modelling, *Bioinformatics*, 22 (2006) 195-201.
- [285] N.M. O'Boyle, M. Banck, C.A. James, C. Morley, T. Vandermeersch, G.R. Hutchison, Open Babel: An open chemical toolbox, *Journal of cheminformatics*, 3 (2011) 33.
- [286] S. Dallakyan, A.J. Olson, *Small-molecule library screening by docking with PyRx*, Chemical Biology, Springer, Place Published, 2015, pp. 243-250.
- [287] J.J. Irwin, B.K. Shoichet, ZINC– a free database of commercially available compounds for virtual screening, *Journal of chemical information and modeling*, 45 (2005) 177-182.
- [288] A. Daina, O. Michielin, V. Zoete, SwissADME: a free web tool to evaluate pharmacokinetics, drug-likeness and medicinal chemistry friendliness of small molecules, *Scientific reports*, 7 (2017) 42717.
- [289] C.A. Lipinski, F. Lombardo, B.W. Dominy, P.J. Feeney, Experimental and computational approaches to estimate solubility and permeability in drug discovery and development settings, *Advanced drug delivery reviews*, 64 (2012) 4-17.
- [290] G.M. Morris, R. Huey, W. Lindstrom, M.F. Sanner, R.K. Belew, D.S. Goodsell, A.J. Olson, AutoDock4 and AutoDockTools4: Automated docking with selective receptor flexibility, *Journal of computational chemistry*, 30 (2009) 2785-2791.
- [291] S. Release, 2: Maestro; Schrödinger, LLC: New York, 2016, There is no corresponding record for this reference, (2017).
- [292] D. Van Der Spoel, E. Lindahl, B. Hess, G. Groenhof, A.E. Mark, H.J. Berendsen, GROMACS: fast, flexible, and free, *Journal of computational chemistry*, 26 (2005) 1701-1718.
- [293] W.F. van Gunsteren, S.R. Billeter, A.A. Eising, P.H. Hünenberger, P. Krüger, A.E. Mark, W.R. Scott, I.G. Tironi, *Biomolecular simulation: the {GROMOS96} manual and user guide*, (1996).
- [294] A.W. SchuÈttelkopf, D.M. Van Aalten, PRODRG: a tool for high-throughput crystallography of protein–ligand complexes, *Acta Crystallographica Section D: Biological Crystallography*, 60 (2004) 1355-1363.

- [295] H.-C. Lee, W.-C. Hsu, A.-L. Liu, C.-J. Hsu, Y.-C. Sun, Using thermodynamic integration MD simulation to compute relative protein–ligand binding free energy of a GSK3 $\beta$  kinase inhibitor and its analogs, *Journal of Molecular Graphics and Modelling*, 51 (2014) 37-49.
- [296] M.J. Abraham, J.E. Gready, Optimization of parameters for molecular dynamics simulation using smooth particle-mesh Ewald in GROMACS 4.5, *Journal of computational chemistry*, 32 (2011) 2031-2040.
- [297] R. Kumari, R. Kumar, O.S.D.D. Consortium, A. Lynn, g\_mmpbsa □ A GROMACS tool for high-throughput MM-PBSA calculations, *Journal of chemical information and modeling*, 54 (2014) 1951-1962.
- [298] S. Jagoueix, J.M. Bové, M. Garnier, PCR detection of the two «Candidatus» liberobacter species associated with greening disease of citrus, *Molecular and cellular probes*, 10 (1996) 43-50.
- [299] D.R. Boina, J.R. Bloomquist, Chemical control of the Asian citrus psyllid and of huanglongbing disease in citrus, *Pest management science*, 71 (2015) 808-823.
- [300] M. Doud, M.-Q. Zhang, C.A. Powell, Y.-P. Duan, Thermo-therapy and chemotherapy to control citrus HLB in the field, *Journal of Citrus Pathology*, 1 (2014).
- [301] Z. Jia, J. Zheng, Y. Huang, H. Zhou, R. Ehsani, Review and prospect of thermo-therapy for citrus huanglongbing, *Transactions of the Chinese Society of Agricultural Engineering*, 31 (2015) 1-9.
- [302] N. Akula, P. Trivedi, F.Q. Han, N. Wang, Identification of small molecule inhibitors against SecA of Candidatus Liberibacter asiaticus by structure based design, *European journal of medicinal chemistry*, 54 (2012) 919-924.
- [303] D.B. Kitchen, H. Decornez, J.R. Furr, J. Bajorath, Docking and scoring in virtual screening for drug discovery: methods and applications, *Nature reviews Drug discovery*, 3 (2004) 935.
- [304] N. Singh, V. Dalal, P. Kumar, Structure based mimicking of Phthalic acid esters (PAEs) and inhibition of hACMSD, an important enzyme of the tryptophan kynurenine metabolism pathway, *International journal of biological macromolecules*, 108 (2018) 214-224.
- [305] N. Singh, V. Dalal, J.K. Mahto, P. Kumar, Biodegradation of phthalic acid esters (PAEs) and in silico structural characterization of mono-2-ethylhexyl phthalate (MEHP) hydrolase on the basis of close structural homolog, *Journal of hazardous materials*, 338 (2017) 11-22.

- [306] D.A. Lewis, J. Klesney-Tait, S.R. Lumbley, C.K. Ward, J.L. Latimer, C.A. Ison, E.J. Hansen, Identification of the *znuA*-encoded periplasmic zinc transport protein of *Haemophilus ducreyi*, *Infection and immunity*, 67 (1999) 5060-5068.
- [307] G. Schneider, Virtual screening: an endless staircase?, *Nature Reviews Drug Discovery*, 9 (2010) 273.
- [308] B.K. Shoichet, Virtual screening of chemical libraries, *Nature*, 432 (2004) 862.
- [309] W. Huang, A. Wilks, Extracellular heme uptake and the challenge of bacterial cell membranes, *Annual review of biochemistry*, 86 (2017) 799-823.
- [310] V. Braun, H. Killmann, Bacterial solutions to the iron-supply problem, *Trends in biochemical sciences*, 24 (1999) 104-109.
- [311] A.C. Dlouhy, C.E. Outten, The iron metallome in eukaryotic organisms, *Metallomics and the Cell*, Springer, Place Published, 2013, pp. 241-278.
- [312] K.W. Becker, E.P. Skaar, Metal limitation and toxicity at the interface between host and pathogen, *FEMS microbiology reviews*, 38 (2014) 1235-1249.
- [313] J. Neilands, Siderophores: structure and function of microbial iron transport compounds, *Journal of Biological Chemistry*, 270 (1995) 26723-26726.
- [314] K.N. Raymond, E.A. Dertz, S.S. Kim, Enterobactin: an archetype for microbial iron transport, *Proceedings of the National Academy of Sciences*, 100 (2003) 3584-3588.
- [315] J.H. Crosa, C.T. Walsh, Genetics and assembly line enzymology of siderophore biosynthesis in bacteria, *Microbiology and molecular biology reviews*, 66 (2002) 223-249.
- [316] S.M. Barry, G.L. Challis, Recent advances in siderophore biosynthesis, *Current opinion in chemical biology*, 13 (2009) 205-215.
- [317] D.I. Chan, H.J. Vogel, Current understanding of fatty acid biosynthesis and the acyl carrier protein, *Biochemical Journal*, 430 (2010) 1-19.
- [318] B.F. Matzanke, S. Anemüller, V. Schünemann, A.X. Trautwein, K. Hantke, FhuF, part of a siderophore– reductase system, *Biochemistry*, 43 (2004) 1386-1392.
- [319] E. Chiancone, P. Ceci, A. Ilari, F. Ribacchi, S. Stefanini, Iron and proteins for iron storage and detoxification, *Biometals*, 17 (2004) 197-202.
- [320] S.D. Gray-Owen, A.B. Schyvers, Bacterial transferrin and lactoferrin receptors, *Trends in microbiology*, 4 (1996) 185-191.
- [321] A.B. Schryvers, I. Stojiljkovic, Iron acquisition systems in the pathogenic *Neisseria*, *Molecular microbiology*, 32 (1999) 1117-1123.

- [322] S. Release, 2: Maestro, Schrödinger, LLC, New York, NY, 2017, Received: February, 21 (2016) 2018.
- [323] A.W. Schüttelkopf, D.M. Van Aalten, PRODRG: a tool for high-throughput crystallography of protein–ligand complexes, *Acta Crystallographica Section D: Biological Crystallography*, 60 (2004) 1355-1363.
- [324] M. Zhang, Y. Guo, C.A. Powell, M.S. Doud, C. Yang, Y. Duan, Effective antibiotics against ‘*Candidatus Liberibacter asiaticus*’ in HLB-affected citrus plants identified via the graft-based evaluation, *PloS one*, 9 (2014) e111032.
- [325] S. Lopes, G. Frare, Graft transmission and cultivar reaction of citrus to ‘*Candidatus Liberibacter americanus*’, *Plant Disease*, 92 (2008) 21-24.
- [326] T. Nariani, S. Raychaudhuri, S. Viswanath, Tolerance to greening disease in certain citrus species, *Current Science*, 42 (1973) 513-514.

